Summer 8-7-2012

Biophysical Characterization of the Binding of Homologous Anthraquinone Amides to DNA

Shirlene R. Jackson Beckford
Georgia State University

BIOPHYSICAL CHARACTERIZATION OF THE BINDING OF HOMOLOGOUS ANTHRAQUINONE AMIDES TO DNA

by

SHIRLENE JACKSON BECKFORD

Under the Direction of Dr. Dabney Dixon

ABSTRACT

The synthesis of four homologous anthraquinones (**AQ I-IV**) bearing increasing lengths of polyethylene glycol (PEG) side chains and their binding to AT- and GC-rich DNA hairpins are reported. The molecules were designed such that the cationic charge is at a constant position and the ethylene glycol units chosen to allow significant increases in size with minimal changes in hydrophobicity. The mode and affinity of binding were assessed using circular dichroism (CD), nuclear magnetic resonance (NMR), surface plasmon resonance (SPR), and isothermal titration calorimetry (ITC). The binding affinity decreased as the AQ chain length increased along the series with both AT- and GC-rich DNA. ITC measurements showed that the thermodynamic parameters of **AQ I-IV** binding to DNA exhibited significant enthalpy-entropy compensation. The enthalpy became more favorable while the entropy became less favorable. The correlation

between enthalpy and entropy may involve not only the side chains, but also changes in the binding of water and associated counterions and hydrogen bonding.

The interactions of **AQ I-IV** with GC-rich DNA have been studied via molecular dynamics (MD) simulations. The geometry, conformation, interactions, and hydration of the complexes were examined. As the side chain lengthened, binding to DNA reduced the conformational space, resulting in an increase in unfavorable entropy. Increased localization of the PEG side chain in the DNA groove, indicating some interaction of the side chain with DNA, also contributed unfavorably to the entropy. The changes in free energy of binding due to entropic considerations (-3.9 to -6.3 kcal/mol) of **AQ I-IV** were significant.

The kinetics of a homologous series of anthraquinone threading intercalators, **AQT I-IV** with calf thymus DNA was studied using the stopped-flow. The threading mechanisms of the anthraquinones binding to DNA showed sensitivity to their side chain length. Fitting of the kinetic data led to our proposal of a two step mechanism for binding of **AQT I**, bearing the shortest side chain, and a three step mechanism for binding of the three longer homologs. Binding involves formation of an externally bound anthraquinone-DNA complex, followed by intercalation of the anthraquinone for **AQT I-IV**, then isomerization to another complex with similar thermodynamic stability for **AQT II-IV**.

INDEX WORDS: Anthraquinone amide, Polyethylene glycol, Homologous, DNA, Hairpin, AT-rich, GC-rich, ct-DNA, Intercalate, Enthalpy-entropy compensation, Surface plasmon resonance, Isothermal titration calorimetry, Circular dichroism, Nuclear magnetic resonance, Molecular dynamics simulation, Hydration, Kinetics

BIOPHYSICAL CHARACTERIZATION OF THE BINDNG OF HOMOLOGOUS ANTHRAQUINONE AMIDES TO DNA

by

SHIRLENE JACKSON BECKFORD

A Dissertation Submitted in Partial Fulfillment of the Requirements for the Degree of

Doctor of Philosophy

in the College of Arts and Sciences

Georgia State University

2012

BIOPHYSICAL CHARACTERIZATION OF THE BINDNG OF HOMOLOGOUS ANTHRAQUINONE AMIDES TO DNA

by

SHIRLENE JACKSON BECKFORD

Committee Chair: Dabney W. Dixon

Committee: David Wilson

Donald Hamelberg

Electronic Version Approved:

Office of Graduate Studies

College of Arts and Sciences

Georgia State University

August 2012

DEDICATION

To Garfield and Jewelle

You have given me strength and purpose to complete this project.

ACKNOWLEDGEMENTS

I would like to thank God, who has given me this opportunity and the strength to complete this project.

Thanks to my advisor, Dr. Dabney Dixon, for the guidance, patience, and motivation that she was able to provide. She has been a constant source of intellectual stimulation throughout the years and a reminder of the importance of interpersonal relationships.

To Neval, Yu, Joy, and Elizabeth, it goes without saying, that the dynamic in our lab is one of friendship and trust. Thanks for the constant support and humor that you have provided, in helping me find my way though graduate school.

I would also like to thank my family, Mom, Dad, my brothers and sisters for the joy, perspective, and support they bring. I know you are truly happy about the completion of my doctoral studies.

Special thanks to my committee advisors, Dr. Wilson and Dr. Hamelberg. Thanks for your time and helpful discussions in helping me to complete my studies. I also want to say thanks to Dr. Gadda who was very instrumental in collecting and interpreting the kinetic data.

TABLE OF CONTENTS

LIST OF TABLES

LIST OF FIGURES

1 OVERVIEW OF SMALL MOLECULES BINDING TO DNA

1.1 DNA as a Target for Drug Design

The discovery and development of new therapeutics has been a topic of interest for several decades. Technology and innovation have brought about the advent of new high throughput screening methods [1-3] and the application of both rational [4-6], and structure based drug design [7-9] in searching for potentially interesting therapeutic agents and to the understanding of metabolic processes. One major aspect of drug discovery in both academia and industry has been the specific molecular recognition of gene sequences by ligands [10-14].

The design of small molecules that selectively target DNA has led to the development of many anticancer, antibiotic, antiprotozoal and antiviral drugs [12, 15-21]. These drugs are generally thought to exert their biological activities through binding with target DNA sequences and subsequently interference with DNA replication and transcription, and inhibition of gene expression. The development of new molecules that can target specific DNA sequences with high binding affinities requires elucidation of their molecular recognition patterns, and the driving forces that gives rise to their binding affinities as well as their binding mechanisms.

1.2 Binding of Small Molecules to DNA

Small molecules that bind to DNA have proven that they can be effective therapeutic agents [18, 22-23]; however, one of the most challenging goals in this area is the design of molecules which bind to DNA with high selectivity and large association constants. There are four general factors that are generally considered when designing small molecules that target DNA [16, 24-29]; first, the structural properties of the molecule which include its stereoelectronic properties and attached functional groups that promote different types of bonding. Structure activity relation-

ships studies are generally used for optimization. A second important consideration is how the spatial characteristics of the molecule (configuration and conformation) affect its interactions with DNA. Third, the physiochemical properties of the molecules need to be considered. These include their solubility, ionization, partition coefficients and phase behaviors which in part dictate the binding interaction of the molecule, as well as the transport and activity of the drug in the body. Fourth, the dose and effective drug concentration are important in drug-DNA interactions since they are important in qualifying a drug as both potent and effective. Work on the interactions of small molecules with DNA continues to advance with developments in molecular biology, chemical synthesis, biophysical methods, computational capabilities, and analytical instrumentation.

1.3 Mode of Binding of Small Molecules to DNA

Small molecules generally bind to DNA covalently or non-covalently by through π-stacking, hydrogen bond, electrostatic and hydrophobic interactions. These non-covalent binders associate by major or minor groove binding as well as intercalation and outside binding.

1.3.1 *Minor Groove Binding*

Groove binding occurs when a molecule fits into the DNA groove and interacts with the base pairs on the floor and walls of the DNA. The functional groups of the DNA bases are accessible in the grooves and thus, binding of a molecule is significantly more selective than intercalation because it makes direct contact with more base pairs and their functional groups [30]. Both the major and minor groove exhibit different electrostatic potential, hydrogen bonding characteristics, steric effects, micro-environmental polarity, and hydration [30]. These characteristics vary depending on the DNA sequence. The DNA structure and conformation are also dependent on the sequence. The major groove is wide and accessible and usually accommodates

proteins. In contrast, the minor groove is much smaller and binds mostly small molecules and displays specific contacts with the narrower groove. Typical minor groove binders include the polyamides, the bis-benzimidazoles such as Hoechst 33258, the diarylamidines (DAPI, berenil, and pentamidine), distamycin A, and netropsin, (Figure 1).

In general, minor groove binders contain unfused aromatic rings and are linked by bonds that allow rotation of the molecule to fit the curvature of the DNA groove [31]. Their flexibility allows the molecule to twist appropriately to complement the shape to the DNA groove, while promoting favorable placement of its functional groups, through the formation of H-bonds, electrostatic interactions and van der Waals contacts in the groove. Minor groove binders usually favor AT-rich sequences because the amino group of guanine and the carbonyl oxygen of cytosine in GC-rich sequences sterically inhibit the ligand's interaction with these bases [32]. In addition, the DNA minor groove is narrower in AT-rich sequences compared to GC-rich sequences, thus, allowing the small molecule to make better van der Waals contacts with the walls of the groove. The electrostatic potential of the AT-rich minor groove is more negative than that in the GC-rich minor groove [33]. Because most minor groove binders are positively charged, this also promotes binding at AT-rich sites. Small molecules typically bind to the DNA minor groove with binding affinities in the order of ~10^5 – 10^9 M, and usually cause little disturbance of the DNA structure [31].

Interaction of groove binders with DNA has shown a wide range of biological activity including antitumor, antiviral, antifungal and antimicrobial effects [34]. Diarylamidines are effective in the treatment of trypanosomiasis and leishmaniasis [16, 35]. Some examples include DAPI, berenil, stilbamidine, and pentamidine. DAPI targets AT-rich regions of duplex DNA, binding to the minor groove with its phenyl and indole rings parallel to the groove walls covering the

three-base pair sequence ATT [18]. However, DAPI has numerous undesirable side effects, so its use in the clinic as an anti-microbial has been limited [18]. Berenil also binds with high affinity to ATT-DNA sequences [18]. It is widely used in veterinary medicine for the treatment of trypanosomaisis[36]. Pentamidine also preferentially target AT-rich sequences in the DNA minor groove [18]. It is active against a variety of protozoa including *Pneumocystis carinii*; however, it displays side effects such as nephrotoxicity, cardiotoxicity, and hepatotoxiticy [37-39]. Pentamidine is also known to inhibit oncogenic PRL phosphatases [40]. These proteins play an important role in many cancers and, as such, can be therapeutic targets for diseases such as pancreatic cancer [40-42]. Most antitumor drugs bind non-specifically to DNA, causing damage to normal cells. However, minor groove binders usually targets AT-rich regions of DNA with high specificity.

Distamycin A is another minor groove binding agent that displays significant biological activities. The drug is a naturally occurring tripyrrole peptide, isolated from the cultures of Streptomyces distallicus [43]. It has been subsequently synthesized both in solution and on solid phase [44]. This antibiotic has antibacterial and antiviral activities; however, it is inactive as an antitumor agent [45]. The most important antiviral effects are directed against DNA-containing viruses (herpes simplex, herpes zoster, and vaccine virus); it is not active against RNA virus. Distamycin A has also been shown to possess antiprotozoal activity against *Plasmodium falcipa-rum* [46]. Distamycin selectively binds to the minor groove of A/T-containing DNA; each NH group in the amide unit participates in hydrogen bonding with a thymine O2 and/or an adenine N3 [47]. Modifications have since been made to the methylpyrrole groups which bind to DNA as a stacked dimer and alters the sequence recognition pattern from an AT to GC base-pair [48].

1.3.2 *Classical Intercalators*

Leonard Lerman was the first to propose the intercalation model for a ligand binding to DNA in the early 1960s [49]. Intercalators possess a common structural feature which is an extended, electron-deficient planar aromatic ring structure. The almost coplanar arrangement of the DNA bases allows intercalation of the planar aromatic ring of the intercalator in between the bases. Although intercalation occurs without interfering with the hydrogen bonding of the base pairs, this binding mode requires extensive conformational change of the DNA double helix [50]. The DNA has to unwind so that the intercalator fits between the two base pairs. This unwinding leads to a lengthening of the helix by approximately 3.4 Å, which subsequently causes significant conformational changes of some involved sugar moieties [31]. It has also been shown that during unwinding, the sugar group may be changed from C2'-endo to C3'-endo. Unwinding and lengthening of the DNA increases the phosphate spacing and therefore causes a decrease in the charge density along the DNA backbone. The decrease in charge density leads to a release of condensed counterions from the grooves and provides an energetically favorable contribution to the free energy of binding. Intercalators also establish favorable electrostatic, dipole-dipole, van der Waals, and π-stacking interactions with the DNA. The favorable contributions usually result in association constants of 10^4 to 10^6 M^{-1} [31].

Most intercalators have a variety of chemical substituents, including sugar rings or peptide groups. These substituents have a major role in the DNA sequence specificity, thermodynamic stability and structural orientation of the intercalator. Substituents usually occupy the DNA grooves and form favorable non-covalent contacts such as electrostatic interactions, van der Waals interactions, hydrophobic interactions and hydrogen-bonding interactions. For more complex intercalators, the functional group substituents can give rise to direct sequence readout

and hence sequence selectivity [51-52]. Typical examples of intercalators include ethidium , daunomycin, proflavin, acridines, *m*-AMSA, and actinomycin (Figure 2).

The main interest in intercalating drugs lies in their antitumor properties, several intercalating molecules have shown anticancer properties. The mechanism by which these molecules act is not fully understood, however, it is generally accepted that these drugs act as cellular topoisomerase I and II inhibitors [53]. Intercalators currently in clinical use for antitumor treatment include the anthracycline antibiotics adriamycin and daunomycin, mitoxantrone, ametantrone, and amsacrine [54-59].

The anthraquinone related intercalator, daunomycin, is probably the best studied intercalating drug with over 20 high resolution structures known. Daunomycin binds to DNA with its long axis almost perpendicular to the long axis of the adjacent base pairs [60]. The amino sugar group, attached to ring A, resides in the minor groove and is stabilized by van der Waals interactions and hydrogen bonds. The hydroxyl group on ring A acts as a hydrogen donor and acceptor which gives rise to a favorable enthalpy of intercalation as well as the specificity and orientation of binding. The minor groove of the DNA is filled with the amino sugar, as well as ring A which causes bound water molecules and ions to be expelled. This gives rise to a favorable binding entropy. Ring D of daunomycin occupies the major groove.

1.4 The Anthraquinone Drug Class

Anthraquinones form the basis of several anticancer drugs including daunomycin, doxorubicin, mitoxantrone and ametantrone [54-59]. They exert their cytotoxic activities through several modes [57]. First, they interact with DNA, preferentially at 5'-pyrimidine-purine- 3' GC-rich sites. This causes significant conformational changes in the DNA leading to inhibited synthesis of the DNA. Second, anthraquinone intercalation may produce damaging free radicals or radical-ion

intermediates as a consequence of its redox properties. This may lead to DNA damage or lipid peroxidation. Third, they can cause inhibition of topoisomerase II activity, leading to DNA damage or induction of apoptosis. Fourth, certain derivatives can cause DNA cross-linking or alkylation. Fifth, examples of interference with DNA unwinding or DNA strand separation and helicase activity are known. Finally, direct membrane effects have been shown in some instances.

Numerous high-resolution crystal structures of anthraquinones binding to duplex DNA are in the Nucleic Acids Structure Database [61-69]. The classical feature of anthraquinone-DNA interactions is exhibited by adriamycin and daunomycin [62]. Adriamycin, which has been used in the clinic for more than 30 years and is still a widely used cancer chemotherapeutic, intercalates into DNA with rings B and C between the adjacent base pairs of DNA. The drug intercalates at a pyrimidine-purine step with a preference for the CG sequence, with its sugar moiety interacting with the minor groove of DNA [62]. Daunomycin, which differs from adriamycin by only a hydroxyl group displays a similar binding mode [62]. However, the molecules have significant differences in their binding interactions, including sequence specificities and solvent interactions.

The DNA binding properties and biological activities of anthraquinone intercalators are significantly affected by the different substituents of the planar ring system [22, 70-83]. These changes mostly involve structural alterations such as the number and position of substituents [70-71, 76, 79], the number of charges [71], and variation in the type of substituents [72-73, 79, 82]. These properties have been shown to significantly affect their binding modes and affinity to DNA, as well as their biological activities [70-71, 76-83], which are discussed below.

In early work, Tanious et al. found that anthraquinone derivatives with substituents in the 1,4 and 1,8 positions intercalated classically in DNA, while 1,5 derivatives were threading intercalators, with one side chain in each groove [70]. This was in line with previous molecular

modeling work of Neidle and colleagues [76]. Spectrophotometric titration showed that the binding affinities of substituted amido-anthraquinones with duplex DNA was in the order 1,5-bis > 1,4-bis > 1,8-bis > monosubstituted anthraquinones [84]. The 1,5-isomer bearing alkyl-amino side chains had an affinity for duplex DNA of $3.97 \times 10^6 M^{-1}$, two and a half times that of the analogous monosubstituted anthraquinone.

2,6-Amidoanthraquinones bearing substituents such as morpholino-, diethylamino-, and piperidino- groups were shown to increase the melting temperature of duplex DNA in proportion to the amount of ligand added [79]. Diethylamino and piperidino analogs showed a higher T_m than the morpholino analog, which was assumed to arise from the reduced basicity of the side chain. Diethyl hydroxyamines showed lower melting temperatures and computed higher binding enthalpies than the piperidine analogues indicating a lower binding constant with the DNA plasmid used. Molecular modeling studies suggested this might be due to the inability of the diethyl hydroxy amino groups to follow the helical coil of the DNA grooves, resulting in decreased interaction.

Breslin et al. have described the binding of mono-, di-, and tetracationic anthraquinones to DNA[81]. They have shown that both monocationic and dicationic anthraquinones bind to DNA via an intercalative mode, using NMR and UV/VIS studies. However, the tetracationic anthraquinone investigated binds primarily to the minor groove of duplex DNA. Docking studies have shown that in this mode, the positively charged ammonium groups can be placed within van der Waals contact of the negatively charged phosphate group. As such, significant electrostatic contacts are made, stabilizing the AQ-DNA groove bound complex.

Our group has previously demonstrated that binding affinity depends on side chain length of a homologous series of anthraquinone threading intercalators, using surface plasmon reso-

nance [82]. Binding constants of anthraquinone bearing 1-4 ethylene glycol units in their side chain were investigated with AT and GC rich sequences. The binding constant for the 2,6-anthraquinone with one ethylene glycol unit and AT rich DNA was 7.6 x 10^5 M^{-1}, four times that of the largest member of the homologous series. These results were consistent with melting temperature studies with the first member of the homologous series melting at ~ 7 ^oC higher than the last member. The effect of the side chain may be the result of a loss of rotational degrees of freedom of the rotatable bonds in the side chain when bound to DNA. The free energy of the anthraquinone system is thereby reduced as the side chain increases in length resulting in a higher energetic cost. Agbandje et al. have also noted a decrease in binding affinity with increases in the number of methylene units in the anthraquinone side chain, as determined by molecular modeling [79]. This decrease in binding affinity was attributed to a decrease in stacking interactions at the intercalation sites for the monosubstituted anthraquinones. They postulated that the short chain reduces the rotational degrees of freedom of the side arm which could otherwise be maneuvered to eliminate unfavorable steric hindrances.

The binding of a series of anthraquinone amides with one or two peptide chains at positions 1 and/or 4 to DNA have also been investigated [71]. These peptidyl anthraquinones maintained their ability to intercalate, but somewhat changed their orientation within the base pair pocket compared to the parent compounds. 1,4-Anthraquinones with glycine substituent(s) in their side chain showed similar DNA binding affinity to that of other 1,4-disubstituted anthraquinones studied previously, e.g., ametantrone (3.4 x 10^5 M^{-1}) . Replacing a glycine with a L-lysine in the anthraquinone side chain increased the binding affinity to 18.5 x 10^5 M^{-1} while the D-isomer was even more effective with a binding constant of 33.0 x 10^5 M^{-1}. The D-isomer had two times the affinity of the L-isomer to DNA duplex and about fourteen times that of di-glycine

substituent. The increased basicity of the side chain due to the presence of the lysine results in favorable interaction with the phosphodiester backbone. A higher binding constant was thus observed.

Construction of an anthraquinone-cisplatin complex has been synthesized to investigate the cooperative binding effect of cisplatin and anthraquinone with dsDNA [72-73]. The anthraquinones studied were linked to the cisplatin complex at various positions as either a monodentate ligand or a bidentate ligand. The monodentate anthraquinone complex showed similar activity (ED_{50} of 45 μM) to the free ligand against P388 leukemic cells. The bidentate ligands (3-C and 6-C alkyl chain between the anthraquinone and platinum complex) substituted in position 2 of the anthraquinone showed activity 10-fold less than the free ligand. The bidentate ligands substituted at position 1 of the anthraquinone exhibited higher activity than the free ligand. Complexes with a 3-C alkyl spacer showed an almost 100-fold greater activity compared to its analog which is substituted in position 2. Both bidentate complexes with 6-C alkyl linker were not very active. In general, cisplatin-anthraquinone complexes substituted at position 1 had a higher binding constant ($10^6\ M^{-1}$) than complexes substituted at position 2 ($10^4\ M^{-1}$).

The affinities of anthraquinone, cyclam-anthraquinone and, copper-cyclam-anthraquinone for duplex DNA have been studied[74]. As indicated by UV spectrophotometric titrations, addition of a macrocycle increased the binding of anthraquinone to DNA, K_a of 4.7 x $10^3\ M^{-1}$ and addition of copper to this complex further increased its affinity K_a of 6.2 x $10^3\ M^{-1}$. The binding constant for the Cu complex was ~3 times greater than that of the Zn complex which had a binding constant of 2.8 x $10^4\ M^{-1}$.

Zinc complexes of anthraquinone have also been investigated due to their ability to act as a Lewis acid and hence perhaps play a role in the hydrolytic cleavage of DNA[75]. The com-

pounds showed highest activity when the alkyl spacer between the zinc unit and the anthraquinone unit was largest, that is C_8. Up to a 15-fold increase in cleavage for the conjugated metal complexes was observed when compared to the metal-triaminocyclohexane complex alone. These results were confirmed by molecular mechanics calculations where it was seen that after intercalation of the anthraquinone, the alkyl side chain folds in a manner to position the zinc complex close to the phosphate backbone and promote cleavage. Alkyl chains that are shorter resulted in less interaction of the metal with the phosphate group.

Ihmels and Otto have given an overview of anthraquinone modifications including those substituted with amine-containing side groups, those with DNA cross-linking potential, those that generate free radicals upon intercalation, and those in combination with transition metal complexes [31].

1.4.1 *Kinetic Studies on Threading Anthraquinones*

Threading intercalators represent a class of high affinity DNA binding agents that interact by inserting the chromophore between the DNA bases and locating one substituent into each groove [22, 85-90]. One substituent of the intercalator binds in the major groove and the other substituent interacts with the minor groove. Several representative threading intercalators can be seen in Figure 3; these include the 2,7-disubstituted anthraquinones, 9,10-disubstituted anthracenes, and the napthalene bis(carboximide).

Perhaps the first threading intercalator to be studied kinetically was nogalamycin, with an anthraquinone core flanked by two bulky sugar moieties [91-93]. The two bulky sugar substituents on opposite sides of nogalamycin requires that one of the sugar groups thread through the stacked nucleobases of the double helix to bind via threading intercalation [94]. Crystal structure of nogalamycin bound to the 5' cytosine methylated duplex, $d(CGTACG)_2$, shows the neutral

nogalose sugar and the methyl ester residing in the minor groove and the positively charged bi-cyclic amino sugar residing in the major groove stabilized by hydrogen bonds to the CG base pair [94]. The reaction kinetics of nogalamycin with ct-DNA is complex, requiring at least three exponentials to fit [93]. Threading of nogalamycin is thought to involve an initial threading intercalated state followed by reorganization, and shuffling to a more favored thermodynamic binding site. Nogalamycin has a slow rate of dissociation from DNA(k_d = ~ 10^{-3} s^{-1}) [91].

Daunomycin is also an anthraquinone-based structure. Although it is best viewed as a classical intercalator, the kinetics of intercalation have similarities to those of nogalamycin. It has dissociation rates >1.0 s^{-1} [95]. Detailed kinetic analysis showed three relaxation processes [95]. The kinetic data was interpreted as a model which involved a rapid bimolecular association step followed by two sequential isomerization steps. This is believed to correspond to a rapid "outside" binding of daunomycin to DNA, followed by intercalation of the drug, then either conformational adjustment of the drug or DNA binding site or redistribution of bound drug to preferred sites.

The kinetics of smaller, less complex, anthraquinone structures have also been evaluated. Tanious et al. have studied the kinetics of 1,4-, 1,8-, 1,5-, and 2,6-anthraquinone derivatives substituted with amino alkyl side chains [70]. Association and dissociation rates for the threading mode were shown to be approximately 10 times lower than the classical modes. The kinetic data required two exponentials to fit with rate constants for both phases ≤ 6. The two closely related intercalated complexes were believed to perhaps represent binding to two classes of binding site or from either groove of the DNA. One of the goals of the current study is to extend our understanding of the threading intercalation mechanism.

1.4.2 *Energetics of Anthraquinone Binding to DNA*

The free energy, ΔG, of intercalation may be obtained from the experimentally determined binding constants. Parsing the free energy of binding of a ligand to DNA is of interest in several groups [96-102]. Chaires have parsed the binding free energy of an anthraquinone-related intercalator into five additive terms [103] which are described below.

$$\Delta G_{obs} = \Delta G_{conf} + \Delta G_{hyd} + \Delta G_{t+r} + \Delta G_{pe} + \Delta G_{mol} \qquad \text{Equation 1.1}$$

where ΔG_{conf} is free energy contribution from conformational changes in the ligand and DNA, ΔG_{hyd} is the free energy of hydrophobic transfer of a molecule from solution to its binding site, ΔG_{t+r} is the free energy loss from translational and rotational motion upon complex formation, ΔG_{pe} is the polyelectrolyte contribution to the binding free energy, and ΔG_{mol} is the free energy arising from molecular interactions with the ligand and DNA.

For formation of the intercalation complex, the DNA undergoes significant conformational changes. The helix has to unwind and lengthen to separate adjacent base-pair to create an intercalation site. These structural changes in the DNA are energetically unfavorable and represent an endergonic contribution to ΔG_{obs}. Several attempts to estimate the magnitude of this contribution have been made [50]; however, ΔG_{conf} is generally accepted to be ~4 kcal mol^{-1}, as determined by detailed kinetic studies by Macgregor et al [104]. The kinetic mechanism for the binding of ethidium to DNA was determined, and showed an obligatory DNA conformational transition, interpreted as opening of the helix prior to ethidium intercalation. The corresponding equilibrium constant yielded a free energy cost of ~ 4 kcal mol^{-1}. Benight et al. have shown that the unstacking free energy of DNA is sequence dependent and therefore, postulated that the sequence selectivities of particular intercalators may be governed by conformational changes in the DNA [105]. In contrast, there has been little evidence to suggest that the intercalator undergoes signifi-

cant conformational change. As such, formation of the intercalation site is the primary contributor to ΔG_{conf} [50].

The largest favorable free energy contribution comes from the hydrophobic effect, ΔG_{hyd} [50]. Intercalators have aromatic ring systems that are intrinsically hydrophobic in nature; transfer of these rings from a hydrophilic solution to the hydrophobic binding site of the DNA is energetically favorable. Estimates from hydrophobic transfer energies may be obtained from changes in the heat capacity upon intercalation, [$\Delta G_{hyd} \sim 80\ (\pm 10) \times \Delta Cp$] [106]. ΔG_{hyd} can also be estimated from the change in the solvent accessible surface area (SASA) upon complex formation, $\Delta G_{hyd} \sim -22(\pm 5) \times \Delta$SASA [106-108]. The hydrophobic contribution to the overall binding free energy of daunomycin to DNA was estimated to be $\Delta G_{hyd} \sim -13$ kcalmol^{-1} [50].

ΔG_{t+r} is the free energy cost resulting from losses in translational and rotational degrees of freedom upon complex formation. When a bimolecular complex is formed, three rotational and three translational degrees of freedom for each reactant are replaced by a single set for the complex. This results in a significant loss of entropy, corresponding to an unfavorable free energy contribution; however, some of this energetic loss is compensated for by six internal vibrational modes [109]. The magnitude of the loss of translational and rotational entropy is still under debate, because of the difficulty of obtaining experimental data along these lines. Spolar and Record have empirically derived a value for the free energy of translational and rotational freedom, from the consideration of the thermodynamics of specific cases that appeared to represent rigid body association [110]. An average value of 14.9 (±3.0) kcal mol^{-1} was obtained for ΔG_{r+t}.

The polyelectrolyte contribution to the binding free energy, ΔG_{pe}, arises from the release of condensed counterions from DNA upon complex formation. The free energy of polyelectrolyte contribution is given by the equation

$$\Delta G_{pe} = Z\varphi RT(m\psi) \ln [M^+] \quad \text{Equation 1.2}$$

where Z is the charge on the ligand, φ is the fraction of monovalent cation associated per DNA phosphate, and M^+ is the monovalent salt concentration. Zφ can be derived from the equation derived by Record and coworkers [111]:

$$-Z\varphi = (\delta \ln K/\delta \ln M^+) \quad \text{Equation 1.3}$$

in which K is the ligand binding constant. The magnitude of ΔG_{pe} depends on the charge of the ligand. The polyelectrolyte contribution, ΔG_{pe}, to the overall free energy, ΔG_{obs}, of daunomycin binding to DNA is approximately -1 kcalmol^{-1} [50]. The majority of this contribution is due to the release of condensed counter ions from the DNA upon binding. Uncharged intercalators also have a favorable polyelectrolyte contribution, since the lengthening of the DNA upon complex formation leads to a decrease of its charge density along the backbone and subsequently to a release of counter ions [112-113]. Overall, the polyelectrolyte contribution for an intercalator with a +1 charge will range from 0 to -4 kcalmol^{-1} [114].

The free energy of molecular interactions, ΔG_{mol}, in a complex is usually difficult to quantify [50]. It has contributions from noncovalent bonding interactions such as hydrogen bonding, π-stacking, and Lewis acid–base interactions. Few data for ΔG_{mol} of intercalation complexes are known. The most efficient approach to determine ΔG_{mol} is through structure-activity relationship by varying the substitution pattern of a known intercalator and then conducting detailed binding studies [50]. The results will give a structure-property correlation that allows the determination of ΔG_{mol}. One such example is that of daunomycin and doxorubicin, which differ by a single OH group at position 9. Removal of the 9-OH group from doxorubicin (to form daunomycin) resulted in a 1.1 kcal mol^{-1} loss in binding free energy, a magnitude that is consistent with estimates of the energy for formation of a single hydrogen bond [115]. This is con-

sistent with X-ray crystal structure which shows the 9-OH substituent of doxorubicin forms a hydrogen bond with the central guanine within the drug binding site [62].

1.5 Research Goals

The objective of this research project is to understand the effect of side chain length on the binding interactions and mechanism of anthraquinones intercalators with AT-rich, GC-rich, and CT- DNA.

To achieve this goal, three homologous series of anthraquinone intercalators, (classical and threading) were synthesized. An array of biophysical techniques, ultraviolet-visible (UV-VIS), circular dichroism (CD), biosensor-surface plasmon resonance (SPR), isothermal titration calorimetry (ITC), fluorescence, stopped-flow, and molecular dynamics (MD) simulations were utilized. The mode of binding, affinities, thermodynamics, kinetics, and molecular dynamics with various DNA sequences are discussed. This dissertation is divided into five chapters which are described below:

Chapter 1, the current chapter, gives a general introduction to targeting DNA with small molecules as an effective strategy for drug design.

Chapter 2 is divided into two sections: The first section is a direct copy of our work for publication: Jackson Beckford, S., Dixon, D.W. Synthesis and Biophysical Characterization of the Binding of a Homologous Series of Anthraquinone Intercalators with DNA, (*intended publication to Biochemistry*). This section presents the synthesis and characterization of the binding interactions of a homologous series of classical anthraquinone intercalators with DNA. The binding interactions with both AT- and GC-rich DNA were characterized using CD, SPR, and ITC. The SPR experiments were performed by Dr. Yang Liu, and analyzed by SJB. All other experiments were performed and analyzed by SJB.

The second section presents additional experimental data which will not be reported in the publication. These include additional NMR, CD, SPR and ITC data used in our analysis of the data presented in the first section.

Chapter 3 describes the synthesis and thermodynamic analysis of a homologous series of dicationic anthraquinone amides.

Chapter 4 is a direct copy of our published work: Jackson Beckford, S., Dixon, D.W. (2012) Molecular Dynamics of Anthraquinone DNA Intercalators with Polyethylene Glycol Side Chains. *JBSD* **29**(5): 1065-1080. This article describes a detailed molecular dynamic simulation of the homologous series of intercalators discussed in Chapter 2 with GC-rich DNA.

Chapter 5 discusses kinetic studies of both threading and classical intercalators.

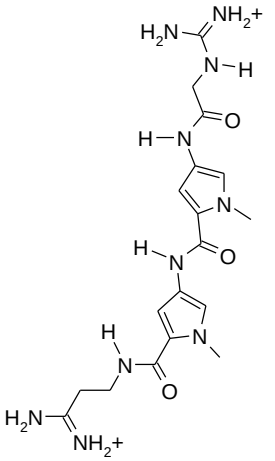

Netropsin

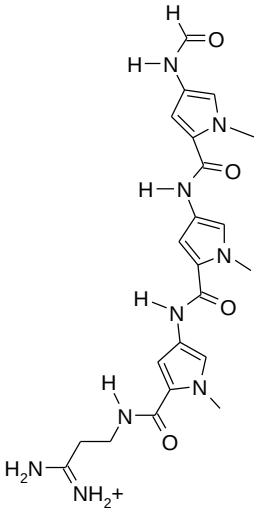

Distamycin A

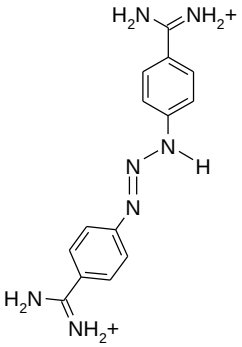

Berenil

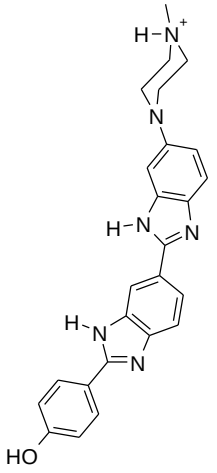

Hoechst 33258

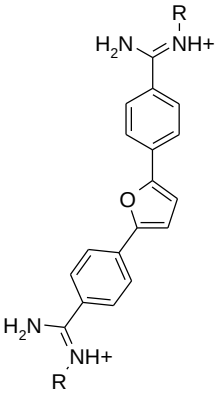

Diphenyfuran derivatives
R = H = DB75

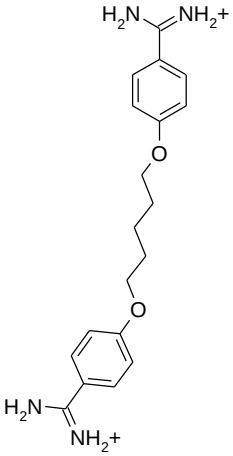

Pentamidine

Figure 1.1: Structures of minor groove binding ligands

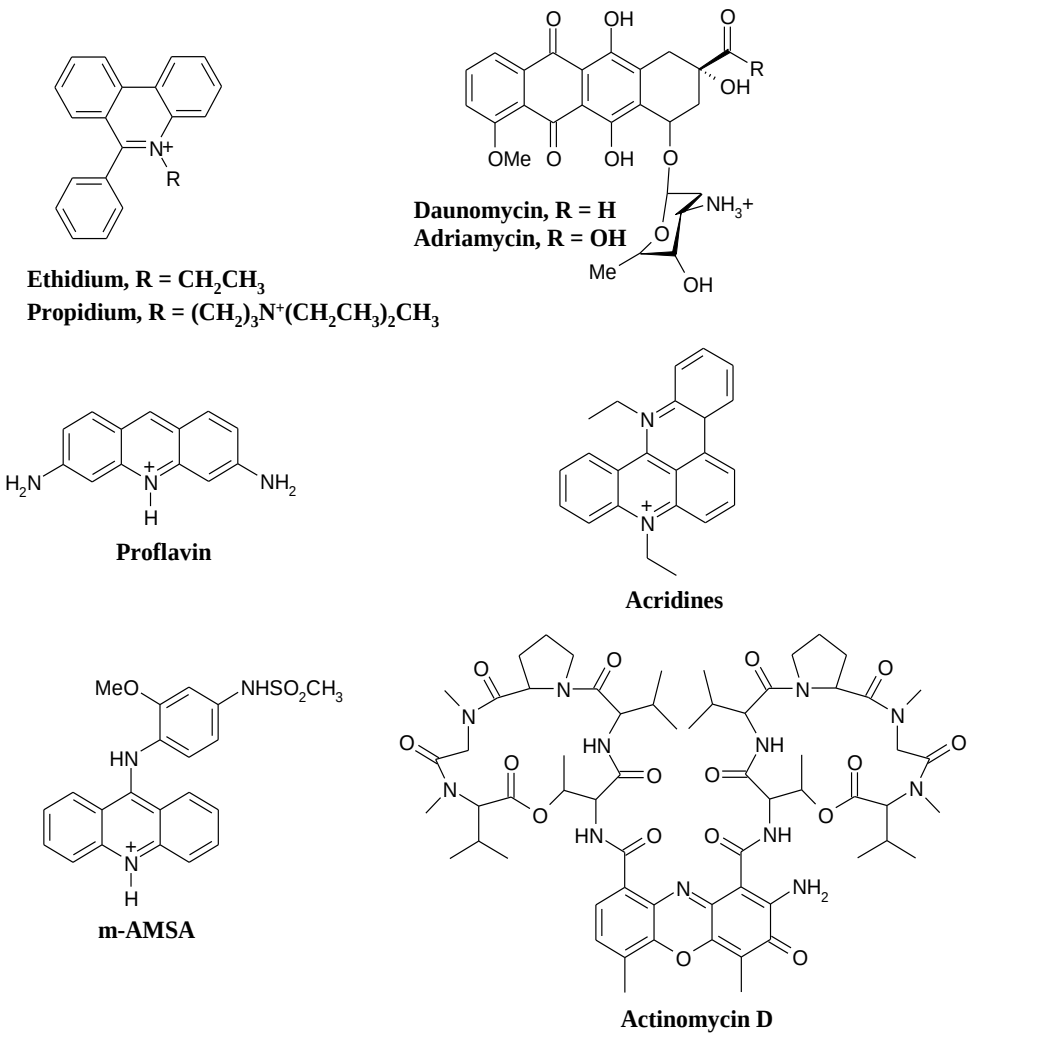

Figure 1.2: Structures of classical intercalating ligands

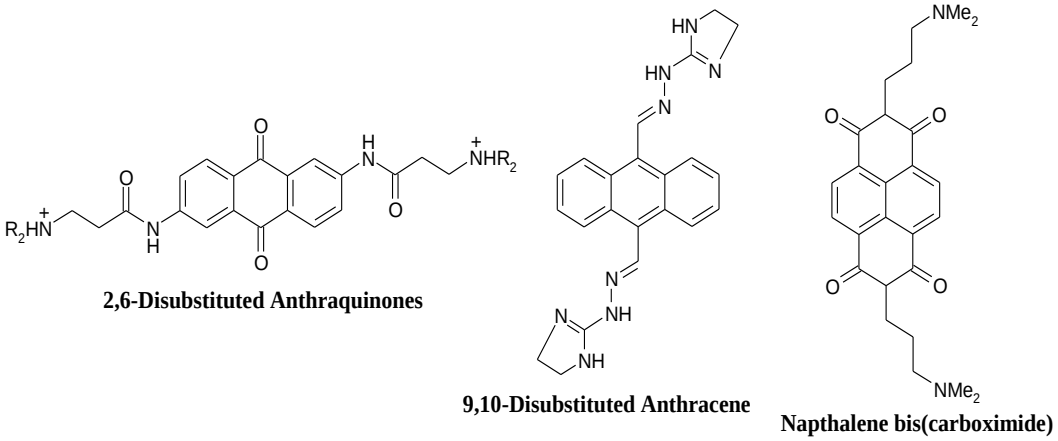

Figure 1.3: Structures of threading intercalating ligands.

1.6 References

1. Zhang, J. H., Chung, T. D. Y., and Oldenburg, K. R. (1999) A simple statistical parameter for use in evaluation and validation of high throughput screening assays, *J. Biomol. Screen. 4*, 67-73.
2. Rishi, V., Potter, T., Laudeman, J., Reinhart, R., Silvers, T., Selby, M., Stevenson, T., Krosky, P., Stephen, A. G., Acharya, A., Moll, J., Oh, W. J., Scudiero, D., Shoemaker, R. H., and Vinson, C. (2005) A high-throughput fluorescence-anisotropy screen that identifies small molecule inhibitors of the DNA binding of B-ZIP transcription factors, *Anal. Biochem. 340*, 259-271.
3. Hallikas, O., and Taipale, J. (2006) High-throughput assay for determining specificity and affinity of protein-DNA binding interactions, *Nat. Protoc. 1*, 215-222.
4. Huttunen, K. M., Raunio, H., and Rautio, J. (2011) Prodrugs-from serendipity to rational design, *Pharmacol. Rev. 63*, 750-771.
5. Mavromoustakos, T., Durdagi, S., Koukoulitsa, C., Simcic, M., Papadopoulos, M. G., Hodoscek, M., and Grdadolnik, S. G. (2011) Strategies in the rational drug design, *Curr. Med. Chem. 18*, 2517-2530.
6. Shim, J., and MacKerell, A. D., Jr. (2011) Computational ligand-based rational design: Role of conformational sampling and force fields in model development, *Medchemcomm 2*, 356-370.
7. Kalyaanamoorthy, S., and Chen, Y. P. (2011) Structure-based drug design to augment hit discovery, *Drug Discov. Today 16*, 831-839.
8. Ma, D., Chan, D. S., Lee, P., Kwan, M. H., and Leung, C. (2011) Molecular modeling of drug-DNA interactions: Virtual screening to structure-based design, *Biochimie 93*, 1252-1266.
9. Congreve, M., Langmead, C. J., Mason, J. S., and Marshall, F. H. (2011) Progress in structure based drug design for G protein-coupled receptors, *J. Med. Chem. 54*, 4283-4311.
10. Dervan, P. B., and Burli, R. W. (1999) Sequence-specific DNA recognition by polyamides, *Curr. Opin. Chem. Biol. 3*, 688-693.
11. Han, X. G., and Gao, X. L. (2001) Sequence specific recognition of ligand-DNA complexes studied by NMR, *Curr. Med. Chem. 8*, 551-581.
12. Dervan, P. B. (2001) Molecular recognition of DNA by small molecules, *Bioorg. Med. Chem. 9*, 2215-2235.
13. Marmorstein, R., and Fitzgerald, M. X. (2003) Modulation of DNA-binding domains for sequence-specific DNA recognition, *Gene 304*, 1-12.
14. Du, Y. H., Huang, J., Weng, X. C., and Zhou, X. (2010) Specific recognition of DNA by small molecules, *Curr. Med. Chem. 17*, 173-189.
15. Kreuzer, K. N. (1989) DNA topoisomerases as potential targets of antiviral action, *Pharmacol. Ther. 43*, 377-395.
16. Tidwell, R. R., and Boykin, D. W. (2004) Dicationic DNA minor groove binders as antimicrobial agents, In *Small Molecule DNA and RNA Binders* (Demeunynck, M., Bailly, C., and Wilson, W. D., Eds.), pp 414-460, Wiley-VCH Verlag GmbH & Co. KGaA, Weinheim.
17. Melander, C., Burnett, R., and Gottesfeld, J. M. (2004) Regulation of gene expression with pyrrole-imidazole polyamides, *J. Biotechnol. 112*, 195-220.

18. Baraldi, P. G., Bovero, A., Fruttarolo, F., Preti, D., Tabrizi, M. A., Pavani, M. G., and Romagnoli, R. (2004) DNA minor groove binders as potential antitumor and antimicrobial agents, *Med. Res. Rev. 24*, 475-528.
19. Neto, B. A. D., and Lapis, A. A. M. (2009) Recent developments in the chemistry of deoxyribonucleic acid (DNA) intercalators: Principles, design, synthesis, applications and trends, *Molecules 14*, 1725-1746.
20. Palchaudhuri, R., and Hergenrother, P. J. (2007) DNA as a target for anticancer compounds: methods to determine the mode of binding and the mechanism of action, *Curr. Opin. Biotechnol. 18*, 497-503.
21. Gurova, K. (2009) New hopes from old drugs: revisiting DNA-binding small molecules as anticancer agents, *Future Oncology 5*, 1685-1704.
22. Braña, M. F., Cacho, M., Gradillas, A., de Pascual-Teresa, B., and Ramos, A. (2001) Intercalators as anticancer drugs, *Curr. Pharm. Des. 7*, 1745-1780.
23. Martínez, R., and Chacón-García, L. (2005) The search of DNA-intercalators as antitumoral drugs: What it worked and what did not work, *Curr. Med. Chem. 12*, 127-151.
24. Bischoff, G., and Hoffmann, S. (2002) DNA-binding of drugs used in medicinal therapies, *Curr. Med. Chem. 9*, 321-348.
25. Neidle, S., and Editor (2008) *Cancer: Drug Design and Discovery*.
26. Cayen, M. N., and Editor (2010) *Early Drug Development: Strategies and Routes to First-in-Human Trials*.
27. Jampilek, J., and Editor (2011) *Prodrugs: Pharmaceutical Design And Current Perspectives.* .
28. Livingstone, D. J., Davis, A. M., and Editors (2012) *Drug Design Strategies: Quantitative Approaches.*
29. Kelley, M. R. (2012) *DNA Repair in Cancer Therapy: Molecular Targets and Clinical Applications*.
30. (2006) Reversible small molecule-nucleic acid interactions, In *Nucleic Acids in Chemistry and Biology* (Blackburn, M., Gait, M., Loakes, D., and Williams, D., Eds.) 3rd ed., pp 341-382, The Royal Society of Chemistry, Cambridge.
31. Ihmels, H., and Otto, D. (2005) Intercalation of organic dye molecules into double-stranded DNA general principles and recent developments, In *Supermolecular Dye Chemistry*, pp 161-204.
32. Bailly, C., and Chaires, J. B. (1998) Sequence-specific DNA minor groove binders. Design and synthesis of netropsin and distamycin analogues, *Bioconjug. Chem. 9*, 513-538.
33. Lavery, R., Zakrzewska, K., and Pullman, B. (1986) Binding of non-intercalating antibiotics to B-DNA: A theoretical study taking into account nucleic acid flexibility, *J. Biomol. Struct. Dyn. 3*, 1155-1170.
34. Geierstanger, B. H., and Wemmer, D. E. (1995) Complexes of the minor groove of DNA, *Annu. Rev. Biophys. Biomol. Struct. 24*, 463-493.
35. Bray, P. G., Barrett, M. P., Ward, S. A., and de Koning, H. P. (2003) Pentamidine uptake and resistance in pathogenic protozoa: past, present and future, *Trends Parasitol. 19*, 232-239.
36. Rogers, D. J. (1985) Trypanosomiasis 'risk' or 'challenge': a review, *Acta Trop. 42*, 5-23.

37. Coyle, P., Carr, A. D., Depczynski, B. B., and Chisholm, D. J. (1996) Diabetes mellitus associated with pentamidine use in HIV-infected patients, *Med. J. Aust. 165*, 587-588.
38. Kuryshev, Y. A., Ficker, E., Wang, L., Hawryluk, P., Dennis, A. T., Wible, B. A., Brown, A. M., Kang, J. S., Chen, X. L., Sawamura, K., Reynolds, W., and Rampe, D. (2005) Pentamidine-induced long QT syndrome and block of hERG trafficking, *J. Pharmacol. Exp. Ther. 312*, 316-323.
39. Milligan, K. S., and Phillips, D. L. (2007) Perioral numbness associated with intravenous pentamidine administration, *Ann. Pharmacother. 41*, 153-156.
40. Pathak, M. K., Dhawan, D., Lindner, D. J., Borden, E. C., Farver, C., and Yi, T. L. (2002) Pentamidine is an inhibitor of PRL phosphatases with anticancer activity, *Mol. Cancer Ther. 1*, 1255-1264.
41. Al-Aidaroos, A. Q. O., and Zeng, Q. (2010) PRL-3 Phosphatase and Cancer Metastasis, *J. Cell. Biochem. 111*, 1087-1098.
42. Dumaual, C. M., Sandusky, G. E., Soo, H. W., Werner, S. R., Crowell, P. L., and Randall, S. K. (2012) Tissue-specific alterations of PRL-1 and PRL-2 expression in cancer, *American journal of translational research 4*, 83-101.
43. Arcamone, F., Penco, S., Orezzi, P., Nicolella, V., and Pirelli, A. (1964) Structure and synthesis of distamycin A, *Nature 203*, 1064-1065.
44. Boger, D. L., Fink, B. E., and Hedrick, M. P. (2000) Total synthesis of distamycin A and 2640 analogues: A solution-phase combinatorial approach to the discovery of new, bioactive DNA binding agents and development of a rapid, high-throughput screen for determining relative DNA binding affinity or DNA binding sequence selectivity, *J. Am. Chem. Soc. 122*, 6382-6394.
45. Cai, X., Gray, P. J., Jr., and Von Hoff, D. D. (2009) DNA minor groove binders: Back in the groove, *Cancer Treat. Rev. 35*, 437-450.
46. Ginsburg, H., Nissani, E., Krugliak, M., and Williamson, D. H. (1993) Selective tozicity to malaria parasites by non-intercalating DNA binding ligands, *Mol. Biochem. Parasitol. 58*, 7-15.
47. Kopka, M. L., Yoon, C., Goodsell, D., Pjura, P., and Dickerson, R. E. (1985) The molecular origin of DNA-drug specificity in netropsin and distamycin, *Proc. Natl. Acad. Sci. U. S. A. 82*, 1376-1380.
48. Dervan, P. B., and Edelson, B. S. (2003) Recognition of the DNA minor groove by pyrrole-imidazole polyamides, *Curr. Opin. Struct. Biol. 13*, 284-299.
49. Lerman, L. S. (1961) Structural considerations in the interaction of DNA and acridines, *J. Mol. Biol. 3*, 18-30.
50. Chaires, J. B. (1997) Energetics of drug-DNA interactions, *Biopolymers 44*, 201-215.
51. Chaires, J. B. (2005) Structural selectivity of drug-nucleic acid interactions probed by competition dialysis, In *DNA Binders and Related Subjects* (Waring, M. J. C. J. B., Ed.), pp 33-53.
52. Holman, G. G., Zewail-Foote, M., Smith, A. R., Johnson, K. A., and Iverson, B. L. (2011) A sequence-specific threading tetra-intercalator with an extremely slow dissociation rate constant, *Nat. Chem. 3*, 875-881.
53. Pommier, Y., Pourquier, P., Fan, Y., and Strumberg, D. (1998) Mechanism of action of eukaryotic DNA topoisomerase I and drugs targeted to the enzyme, *Biochim. Biophys. Acta, Gene Struct. Expression 1400*, 83-106.

54. Lown, J. W. (1993) Anthracycline and anthraquinone anticancer agents: Current status and recent developments, *Pharmacol. Ther. 60*, 185-214.
55. Arcamone, F., Animati, F., Capranico, G., Lombardi, P., Pratesi, G., Manzini, S., Supino, R., and Zunino, F. (1997) New developments in antitumor anthracyclines, *Pharmacol. Ther. 76*, 117-124.
56. Monneret, C. (2001) Recent developments in the field of antitumour anthracyclines, *Eur. J. Med. Chem. 36*, 483-493.
57. Minotti, G., Menna, P., Salvatorelli, E., Cairo, G., and Gianni, L. (2004) Anthracyclines: Molecular advances and pharmacologic developments in antitumor activity and cardiotoxicity, *Pharmacol. Rev. 56*, 185-229.
58. Asche, C. (2005) Antitumour quinones, *Mini-Rev. Med. Chem. 5*, 449-467.
59. Kratz, F., Warnecke, A., Schmid, B., Chung, D. E., and Gitzel, M. (2006) Prodrugs of anthracyclines in cancer chemotherapy, *Curr. Med. Chem. 13*, 477-523.
60. Moore, M. H., Hunter, W. N., d'Estaintot, B. L., and Kennard, O. (1989) DNA-drug interactions. The crystal structure of d(CGATCG) complexed with daunomycin, *J. Mol. Biol. 206*, 693-705.
61. Wang, A. H., Ughetto, G., Quigley, G. J., and Rich, A. (1987) Interactions between an anthracycline antibiotic and DNA: Molecular structure of daunomycin complexed to d(CpGpTpApCpG) at 1.2 Å resolution, *Biochemistry 26*, 1152-1163.
62. Frederick, C. A., Williams, L. D., Ughetto, G., Van der Marel, G. A., Van Boom, J. H., Rich, A., and Wang, A. H. J. (1990) Structural comparison of anticancer drug-DNA complexes: adriamycin and daunomycin, *Biochemistry 29*, 2538-2549.
63. Berman, H. M., Olson, W. K., Beveridge, D. L., Westbrook, J., Gelbin, A., Demeny, T., Hsieh, S. H., Srinivasan, A. R., and Schneider, B. (1992) Tne nucleic acid database - A comprehensive relational database of 3-dimensional structures of nucleic acids, *Biophys. J. 63*, 751-759.
64. Wang, A. H. J. (1996) X-ray crystallographic and NMR structural studies of anthracycline anticancer drugs: Implication in drug design, In *Advances in DNA Sequence-Specific Agents* (Laurence, H. H., and Jonathan, B. C., Eds.), pp 59-100, Elsevier.
65. Robinson, H., Priebe, W., Chaires, J. B., and Wang, A. H. J. (1997) Binding of two novel bisdaunorubicins to DNA studied by NMR spectroscopy, *Biochemistry 36*, 8663-8670.
66. Searle, M. S., Maynard, A. J., and Williams, H. E. L. (2003) DNA recognition by the anthracycline antibiotic respinomycin D: NMR structure of the intercalation complex with d(AGACGTCT)(2), *Org. Biomol. Chem. 1*, 60-66.
67. Shi, K., Pan, B. C., and Sundaralingam, M. (2003) Structure of a B-form DNA/RNA chimera (dC)(rG)d(ATCG) complexed with daunomycin at 1.5 angstrom resolution, *Acta Crystallographica Section D-Biological Crystallography 59*, 1377-1383.
68. Temperini, C., Cirilli, M., Aschi, M., and Ughetto, G. (2005) Role of the amino sugar in the DNA binding of disaccharide anthracyclines: crystal structure of the complex MAR70/d(CGATCG), *Bioorg. Med. Chem. 13*, 1673-1679.
69. De Luchi, D., Uson, I., Wright, G., Gouyette, C., and Subirana, J. A. (2010) Structure of a stacked anthraquinone-DNA complex, *Acta Crystallographica, Section F: Structural Biology and Crystallization Communications F66*, 1019-1022.

70. Tanious, F. A., Jenkins, T. C., Neidle, S., and Wilson, W. D. (1992) Substituent position dictates the intercalative DNA-binding mode for anthracene-9,10-dione antitumor drugs, *Biochemistry 31*, 11632-11640.
71. Gatto, B., Zagotto, G., Sissi, C., Cera, C., Uriarte, E., Palu, G., Capranico, G., and Palumbo, M. (1996) Peptidyl anthraquinones as potential antineoplastic drugs: Synthesis, DNA binding, redox cycling, and biological activity, *J. Med. Chem. 39*, 3114-3122.
72. Gibson, D., Mansur, N., and Gean, K. F. (1995) Preparation, characterization, and antitumor properties of cis-$PtCl_2$ complexes linked to anthraquinones through position number 2., *J. Inorg. Biochem. 58*, 79-88.
73. Gibson, D., Gean, K. F., Ben-Shoshan, R., Ramu, A., Ringel, I., and Katzhendler, J. (1991) Preparation, characterization, and anticancer activity of a series of cis-$PtCl_2$ platinum dichloride complexes linked to anthraquinone intercalators., *J. Med. Chem. 34*, 414-420.
74. Ellis, L. T., Perkins, D. F., Turner, P., and Hambley, T. W. (2003) The preparation and characterisation of cyclam/anthraquinone macrocyle/intercalator complexes and their interactions with DNA, *Dalton Trans.*, 2728-2736.
75. Boseggia, E., Gatos, M., Lucatello, L., Mancin, F., Moro, S., Palumbo, M., Sissi, C., Tecilla, P., Tonellato, U., and Zagotto, G. (2004) Toward efficient Zn(II)-based artificial nucleases, *J. Am. Chem. Soc. 126*, 4543-4549.
76. Islam, S. A., Neidle, S., Gandecha, B. M., and Brown, J. R. (1983) Experimental and computer graphics simulation analyses of the DNA interaction of 1,8-bis-(2-diethylaminoethylamino)-anthracene-9, 10-dione, a compound modelled on doxorubicin, *Biochem. Pharmacol. 32*, 2801-2808.
77. Palu, G., Palumbo, M., Antonello, C., Meloni, G. A., and Marciani-Magno, S. (1986) A search for potential antitumor agents: biological effects and DNA binding of a series of anthraquinone derivatives, *Mol. Pharmacol. 29*, 211-217.
78. Neidle, S., Jenkins, T. C., and Agbandje, M. (1991) Preparation of 2,6-bis(aminoalkanoylamino)anthracene-9,10-diones as intercalating agents, p 52 pp, (Cancer Research Technology Ltd., UK). Application: WO.
79. Agbandje, M., Jenkins, T. C., McKenna, R., Reszka, A. P., and Neidle, S. (1992) Anthracene-9,10-diones as potential anticancer agents. Synthesis, DNA-binding, and biological studies on a series of 2,6-disubstituted derivatives, *J. Med. Chem. 35*, 1418-1429.
80. Haq, I., Ladbury, J. E., Chowdhry, B. Z., and Jenkins, T. C. (1996) Molecular anchoring of duplex and triplex DNA by disubstituted anthracene-9,10-diones: Calorimetric, UV melting, and competition dialysis studies, *J. Am. Chem. Soc. 118*, 10693-10701.
81. Breslin, D. T., Yu, C. J., Ly, D., and Schuster, G. B. (1997) Structural modification changes the DNA binding mode of cation-substituted anthraquinone photonucleases: Association by intercalation or minor groove binding determines the DNA cleavage efficiency, *Biochemistry 36*, 10463-10473.
82. McKnight, R. E., Zhang, J. G., and Dixon, D. W. (2004) Binding of a homologous series of anthraquinones to DNA, *Bioorg. Med. Chem. Lett. 14*, 401-404.
83. Jackson Beckford, S., and Dixon, D. W. (2012) Molecular dynamics of anthraquinone DNA intercalators with polyethylene glycol side chains, *J. Biomol. Struct. Dyn. 29*, 1065-1080.

84. Islam, S. A., Neidle, S., Gandecha, B. M., Partridge, M., Patterson, L. H., and Brown, J. R. (1985) Comparative computer graphics and solution studies of the DNA interaction of substituted anthraquinones based on doxorubicin and mitoxantrone, *J. Med. Chem. 28*, 857-864.
85. Takenaka, S., and Takagi, M. (1999) Threading intercalators as a new DNA structural probe, *Bull. Chem. Soc. Jpn. 72*, 327-337.
86. Wilson, W. D. (1999) DNA Intercalators, In *DNA and Aspects of Molecular Biology* (Kool, E. T., Ed.), pp 427-476, Pergamon, New York.
87. Guelev, V. M., Cubberley, M. S., Murr, M. M., Lokey, R. S., and Iverson, B. L. (2001) Design, synthesis, and characterization of polyintercalating ligands, In *Methods Enzymol.* (Chaires, J. B., and Waring, M. J., Eds.), pp 556-570, Academic Press, New York.
88. Wilhelmsson, L. M., Lincoln, P., and Nordell, P. (2006) Slow DNA Binding, In *Sequence-Specific DNA Binding Agents* (Waring, M., Ed.), pp 69-95, The Royal Society of Chemistry, Cambridge, UK.
89. Wheate, N. J., Brodie, C. R., Collins, J. G., Kemp, S., and Aldrich-Wright, J. R. (2007) DNA intercalators in cancer therapy: Organic and inorganic drugs and their spectroscopic tools of analysis, *Mini Rev. Med. Chem. 7*, 627-648.
90. Strekowski, L., and Wilson, B. (2007) Noncovalent interactions with DNA: An overview, *Mutat. Res. Fund. Mol. Mech. Mut. 623*, 3-13.
91. Fox, K. R., Brassett, C., and Waring, M. J. (1985) Kinetics of dissociation of nogalamycin from DNA: Comparison with other anthracycline antibiotics, *Biochim Biophys Acta. 830*, 383-392.
92. Fox, K. R., and Waring, M. J. (1984) Evidence of different binding sites for nogalamycin in DNA revealed by association kinetics, *Biochim. Biophys. Acta 802*, 162-168.
93. Fox, K. R., and Waring, M. J. (1986) Footprinting reveals that nogalamycin and actinomycin shuffle between DNA binding sites, *Nucleic Acids Res. 14*, 2001-2014.
94. Williams, L. D., Egli, M., Gao, Q., Bash, P., Van Der Marel, G. A., Van Boom, J. H., Rich, A., and Frederick, C. A. (1990) Structure of nogalamycin bound to DNA hexamer, *Proc. Natl. Acad. Sci. U. S. A. 87*, 2225-2229.
95. Chaires, J. B., Dattagupta, N., and Crothers, D. M. (1985) Kinetics of the daunomycin-DNA interaction, *Biochemistry 24*, 260-267.
96. Baginski, M., Fogolari, F., and Briggs, J. M. (1997) Electrostatic and non-electrostatic contributions to the binding free energies of anthracycline antibiotics to DNA, *J. Mol. Biol. 274*, 253-267.
97. Haq, I., Jenkins, T. C., Chowdhry, B. Z., Ren, J. S., and Chaires, J. B. (2000) Parsing free energies of drug-DNA interactions, In *Energetics of Biological Macromolecules, Pt C*, pp 373-405.
98. Ren, J., Jenkins, T. C., and Chaires, J. B. (2000) Energetics of DNA intercalation reactions, *Biochemistry 39*, 8439-8447.
99. Chaires, J. B. (2001) Analysis and interpretation of ligand-DNA binding isotherms, In *Drug-Nucleic Acid Interactions*, pp 3-22.
100. Mukherjee, A., Lavery, R., Bagchi, B., and Hynes, J. T. (2008) On the molecular mechanism of drug intercalation into DNA: A simulation study of the intercalation pathway, free energy, and DNA structural changes, *J. Am. Chem. Soc. 130*, 9747-9755.
101. Kostjukov, V. V., Khomytova, N. M., and Evstigneev, M. P. (2009) Partition of thermodynamic energies of drug-DNA complexation, *Biopolymers 91*, 773-790.

102. Chang, Y.-M., Chen, C. K. M., and Hou, M.-H. (2012) Conformational Changes in DNA upon Ligand Binding Monitored by Circular Dichroism, *International Journal of Molecular Sciences 13*, 3394-3413.
103. Chaires, J. B. (2006) A thermodynamic signature for drug-DNA binding mode, *Arch. Biochem. Biophys. 453*, 26-31.
104. Macgregor, R. B., Jr., Clegg, R. M., and Jovin, T. M. (1985) Pressure-jump study of the kinetics of ethidium bromide binding to DNA, *Biochemistry 24*, 5503-5510.
105. Benight, A. S., Gallo, F. J., Paner, T. M., Bishop, K. D., Faldasz, B. D., and Lane, M. J. (1995) *Advances in Biophysical Chemistry*, Vol. 5, JAI Press Inc., Greenwich, CT.
106. Ha, J. H., Spolar, R. S., and Record, M. T. J. (1989) Role of hydrophobic effects in stability of site-specific protein DNA complexes, *J. Mol. Biol. 209*, 801-816.
107. Livingstone, J. R., Spolar, R. S., and Record, M. T. J. (1991) Cntribution to the thermodynamics of protein folding from the reduction in water accessible non-polar surface area, *Biochemistry 30*, 4237-4244.
108. Spolar, R. S., Livingstone, J. R., and Record, M. T. (1992) Use of liquid-hydrocarbon and amide transfer data to estimate contributions to thermodynamic functions of protein folding from the removal of non-polar and polar surface from water, *Biochemistry 31*, 3947-3955.
109. Finkelstein, A. V., and Janin, J. (1989) The price of lost freedom: Entropy of bimolecular complex formation, *Protein Eng. 3*, 1-3.
110. Spolar, R., and Record, M. (1994) Coupling of local folding to site-specific binding of proteins to DNA, *Science 263*, 777-784.
111. Record, M. T., Jr., Anderson, C. F., and Lohman, T. M. (1978) Thermodynamic analysis of ion effects on the binding and conformational equilibria of proteins and nucleic acids: the roles of ion association or release, screening, and ion effects on water activity, *Q. Rev. Biophys. 11*, 103-178.
112. Wilson, W. D., and Lopp, I. G. (1979) Analysis of cooperativity and ion effects in the interaction of quinacrine with DNA, *Biopolymers 18*, 3025-3041.
113. Friedman, R. A. G., and Manning, G. S. (1984) Polyelectrolyte effects on site-binding equilibria with application to the intercalation of drugs into DNA, *Biopolymers 23*, 2671-2714.
114. Chaires, J. B. (1996) Dissecting the free energy of drug binding to DNA, *Anticancer. Drug Des. 11*, 569-580.
115. Chaires, J. B., Satyanarayana, S., Suh, D., Fokt, I., Przewloka, T., and Priebe, W. (1996) Parsing the free energy of anthracycline antibiotic binding to DNA, *Biochemistry 35*, 2047-2053.

2 EFFECT OF SIDE CHAIN LENGTH ON DNA BINDING AFFINITY

2.1 Work to be published

Synthesis and characterization of a homologous series of anthraquinone intercalators binding to DNA

2.1.1 ***Abstract***

The synthesis of four homologous anthraquinones (**AQ I-IV**) bearing increasing lengths of polyethylene glycol (PEG) side chains and their binding to AT- and GC-rich DNA hairpins are reported. The molecules were designed such that the cationic charge is at a constant position and the ethylene glycol units chosen to allow significant increases in chain length with minimal changes in hydrophobicity. The mode and affinity of binding were assessed using circular dichroism (CD), nuclear magnetic resonance (NMR), surface plasmon resonance (SPR), and isothermal titration calorimetry (ITC). The binding affinity decreased as the AQ chain length increased along the series with both AT- and GC-rich DNA. ITC measurements showed that the thermodynamic parameters of **AQ I-IV** binding to DNA exhibited significant enthalpy-entropy compensation. The enthalpy became more favorable while the entropy became less favorable. Changes in the enthalpic term along the series partly reflect interactions of the PEG side chain with DNA; a decrease in the conformational freedom of the side chains upon binding contributes to the entropic term. The correlation between enthalpy and entropy may involve not only the side chains, but also changes in the binding of water and associated counterions and hydrogen bonding. The importance of entropic considerations is also seen in the observation that DNA binding of intercalators shows more dependence on the number of rotatable bonds in the side chain than on the hydrophobicity of the ligand.

2.1.2 *Introduction*

The design of small molecules that target duplex DNA sequences is an area of continued interest in chemistry, biology and medicine.[1-5] A major goal is to design molecules, both intercalators and groove binders, which target DNA with greater specificity and increased binding affinity. Characterization of ligand-DNA complexes with X-ray crystallography[6-8] and NMR spectroscopy[9-14] has led to fairly detailed understanding of the structural factors involved in DNA binding. Structural data, however, need to be accompanied by thermodynamic[15-18] and kinetic[19-22] studies to elucidate the driving forces for binding interactions and for a complete understanding of the effects of substituent changes on binding affinity and specificity.

Intercalators that interact with DNA can be thought of in terms of the aromatic core and the appended side chains. The designs of their side chains may result in important differences in their DNA-binding behaviors. Modifications to the intercalators' side chains have been implicated in altering the solubility of the molecule,[23-24] creating additional interactions that enhance DNA binding affinity and specificity,[25-29] changing the kinetics of interactions,[30-31] and their biological activities.[32-34]

The anthraquinone-related molecules have many applications as biologically relevant chromophores, including in chemotherapy[35] and studies of electron transfer in DNA.[36-40] The introduction of an amide substituent into the anthraquinone (AQ) ring system allows elaboration of the system through the attachment of various side chains. In this context, the position and/or nature of the side chain on the AQ amides with the nitrogen bound in the 2-position, has been shown to affect its DNA binding mode,[41-42] binding affinity,[42-43] specificity,[42] recognition of different DNA structures,[44] extent to which it stabilizes DNA,[45-47] cytotoxicity,[43, 48-49] and DNA

cleavage.[50-52] The direction of the amide bond is known to modulate DNA recognition and inhibition.[53]

In the present study, we have systematically increased the side chain length of anthraquinone DNA intercalators to reveal fundamental contributions of the side chain in terms of the ligand's affinity for DNA and the entropy and enthalpy of binding. For the side chains, we have used increasing lengths of polyethylene glycol (PEG). PEG, a neutral molecule, is used as an osmolyte in studies with DNA due to its minimal interaction with DNA, water solubility, lack of toxicity, stability, commercial availability, and varying molecular weights.[54-61] A PEG side chain allows for a significant increase in chain length with minimal changes in hydrophobicity.[62] The cationic charge has been maintained at a constant position in the series to facilitate direct comparison, since it is known that that the position of the cation can affect the binding characteristics of AQ.[63]

A previous study in our group involved a homologous series of AQ derivatives with two symmetrical side chains on opposite side of the central core. Those derivatives bound to DNA via a threading mechanism;[64] a decrease in DNA binding affinity with an increase in side chain length was observed. The current series involves derivatives with a single side chain (**AQ I-IV**, Figure 1). Both surface plasmon resonance (SPR) and isothermal titration calorimetry (ITC) have been used to assess the thermodynamic effects of molecular size on DNA binding affinity. For these derivatives, the binding constant also decreased as the PEG side chain increased in length, with an increase in favorable enthalpy and decrease in entropy (more negative $T\Delta S$) along the series. Molecular dynamics (MD) simulations have provided an important complement to the thermodynamic data in defining the molecular forces that drive binding.[65]

For a ligand binding to DNA, the enthalpic and entropic contributions dictate the Gibbs free energy and thus the ligand's binding affinity. The enthalpy is associated with two main contributors: non-covalent interactions between the ligand and DNA and rearrangement of water molecules upon ligand interaction with DNA.[66] The entropy is also associated with two main contributors upon complexation: release or uptake of water molecules and counterions and conformational restriction of the ligand when bound to DNA.[66] Tighter binding affinities can be achieved by favorable changes in either the enthalpic term or the entropic term, or both. However, enthalpy-entropy compensations are frequently evident and a favorable enthalpy is often compensated by an unfavorable entropy.[67-69] The homologous series used allow a close look at the effect of defined changes in the side chains on both the enthalpy and entropy of binding.

For both of our series, as well as other homologous intercalators binding to DNA,[64-65, 70-74] there seems to be a strong dependence of the binding affinity on the side chain length rather than the hydrophobicity of the molecule. In our series, this effect was only partly due to the effect of DNA in restricting the space available to the side chains. A significant enthalpy-entropy compensation of the binding of ligands to DNA indicates that the situation is complex, involving not only the ligand and DNA, but presumably also water and counterions.

2.1.3 ***Materials and Methods***

2.1.3.1 Synthesis of AQ I, N-*(3-[(3-methoxy-propylamino]-propionylamino]-9,10-dioxo-9,10-dihydro-anthracen-2-yl)-propionamide.*

Following the procedure from Agbandje et al.,[43] a mixture of 3-bromopropionyl chloride (5.0 mL, 50 mmol) and 2-aminoanthraquinone (1.0 g, 4.5 mmol) was heated at 85 ^{o}C for 2 h. The mixture was allowed to cool to room temperature, filtered and the product washed with diethyl ether to afford 3-bromo-*N*-(9,10-dihydro-anthracen-2-yl)-propionamide (1.2 g, 3.4 mmol)

as a yellow green powder.[43, 52] This product (1.2 g, 3.4 mmol), potassium carbonate (2.9 g, 21 mmol) and methoxypropylamine (1.9 g, 21 mmol) were refluxed in absolute ethanol (30 mL) for 4 h. The product was filtered and the filtrate evaporated under reduced pressure. The anthraquinone amide was partially purified by silica gel chromatography eluting with CH_2Cl_2/MeOH, 1:1. The amide was further purified by HPLC on a Shimadzu LC-10AT VP system and a Zobax C18 reverse phase column. Elution conditions: CH_3CN-MeOH (flow rate = 1.5 mL/min), 0-10 min (CH_3CN 0%-100%), 10-35 min (CH_3CN 100%-50%) to yield a yellow solid (37 mg, 0.10 mmol, 2.9%). ^{1}H NMR (400 MHz, $CDCl_3$) δ 11.65 (br s, 1H), 8.27 (m, 4H), 8.12 (s, 1H), 7.89 (m, 2H), 3.57 (t, *J* = 6.3, 2H), 3.38 (s, 3H), 3.04 (t, *J* = 5.6, 2H), 2.88 (t, *J* = 6.3, 2H), 2.57 (t, *J* = 5.6, 2H), 2.18 (br s, 1H), 1.92 (quintet, *J* = 6.3, 2H); ^{13}C NMR δ 182.5, 181.8, 171.9, 144.5, 134.7, 134.5, 134.3, 129.0, 128.8, 127.5, 124.9, 116.4, 71.1, 58.6, 46.3, 45.0, 35.2, 29.8 (^{1}H and ^{13}C NMR spectra are in Supplemetal Material). HRMS (ESI) calcd for $C_{21}H_{23}N_2O_4$ $[M]^+$: 367.1658, found: 367.1671.

2.1.3.2 Synthesis of AQ II, N-*(3-[3-{2-methoxy-ethoxy}-propylamino]-propionylamino}-9,10-dioxo-9, 10-dihydro-anthracen-2-yl)-propionamide.*

Following the procedure for the synthesis of **AQ I**, 3-bromo-*N*-(9,10-dihydro-anthracen-2-yl)-propionamide (1.5 g, 4.2 mmol), potassium carbonate (2.9 g, 12 mmol) and 3-(2-methoxyethoxy)propylamine (2.8 g, 21 mmol) were refluxed in absolute ethanol (30 mL) for 4 h. After purification, **AQ II** was obtained as a yellow solid (49 mg, 0.12 mmol, 2.9%). ^{1}H NMR (400 MHz, $CDCl_3$) δ 11.63 (br s, 1H), 8.48 (s, 1H), 8.10 (m, 4H), 7.68 (m, 2H), 3.60 (t, *J* = 5.9, 2H), 3.49 (m, 4H), 3.36 (s, 3H), 3.04 (t, *J* = 5.8, 2H), 2.87 (t, *J* = 5.9, 2H), 2.58 (t, *J* = 5.8, 2H), 1.94 (quintet, *J* = 5.9, 2H); ^{13}C NMR δ 182.5, 181.7, 171.8, 144.7, 134.6, 134.4, 134.3, 129.2, 128.8, 127.5, 124.8, 116.8, 71.7, 70.1, 70.0, 59.0, 46.9, 45.1, 35.5, 29.8 (^{1}H and ^{13}C NMR

spectra are in Supplemetal Material). HRMS (ESI) calcd for $C_{23}H_{27}N_2O_5$ $[M]^+$: 411.1920, found: 411.1900.

2.1.3.3 Synthesis of AQ III, N-*(3-[3-{2-methoxyethoxy-ethoxy-propylamino]-propionylamino}-9,10-dioxo-9,10-dihydro-anthracen-2-yl)-propionamide.*

Following the procedure from Brustolin et al. [75] for Michael addition, a catalytic amount of sodium methoxide (0.6 g) was added to a well-stirred solution of di(ethylene gycol) methyl ether (28 g, 0.23 mol) in acrylonitrile (25 g, 0.46 mol); the mixture was stirred for 2 h at 0 ^oC. Three drops of concentrated hydrochloric acid were added and the unreacted acrylonitrile evaporated *in vacuo*. After addition of chloroform, the insoluble side products were filtered and the product concentrated under vacuum to give 3-[2-(2-methoxyethoxy)ethoxy]propionitrile (15 g, 0.091 moles).[76] Under 60 psi H_2 pressure, the nitrile (2.9 g, 0.017 mol) in 2 M ethanolic ammonia (40 mL) was catalytically hydrogenated in the presence of Raney-nickel in water (2 g) using a Parr apparatus. When no more H_2 was consumed, the reaction mixture was filtered over Celite and the filtrate evaporated *in vacuo* yielding 3-[2-(2-methoxyethoxy)ethoxy]propylamine (2.3 g, 0.013 moles).[76]

The amine (13 mmol) was allowed to react with 3-bromo-*N*-(9,10-dihydro-anthracen-2-yl)-propionamide (4.2 mmol) in potassium carbonate (2.1 g, 15 mmol) under reflux in absolute ethanol (30 mL) for 4 h. The product was filtered and the filtrate evaporated under reduced pressure. The anthraquinone amide was partially purified by silica gel chromatography eluting with CH_2Cl_2/MeOH, 1:1. The amide was further purified by HPLC and the product obtained as yellow solid (77 mg, 0.17 mmol, 4.0%). ^1H NMR (400 MHz, $CDCl_3$) δ 11.60 (br s, 1H), 8.28 (m, 4H), 8.12 (s, 1H), 7.77 (m, 2H), 3.67 (m, 8H), 3.63 (t, *J* = 6.1, 2H), 3.38 (s, 3H), 3.03 (t, *J* = 5.7, 2H), 2.88 (t, *J* = 6.1, 2H), 2.56 (t, *J* = 5.7, 2H), 1.93 (quintet, *J* = 6.1, 2H), ^{13}C

NMR δ 182.4, 181.7, 171.7, 144.6, 134.8, 134.7, 134.5, 129.2, 128.8, 127.4, 124.8, 116.9, 71.7, 70.1, 69.9, 58.8, 46.7, 45.0, 35.5, 29.7 (^{1}H and ^{13}C NMR spectra are in Supplemetal Material). HRMS (ESI) calcd for $C_{25}H_{31}N_2O_6$ $[M]^+$: 455.2182, found: 455.2173.

2.1.3.4 Synthesis of AQ IV, N-*(3-[2-{2-(2-methoxy-ethoxy)-ethoxy-ethoxy-propylamine}-propionylamino]-9,10-dioxo-9,10-dihydro-anthracen-2-yl)-propionamide.*

Tri(ethylene glycol) monomethyl ether (24 g, 0.14 mol) was reacted as described above (synthesis of **AQ III**) and purified by HPLC to give **AQ IV** as a yellow solid (50 mg, 0.10 mmol, 2.4%). ^{1}H NMR (400 MHz, $CDCl_3$) δ 11.55 (br s, 1H), 8.34 (m, 4H), 8.29 (s, 1H), 7.81 (m, 2H), 3.66 (m, 12H), 3.54 (m, 2H), 3.37 (s, 3H), 3.05 (t, *J* = 5.2, 2H), 2.90 (t, *J* = 6.2, 2H), 2.58 (t, *J* = 5.2, 2H), 1.92 (quintet, *J* = 6.2, 2H), ^{13}C NMR δ 182.5, 181.7, 172.0, 144.9, 134.8, 134.6, 134.4, 129.0, 128.8, 127.4, 124.9, 116.9, 71.8, 71.7, 70.3, 70.1, 69.9, 59.2, 46.8, 45.1, 35.5, 29.9 (^{1}H and ^{13}C NMR spectra are in Supplemetal Material). HRMS (ESI) calcd for $C_{27}H_{35}N_2O_7$ $[M]^+$: 499.2444, found: 499.2465.

2.1.3.5 Determination of Binding Mode using NMR

NMR spectra were obtained on a Varian Unity plus 500 MHz spectrometer. DNA samples (150 µM) were dissolved in 0.5 mL of phosphate buffer, (10 mM NaH_2PO_4, 10 µM EDTA, 100 mM NaCl, pH 7.0), dried under N_2 gas and finally dissolved in 90% H_20 - 10% D_2O. An initial temperature study was conducted from 25 ^{o}C to 5 ^{o}C on the NMR spectrophotometer. All imino protons were seen at 5 ^{o}C. Titrations of **AQ II** with both AT- and GC-rich DNA hairpins were conducted over a range of AQ-DNA ratios from 0.5 to 10 under slow exchange conditions (5 ^{o}C). The complete sequences are 5'-biotin-CGCGCGCG<u>TTTT</u>CGCGCGCG and 5'-biotin-CATATATAT<u>CCCC</u>ATATATATG where the hairpin loops are underlined. The GC base pair was placed at the end of the AT-rich hairpin to minimize fraying. The Jump-Return pulse se-

quence was used for water suppression. The NMR experiments were obtained with a spectral width of 5000 Hz, ~ 16,000 data points, a relaxation delay time of 1.5 s, and 2 Hz line broadening. Data were processed by MestReNova 5.0.3 software.

2.1.3.6 Determination of Binding Mode using Circular Dichroism

CD spectra were obtained on a Jasco J-710 spectrometer (software supplied by Jasco) in a 1 cm cell in the range 200-650 nm. A buffer baseline scan was initially collected and subsequently subtracted from the average scan for each CD experiment. The hairpin concentration in all cases refers to the strand concentration, which is also the duplex concentration. DNA hairpin samples, 10 μM were incubated with **AQ II** at various ratios (r_i = 0, 0.5, 1.0, 2.0, 3.0, 4.0, 5.0, 6.0, 7.0, 8.0) at 25 ^{o}C in MES10 buffer (1.0 mM EDTA, 0.1 M NaCl and 10 mM MES, pH 6.24) for 5 min at room temperature before each spectral analysis. Measurements were collected at 50 nm/min using a 0.5 nm step and a response time of 0.5 s. Five scans were accumulated and automatically averaged. Data manipulation and plotting was done using the program Kaleidagraph version 4.0. To obtain the binding constant of anthraquinone to DNA, the data for GC-rich hairpin with **AQ II** were fitted to the following interaction model for nonlinear least-squares optimization of the binding parameters:

$$E_i = E_0 + (E_f - E_0) * \sqrt{(L_t + D_t + K_d)}-((L_t + D_t + K_d)^2 - 4D_tL_t) / 2[D_t] \qquad eq\ 1$$

where E_i is the ellipticity at a given concentration, *i* throughout the titration, E_0 is the initial ellipticity of DNA, E_f is the ellipticity of the fully formed DNA-complex, L_t is the total ligand concentration added at time *i*, D_t is the total DNA concentration used and, K_d is the dissociation

constant. E_f was fitted to -4 mdeg which was close to the ellipticity obtained at the end of the titration, -5 mdeg at 250 nm.

Binding interaction with AT-rich DNA did not fit the one-binding site model, instead, it required a two binding site interaction model. A two binding site model requires four complex variables for fitting;[77] variable correlation can be a significant issue with this many parameters. A binding curve was therefore calculated from the SPR K_1 and K_2 using equation 2 below:[78]

$$E_i = E_i[\text{DNA}] + E_i[\text{AQ-DNA}] + E_i[\text{AQ}_2\text{-DNA}] \qquad \textit{eq 2}$$

where [AQ-DNA] is the concentration of the DNA-complex after the first AQ ligand is bound and [AQ_2-DNA] is the concentration of the DNA-complex after the second ligand is bound. This equation is expanded to give equation 3 to solve for the predicted E_i:

$$E_i = E_{\text{DNA}} + E_{\text{AQ-DNA}}K_1[\text{AQ}] + E_{\text{AQ}_2\text{-DNA}}K_1K_2[\text{AQ}]^2[\text{DNA}]_t/(1+K_1[\text{AQ}]+K_1K_2[\text{AQ}]^2) \qquad \textit{eq 3}$$

The ellipticity values for AQ-DNA and AQ_2-DNA were assumed to be -3 and -4, respectively.

2.1.3.7 Surface Plasmon Resonance (SPR).

SPR analysis was conducted using a four-channel BIACORE 3000 system (BIAcore, Inc.) to measure real-time interactions between DNA coupled to a streptavidin coated sensor chip (SA) and anthraquinones under constant flow. The anthraquinone solutions were prepared in sterile filtered and degassed MES buffers: 10 mM MES, (pH 6.4), 0.1 mM EDTA, 0.1 M NaCl and 0.005% surfactant P20 by serial dilutions from stock solution. Anthraquinone concentrations varied from 10 nM - 14 µM; a Cary 50 Bio UV-Visible spectrophotometer was used to

measure the concentration of the stock, the molar absorptivity assumed to be 9,800 $mol^{-1}dm^3cm^{-1}$.[64] The sensor chip was conditioned with three consecutive 1-min injections of 1 M NaCl in 50 mM NaOH followed by extensive washing with HBS-EP buffer (10 mM HEPES, 0.15 M NaCl, 3 mM EDTA, 0.005% surfactant P20, pH 7.4); surfactant P20 was purchased from Biacore. Two flow cells were used to immobilize the 5'-biotinylated DNA hairpins in HBS-EP buffer to the sensor chip via biotin capture while the third was left blank as a control. A flow rate of 2 µL/min was used to control the amount of DNA bound; approximately 350 RU of DNA was captured in each case. The experiments were carried out in MES10 buffer and samples injected at a flow rate of 20 µL/min. Interaction analysis was performed by steady-state methods with multiple injections of different compound concentrations at 25 ºC. The compounds were dissociated and the surface regenerated using the running buffer and regeneration buffer (10 mM Gly, pH 2). The baseline was then reestablished, and the next sample injected. The SPR data was evaluated using the BIAevaluation software and the binding constants determined using Kaleidagraph (version 3.5, Synergy Software, PA, USA).

The reference response from the blank cell was subtracted from the response in each cell containing DNA to give a signal (RU, response units) that is directly proportional to the amount of bound compound. The predicted maximum response per bound compound in the steady-state region ($RU_{max.pred.}$) was determined from the DNA molecular weight (MW_{DNA}), the response of the DNA itself on the flow cell (RU_{DNA}), the compound molecular weight ($MW_{compound}$) and the refractive index gradient ratio of the compound and DNA (RI). For this series of compound, RI was taken to be 1.2.[79]

$$RU_{max.\ pred.} = (RU_{DNA} \times MW_{compound} \times RI)/MW_{DNA} \qquad \textit{eq 4}$$

To obtain the affinity constants, the data were fitted to a one- or two binding site interaction model using Kaleidagraph as shown below:

$$RU = RU_{pred} * (K_1C_{free} + 2K_1K_2C_{free}^2) / (1 + K_1C_{free} + K_1K_2C_{free}^2) \qquad eq\ 5$$

where K_1 and K_2 are macroscopic equilibrium constants for two binding sites (for a single site model, K_2 is zero). C_{free} is the concentration of free compound (and remains constant during the experiment due to continuous flow of the compound).

The observed RU values for AQ binding to the GC-rich hairpin were about 3 times lower than that observed for the AT-rich hairpin. However, the AQ ligands binding to the GC-rich hairpin required one binding constant while binding to the AT-rich hairpin required two binding constants. The reason for this irregularity was due to the GC-rich hairpin requiring a larger concentration of the AQ-ligand for saturation, due to its lower binding constants. We however used similar AQ-concentrations for both AT- and GC-rich experiments for two reasons. Firstly, using higher AQ concentrations was avoided to prevent problems such as excessive dimerization or adhering to the container surface. Secondly, both AT- and GC-rich hairpins were placed on the same chip for direct comparison of results. The data was sufficient to fit to a one-site binding model. A calculated plot using the K_a obtained from SPR, RU_{pred} and the concentrations used gave similar RU_{obs} values.

2.1.3.8 Isothermal Titration Calorimetry (ITC)

ITC experiments were carried at 25 ^oC using a VP-ITC microtitration calorimeter (Microcal, Inc., Northhampton, MA). ITC experiments were conducted by injecting 3 μL of the

0.3 mM anthraquinone solution in MES10 buffer every 300 s for a total of 98 injections into a 0.01 mM AT or GC-rich DNA hairpin solution in the same buffer. Integration of the area under each peak of the titration plot as a function of time gave the heat produced for each injection. Control experiments to determine the heats of dilution for the DNA and each AQ-ligand were carried out by injecting MES buffer solution into DNA or ligand into buffer alone. The dilution heat for the DNA was negligible and constant and was therefore subtracted from the interaction heats of ligand into DNA titration. The corrected binding isotherm for ligand binding to DNA was fit to an appropriate binding model with Origin 7.0, using equilibrium binding constants obtained from SPR to determine the binding parameter $\Delta H_{observed}$.

The heat of dilution titration profile for each ligand was typical for a molecule that self-associates. The dilution isotherm was therefore fit to a dimer dissociation model (Microcal Origin 7.0 software) as described in the equation below.[80-81]

$$q_i = \Delta H_{diss} [AQ_2]_{syr} dV_i - \Delta H_{diss} ([AQ_2]_i - [AQ_2]_{i-1}) * (V_o + dV_i/2) \qquad eq\ 6$$

where q_i is the heat change with each successive addition of AQ, ΔH_{diss} is the heat of dissociation of the dimer, $[AQ_2]_{syr}$, $[AQ_2]_i$ and $[AQ_2]_{i-1}$ are the dimer concentrations in the syringe, after the i^{th} and $(i-1)^{th}$ injection, respectively, dV_i is the volume of concentrated solution injected into the calorimeter cell of constant volume V_o. The $(V_o + dV_i/2)$ term is an effective volume which takes into account the displacement which occurs in a total filled cell.

The determined $\Delta H_{dissociation}$ value was subtracted from the $\Delta H_{observed}$ value to give a corrected value for the binding-induced enthalpy change. The change in entropy, ΔS, was calculated from $\Delta G = \Delta H_{binding} - T\Delta S$.

2.1.4 ***Results***

2.1.4.1 Determination of Binding Mode (NMR and Circular Dichroism).

Although anthraquinones are usually intercalators, in some instances they have been shown to interact with the DNA also as groove binders.[63, 82-83] Therefore, we began by evaluating the binding mode using NMR and circular dichroism (CD). One-dimensional spectra of exchangeable protons were acquired at 5 ^{o}C to 25 ^{o}C in 5 ^{o}C increments. The imino signals were most well resolved at 5 ^{o}C, so all other NMR experiments were conducted at this temperature. Titration of the AT-rich hairpin with **AQ II** to a stoichiometry of 1:10, Figure 2, showed perturbation of the imino resonances. The spectrum integrated for the nine imino resonances of the AT-rich hairpin. Over the course of the titration, most resonances appeared to have shifted upfield by 0.1 ppm or greater compared to the free DNA. Similarly, eight imino resonances were seen for the GC-rich hairpin and about half the signals appeared to have shifted upfield at the end of the titration (data not shown). An upfield shift in DNA imino resonances is indicative of intercalation.[84]

Circular dichroism experiments were performed to study the DNA binding properties of the AQ ligands, which do not exhibit any optical activity in the absence of DNA. Figure 3 shows the CD spectra of **AQ II** titrated with the AT-rich DNA hairpin. The uncomplexed AT-rich hairpin exhibited a negative band at approximately 244 nm due to base stacking and a positive band at about 280 nm due to the hairpin's helicity, typical of B-DNA.[85] Significant hypochromicity was seen for both bands over the course of the titration. In addition, the positive band showed a bathochromicity of about 10 nm.

The CD spectra in the GC-rich hairpin titration were qualitatively similar to that of the AT-rich DNA titration. The GC-rich DNA hairpin complex exhibited significant

hypochromicity at wavelengths 250 and 280 nm, Figure 4. A bathochromic shift of about 12 nm was also observed for the positive band. However, the AT- and GC-rich hairpin spectra were quantitatively distinct from each other, with a higher concentration of **AQ II** required for saturation of the GC-rich hairpin.

The circular dichroic effect arising from binding of **AQ II** to both AT- and GC-rich DNA hairpins allowed for an estimation of the binding constant. Figure 4 (bottom) shows the change in ellipticity at 250 nm as a function of the concentration of **AQ II** for the GC-rich hairpin. The data was fitted to a one-binding site model to obtain a binding constant of $1.4 \pm 0.2 \times 10^4\ M^{-1}$. In contrast, the binding data for AT-rich DNA hairpin did not fit to a one binding site model. However, the molar ellipticity at 244 nm as a function of **AQ II** concentration was consistent with a curve generated from the SPR binding constants (*vide infra*) for this system (Figure 3, bottom).

2.1.4.2 SPR Analysis to Determine the Binding Affinity.

To investigate the binding interactions of **AQ I-IV** with AT- and GC- rich DNA, SPR was used. SPR can provide useful information on the binding affinity and stoichiometry of DNA interactions. Representative sensograms for the binding of **AQ I** to AT- and GC-rich hairpins are shown in Figure 5; sensograms for **AQ II-IV** can be found in the Supporting Information. The SPR showed fast association and dissociation kinetics in the concentration range studied. RU values at steady state were used to generate binding plots as a function of ligand concentration.

Table I lists the binding constants of compounds **AQ I-IV** for both AT- and GC-rich DNA hairpins. The binding of **AQ I-IV** with the AT-rich DNA had a 2:1 stoichiometry for all compounds studied. The equilibrium constants for binding of the first ligand, K_1, were two to

four times higher than binding of the second ligand, K_2. Binding constants for the primary binding site decreased from 11.3 x 10^4 – 7.2 x 10^4 M^{-1} as the length of the side chain increased. The equilibrium binding constants obtained for binding of the second ligand, K_2, did not show a pattern in going from **AQ I-IV**.

In contrast to the AT-rich hairpin, the best fit for the binding to the GC-hairpin required one binding constant, consistent with the results obtained from CD. **AQ I-IV** showed a somewhat weaker affinity for binding GC-rich hairpin in comparison to the AT-rich hairpin; however, the trend was very similar. Equilibrium binding constants decreased over the range 4.1 – 1.8 x 10^4 M^{-1} as the length of the side chain increased (Table I). The anthraquinone with the shortest side chain (**AQ I**) bound approximately two times more tightly in comparison to that with the longest side chain.

2.1.4.3 Isothermal Titration Calorimetry.

ITC experiments were performed with both the AT- and GC-rich DNA hairpins to obtain a full thermodynamic profile of the interactions of **AQ I-IV**. Figure 6 shows ITC profiles of the binding to the AT-rich hairpin. The upper panels in the figures represent the raw ITC curves resulting from the injection of **AQ I-IV** into the DNA hairpin solution. The data were corrected separately for the heats of dilution of the DNA and the ligand. The heat of dilution of the DNA was found to be constant and very small. This was subtracted from the raw calorimetric data. Plots of the corrected heat released versus the AQ-DNA molar ratio are shown in the lower panels of Figure 6.

The heats of dilution for the AQ ligands were not constant, which is typical for a ligand undergoing dissociation. A review of the literature showed that anthraquinones can form dimers in solution.[46, 86-88] A closely related anthraquinone amide has been shown to have a dissociation

constant of 3.1 x 10^{-4} M.[46] In our work, the dilution curves were fitted to the dimer dissociation model described in the experimental using the literature dissociation constant.

The heat of dissociation of the dimers for **AQ I-IV** was 1.0 ± 0.1 kcal/mol. This value was used in each case to correct the observed enthalpy of interaction of AQ ligands with DNA:

$$\Delta H_{observed} = \Delta H_{dissociation} + \Delta H_{binding} \qquad \textit{eq 7}$$

Equation 7 assumes that the ligand is fully dissociated in the calorimeter cell. This was a reasonable approximation in these experiments, with more than 90% of the AQ in its monomeric form even at the highest concentration of AQ used.

The data for **AQ I-IV** binding to the AT-rich DNA was fitted to a two site binding model using the K_1 and K_2 values obtained from SPR. For the first ligand, binding enthalpies with the AT-rich DNA hairpin became more favorable as the length of the AQ side chain increased, ranging from -7.08 kcal/mol to -13.6 kcal/mol (Table I). The entropy values, on the other hand, became more unfavorable as the chain length increased ($T\Delta S$ = 0.15 to -7.20 kcal/mol). The fitted ΔH_2 and calculated $T\Delta S_2$ for the second (weaker) binding site for each complex showed no pattern as a function of side chain length. In addition, some compounds had relatively high values for both ΔH and $T\Delta S$, presumably resulting from the low binding constant (SPR) and possible correlation of data. ΔH values, therefore, are reported only for the first binding process in Table I.

Binding parameters for **AQ I-IV** with GC-rich DNA are also shown in Table I (figures are in the Supporting Information). The SPR data fitted well to a single binding constant, given as K_1 in the Table. The ITC experiments were better fitted by a two-site sequential binding

model. In this fitting, K_1 was assigned to the value determined by SPR while the K_2 and ΔH parameters were allowed to float. The second binding constant ($\sim 10^3$ M^{-1}) was taken as weak, non-specific binding to the GC-rich DNA hairpin, perhaps due to the high ratios of ligand to DNA used in the ITC titrations (ratios of up to 5 AQ:1 DNA). For the first (primary) binding site in the GC hairpin, as the AQ side chain increased in length, the enthalpy became more favorable, from -4.95 kcal/mol to -11.7 kcal/mol, and the entropy became more unfavorable, from 1.24 kcal/mol to -5.98 kcal/mol. This pattern was very similar to that observed for binding to the AT-rich hairpin. However, binding enthalpies for the GC-rich hairpin were generally about 2-3 kcal/mol less favorable and binding entropies about 1-2.5 kcal/mol more favorable than for the AT-rich hairpin.

2.1.5 ***Discussion***

2.1.5.1 Spectral Evidence Showing AQ Intercalation in DNA.

The changes in the chemical shifts and line widths of the imino protons of DNA when bound to a ligand are indicative of its binding mode.[84] Intercalation leads to line-broadened signals and upfield chemical shifts of the imino protons due to the ring currents exerted by the aromatic chromophore. In contrast, groove binding induces small downfield shifts of the resonances. The anthraquinone-based intercalators nogalamycin,[89] daunomycin,[84] sabarubicin,[90] doxorubicin derivatives,[91] and an anthraquinone sulfonamide [63] have been studied by NMR techniques. Binding of these anthraquinone intercalators to DNA caused an upfield shift of the imino resonances. In our work, binding of anthraquinone to both AT- and GC-rich DNA resulted in an upfield shift of the imino protons, indicative of intercalation.

2.1.5.2 Conformational Changes in DNA Monitored by Circular Dichroism.

The conformational changes in the DNA upon binding to the AQ ligands were monitored by circular dichroism. The CD spectrum of B-form DNA exhibits a positive band at about 280 nm due to base stacking and a negative band at about 250 nm due to the helicity of the DNA.[92] Upon AQ binding, both the AT- and GC-rich hairpins showed significant hypochromicity for both the 280 and 250 nm bands and bathochromicity of the peak at 280 nm. Intercalators are known to unwind the DNA helix to allow the DNA base pairs to separate for binding. The changes seen in the DNA CD signals signify alterations in both the DNA base stacking and helicity upon AQ binding, observed also for the anthraquinone intercalators nogalamycin and daunomycin.[93-94]

An induced signal for the AQ bound to either AT- or GC-rich DNA was not seen. Breslin et al. have made a similar observation with an anthraquinone sulfonamide.[63] They found that at low concentrations of the AQ-DNA complex (similar to ours), the induced CD ligand signal was too weak to be measurable. In general, groove binders exhibit much stronger induced CD signal intensity than do intercalated compounds.[95-96]

2.1.5.3 Binding Affinity.

Binding constants determined by SPR indicated moderate ligand-DNA affinities with values of $K_a \sim 10^4\ M^{-1}$. Association constants of 10^4 - $10^5\ M^{-1}$ have been previously determined for the binding of other AQ amides to DNA.[42-43, 46, 52, 63, 82, 97-100] The AQ ligands in our study had a moderate preference for AT-rich DNA, binding approximately three-fold more tightly than with GC-rich DNA (Table I). Other anthraquinone amides showing AT-selectivity have been reported.[63-64, 98] Preferential intercalator binding at AT-sites may be due to specific hydrogen-bonding interactions between the side chain atoms and the AT base pairs.[101]

2.1.5.4 Thermodynamic Characterization of AQ I-IV Binding to DNA.

Binding of **AQ I-IV** to the primary binding sites of both AT- and GC-rich DNA was enthalpically driven. Calculations showed that the favorable enthalpies of binding had contributions from electrostatic interactions between the side chain ammonium group and phosphate groups, a hydrogen bond between the side chain amide and DNA, and water bridges between the AQ chromophore and DNA.[65]

The binding enthalpy became more negative along the series **AQ I-IV**, decreasing from -7.08 to -13.6 kcal/mol for AT-rich DNA and -4.95 to -11.7 kcal/mol for the CG-rich DNA. Molecular dynamics (MD) simulations showed that the PEG side chain was more localized in the groove as the side chain became longer.[65] PEG is a neutral molecule widely used as an osmolyte in DNA studies; it is generally viewed as having minimal interaction with the DNA. The MD results, however, suggest interactions between the side chain and the DNA, presumably due to the forced high local concentration of the PEG in the DNA groove. This is expected to contribute favorably to the enthalpy.

The MD simulations also showed release of water molecules hydrogen bonded to the PEG side chain. This effect increased with the length of the side chain, with approximately 10% (**AQ I**) to 25% (**AQ IV**) of the side chain PEG-bound water molecules released upon ligand binding to the DNA. For **AQ IV** there was a high correlation between conformations with the side chains localized in the DNA groove and a decrease in the number of internal water bridges in the side chain, presumably due to the formation of favorable side chain-DNA interactions for this structure. The water molecules released from the side chain ether oxygens form hydrogen bonds with bulk water. The change in hydrogen bonding of these water molecules from a water-ether linkage to a water-water linkage presumably results in a net strengthening of hydrogen

bonding, thus contributing favorably to the enthalpy. Lu et al. showed that water molecules tend to cluster with increasing concentration of 1,2-dimethoxyethane solution,[102] which may be indicative of the stronger hydrogen bonds formed between water molecules.

The entropic component of the free energy became more unfavorable as the length of the side chain increased. $T\Delta S$ decreased from 0.15 to -7.20 kcal/mol along the AT series and 1.24 to -5.98 kcal/mol along the GC series. MD simulations showed the motions of the AQ side chains, when bound to DNA, were inhibited by the groove wall and therefore could only sample space away from the AQ chromophore. This effect became more significant as the side chain lengthened. Increased localization of the PEG side chain in the DNA groove also contributed unfavorably to the binding entropy by further restricting the motions of the side chain.

MD simulations comparing the free and bound AQ, showed a net change in $T\Delta S_{conf}$ of 3.4 kcal/mol for the complexes with the GC hairpin. This compares with a net change found in the experiments for $T\Delta S$ of 7.22 kcal/mol. Thus, the $T\Delta S$ range in the experiments is approximately twice that in the MD simulation. This is presumably because the entropy derived from MD simulation only accounted for the range of motions of the side chain, but not for other controlling aspects such as entropy due to loss or gain in water and/or counter ions during binding of the ligand to DNA.

The change in entropy may also be influenced by the release of water molecules from the side chain. If the released water molecules undergo strengthening of hydrogen bonds due a change from water-ether to water-water interactions, the change in entropy could be unfavorably affected (discussed in more detail below). Higher density water regions appeared to decrease as the side chain increased in length. Overall, the free energy of conformational change for

intercalators bearing a long or flexible side chains can contribute significantly to the free energy of binding of a ligand to DNA and ultimately, its binding affinity.

2.1.5.5 Enthalpy-Entropy Compensation.

The magnitude of the changes over the series in the enthalpies ($\Delta H > 6$ kcal/mol) and entropies ($T\Delta S > 3$ kcal/mol) for binding were not reflected in the change in the free energy of binding; the change in ΔG was < 1 kcal/mol from **AQ I** to **AQ IV**. Enthalpy-entropy compensation has been observed in previous studies of DNA binding. Figure 7 shows an enthalpy-entropy compensation plot of data obtained from binding of the AQ ligands studied herein as well as data obtained from the literature (compiled by J.B. Chaires). [69] The data chosen by Chaires were selected on the basis that enthalpy values were calorimetrically determined, binding free energies were determined from independently measured binding constants, and the data were acquired under solution conditions of 25 °C, pH 7, 0.2 M NaCl. Our data met the first two criteria and solution conditions were similar to those in the previous compilation (25 °C, pH 6.4, 0.15 M NaCl).

Groove binders and intercalators fall along different parts of the correlation, with the former having more unfavorable enthalpies and more favorable entropies than the latter. Our data set falls along the line of other mono-intercalators, extending the series in the data for **AQ III** and **AQ IV**. Bis-intercalators (the two points in the lower right of the graph, Figure 7)[103-104] show much more favorable enthalpies and unfavorable entropies, as might be expected for the binding of two moieties to the DNA. The enthalpy-entropy correlation is seen over a large number of different structures of DNA binding molecules and appears independent of even the mode of binding (groove binding or intercalation). In our series, the compensation increases smoothly

in the order **AQ I** < **AQ II** < **AQ III** < **AQ IV**. Thus, the longer side chains result in a higher compensation.

Enthalpy-entropy compensation has been previously observed in a variety of processes involving nucleic acids, including melting of single strands, hairpins and duplexes,[105-109] nucleic acid folding,[110] and the interactions of nucleic acids with ligands.[67-69, 111] For the examples in Figure 7, the interactions of groove binders are entropically driven and those of intercalators are enthalpically driven. The reasons for the enthalpy-entropy correlations are unclear, but may involve changes in the binding of water and associated counterions, hydrogen bonding, and the collective dynamics of the ligand-DNA complex.

The role of water may be significant in enthalpy-entropy compensations in ligand-DNA interactions.[67] Ligands that bind to the minor groove of DNA have been shown to effect the release of water from the groove e.g., Hoechst 33258,[112] DAPI,[113] the benzimidazole derivatives DB183 and DB185,[114] and netropsin.[115] The release of water molecules from the groove binder-DNA complex would be expected to result in favorable entropy. In contrast, intercalator binding is often accompanied by water uptake; e.g., for propidium, proflavine, daunomycin, and 7-aminoactinomycin D.[116] This results in more negative entropies of complex formation. In addition, the formation of new hydrogen bonds between water and the DNA complex could result in a more favorable enthalpic term.

The role of water can also be viewed in terms of hydrogen bonds formed and broken.[111] In this model, release or uptake of water molecules is viewed primarily as a redistribution of hydrogen bonds. Work by Pimentel et al. on model systems has indicated that hydrogen bond formation (favorable enthalpy) is accompanied by an unfavorable entropy,[117] presumably due to a loss in molecular motion. The observed enthalpy-entropy compensation could therefore arise

from the release of waters from the side chain to form hydrogen-bonds with bulk water molecules. The increase in enthalpy due to formation of hydrogen-bonds is compensated by the loss in molecular motions of the water molecules.

A third aspect of enthalpy-entropy compensation is the restriction of molecular motion due to intermolecular forces including hydrophobic interactions, hydrogen bonds and electrostatic interactions. Searle and Williams have postulated the compensating effect of these non-covalent interactions in nucleic acid melting studies.[105] Dunitz has used a statistical mechanical model to derive a semi-quantitative estimate for enthalpic and entropic components when two molecules interact.[118] This model suggests that an increase in enthalpic contributions from non-covalent interactions of the ligand and DNA is accompanied by a restriction of the motions of the ligand and DNA, resulting in a decrease in entropy. Whatever the mixture of physical effects that underlie enthalpy-entropy compensation, it is clear that this phenomenon is seen for a variety of different molecules binding to DNA as both groove binders and intercalators.

2.1.5.6 Effect of Increasing Side Chain Length on DNA Binding Affinity..

Our data may be compared with other quantitative studies of homologous intercalators binding to DNA. Most homologous series are created with addition of methylene units to the side chain(s). Maleev and co-workers looked at the binding of actinocin derivatives with CT-DNA.[72] Wakelin et al. [70] and Atwell et al. [71] measured binding of similar homologous series of aminoacridine and acridines, respectively, to both AT-and GC-rich DNA. Zhang et al. studied two sets of acenaptho[1,2-b] pyrrole derivatives.[73] Ovchinikov et al. investigated the binding of actinomycin homologs.[74] In all five of these series, the extension of the side chains by methylene units resulted in structures that became more hydrophobic as the side chains became longer. There are two studies of homologous series in which the side chains are increased by –

CH_2CH_2O– groups, the current study and previous work in this laboratory on threading intercalators by McKnight et al.[64] For both of these series, the structures became more hydrophilic and the binding constant decreased as the side chains became longer. All of the data are plotted in Figure 8a. Overall, there is no dependence of the binding constant on hydrophobicity (expressed as XlogP of the molecule[62]).

In all the seven series studied, however, there is a decrease in binding constant as the number of rotatable bonds in the side chain increases; the data are plotted in Figure 8b. This change in binding constant is independent of increasing or decreasing hydrophobicity, one or two side chains, threading or "classical" modes of binding, and mono- or dicationic structures. This significant correlation of binding constant in each series with the number of rotatable bonds indicates the importance of the side chain in controlling the DNA binding constant. However, control is only partly due to the effect of DNA in restricting the space available to the side chains. The significant enthalpy-entropy compensation of the binding of ligands to DNA indicates that the situation is complex, involving not only the ligand and DNA, but also water and counterions.

2.1.6 ***Conclusions.***

This study has reported the binding of four homologous anthraquinones (AQ) bearing PEG-based side chains to both AT- and GC-rich hairpins. The binding affinity and thermodynamic parameters were assessed via SPR and ITC measurements. The AT-rich sequence bound two AQ while the GC-rich sequence bound one AQ ligand. The binding affinity decreased slightly as the AQ chain length increased along the series **AQ I-IV** with both AT- and GC-rich DNA. Conversion of the binding constants to binding free energy showed small changes in $\Delta\Delta G$ of less than 1 kcal/mol along the series; this small change arose from enthalpy-entropy compen-

sation, that is, the enthalpic term became more favorable and the entropic term became less favorable along the series.

Changes in the enthalpic term along the series probably reflect increased interactions of the side chain with DNA as the chain length increases. This is consistent with related molecular dynamics studies on this system that show increasing localization of the PEG chain in the groove as it becomes longer. PEG is generally viewed as having minimal interaction with DNA; our work indicates that PEG does interact with the DNA, presumably due to the forced high local concentration in the DNA groove. The enthalpic term may also be affected by the rearrangement of water molecules upon AQ-DNA interaction. The water molecules released from the side chain can form hydrogen bonds with bulk water; the hydrogen bonds involving water are stronger than those with the ether linkage, resulting in a net increase in favorable enthalpy.

Changes in the entropic term are thought to arise from two main factors. First, upon binding to DNA, the conformational freedom of the PEG side chains is restricted by the DNA. Ligands bearing longer side chains are expected to pay a higher entropic cost because the side chains can no longer sample space above and below the chromophore. Second, formation of hydrogen-bonds by the release or uptake of water molecules by the AQ-DNA complex restricts the molecular motions of water molecules, which also contributes unfavorably to the entropy.

Binding of intercalators to DNA can be parsed in terms of a series of free energy contributions, including ΔG_{conf}, the free energy contribution from conformational changes in the DNA and ligand upon binding. Conformational changes for intercalators binding to DNA are often neglected, both because many intercalators do not have significant numbers of rotatable bonds, and because $T\Delta S$ for many is small. This study shows that there is an entropic cost when intercalators with long side chains bind to DNA. This is greater the longer the side chain and is

significant enough to cause a decrease in DNA binding affinity. The importance of entropic considerations is also seen in the observation that DNA binding of intercalators shows more dependence on the number of rotatable bonds in the side chain than on the hydrophobicity of the ligand.

More generally, not only this series of DNA binding molecules but many others show significant enthalpy-entropy compensation. Enthalpy-entropy compensation is a complex phenomenon, involving not only noncovalent interactions between the ligand and DNA, but also rearrangement of the water molecules involved in the complex with the resulting changes in hydrogen bonding.

2.2 Unpublished Work.

2.2.1 *NMR: Determination of the Binding Mode of AQ to GC-rich DNA.*

Titration of the GC-rich hairpin with **AQ II** to a stoichiometry of 1:10, Figure 2.9, showed perturbation of the imino resonances. The spectrum integrated for the eight imino resonances of the GC-rich hairpin. Over the course of titration, about half the resonances appeared to have shifted upfield by 0.1 ppm or greater compared to the free DNA. An upfield shift in DNA imino resonances is indicative of intercalation.[84]

2.2.2 *CD: Derivation of the Binding Constant of AQ II binding to DNA*

The binding affinities of small molecules binding to DNA can be estimated from non-linear curve fitting of the CD binding isotherm at specific wavelengths using various software programs, such as Kaleidagraph. Derivation of the binding constant for systems of 1:1 binding stoichiometry has been previously reported,[78] and is shown in equations 2.1-2.9. The binding of **AQ II** to GC-rich hairpin was fitted to a 1:1 binding stoichiometry. Binding interaction of **AQ II** with AT-rich DNA did not fit the one-binding site model. Binding models with two interaction

sites or greater requires four or more complex variables for fitting; [78] variable correlation can be a significant issue with this many parameters. A binding curve was therefore calculated from the SPR K_1 and K_2 using the derivation described in equations 2.10-2.19 below.[78]

2.2.2.1 Derivation of one-site binding isotherm.

The AQ ligand, L is assumed to bind reversibly to the DNA macromolecule, M to form ML with a dissociation constant, K_d. The total concentrations of M and L are denoted M_t and L_t, respectively, and the ellipticity of M and ML is given by *E*. The drug has no ellipticity. From the equilibrium condition and mass conservation, the following is obtained:

$$M + L \rightleftharpoons ML$$

$$K_d = [M][L]/[ML] \quad \textbf{(2.1)}$$

$$M_t = [M] + [ML] \quad \textbf{(2.2)}$$

$$L_t = [L] + [ML] \quad \textbf{(2.3)}$$

Substitute equations 2.2 and 2.3 into 2.1, it follows that

$$K_d = [M_t - ML][L_t - ML]/[ML] \quad \textbf{(2.4)}$$

$$[ML]K_d = [M_t][L_t] - [ML][L_t] - [ML][M_t] + [ML]^2 \text{ or} \quad \textbf{(2.5)}$$

$$[ML]^2 - (L_t + M_t + K_d) - (L_t + M_t) = 0 \quad \textbf{(2.6)}$$

which is expressed as

$$ML = \sqrt{(L_t + M_t + K_d)} - ((L_t + M_t + K_d)^2 - 4M_tL_t)/2 \quad \textbf{(2.7)}$$

Since,

$$[ML]/[M_t] = (E_i - E_0) / (E_f - E_0), \quad \textbf{(2.8)}$$

where E_0 is ellipticity of free macromolecule, E_f is the ellipticity when all the macromolecule is fully bound and E_i is the ellipticity at any given concentration of ligand, then, ML is given as

$$E_i = E_0 + (E_f - E_0) * \sqrt{(L_t + M_t + K_d)} - ((L_t + M_t + K_d)^2 - 4M_tL_t)/2\ [M_t] \quad \textbf{(2.9)}$$

2.2.2.2 Derivation of two-site binding isotherm.

The derivation of the 1:2 binding starts with two equilibrium binding constant expression (2.10 and 2.11) and two mass balance equations (2.12 and 2.13) obtained from two equilibrium equations. The AQ ligand, L is assumed to bind reversibly to macromolecule, M to form ML with association constant K_1. A second ligand L then binds to ML with an association constant, K_2. The total concentrations of M and L are denoted M_t and L_t, respectively, and the combined ellipticity of M, ML, and ML_2 is given by *E*. From the equilibrium condition and mass conservation, the following is obtained:

$$M + L \rightleftharpoons ML$$

$$ML + L \rightleftharpoons ML_2$$

$$K_1 = [ML]/([M][L]) \quad \textbf{(2.10)}$$

$$K_2 = [ML_2]/([ML][L]) \quad \textbf{(2.11)}$$

$$M_t = [M] + [ML] + [ML_2] \quad \textbf{(2.12)}$$

$$L_t = [L] + [ML] + 2[ML_2] \quad \textbf{(2.13)}$$

Substituting equations 2.10 and 2.11 into 2.12, it follows that

$$[M] = [M_t]/1+K_1[L] + K_1K_2[L]^2 \quad \textbf{(2.14)}$$

$$[ML] = K_1[L][M_t]/1+K_1[G] + K_1K_2[L]^2 \quad \textbf{(2.15)}$$

$$[ML_2] = K_1K_2[L]^2[M_t]/1+K_1[G] + K_1K_2[L]^2 \quad \textbf{(2.16)}$$

Substituting equations 2.15 and 2.16 into equation 2.13 yields equation 2.17, in which the unknown variables are [L], K_1, and K_2.

$$[L]_t = [L] + (K_1[L] + 2K_1K_2[L]^2)[M_t]/1+K_1[L] + K_1K_2[L]^2 \quad \textbf{(2.17)}$$

Rearranging equation 2.17 results in a cubic equation for [L],

$$A[L]^3 + B[L]^3 + C[L] + D = 0$$

where,

$$A = K_1K_2$$

$$B = K_1 + 2K_1K_2[M_t] – K_1K_2[L_t]$$

$$C = 1 + K_1[M_t] – K_1[L_t]$$

$$D = - [L_t]$$

The relationship of the ellipticity data to [L] and [M] is:

$$E_i = E_M[M] + E_{ML}[ML] + E_{ML2}[ML_2] \quad \textbf{(2.18)}$$

(L does not have an ellipticity value).

Substituting equations 2.14-2.16 into equation 2.18 yields

$$E_i = (E_M + E_{ML}K_1[L] + E_{ML2}K_1K_2[L]^2)[M_t]/1+K_1[L] + K_1K_2[L]^2 \quad \textbf{(2.19)}$$

Equation 2.19 was used to generate a binding curve for **AQ II** with DNA. The ellipticity value for **M** was -21 and those for **ML** and **ML_2** were assumed to be -4 and -3, respectively.

2.2.3 *SPR: Calculated RU versus Observed RU versus Fitted RU values.*

SPR is an effective tool to measure the affinity and study the kinetics of most biomolecular interactions because of its high sensitivity.[119-120] As such, SPR was used to quantitatively evaluate interactions between **AQ I-IV** and AT- and GC-rich DNA to gain insights into their binding affinities. The SPR experiments were performed with a four-channel BIAcore 2000 optical biosensor system (BIAcore, Inc.) and streptavidin coated sensor chip as previously described in Section 2.1.3.7. The instrument response (RU) in the steady state region is proportional to the amount of bound drug.

The predicted maximum response per bound compound in the steady state region ($RU_{max.pred}$) was determined from the DNA molecular weight (MW_{DNA}), the amount of DNA on

the flow cell, the compound molecular weight ($MW_{compound}$), and the refractive index gradient ratio of the compound and DNA (RI). For this series of compound, RI was taken to be 1.2.[79]

$$RU_{max.\ pred.} = (RU_{DNA} \times MW_{compound} \times RI)/MW_{DNA} \quad \textbf{(2.19)}$$

The predicted response for each AQ ligand is given in Table 2.2. We noted that, as the side chain increased in length from **AQ I-IV**,

a. the maximum RU values observed were increasingly lower than the $RU_{max.pred}$ values
b. the maximum RU values observed for the GC-rich series were much lower than the AT-rich series

The data was refitted with $RU_{max.pred}$ as an unknown variable using equation 2.2. The fitted values obtained for $RU_{max.pred}$ from non-linear least square fitting was similar to the calculated values for $RU_{max.pred}$ (Table 2.2).

The low values obtained for the maximum RU observed can be rationalized as:

- The binding constant decreased as the AQ side chain increased in length; therefore, the DNA required a larger concentration along the AQ series for saturation. Since similar concentrations of AQ ligands were used for titration of **AQ I-IV**, the DNA will be less saturated along the series, hence the lower RU values.

- The binding constants for the AT-rich series were ≥ 3 that of the GC-rich sequence. Therefore, the GC-rich series required a higher concentration of ligand for saturation. Since similar concentrations of ligand were used for both series, the GC-rich series displayed lower RU vales.

2.2.4 *ITC: Determination of the heats of dilution for AQ I-IV.*

Control experiments to determine the heats of dilution for the DNA and each AQ ligand were carried out by injecting MES buffer solution into DNA or ligand into buffer alone. The di-

lution heat for the DNA was small and constant and was subtracted from the heat of the AQ ligand binding to DNA per injection. The corrected binding isotherm for ligand binding to DNA was fit to an appropriate binding model with Origin 7.0, using equilibrium binding constants obtained from SPR to determine the binding parameter $\Delta H_{observed}$.

The heat of dilution titration profile for each ligand was typical for a molecule that self-associate. Calorimetric dilution experiments alone cannot discriminate between dimerization and formation of higher order aggregates,[87] however, Haq and coworkers have shown that similar AQ ligands are predominantly dimers [46]. In addition, a dimer dissociation curve is expected to obey a hyperbolic behavior for the dissociation of strong dimers, that is, each successive injection at the start of an ITC experiment will be expected to result in a slightly lower heat uptake due to the tendency of dimers not to fully dissociate even at lower monomer concentrations in the calorimetric cell.[121] The heat uptake will continue to decrease slowly with further injections and eventually level out at zero as the concentration of monomers in the calorimetric cell reaches beyond the dissociation constant. Dissociation of higher order aggregates is reported to frequently give sigmoidal dilution thermograms, in contrast to the hyperbolic shapes for the dimer dissociation. The dilution isotherm was therefore fit to a dimer dissociation model to determine $\Delta H_{dissociation}$ which was subsequently subtracted from the $\Delta H_{observed}$ value to give a corrected value for the binding-induced enthalpy change, Table 2.3.

2.2.4.1 Derivation of the monomer-dimer equilibrium model.

The derivation of the heat of dissociation due to dimerization is according to that presented in the ITC Data Analysis Origin Tutorial Guide, Version 7.0- January 2004.

The AQ ligand, L is assumed to bind reversibly to another AQ ligand, L to form L_2 with a dissociation constant, K_{diss}. Injection of the L_2 dimer into the calorimetric cell results in some

heat effects, ΔH_{diss} due to dissociation of the ligand as described below (taken from VP-ITC Manual):

$$L_2 \overset{\Delta H_{diss}}{\rightleftharpoons} 2L \qquad K_{diss} = [L]^2/[L_2]$$

The total concentration of ligand (given as equivalent monomer concentration) after the i^{th} injection, C_i, is the sum of the actual monomer concentration $[L]_i$ plus 2 times the aggregate concentration $[L_2]_i$.

$$C_i = [L]_i + 2[L_2]_i \qquad \textbf{(2.22)}$$

Using the expression for the dimer dissociation constant to obtain $[L]_i$ in terms of $[L_2]_i$ leads to the equation:

$$C_i = (K_{diss} * [L_2]_i)^{1/2} + 2[L_2]_i \qquad \textbf{(2.23)}$$

A similar expression applies to the solution in the syringe of fixed concentration C_{syr}

$$C_{syr} = (K_{diss} * [L_2]_{syr})^{1/2} + 2[L_2]_{syr} \qquad \textbf{(2.24)}$$

Since C_{syr} is known and C_i can be determined from C_{syr} knowing injection volumes, then $[L_2]_{syr}$ and $[L_2]_i$ can be determined from equations 2.23 and 2.24 if K_{diss} is assigned.

In the ITC dilution experiment, we measured the heat change q_i when a small volume dV_i of concentrated solution is injected into the calorimeter cell (constant volume V_0) containing initially buffer but, for later injections, more dilute solution. The heat arises from dimers present in higher concentration solution that dissociate upon entering the lower concentration in the cell. For the i^{th} injection of volume dV_i made into a fixed volume cell (V_0) heat is given by:

$$q_i = \Delta H_{diss}[L_2]_{syr}dV_i - \Delta H_{diss}([L_2]_I - [L_2]_{i-1}) * (V_o + dV_i/2) \qquad \textbf{(2.25)}$$

The $(V_o + dV_i/2)$ factor is an effective volume which takes into account the displacement which occurs in a total filled cell.

In the experiments performed, we noted the dilution profile of **AQ IV** had an exothermic portion, which was not seen for the other AQ ligands. The exothermic portion of the **AQ IV** dilution curve may be heat due to differences in the dilution of monomers and dimers that takes place with the injection, assumed to be constant for all injections. Dilution of the AQ ligands involves hydration of the polyethylene glycol side chain. In our MD simulations, we have shown that the hydration of **AQ IV** was significantly more hydrated in solution compared to the other three AQ ligands.[65] It is therefore not surprising that the dilution titration profile for **AQ IV** was somewhat different from the other three ligands.

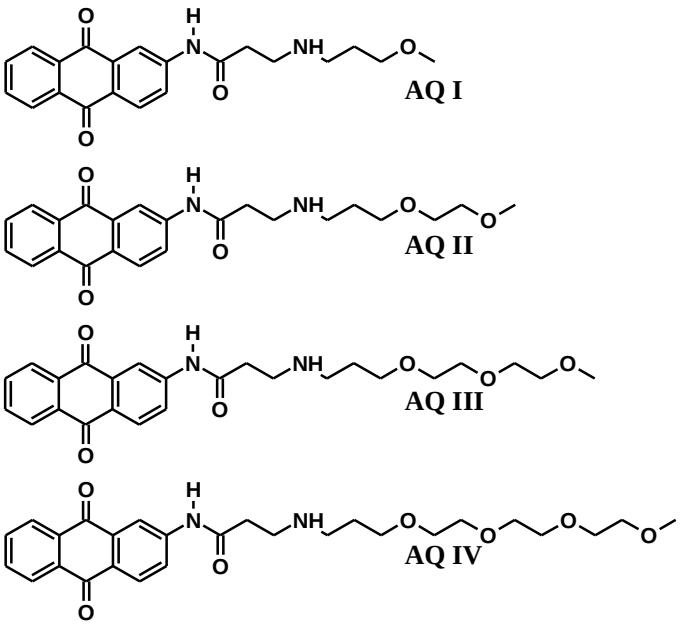

5'-biotin-CGCGCGCGTTTTCGCGCGCG

5'-biotin-CATATATATCCCCATATATATG

Figure 2.1: Anthraquinone intercalators, **AQ I-IV**, used in this study.

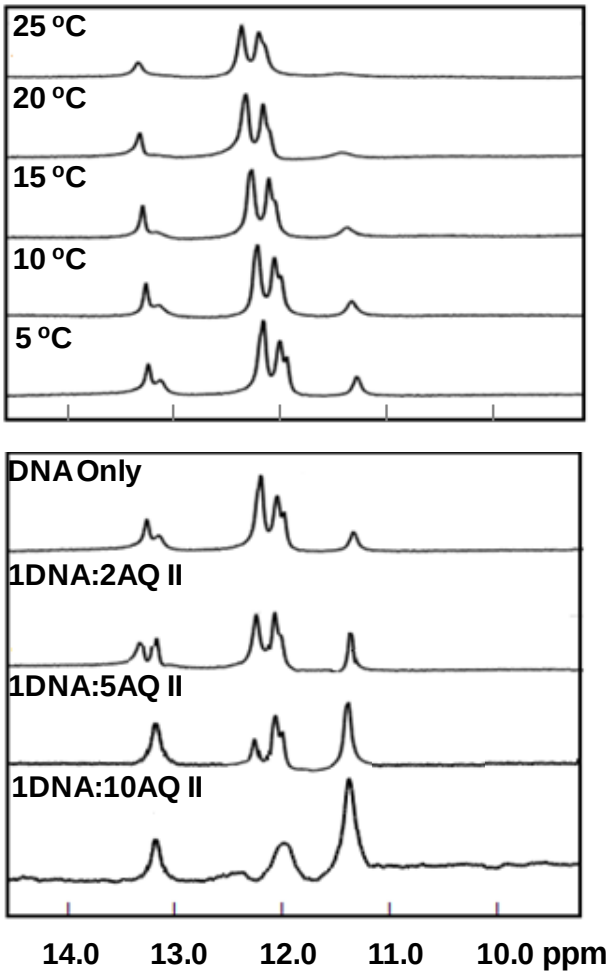

Figure 2.2: Downfield region of the ^{1}H NMR spectra of AT-rich DNA hairpin.
Top: Spectra as a function of temperature. The peaks at 5 ^{o}C had the best resolution. Bottom: ***AQ II****-DNA complex showing resonance of DNA imino protons at 5 ^{o}C; the* ***AQ II****-DNA ratio is given to the left.*

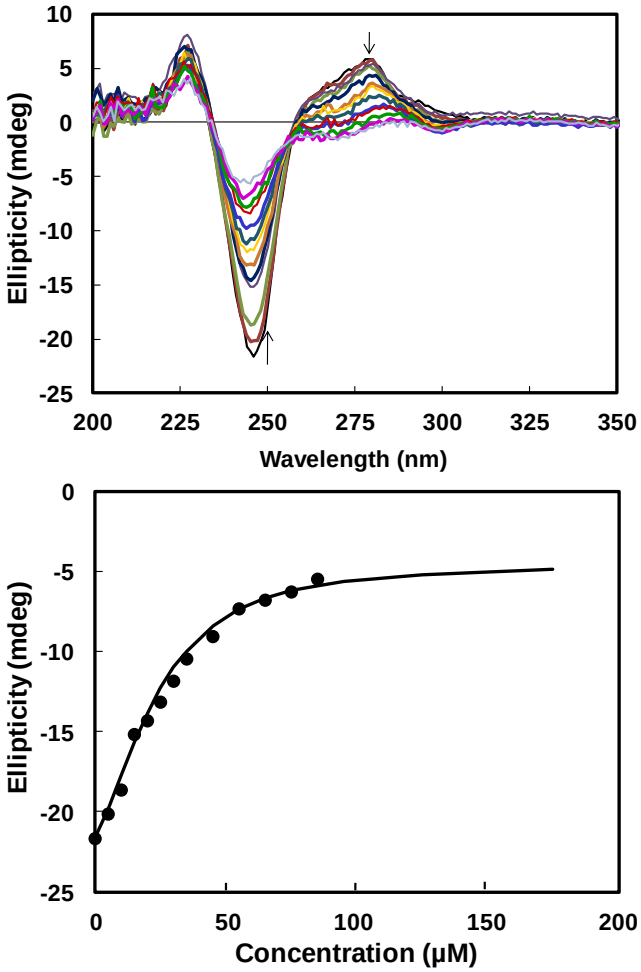

Figure 2.3: CD spectral titration of AQ II with 10 μM AT-rich DNA hairpin in MES10 buffer, pH 6.24 and 25 ^{o}C.
*Top: CD spectra of **AQ II** with AT-rich DNA at various DNA:**AQ II** ratios (r_i = 0 to 8.0). Bottom: The observed ellipticity at 244 nm as a function of the concentration of **AQ II** (closed circles) and a calculated binding curve (solid line) using data from the SPR K_1 and K_2 values.*

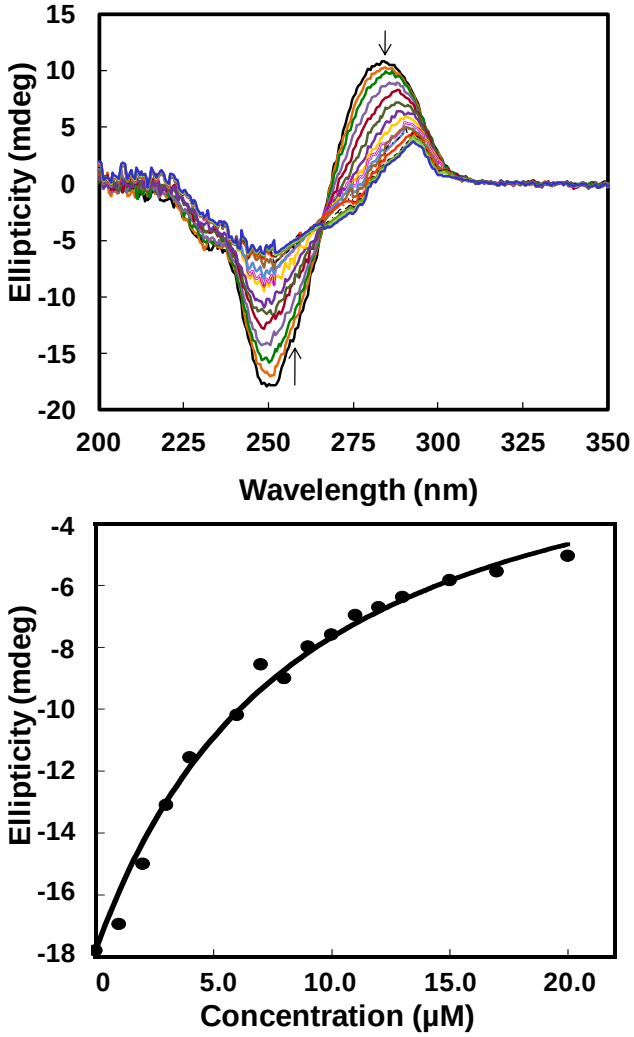

Figure 2.4: CD spectral titration of **AQ II** with 10 μM GC-rich DNA hairpin in MES10 buffer, pH 6.24 and 25 °C.
*Top: CD spectra of **AQ II** with AT-rich DNA at various DNA:**AQ II** ratios (r_i = 0 to 20). Bottom: The observed ellipticity at 250 nm and the concentration of **AQ II** were fitted with a one-site binding model to obtain an equilibrium binding constant, K_1 of 1.4 x 10^4 M^{-1}.*

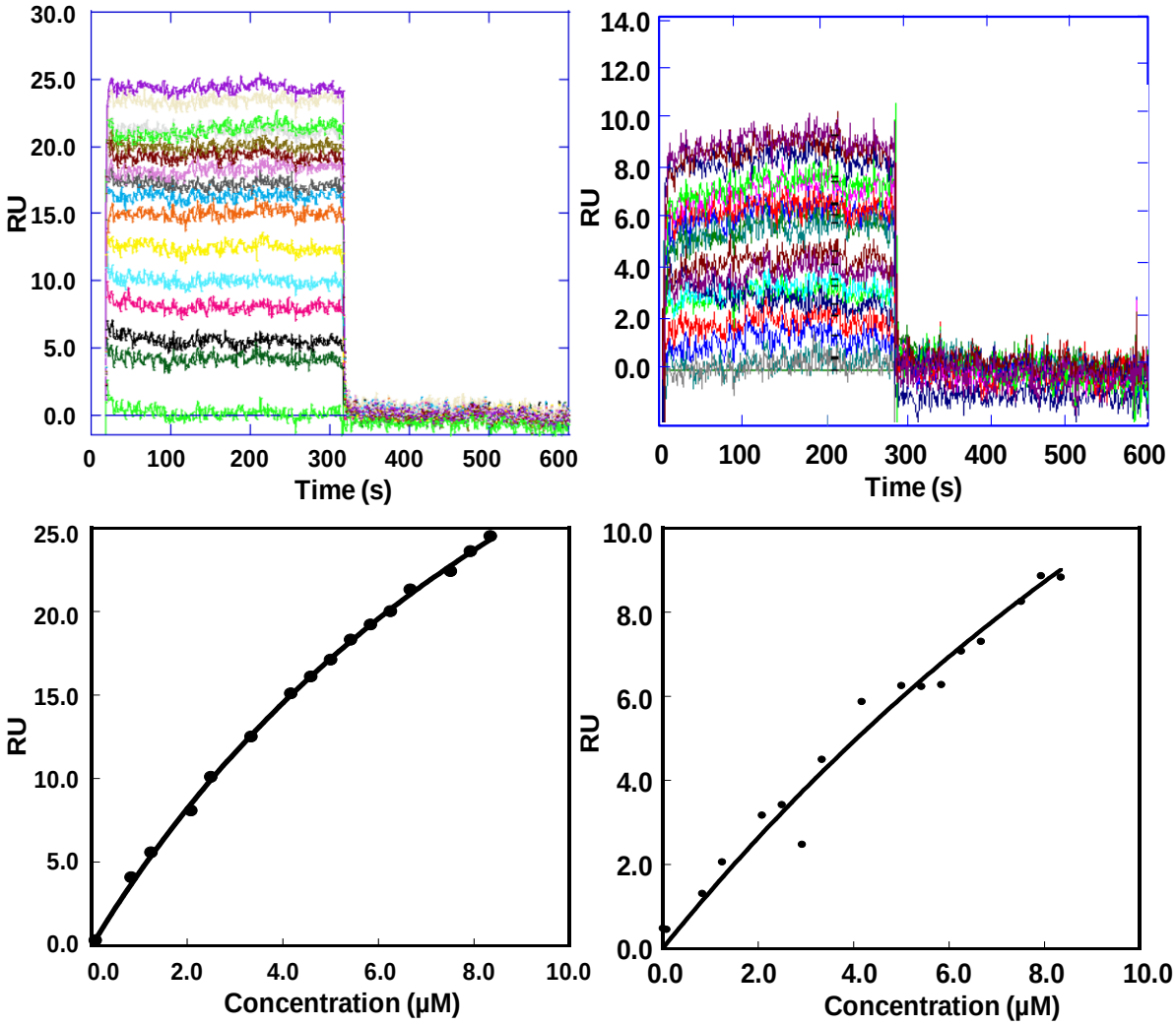

Figure 2.5: SPR sensograms for AQ II with AT-rich and GC-rich DNA.
*Top: SPR sensograms for **AQ II** with AT-rich (left) and GC-rich (right) DNA hairpin in MES 10 buffer, pH 6.24 at 25 °C. Concentrations of **AQ II** ranged from 0-10 μM from bottom to top. Bottom: Conversion of the SPR sensograms to a binding isotherm plotting RU values from the steady-state region of the SPR sensogram versus the **AQ II** concentration. The data were fitted to a two-site binding model for the AT-hairpin and a one-site binding model for the GC-hairpin using eq 5.*

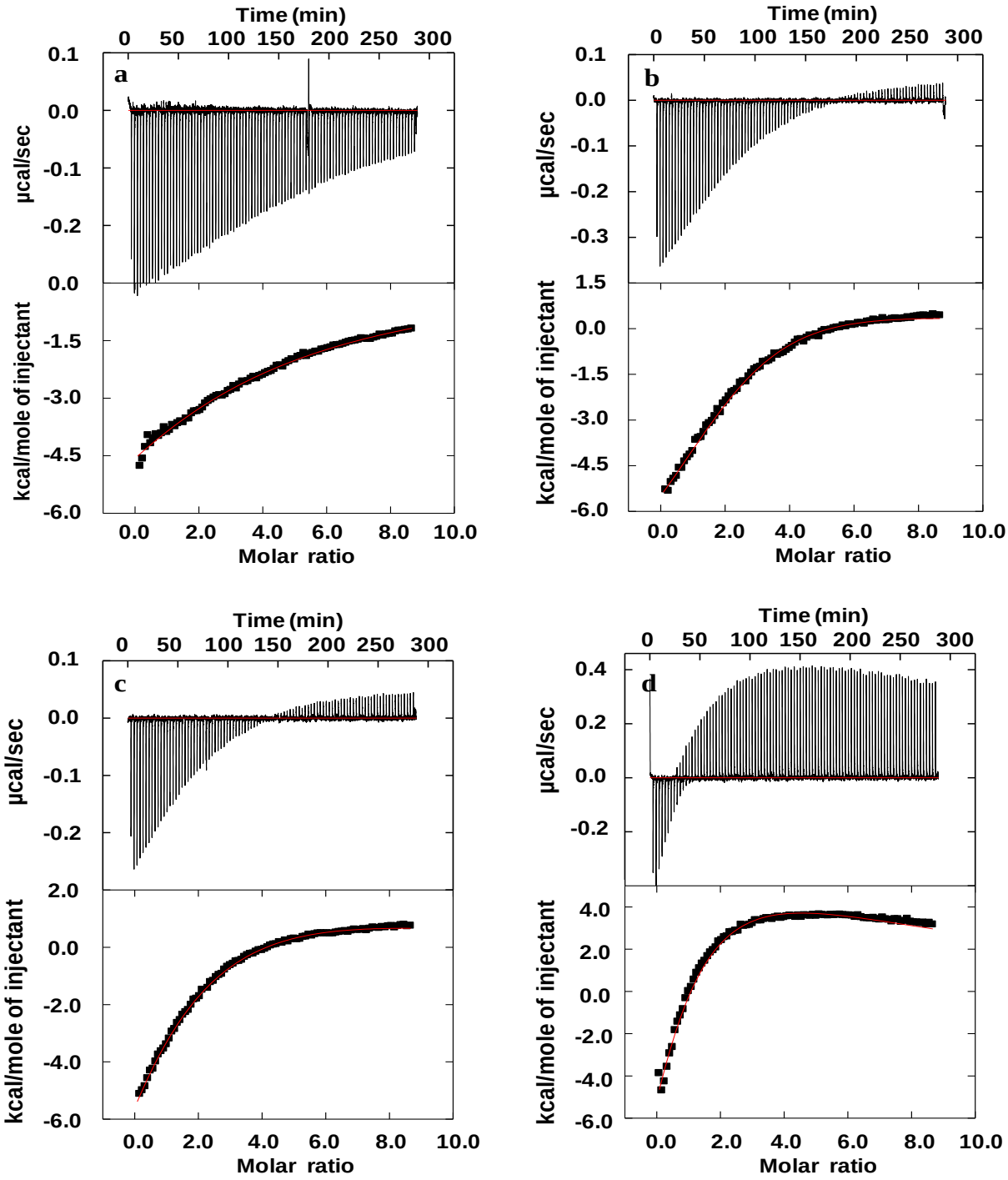

Figure 2.6: ITC curve for the binding of AT-rich DNA hairpin to a) **AQ I**, b) **AQ II**, c) **AQ III**, and d) **AQ IV**.

*Isothermal titrations consisted of ~95 injections (3 µL) of 300 µM **AQ I-IV** ligand into a calorimetric cell containing 10 µM of AT-rich DNA hairpin. The top panels are plots of the baseline corrected experimental data. The lower panels shows the results converted to molar heats and plotted against the compound to DNA molar ratio. Experiments were carried out in MES 10 buffer at 25 ^{o}C. The data were fitted to a two-site binding model.*

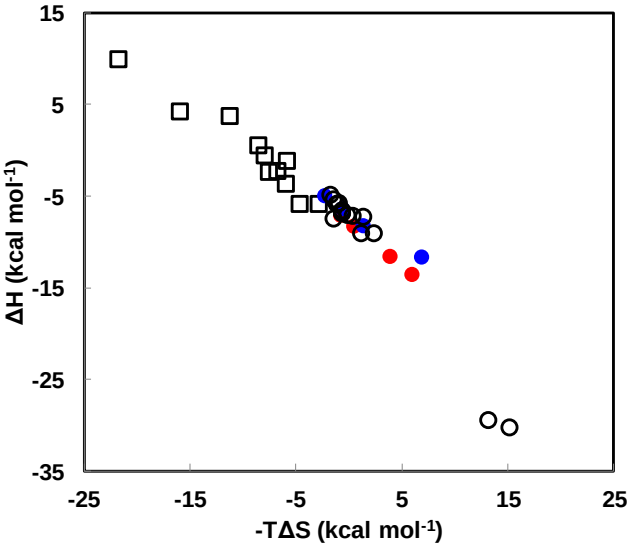

Figure 2.7: Entropy-enthalpy compensation plot for drug-DNA binding data.
*The black open squares are groove binders, and the black open circles are intercalators from the literature. The blue circles are **AQ I-IV** with AT-rich DNA and red circles are **AQ I-IV** with GC-rich DNA. Data were taken from ref 69.*

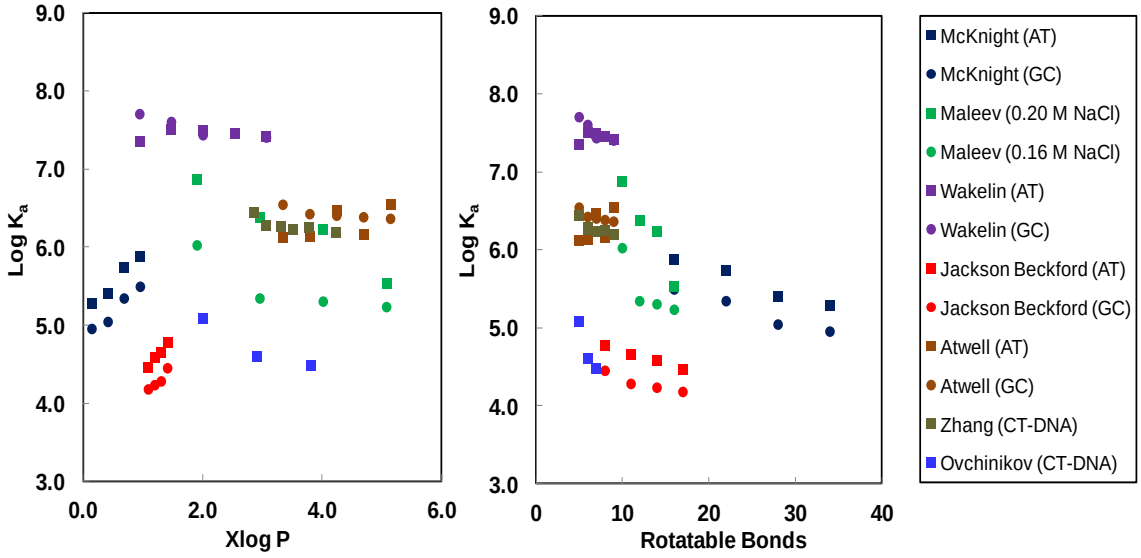

Figure 2.8: Plot of the a) hydrophobicity (Xlog P) and b) rotatable bonds of various intercalators in the literature as a function of their binding constant.
References are given in the text.

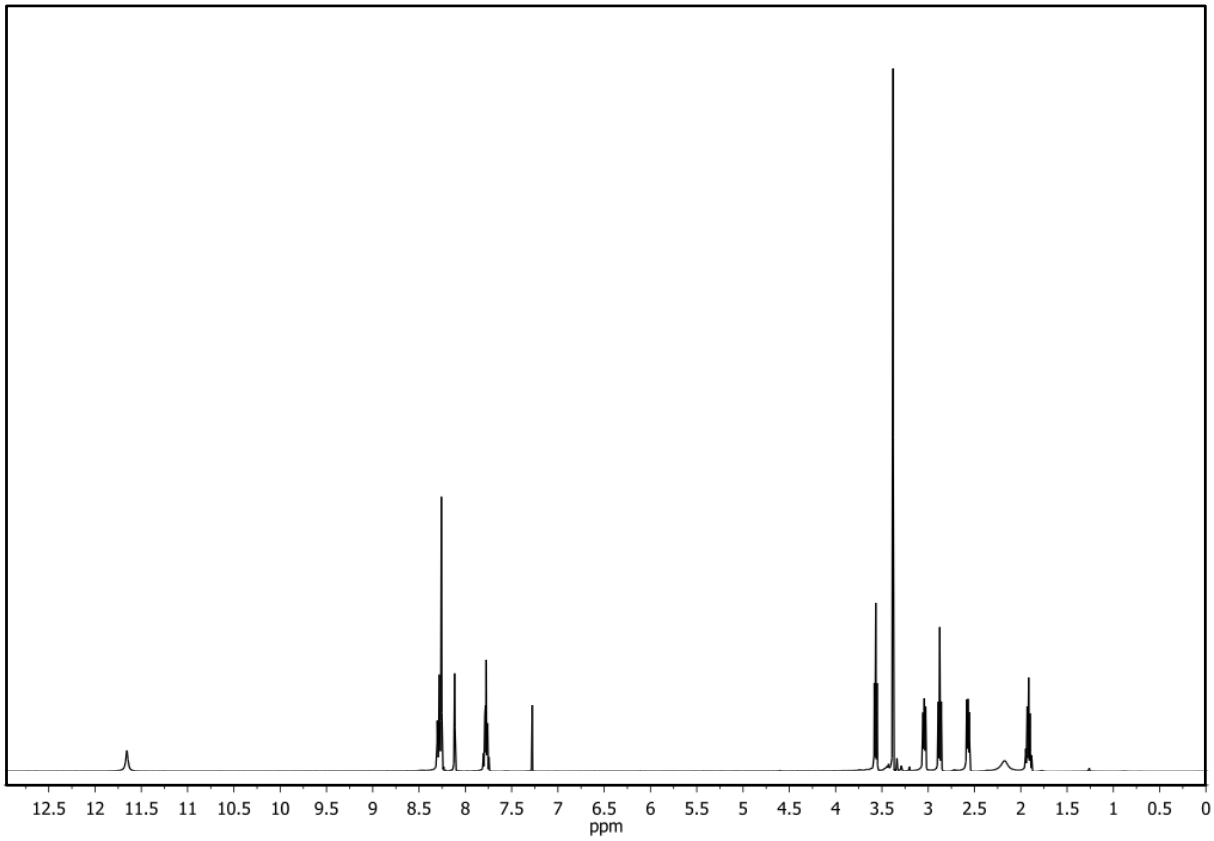

Figure 2.9 (S1): ^{1}H NMR spectrum of **AQ I** in chloroform.

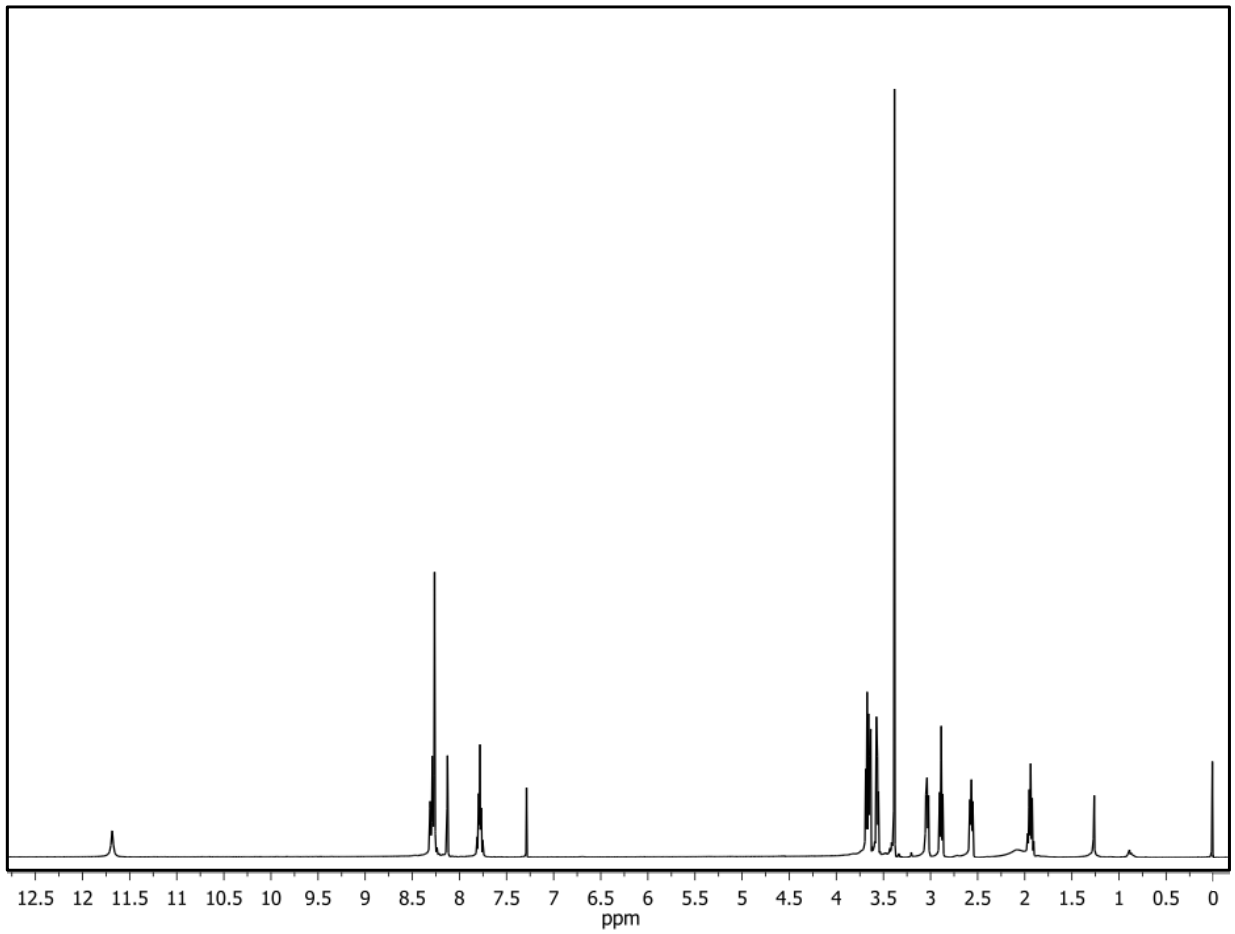

Figure 2.10 (S2): ^{1}H NMR spectrum of **AQ II** in chloroform.

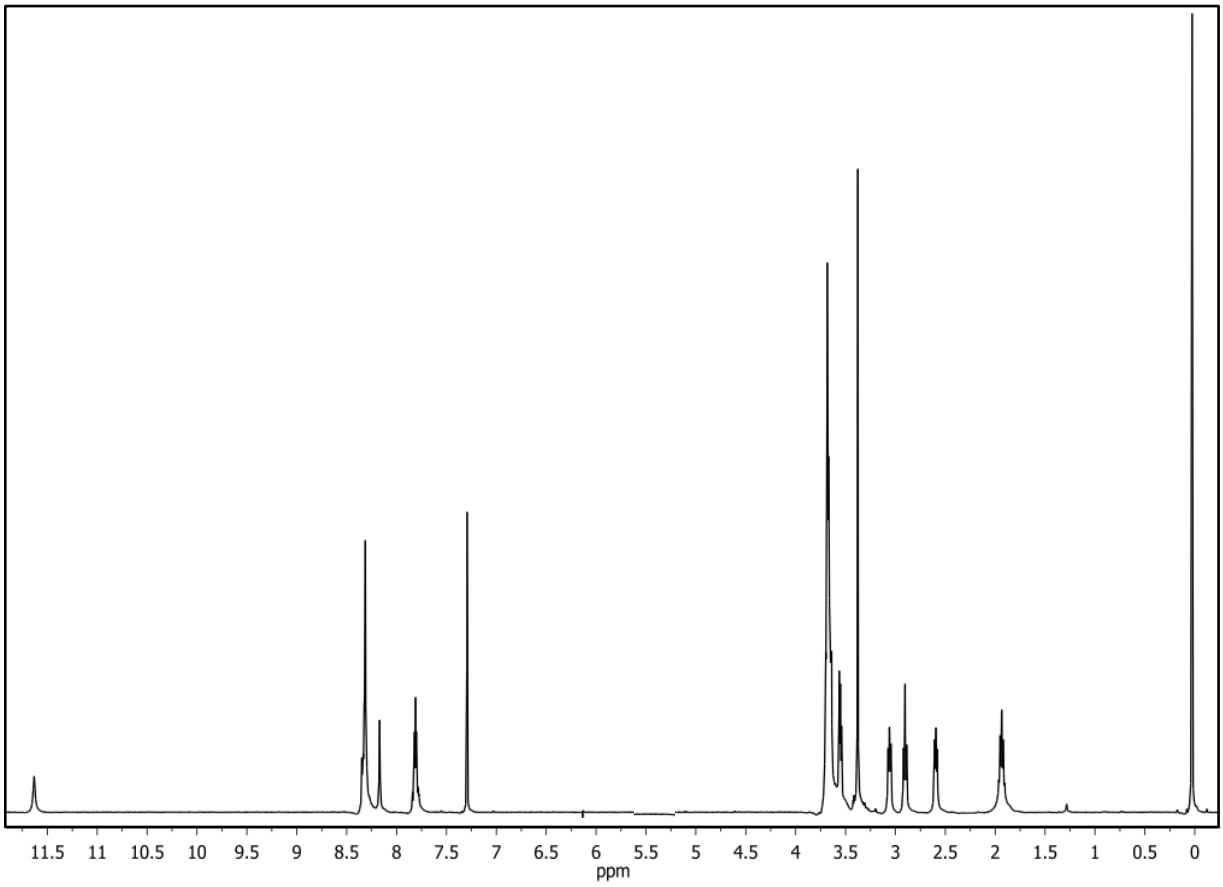

Figure 2.11 (S3): ^{1}H NMR spectrum of **AQ III** in chloroform.

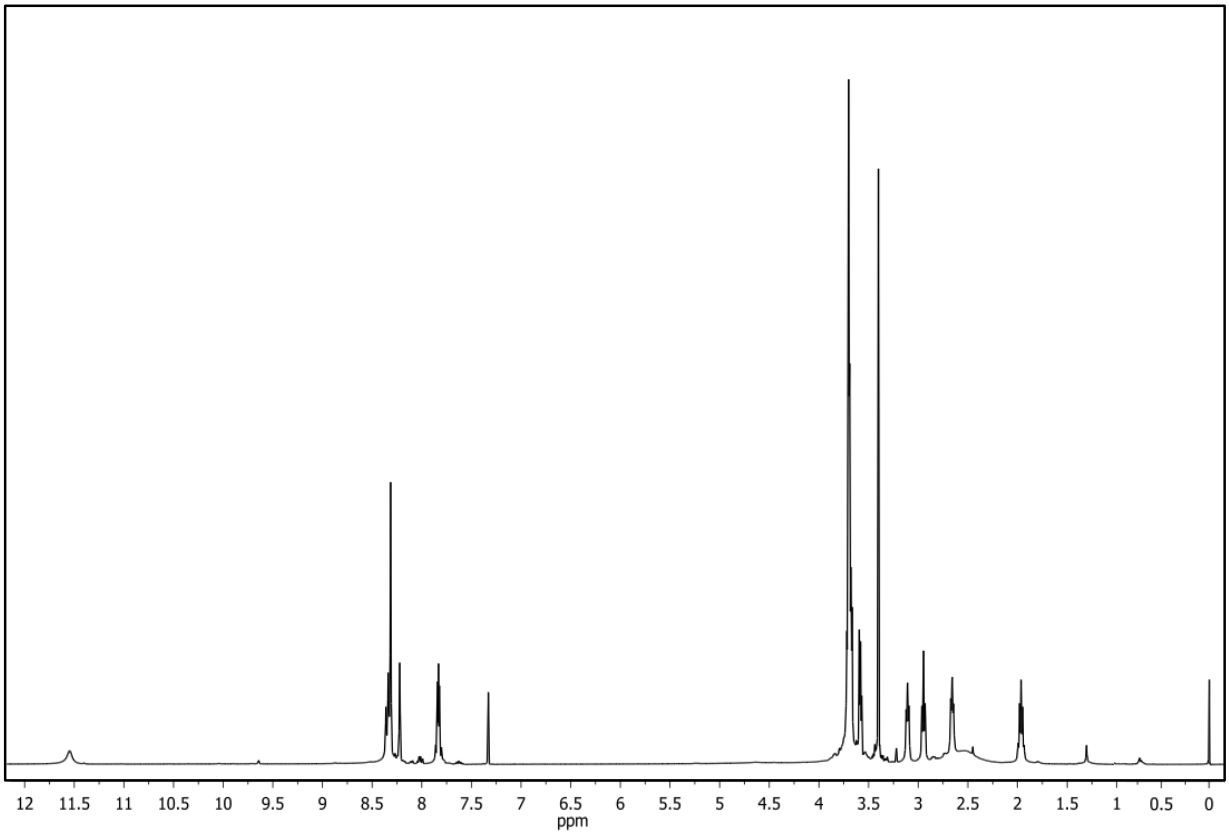

Figure 2.12 (S4): ^{1}H NMR spectrum of **AQ IV** in chloroform.

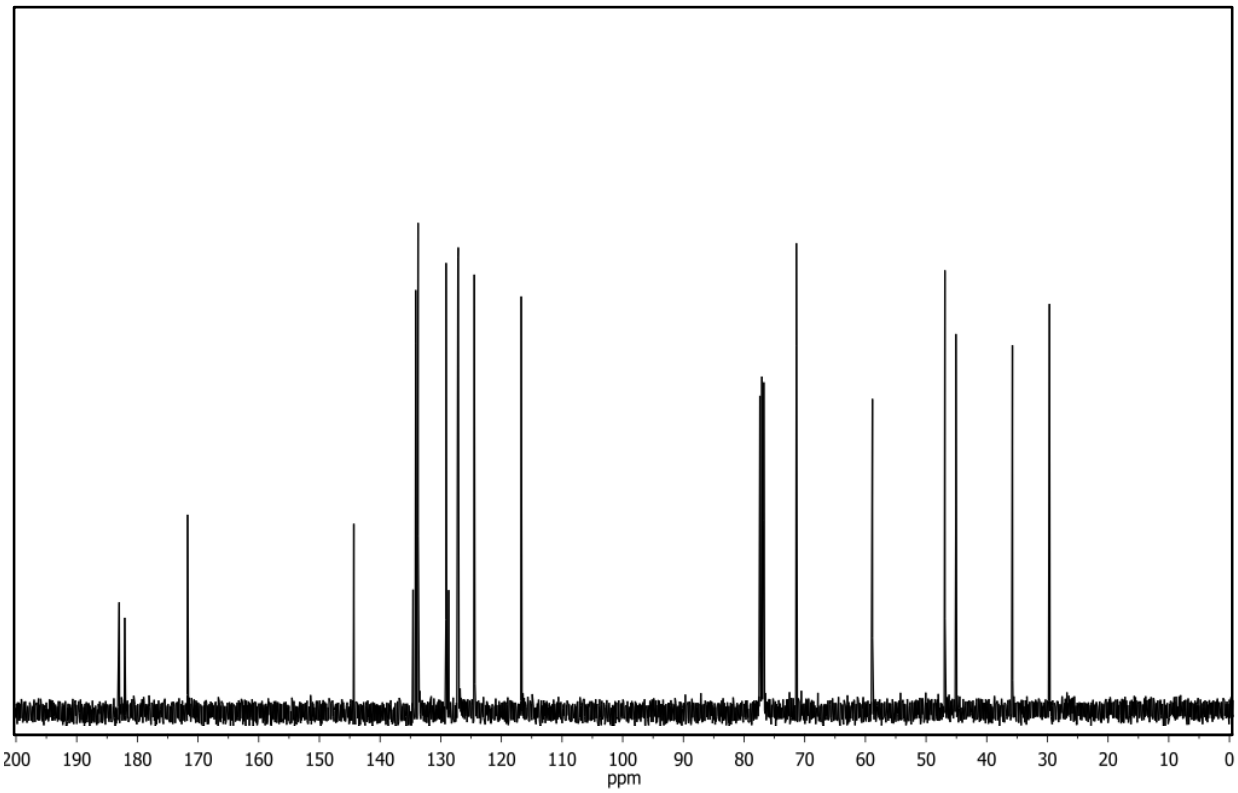

Figure 2.13 (S5): ^{13}C NMR spectrum of **AQ I** in chloroform.

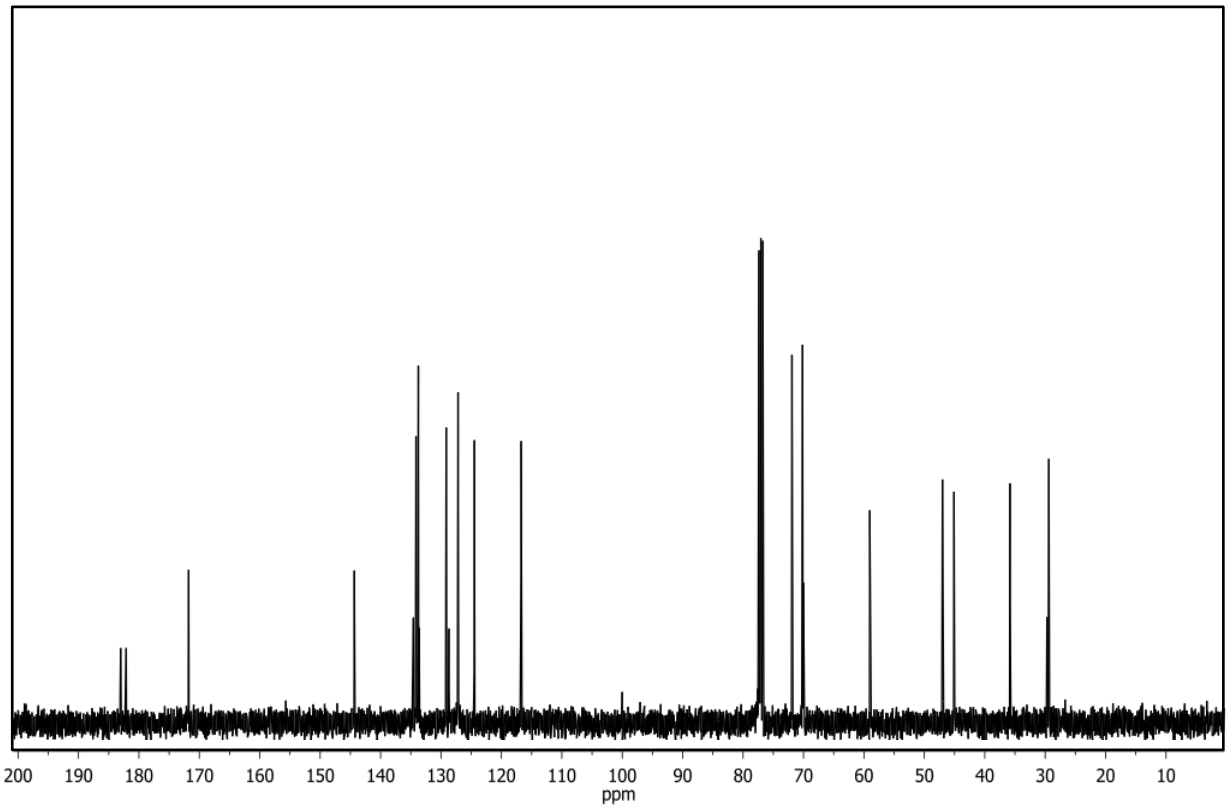

Figure 2.14 (S6): ^{13}C NMR spectrum of **AQ II** in chloroform.

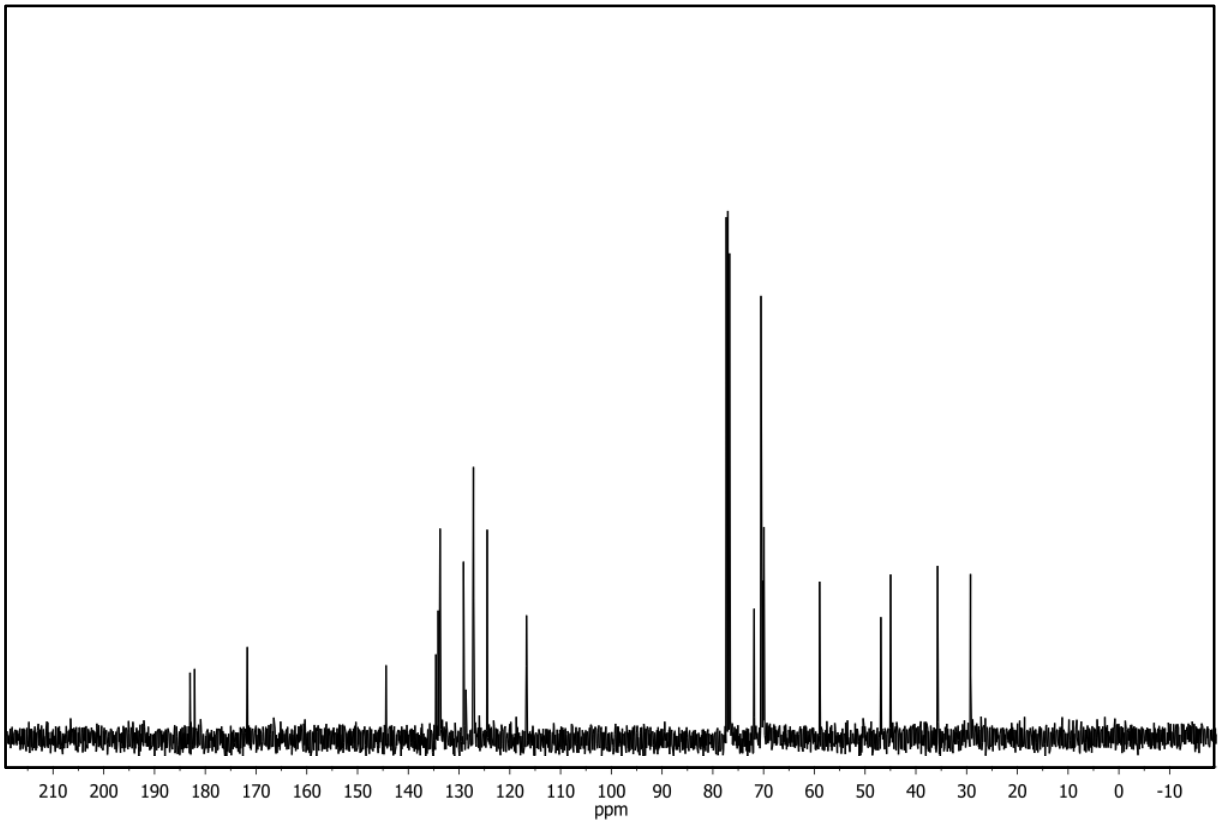

Figure 2.15 (S7): ^{13}C NMR spectrum of **AQ III** in chloroform.

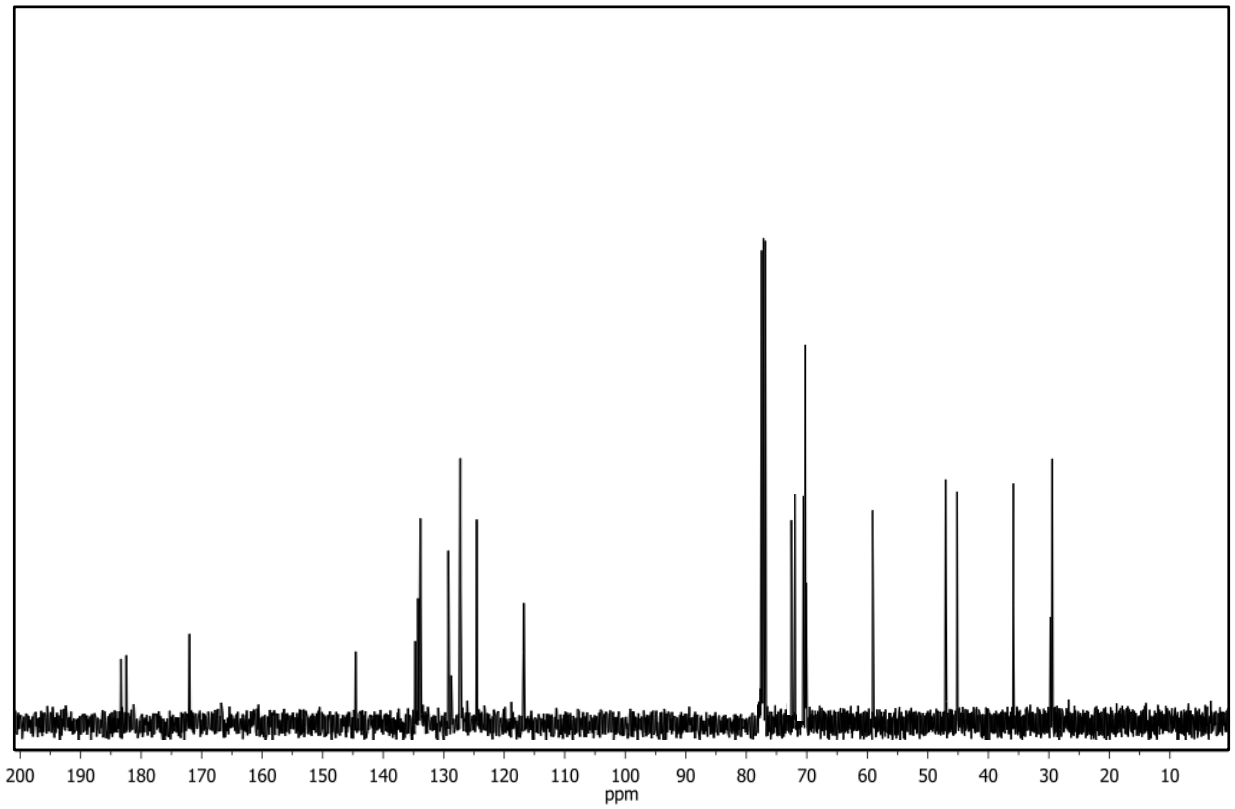

Figure 2.16 (S8): ^{13}C NMR spectrum of AQ IV in chloroform.

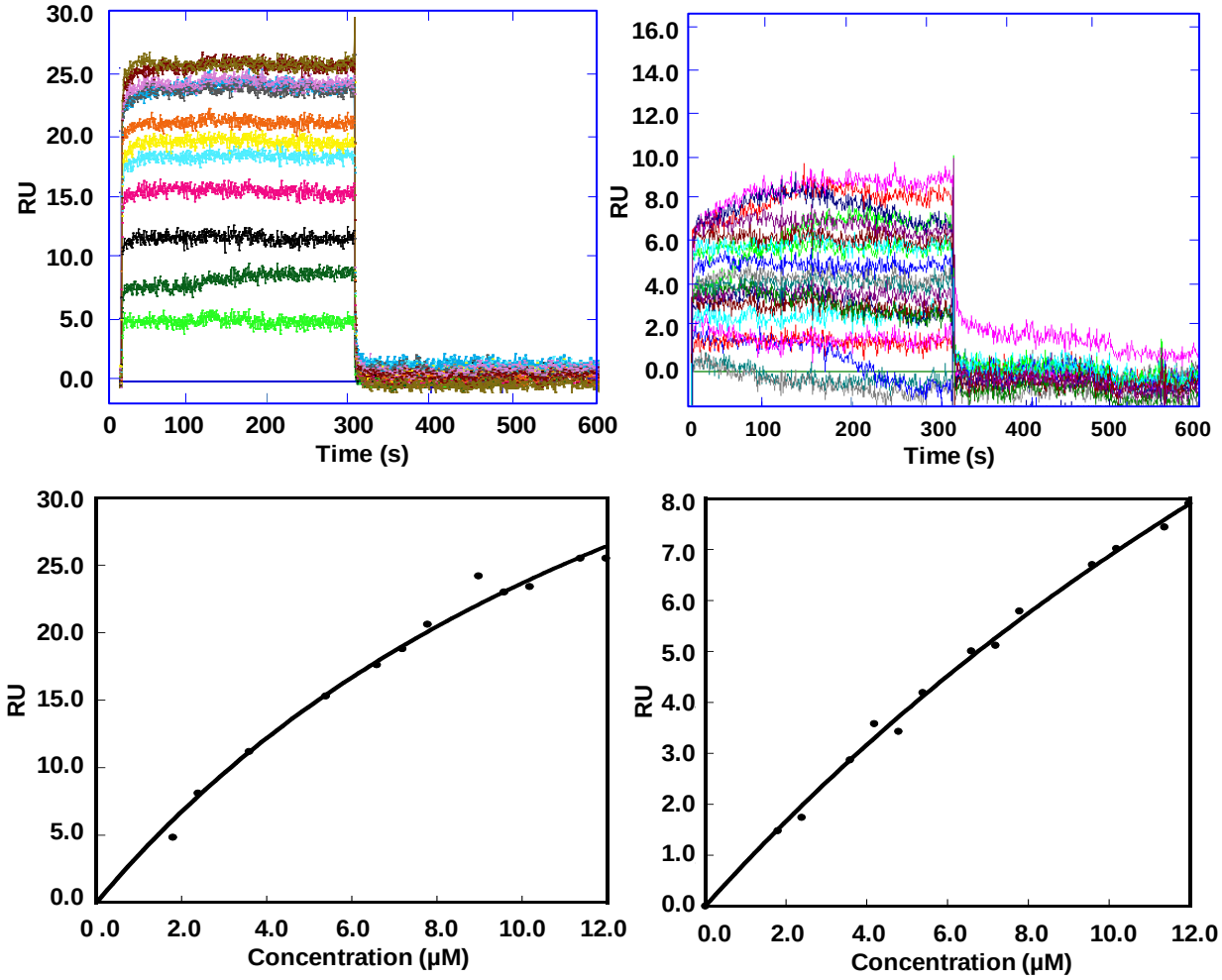

Figure 2.17 (S9): SPR sensograms for **AQ I** with AT-rich and GC-rich DNA.
*Top: SPR sensograms for **AQ I** with AT-rich (left) and GC-rich (right) DNA hairpin in MES 10 buffer, pH 6.24 at 20 ^{o}C. Concentrations of **AQ I** ranged from 0 -12 μM from bottom to top. Bottom: Conversion of the SPR sensograms to a binding isotherm plotting RU values from the steady-state region of the SPR sensogram versus the **AQ II** concentration (bottom). The data were fitted to a two-site binding model for the AT-hairpin and a one-site binding model for the GC-hairpin using eq 5.*

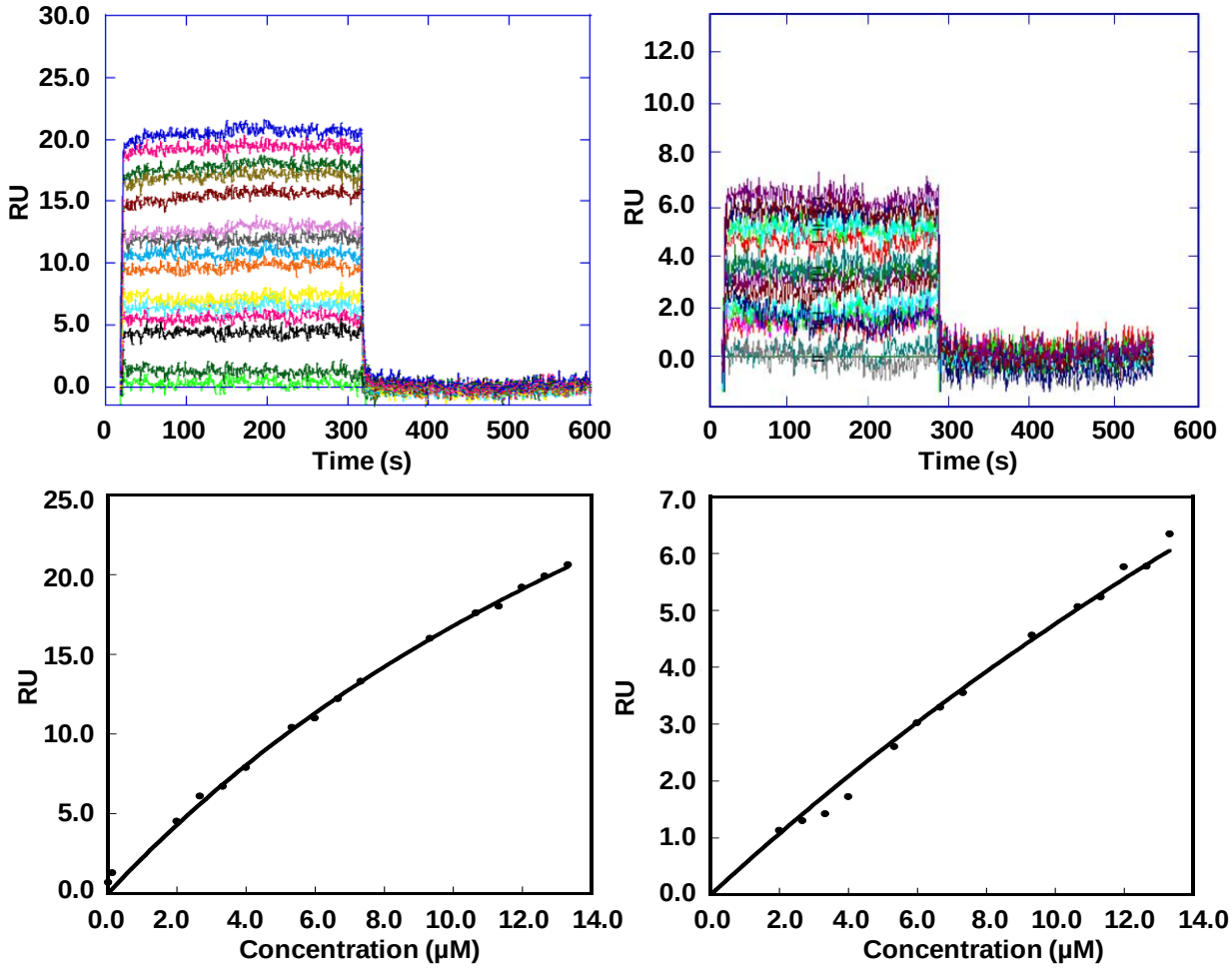

Figure 2.18 (S10): SPR sensograms for **AQ III** with AT-rich and GC-rich DNA.
*Top: SPR sensograms for **AQ III** with AT-rich (left) and GC-rich (right) DNA hairpin in MES 10 buffer, pH 6.24 at 20 °C. Concentrations of **AQ III** ranged from 0 -14 μM from bottom to top. Bottom: Conversion of the SPR sensograms to a binding isotherm plotting RU values from the steady-state region of the SPR sensogram versus the **AQ III** concentration (bottom). The data were fitted to a two-site binding model for the AT-hairpin and a one-site binding model for the GC-hairpin using eq 5.*

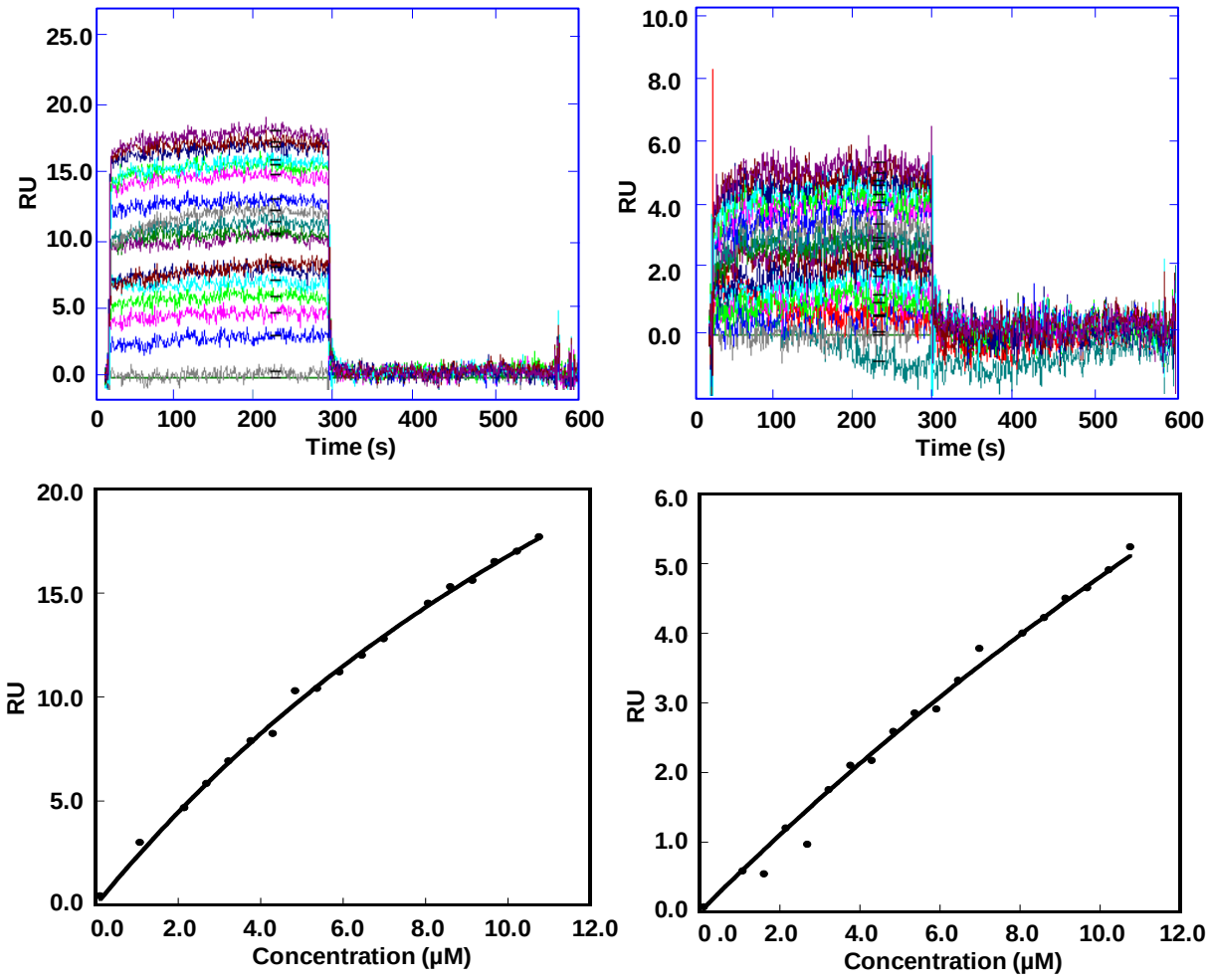

Figure 2.19 (S11): SPR sensograms for **AQ IV** with AT-rich and GC-rich DNA.
*Top: SPR sensograms for **AQ IV** with AT-rich (left) and GC-rich (right) DNA hairpin in MES 10 buffer, pH 6.24 at 25 ^{o}C. Concentrations of **AQ IV** ranged from 0-12 μM from bottom to top. Bottom: Conversion of the SPR sensograms to a binding isotherm plotting RU values from the steady-state region of the SPR sensogram versus the **AQ IV** concentration (bottom). The data were fitted to a two-site binding model for the AT-hairpin and a one-site binding model for the GC-hairpin using eq 5.*

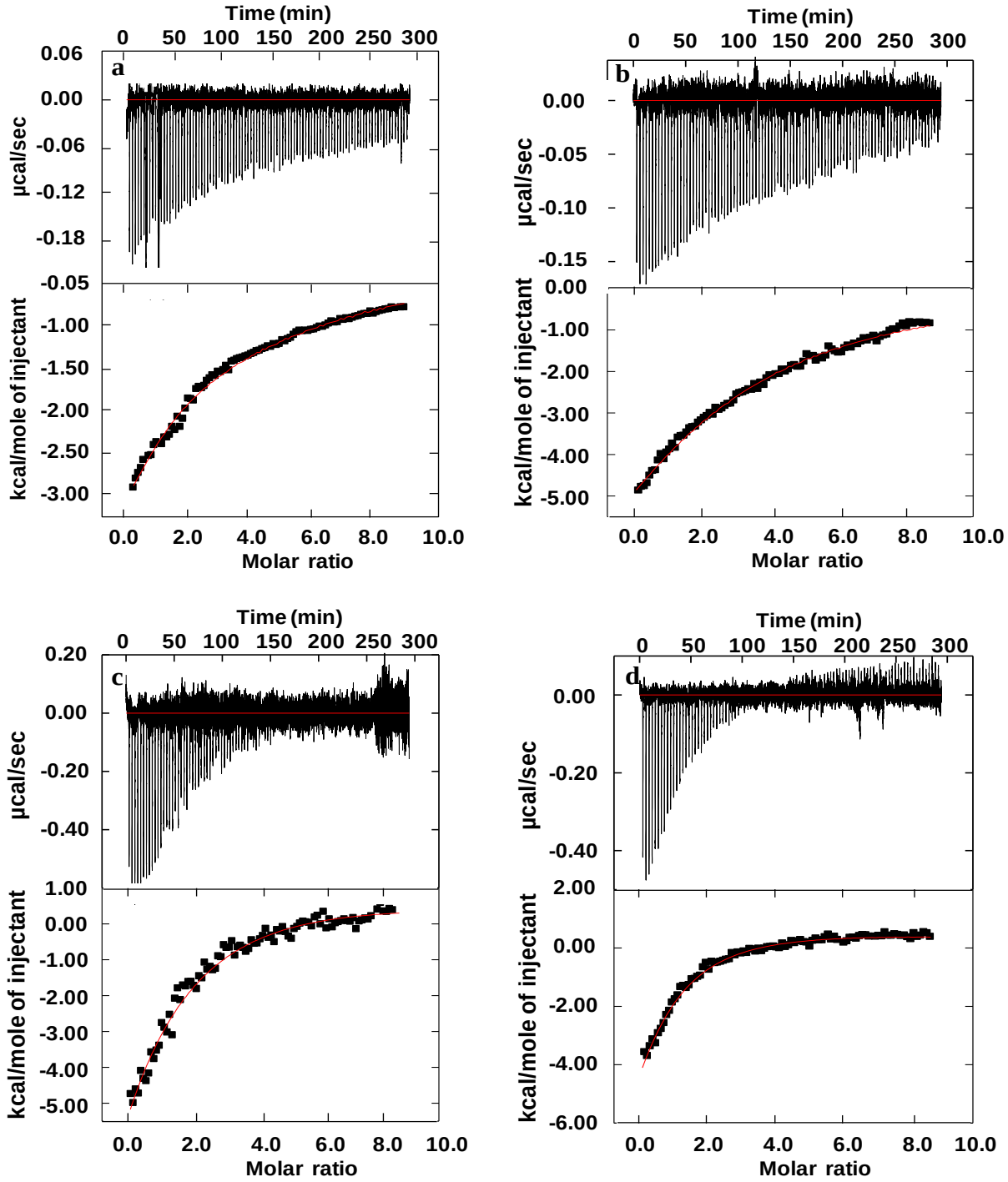

Figure 2.20 (S12): ITC curve for the binding of AT-rich DNA hairpin to a) **AQ I**, b) **AQ II**, c) **AQ III**, and d) **AQ IV**.
*Isothermal titrations consisted of ~95 injections (3 µL) of 300 µM **AQ I-IV** ligand into a calorimetric cell containing 10 µM of GC-rich DNA hairpin. The top panels are plots of the baseline corrected experimental data. The lower panels shows the results converted to molar heats and plotted against the compound to DNA molar ratio. Experiments were carried out in MES 10 buffer at 25 ^{o}C. The data were fitted to a two-site binding model.*

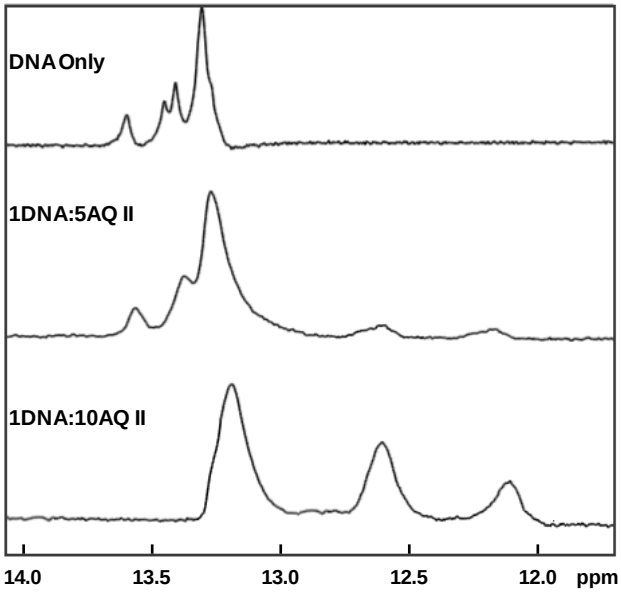

Figure 2.21 (S13): Downfield region of the ^{1}H NMR spectra of GC-rich DNA hairpin with **AQ II**. **AQ II**-DNA complex showing resonance of DNA imino protons at 5 ^{o}C; the **AQ II**-DNA ratio is shown on the left.

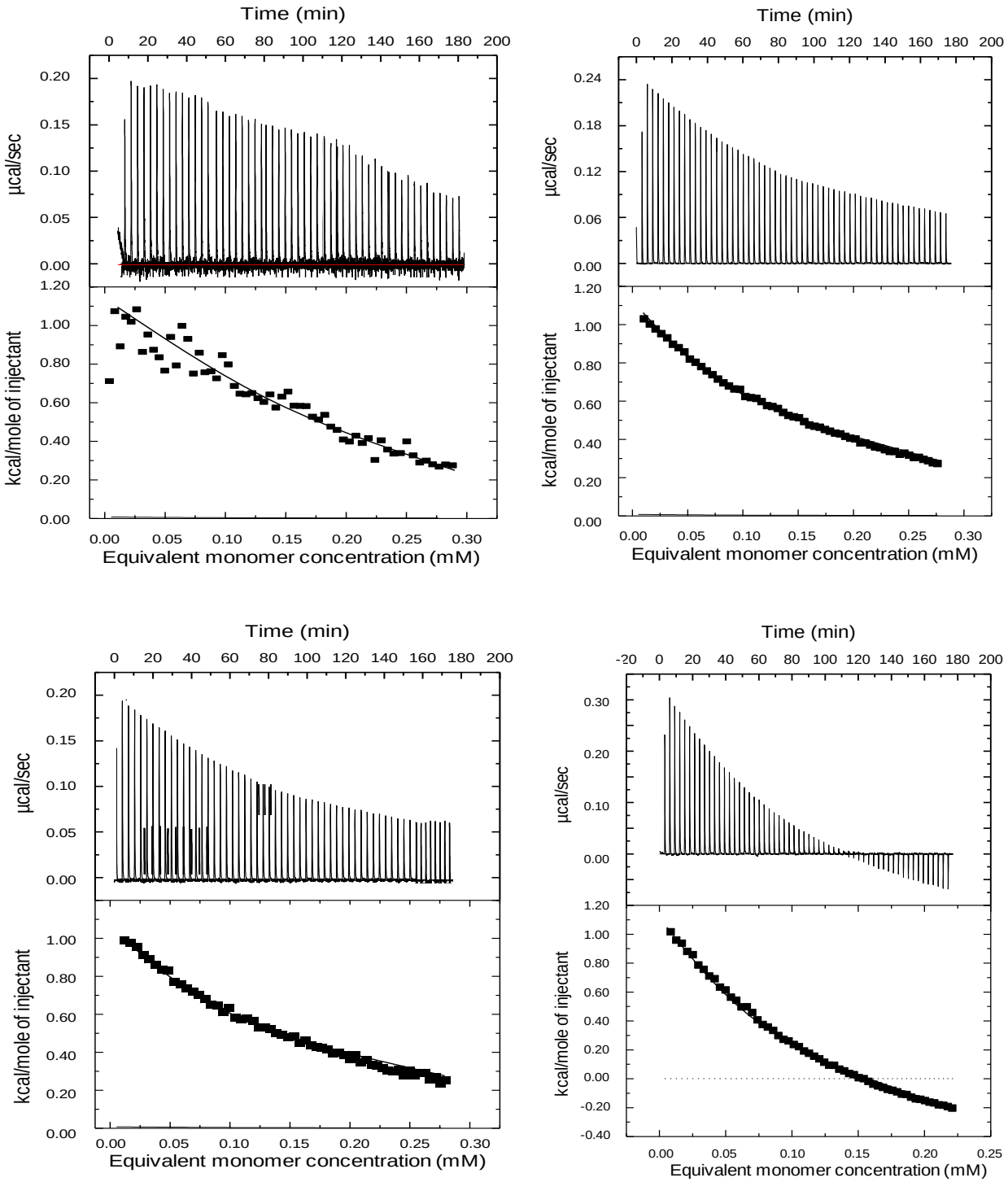

Figure 2.22 (S14): ITC curve for the dilution of 300 µM a) AQ I, b) AQ II, c) AQ III, and d) AQ IV in MES10 buffer.

The top panels are plots of the baseline corrected experimental data. The lower panels shows the results converted to molar heats and plotted against the equivalent monomer concentration of the ligand. All ligands were diluted in MES 10 buffer and experiments were carried out at 20 ^{o}C.

Table 2.1: Thermodynamic data for the interaction of **AQ I-IV** with DNA at 25 °C.*

Compound	DNA	K_1 (10^4 M^{-1})	K_2 (10^4 M^{-1})	ΔH (kcal/mol)	TΔS (kcal/mol)	ΔG_{obs} (kcal/mol)
AQ I	AT	11.3 ± 0.98	2.69 ± 0.50	-7.08 ± 0.34	0.15	-7.23
	GC	4.08 ± 0.06		-4.95 ± 0.07	1.24	-6.19
AQ II	AT	8.93 ± 0.26	2.19 ± 0.19	-8.28 ± 0.33	-0.54	-7.04
	GC	2.21 ± 0.03		-6.37 ± 0.04	0.63	-5.83
AQ III	AT	7.69 ± 0.30	1.93 ± 0.20	-11.6 ± 0.87	-4.69	-6.91
	GC	1.94 ± 0.03		-8.23 ± 0.09	-2.48	-5.75
AQ IV	AT	7.21 ± 0.22	3.09 ± 0.14	-13.6 ± 0.47	-7.20	-6.40
	GC	1.82 ± 0.04		-11.7 ± 0.19	-5.98	-5.72

* K_1 and K_2 are derived from the SPR data; ΔG_{obs} is calculated from K_1. ΔH is from ITC and TΔS is calculated from ΔH and ΔG_{obs}.

Table 2.2: Kaleidagraph fitting of the SPR data from the binding of **AQ I-IV** to AT- and GC-rich DNA hairpins.

Compound	DNA	K_1 (10^4 M^{-1})	K_2 (10^4 M^{-1})	RU_{pred}	RU_{obs}	RU_{fit}
AQ I	AT	11.3 ± 0.98	2.69 ± 0.50	24.3	25.5	25.8
	GC	4.08 ± 0.06		23.4	7.90	26.4
AQ II	AT	8.93 ± 0.26	2.19 ± 0.19	27.2	24.5	25.2
	GC	2.21 ± 0.03		26.5	8.86	30.7
AQ III	AT	7.69 ± 0.30	1.93 ± 0.20	30.2	20.6	24.5
	GC	1.94 ± 0.03		29.3	6.34	33.5
AQ IV	AT	7.21 ± 0.22	3.09 ± 0.14	33.1	17.7	27.2
	GC	1.82 ± 0.04		32.2	5.29	31.5

Table 2.3: Results from the dilution of **AQ I-IV** in MES10 buffer.

Compound	Dimerization Constants (10^3 M^{-1})	Heats of Dissociation (kcal/mol)
AQ I	5.4	0.98
AQ II	5.9	0.97
AQ III	4.3	1.08
AQ IV	5.1	0.95

2.3 References

1. Teulade-Fichou, M.-P., and Vigneron, J.-P. (2004) Interactions of macrocyclic compounds with nucleic acids, In *Small Molecule DNA and RNA Binders* (Demeunynck, M., Bailly, C., and Wilson, W. D., Eds.), pp 278-314, Wiley-VCH Verlag GmbH & Co. KGaA, Weinheim.
2. Tumir, L. M., and Piantanida, I. (2010) Recognition of single stranded and double stranded DNA/RNA sequences in aqueous medium by small bis-aromatic derivatives, *Mini-Rev. Med. Chem. 10*, 299-308.
3. Shinohara, K.-I., Bando, T., and Sugiyama, H. (2010) Anticancer activities of alkylating pyrrole-imidazole polyamides with specific sequence recognition, *Anticancer. Drugs 21*, 228-242.
4. Durai, C. R. S., and Harding, M. M. (2011) Targeting Nucleic Acids using Dynamic Combinatorial Chemistry, *Aust. J. Chem. 64*, 671-680.
5. Tietjen, J. R., Donato, L. J., Bhimisaria, D., and Ansari, A. Z. (2011) Sequence specificity and energy landscapes of DNA-binding molecules, *Methods Enzymol. 497*, 3-30.
6. Muchmore, S. W., and Hajduk, P. J. (2003) Crystallography, NMR and virtual screening: Integrated tools for drug discovery, *Curr. Opin. Drug Disc. 6*, 544-549.
7. Wheate, N. J., Brodie, C. R., Collins, J. G., Kemp, S., and Aldrich-Wright, J. R. (2007) DNA intercalators in cancer therapy: Organic and inorganic drugs and their spectroscopic tools of analysis, *Mini Rev. Med. Chem. 7*, 627-648.
8. Roeland Boer, D., Canals, A., and Coll, M. (2009) DNA-binding drugs caught in action: The latest 3D pictures of drug-DNA complexes, *Dalton Trans.*, 399-414.
9. Van Dongen, M., Weigelt, J., Uppenberg, J., Schultz, J., and Wikstrom, M. (2002) Structure-based screening and design in drug discovery, *Drug Discovery Today 7*, 471-478.
10. Coles, M., Heller, M., and Kessler, H. (2003) NMR-based screening technologies, *Drug Discovery Today 8*, 803-810.
11. Lepre, C. A., Moore, J. M., and Peng, J. W. (2004) Theory and applications of NMR-based screening in pharmaceutical research, *Chem. Rev. 104*, 3641-3675.
12. de Kloe, G. E., Bailey, D., Leurs, R., and de Esch, I. J. P. (2009) Transforming fragments into candidates: Small becomes big in medicinal chemistry, *Drug Discovery Today 14*, 630-646.
13. Cravens, S. L., Navapanich, A. C., Geierstanger, B. H., Tahmassebi, D. C., and Dwyer, T. J. (2010) NMR solution structure of a DNA-actinomycin D complex containing a non-hydrogen-bonding pair in the binding site, *J. Am. Chem. Soc. 132*, 17588-17598.
14. Rettig, M., Langel, W., Kamal, A., and Weisz, K. (2010) NMR structural studies on the covalent DNA binding of a pyrrolobenzodiazepine-naphthalimide conjugate, *Org. Biomol. Chem. 8*, 3179-3187.
15. Haq, I. (2002) Part II: The thermodynamics of drug-bipolymer interaction - Thermodynamics of drug-DNA interactions, *Arch. Biochem. Biophys. 403*, 1-15.
16. Brown, A. (2009) Analysis of cooperativity by isothermal titration calorimetry, *Int. J. Mol. Sci. 10*, 3457-3477.
17. Ball, V., and Maechling, C. (2009) Isothermal microcalorimetry to investigate non specific interactions in biophysical chemistry, *Int. J. Mol. Sci. 10*, 3283-3315.

18. Strawn, R., Stockner, T., Melichercik, M., Jin, L., Xue, W.-F., Carey, J., and Ettrich, R. (2011) Synergy of molecular dynamics and isothermal titration calorimetry in studies of allostery, *Methods Enzymol. 492*, 151-188.
19. Breusegem, S. Y., Loontiens, F. G., Regenfuss, P., and Clegg, R. M. (2001) Kinetics of binding of Hoechst dyes to DNA studied by stopped-flow fluorescence techniques, *Methods Enzymol. 340*, 212-233.
20. Errington, R. J., Ameer-beg, S. M., Vojnovic, B., Patterson, L. H., Zloh, M., and Smith, P. J. (2005) Advanced microscopy solutions for monitoring the kinetics and dynamics of drug-DNA targeting in living cells, *Adv. Drug Deliver Rev. 57*, 153-167.
21. Biver, T., Secco, F., and Venturini, M. (2008) Mechanistic aspects of the interaction of intercalating metal complexes with nucleic acids, *Coord. Chem. Rev. 252*, 1163-1177.
22. Tafvizi, A., Mirny, L. A., and van Oijen, A. M. (2011) Dancing on DNA: Kinetic Aspects of Search Processes on DNA, *Chemphyschem 12*, 1481-1489.
23. Schneider, H. J., and Wang, M. X. (1994) DNA interactions with porphyrins bearing ammonium side chains, *J. Org. Chem. 59*, 7473-7478.
24. Alves, C. M. A., Naik, S., Coutinho, P. J. G., and Goncalves, M. S. T. (2009) Novel long alkyl side chain benzo[*a*]phenoxazinium chlorides: Synthesis, photophysical behaviour and DNA interaction, *Tetrahedron 65*, 10441-10452.
25. Bailly, C., Denny, W. A., Mellor, L. E., Wakelin, L. P. G., and Waring, M. J. (1992) Sequence specificity of the binding of 9-aminoacridine carboxamide and amsacrine-4-carboxamide to DNA studied by DNase I footprinting, *Biochemistry 31*, 3514-3524.
26. Deisabella, P., Capranico, G., Palumbo, M., Sissi, C., Krapcho, A. P., and Zunino, F. (1993) Sequence selectivity of topoisomerase II DNA cleavage stimulated by mitoxantrone derivatives: Relationships to drug-DNA binding and cellular effects, *Mol. Pharmacol. 43*, 715-721.
27. Fairley, T. A., Tidwell, R. R., Donkor, I., Naiman, N. A., Ohemeng, K. A., Lombardy, R. J., Bentley, J. A., and Cory, M. (1993) Structure, DNA minor groove binding, and base pair specificity of alkyl-linked and aryl-linked bis(amidinobenzimidazoles) and bis(amidinoindoles), *J. Med. Chem. 36*, 1746-1753.
28. Mudasir, Wijaya, K., Yoshioka, N., and Inoue, H. (2003) DNA binding of iron(II) complexes with 1,10-phenanthroline and 4,7-diphenyl-1,10-phenanthroline: Salt effect, ligand substituent effect, base pair specificity and binding strength, *J. Inorg. Biochem. 94*, 263-271.
29. White, E. W., Tanious, F., Ismail, M. A., Reszka, A. P., Neidle, S., Boykin, D. W., and Wilson, W. D. (2007) Structure-specific recognition of quadruplex DNA by organic cations: Influence of shape, substituents and charge, *Biophys. Chem. 126*, 140-153.
30. Carr, C. A., Richards, J. M., Ross, S. A., and Lowe, G. (2000) The effect of 4'-substituents on the kinetics of ligand substitution in 2,2': 6',2''-terpyridine platinum(II) complexes, *J. Chem. Res. (S)*, 566-568.
31. Li, M., Lincoln, P., and Andersson, J. (2011) Slow threading intercalation of monomeric Ru(II) complexes with 10,13-diarylsubstituted dppz ligands, *J. Phys. Chem. B 115*, 7923-7931.
32. Huang, H. S., Chiu, H. F., Lu, W. C., and Yuan, C. L. (2005) Synthesis and antitumor activity of 1,8-diaminoanthraquinone derivatives, *Chem. Pharm. Bull. 53*, 1136-1139.

33. Song, M. Y., and Jhon, M. S. (1992) Molecular dynamics study of the effect of ion concentration on the B-DNA, Z-DNA and DNA-daunomycin complex, *THEOCHEM 89*, 33-47.
34. Mansour, O. C., Evison, B. J., Sleebs, B. E., Watson, K. G., Nudelman, A., Rephaeli, A., Buck, D. P., Collins, J. G., Bilardi, R. A., Phillips, D. R., and Cutts, S. M. (2010) New anthracenedione derivatives with improved biological activity by virtue of stable drug-DNA adduct formation, *J. Med. Chem. 53*, 6851-6866.
35. Bartolomei, S. (2012) Chemotherapeutic and biotherapeutic agents and their use, In *Handbook of Cancer Chemotherapy* (Skeel, R. T., and Khleif, S. N., Eds.), pp 53-212, Lippincott Williams & Wilkins, Philadelphia.
36. Schuster, G. B., and Landman, U. (2004) The mechanism of long-distance radical cation transport in duplex DNA: Ion-gated hopping of polaron-like distortions, *Long-Range Charge Transfer in DNA I 236*, 139-161.
37. Lewis, F. D., Thazhathveetil, A. K., Zeidan, T. A., Vura-Weis, J., and Wasielewski, M. R. (2010) Dynamics of ultrafast singlet and triplet charge transfer in anthraquinone-DNA conjugates, *J. Am. Chem. Soc. 132*, 444-445.
38. Shao, F. W., Augustyn, K., and Barton, J. K. (2005) Sequence dependence of charge transport through DNA domains, *J. Am. Chem. Soc. 127*, 17445-17452.
39. Fahlman, R. P., Sharma, R. D., and Sen, D. (2002) The charge conduction properties of DNA holliday junctions depend critically on the identity of the tethered photooxidant, *J. Am. Chem. Soc. 124*, 12477-12485.
40. Bergeron, F., Nair, V. K., and Wagner, J. R. (2006) Near-UV induced interstrand cross-links in anthraquinone-DNA duplexes, *J. Am. Chem. Soc. 128*, 14798-14799.
41. Perry, P. J., Reszka, A. P., Wood, A. A., Read, M. A., Gowan, S. M., Dosanjh, H. S., Trent, J. O., Jenkins, T. C., Kelland, L. R., and Neidle, S. (1998) Human telomerase inhibition by regioisomeric disubstituted amidoanthracene-9,10-diones, *J. Med. Chem. 41*, 4873-4884.
42. Tanious, F. A., Jenkins, T. C., Neidle, S., and Wilson, W. D. (1992) Substituent position dictates the intercalative DNA-binding mode for anthracene-9,10-dione antitumor drugs, *Biochemistry 31*, 11632-11640.
43. Agbandje, M., Jenkins, T. C., McKenna, R., Reszka, A. P., and Neidle, S. (1992) Anthracene-9,10-diones as potential anticancer agents. Synthesis, DNA-binding, and biological studies on a series of 2,6-disubstituted derivatives, *J. Med. Chem. 35*, 1418-1429.
44. Zagotto, G., Ricci, A., Vasquez, E., Sandoli, A., Benedetti, S., Palumbo, M., and Sissi, C. (2011) Tuning G-quadruplex vs double-stranded DNA recognition in regioisomeric lysyl-peptidyl-anthraquinone conjugates, *Bioconjug. Chem. 22*, 2126-2135.
45. Zagotto, G., Sissi, C., Lucatello, L., Pivetta, C., Cadamuro, S. A., Fox, K. R., Neidle, S., and Palumbo, M. (2008) Aminoacyl-anthraquinone conjugates as telomerase inhibitors: Synthesis, biophysical and biological evaluation, *J. Med. Chem. 51*, 5566-5574.
46. Haq, I., Ladbury, J. E., Chowdhry, B. Z., and Jenkins, T. C. (1996) Molecular anchoring of duplex and triplex DNA by disubstituted anthracene-9,10-diones: Calorimetric, UV melting, and competition dialysis studies, *J. Am. Chem. Soc. 118*, 10693-10701.
47. Fox, K. R., Polucci, P., Jenkins, T. C., and Neidle, S. (1995) A molecular anchor for stabilizing triple-helical DNA, *Proc. Natl. Acad. Sci. U. S. A. 92*, 7887-7891.

48. Huang, H.-S., Chen, I.-B., Huang, K.-F., Lu, W.-C., Shieh, F.-Y., Huang, Y.-Y., Huang, F.-C., and Lin, J.-J. (2007) Synthesis and human telomerase inhibition of a series of regioisomeric disubstituted amidoanthraquinones, *Chem. Pharm. Bull. 55*, 284-292.
49. Venitt, S., Crofton-Sleigh, C., Agbandje, M., Jenkins, T. C., and Neidle, S. (1998) Anthracene-9,10-diones as potential anticancer agents: Bacterial mutation studies of amido-substituted derivatives reveal an unexpected lack of mutagenicity, *J. Med. Chem. 41*, 3748-3752.
50. Steullet, V., Edwards-Bennett, S., and Dixon, D. W. (1999) Cleavage of abasic sites in DNA by intercalator-amines, *Bioorg. Med. Chem. 7*, 2531-2540.
51. Helissey, P., Bailly, C., Vishwakarma, J. N., Auclair, C., Waring, M. J., and Giorgi-Renault, S. (1996) DNA minor groove cleaving agents: Synthesis, binding and strand cleaving properties of anthraquinone-oligopyrrolecarboxamide hybrids, *Anticancer. Drug Des. 11*, 527-551.
52. Breslin, D. T., and Schuster, G. B. (1996) Anthraquinone photonucleases: Mechanisms for GG-selective and nonselective cleavage of double-stranded DNA, *J. Am. Chem. Soc. 118*, 2311-2319.
53. Zagotto, G., Sissi, C., Moro, S., Dal Ben, D., Parkinson, G. N., Fox, K. R., Neidle, S., and Palumbo, M. (2008) Amide bond direction modulates G-quadruplex recognition and telomerase inhibition by 2,6- and 2,7-bis-substituted anthracenedione derivatives, *Bioorg. Med. Chem. 16*, 354-361.
54. Lavery, P. E., and Kowalczykowski, S. C. (1992) Enhancement of recA protein-promoted DNA strand exchange activity by volume-occupying agents, *J. Biol. Chem. 267*, 9307-9314.
55. Ellis, R. J. (2001) Macromolecular crowding: Obvious but underappreciated, *Trends Biochem. Sci. 26*, 597-604.
56. Goobes, R., Kahana, N., Cohen, O., and Minsky, A. (2003) Metabolic buffering exerted by macromolecular crowding on DNA-DNA interactions: Origin and physiological significance, *Biochemistry 42*, 2431-2440.
57. Miyoshi, D., and Sugimoto, N. (2008) Molecular crowding effects on structure and stability of DNA, *Biochimie 90*, 1040-1051.
58. Muhuri, S., Mimura, K., Miyoshi, D., and Sugimoto, N. (2009) Stabilization of three-way junctions of DNA under molecular crowding conditions, *J. Am. Chem. Soc. 131*, 9268-9280.
59. Zheng, K., Chen, Z., Hao, Y., and Tan, Z. (2010) Molecular crowding creates an essential environment for the formation of stable G-quadruplexes in long double-stranded DNA, *Nucl. Acids Res. 38*, 327-338.
60. Kilburn, D., Roh, J. H., Guo, L., Briber, R. M., and Woodson, S. A. (2010) Molecular crowding stabilizes folded RNA structure by the excluded volume effect, *J. Am. Chem. Soc. 132*, 8690-8696.
61. Rajendran, A., Nakano, S., and Sugimoto, N. (2010) Molecular crowding of the cosolutes induces an intramolecular i-motif structure of triplet repeat DNA oligomers at neutral pH, *Chem. Commun. 46*, 1299-1301.
62. Mills, N. (2006) ChemDraw ultra 10.0, *J. Am. Chem. Soc. 128*, 13649-13650.
63. Breslin, D. T., Yu, C. J., Ly, D., and Schuster, G. B. (1997) Structural modification changes the DNA binding mode of cation-substituted anthraquinone photonucleases:

Association by intercalation or minor groove binding determines the DNA cleavage efficiency, *Biochemistry 36*, 10463-10473.
64. McKnight, R. E., Zhang, J. G., and Dixon, D. W. (2004) Binding of a homologous series of anthraquinones to DNA, *Bioorg. Med. Chem. Lett. 14*, 401-404.
65. Jackson Beckford, S., and Dixon, D. W. (2012) Molecular dynamics of anthraquinone DNA intercalators with polyethylene glycol side chains, *J. Biomol. Struct. Dyn. 29*, 1065-1080.
66. Freire, E. (2008) Do enthalpy and entropy distinguish first in class from best in class?, *Drug Discovery Today 13*, 869-874.
67. Marky, L. A., and Breslauer, K. J. (1987) Origins of netropsin binding affinity and specificity: Correlations of thermodynamic and structural data, *Proc. Natl. Acad. Sci. U. S. A. 84*, 4359-4363.
68. Qu, X., Ren, J., Riccelli, P. V., Benight, A. S., and Chaires, J. B. (2003) Enthalpy/entropy compensation: Influence of DNA flanking sequence on the binding of 7-amino actinomycin D to its primary binding site in short DNA duplexes, *Biochemistry 42*, 11960-11967.
69. Chaires, J. B. (2006) A thermodynamic signature for drug-DNA binding mode, *Arch. Biochem. Biophys. 453*, 26-31.
70. Wakelin, L. P., Atwell, G. J., Rewcastle, G. W., and Denny, W. A. (1987) Relationships between DNA-binding kinetics and biological activity for the 9-aminoacridine-4-carboxamide class of antitumor agents, *J. Med. Chem. 30*, 855-861.
71. Atwell, G. J., Rewcastle, G. W., Baguley, B. C., and Denny, W. A. (1987) Potential antitumor agents. 50. In vivo solid-tumor activity of derivatives of *N*-[2-(dimethylamino)ethyl]acridine-4-carboxamide, *J. Med. Chem. 30*, 664-669.
72. Maleev, V., Semenov, A., Kruglova, E., Bolbukh, T., Gasan, A., Bereznyak, E., and Shestopalova, A. (2003) Spectroscopic and calorimetric study of DNA interaction with a new series of actinocin derivatives, *J. Mol. Struct. 645*, 145-158.
73. Zhang, Z. C., Yang, Y. Y., Zhang, D. N., Wang, Y. Y., Qian, X. H., and Liu, F. Y. (2006) Acenaphtho[1,2-b]pyrrole derivatives as new family of intercalators: Various DNA binding geometry and interesting antitumor capacity, *Bioorg. Med. Chem. 14*, 6962-6970.
74. Ovchinnikov, A. V., Baranovsky, S. F., Rozvadovska, A. O., Rogova, O. V., Veselkov, K. A., Ermolaev, A. V., ParkeS, H., Davies, D. B., and Evstigneev, M. P. (2007) Structural basis for the binding affinity of a homologous series of synthetic phenoxazone drugs with DNA: NMR and molecular mechanics analysis, *J. Biomol. Struct. Dyn. 24*, 443-453.
75. Brustolin, F., Surin, M., Lemaur, V., Romanazzi, G., Sun, Q., Cornil, J., Lazzaroni, R., Sommerdijk, N., Leclere, P., and Meijer, E. W. (2007) The self-assembly of amphiphilic oligothiophenes: Hydrogen bonding and poly(glutamate) complexation, *Bull. Chem. Soc. Jpn. 80*, 1703-1715.
76. Utermohlen, W. P. (1945) Preparation of γ-alkoxy-n-propylamines, *J. Am. Chem. Soc. 67*, 1505-1506.
77. Wang, Z.-X., and Jiang, R.-F. (1996) A novel two-site binding equation presented in terms of the total ligand concentration, *FEBS Lett. 392*, 245-249.
78. Hargrove, A. E., Zhong, Z., Sessler, J. L., and Anslyn, E. V. (2010) Algorithms for the determination of binding constants and enantiomeric excess in complex host : guest equilibria using optical measurements, *New J. Chem. 34*, 348-354.

79. Davis, T. M., and Wilson, W. D. (2000) Determination of the refractive index increments of small molecules for correction of surface plasmon resonance data, *Anal. Biochem. 284*, 348-353.
80. Edwards, P. M. (2002) Origin 7.0: Scientific graphing and data analysis software, *J. Chem. Inf. Comput. Sci. 42*, 1270-1271.
81. Smith, T. J., and Stevenson, K. J. (2003) Origin 7.0, *J. Am. Chem. Soc. 125*, 3669-3669.
82. Häfliger, P., Agorastos, N., Spingler, B., Georgiev, O., Viola, G., and Alberto, R. (2005) Induction of DNA-double-strand breaks by Auger electrons from 99mTc complexes with DNA-binding ligands, *Chembiochem 6*, 414-421.
83. Qiao, C., Bi, S., Sun, Y., Song, D., Zhang, H., and Zhou, W. (2008) Study of interactions of anthraquinones with DNA using ethidium bromide as a fluorescence probe, *Spectrochim. Acta, Part A 70*, 136-143.
84. Feigon, J., Denny, W. A., Leupin, W., and Kearns, D. R. (1984) Interactions of antitumor drugs with natural DNA: Proton NMR study of binding mode and kinetics, *J. Med. Chem. 27*, 450-465.
85. Gray, D. M., Ratliff, R. L., and Vaughan, M. R. (1992) Circular dichroism spectroscopy of DNA, *Methods Enzymol. 211*, 389-406.
86. Chaires, J. B., Dattagupta, N., and Crothers, D. M. (1982) Self-association of daunomycin, *Biochemistry 21*, 3927-3932.
87. Roche, C. J., Thomson, J. A., and Crothers, D. M. (1994) Site selectivity of daunomycin, *Biochemistry 33*, 926-935.
88. Ren, J., Jenkins, T. C., and Chaires, J. B. (2000) Energetics of DNA intercalation reactions, *Biochemistry 39*, 8439-8447.
89. Colgrave, M. L., Williams, H. E. L., and Searle, M. S. (2001) Binding of anthracycline antibiotic nogalamycin to the site of a DNA single strand break engineered between two co-axially stacked hairpins, *Chem. Commun.*, 315-316.
90. Mazzini, S., Scaglioni, L., Animati, F., and Mondelli, R. (2010) Interaction between double helix DNA fragments and the new antitumor agent sabarubicin, Men10755, *Bioorg. Med. Chem. 18*, 1497-1506.
91. Mazzini, S., Mondelli, R., and Ragg, E. (1998) Structure and dynamics of intercalation complexes of anthracyclines with $d(CGATCG)_2$ and $d(CGTACG)_2$. 2D-^{1}H and ^{31}P NMR investigations, *J. Chem. Soc., Perkin Trans. 2*, 1983-1991.
92. Keller, D. (1996) Theories of circular dichroism from nucleic acids, In *Circular Dichroism and the Conformational Analysis of Biomolecules* (Fasman, G. D., Ed.), pp 469-500, Plenum Press, New York.
93. Dalgleish, D. G., Fey, G., and Kersten, W. (1974) Circular dichroism studies of complexes of the antibiotics daunomycin, nogalamycin, chromomycin, and mithramycin with DNA, *Biopolymers 13*, 1757-1766.
94. Banerjee, T., and Mukhopadhyay, R. (2008) Structural effects of nogalamycin, an antibiotic antitumour agent, on DNA, *Biochem. Biophys. Res. Commun. 374*, 264-268.
95. Lyng, R., Rodger, A., and Nordén, B. (1991) The CD of ligand-DNA systems. I. Poly(dG-dC) B-DNA, *Biopolymers 31*, 1709-1720.
96. Lyng, R., Rodger, A., and Nordén, B. (1992) The CD of ligand-DNA systems. II. Poly(dA-dT) B-DNA, *Biopolymers 32*, 1201-1214.
97. Bennett, S., Sharples, D., and Brown, J. R. (1982) Preparation and evaluation of 2-substituted anthraquinones based on the anthracyclines, *J. Med. Chem. 25*, 369-373.

98. Armitage, B., Yu, C., Devadoss, C., and Schuster, G. B. (1994) Cationic anthraquinone derivatives as catalytic DNA photonucleases: Mechanisms for DNA damage and quinone recycling, *J. Am. Chem. Soc. 116*, 9847-9859.
99. Breslin, D. T., Coury, J. E., Anderson, J. R., McFailIsom, L., Kan, Y. Z., Williams, L. D., Bottomley, L. A., and Schuster, G. B. (1997) Anthraquinone photonuclease structure determines its mode of binding to DNA and the cleavage chemistry observed, *J. Am. Chem. Soc. 119*, 5043-5044.
100. McKnight, R. E., Zhang, J. G., and Dixon, D. W. (2004) Binding of a homologous series of anthraquinones to DNA, *Bioorg. Med. Chem. Lett. 14*, 401-404.
101. Wilson, W. D., Wang, Y. H., Kusuma, S., Chandrasekaran, S., Yang, N. C., and Boykin, D. W. (1985) Binding strength and specificity in DNA interactions: The design of A•T specific intercalators, *J. Am. Chem. Soc. 107*, 4989-4995.
102. Nickolov, Z. S., Goutev, N., and Matsuura, H. (2001) Hydrogen bonding in concentrated aqueous solutions of 1,2-dimethoxyethane: Formation of water clusters, *J. Phys. Chem. A 105*, 10884-10889.
103. Leng, F., Priebe, W., and Chaires, J. B. (1998) Ultratight DNA binding of a new bisintercalating anthracycline antibiotic, *Biochemistry 37*, 1743-1753.
104. Portugal, J., Cashman, D. J., Trent, J. O., Ferrer-Miralles, N., Przewloka, T., Fokt, I., Priebe, W., and Chaires, J. B. (2005) A new bisintercalating anthracycline with picomolar DNA binding affinity, *J. Med. Chem. 48*, 8209-8219.
105. Searle, M. S., and Williams, D. H. (1993) On the stability of nucleic acid structures in solution: Enthalpy-entropy compensations, internal rotations and reversibility, *Nucleic Acids Res. 21*, 2051-2056.
106. Moe, J. G., Folta-Stogniew, E., and Russu, I. M. (1995) Energetics of base pair opening in a DNA dodecamer containing an A_3T_3 tract, *Nucleic Acids Res. 23*, 1984-1989.
107. Petruska, J., and Goodman, M. F. (1995) Enthalpy-entropy compensation in DNA melting thermodynamics, *J. Biol. Chem. 270*, 746-750.
108. Chen, C. J., and Russu, I. M. (2004) Sequence-dependence of the energetics of opening of AT basepairs in DNA, *Biophys. J. 87*, 2545-2551.
109. Starikov, E. B., and Nordén, B. (2009) DNA duplex length and salt concentration dependence of enthalpy-entropy compensation parameters for DNA melting, *J. Phys. Chem. B 113*, 11375-11377.
110. Strazewski, P. (2002) Thermodynamic correlation analysis: Hydration and perturbation sensitivity of RNA secondary structures, *J. Am. Chem. Soc. 124*, 3546-3554.
111. Gilli, P., Ferretti, V., Gilli, G., and Borea, P. A. (1994) Enthalpy-entropy compensation in drug-receptor binding, *J. Phys. Chem. 98*, 1515-1518.
112. Kiser, J. R., Monk, R. W., Smalls, R. L., and Petty, J. T. (2005) Hydration changes in the association of Hoechst 33258 with DNA, *Biochemistry 44*, 16988-16997.
113. Vlieghe, D., Sponer, J., and Meervelt, L. V. (1999) Crystal structure of d(GGCCAATTGG) complexed with DAPI reveals novel binding mode, *Biochemistry 38*, 16443-16451.
114. Tanious, F. A., Hamelberg, D., Bailly, C., Czarny, A., Boykin, D. W., and Wilson, W. D. (2004) DNA sequence dependent monomer-dimer binding modulation of asymmetric benzimidazole derivatives, *J. Am. Chem. Soc. 126*, 143-153.

115. Van Hecke, K., Nam, P. C., Nguyen, M. T., and Van Meervelt, L. (2005) Netropsin interactions in the minor groove of d(GGCCAATTGG) studied by a combination of resolution enhancement and *ab initio* calculations, *FEBS J. 272*, 3531-3541.
116. Qu, X., and Chaires, J. B. (2001) Hydration changes for DNA intercalation reactions, *J. Am. Chem. Soc. 123*, 1-7.
117. Pimentel, G. C., and McClellan, A. L. (1971) Hydrogen bonding, *Annu. Rev. Phys. Chem. 22*, 347-385.
118. Dunitz, J. D. (1995) Win some, lose some: Enthalpy-entropy compensation in weak intermolecular interactions, *Chem. Biol. 2*, 709-712.
119. Tanious, F. A., Nguyen, B., and Wilson, W. D. (2008) Biosensor-surface plasmon resonance methods for quantitative analysis of biomolecular interactions, In *Biophysical Tools for Biologists: Vol 1 in Vitro Techniques* (Correia, J. J. D. H. W., Ed.), pp 53-77.
120. Nguyen, B., Tanious, F. A., and Wilson, W. D. (2007) Biosensor-surface plasmon resonance: Quantitative analysis of small molecule-nucleic acid interactions, *Methods 42*, 150-161.
121. Lovatt, A., Cooper, A., and Camilleri, P. (1996) Energetics of cyclodextrin-induced dissociation of insulin, *European Biophysics Journal with Biophysics Letters 24*, 354-357.

3 SYNTHESIS OF DICATIONIC ANTHRAQUINONE AMIDES

3.1 Introduction

In the design of drugs that bind to DNA with improved affinity, one of the major challenges is to overcome enthalpy-entropy compensation[1-2]; investigation into their structure activity relationships and thermodynamics can yield insights into the origins of their enthalpies and entropies[3]. We have demonstrated, in chapter 2 that the mono-cationic anthraquinone amides, **AQ I-IV**, bind to DNA via intercalation and exhibit moderate binding affinities that decreases with an increase in their side chain length. Binding of **AQ I-IV** to DNA is usually accompanied by an increasing reduction in the conformational space that their side chain can sample, which typically results in an entropic loss. Formation of the AQ-DNA complex typically forms new interactions between the anthraquinone and its binding site, increasing as the chain length increases. However, these interactions between the ligand and DNA limit the ligand's external rotational and translational freedom (as well as ligand and DNA flexibility) and, therefore, represent an entropic penalty. The net effect of these contributions results in a decrease in binding affinity with an increase in anthraquinone chain length.

In this work, we have designed and synthesized a homologous series of dicationic anthraquinone intercalators. The length of the side chains was comparable to the previously synthesized anthraquinone intercalators, **AQD I-IV**, however, bear two cationic charges. The placement of the cationic charges was at either ends of the side chain. ITC studies were conducted and the results are reported in Table 1.

3.2 Materials and Methods

3.2.1 *Synthesis of AQD I.*

Chloroethanol (20 g, 0.25 moles) was added to a mixture of diethylamine (5.6 mL, 0.707 g/cm^3, 0.054 moles), potassium iodide (0.76 g, 0.0046 moles), and potassium carbonate (26.6 g, 0.193 moles). The mixture was refluxed for 20 h then filtered and evaporated under reduced pressure. The product was washed with water, extracted with CH_2Cl_2, then evaporated again to yield 2-(diethylamino)ethanol [4]. Following the procedure from Brustolin et al.[5] for Michael addition, a catalytic amount of sodium methoxide (0.35 g, 0.0065 moles) was added to a well-stirred solution of 2-(diethylamino)ethanol (15 g, 0.13 moles) in acrylonitrile (13.6 g, 0.256 mol). The mixture was stirred for 2 h at 0 ^oC. Three drops of concentrated hydrochloric acid were added and the unreacted acrylonitrile evaporated *in vacuo*. After addition of chloroform, the insoluble side products were filtered and the product concentrated under vacuum to give 3-[2-(diethylamino)ethoxy]propanenitrile.[6] Under 60 psi H_2 pressure, the nitrile (0.07 mol) in 2 M ethanolic ammonia (40 mL) was catalytically hydrogenated in the presence of Raney-nickel in water (2 g) using a Parr apparatus. When no more H_2 was consumed, the reaction mixture was filtered over Celite and the filtrate evaporated *in vacuo* yielding 3-[2-(diethylamino)ethoxy]propane-1-amine.[6]

The amine (40 mmol) was allowed to react with 3-bromo-*N*-(9,10-dihydro-anthracen-2-yl)-propionamide (8 mmol) with potassium carbonate (40 mmol) under reflux in absolute ethanol (30 mL) for 4 h. The product was filtered and the filtrate evaporated under reduced pressure. The anthraquinone amide was purified by silica gel chromatography eluting with CH_2Cl_2/MeOH, 1:1, and the product obtained as yellow solid (550 mg, 15%). ^{1}H NMR (400 MHz, $CDCl_3$) δ8.26 (m, 4H), 8.13 (s, 1H), 7.71 (m, 2H), 3.41 (m, 6H), 2.80 (t, J = 5.6, 2H), 2.62 (t, J = 5.6, 2H), 2.49

(t, J = 5.8, 2H), 2.39 (q, J = 6.2, 4H), 1.63 (quintet, J = 5.6, 2H), 1.02 (t, J = 6.2, 6H); ^{13}C NMR (400 MHz, $CDCl_3$) δ182.1, 181.5, 171.2, 144.8, 135.2, 134.6, 133.7, 128.9, 128.7, 127.3, 124.9, 116.6, 71.0, 65.8, 53.7, 52.6, 50.2, 45.1, 35.9, 29.8, 10.2; (^{1}H NMR & ^{13}C NMR spectra are in list of figures).

3.2.2 ***Synthesis of AQD II.***

Silver oxide was prepared by addition of a solution of sodium hydroxide (6.9 g, 0.172 mol) in water (200 mL, heated to 85 ^{o}C) to a solution of silver nitrate (30.0 g, 0.177 mol) in water (200 mL) and heating to 85 ^{o}C. The resulting suspension was quickly filtered, washed with hot water (200 mL), followed by 95% ethanol (200 mL), and then with absolute ethanol (200 mL). Following the procedure from Bouzide and Sauvé for monotosylation of symmetrical diols,[7] the freshly prepared silver oxide (53.6 g), *p*-toluenesulfonyl chloride (32 g), and potassium iodide (5.1 g) were added to a well stirred solution of diethylene glycol (30 g, 0.29 moles). Following the procedure from Brustolin et al.[5] for Michael addition, a catalytic amount of sodium methoxide (0.35 g, 0.0064 moles) was added to a well-stirred solution of the monotosylate (15 g, 0.057 mol) in acrylonitrile (6.5 g, 0.123 mol); the mixture was stirred for 2 h at 0 ^{o}C. Three drops of concentrated hydrochloric acid were added and the unreacted acrylonitrile evaporated *in vacuo*. After addition of chloroform, the insoluble side products were filtered and the product concentrated under vacuum to give the tosylated nitrile. To a stirred suspension of the nitrile (15 g, 0.048 mol), sodium carbonate (4.95 g, 0.048 mol), in THF, diethylamine (4.8 mL, 0.046 mol) was added. The mixture was refluxed for 24 hrs then cooled and filtered. Under 60 psi H_2 pressure, the nitrile (0.07 mol) in 2 M ethanolic ammonia (40 mL) was catalytically hydrogenated in the presence of Raney-nickel in water (2 g) using a Parr apparatus. When no more H_2 was con-

sumed, the reaction mixture was filtered over Celite and the filtrate evaporated *in vacuo* yielding 3-{2-[2-(diethylamino)ethoxy]ethoxy}propan-1-amine.[6]

The amine (40 mmol) was allowed to react with 3-bromo-*N*-(9,10-dihydro-anthracen-2-yl)-propionamide (8 mmol) in potassium carbonate (40 mmol) under reflux in absolute ethanol (30 mL) for 4 h. The product was filtered and the filtrate evaporated under reduced pressure. The anthraquinone amide was purified by silica gel chromatography eluting with CH_2Cl_2/MeOH, 1:1, and the product obtained as yellow solid (277 mg, 0.56 mmol, 7.0%). ^{1}H NMR (400 MHz, $CDCl_3$) δ 11.65 (br s, 1H), 8.29 (m, 4H), 8.15 (s, 1H), 7.76 (m, 2H), 3.68 (m, 8H), 3.59 (t, *J* = 6.0, 2H), 3.02 (t, *J* = 5.6, 2H), 2.81 (t, *J* = 5.6, 2H), 2.63 (t, *J* = 5.7, 2H), 2.52 (q, *J* = 6.2, 4H), 1.90 (quintet, *J* = 5.8, 2H), 1.04 (t, *J* = 6.2, 6H); ^{13}C NMR (400 MHz, $CDCl_3$) δ182.3, 181.4, 170.4, 144.9, 135.3, 134.8, 133.9, 128.8, 128.6, 127.5, 124.9, 116.8, 73.0, 71.8, 70.5, 66.1, 52.1, 51.6, 50.2, 45.1, 35.8, 29.8, 10.7; (^{1}H NMR & ^{13}C NMR spectra are in list of figures).

3.2.3 ***Synthesis of AQD III.***

AQD III was synthesized using the same procedure as **AQD II**, except using triethylene glycol instead of diethylene glycol. The anthraquinone amide was partially purified by silica gel chromatography eluting with CH_2Cl_2/MeOH, 1:1, and the product obtained as yellow solid (406 mg, 0.75 mmol, 6.1%). ^{1}H NMR (400 MHz, $CDCl_3$) δ 11.52 (br s, 1H), 8.29 (m, 4H), 8.17 (s, 1H), 7.75 (m, 2H), 3.61 (m, 12H), 3.54 (m, 2H), 3.01 (t, *J* = 5.4, 2H), 2.80 (t, *J* = 5.4, 2H), 2.64 (m, 2H), 2.53 (q, *J* = 6.2, 4H), 1.90 (quintet, *J* = 5.8, 2H), 1.04 (t, *J* = 6.2, 6H); ^{13}C NMR (400 MHz, $CDCl_3$) δ182.3, 181.4, 171.3, 145.1, 135.1, 134.9, 133.9, 128.7, 128.5, 127.5, 124.9, 116.7, 72.5, 72.3, 71.8, 70.1, 66.9, 52.1, 51.5, 50.5, 45.0, 35.6, 29.9, 10.6; (^{1}H NMR & ^{13}C NMR spectra are in list of figures).

3.2.4 *Synthesis of AQD IV.*

AQD IV was synthesized using the same procedure as **AQD II**, except using tetraethylene glycol instead of diethylene glycol. The anthraquinone amide was partially purified by silica gel chromatography eluting with CH_2Cl_2/MeOH, 1:1. The amide was further purified by HPLC on a Shimadzu LC-10AT VP system and a Zobax C18 reverse phase column. Elution condition: CH_3CN-MeOH (flow rate = 1.5 mL/min), 0-10 min (CH_3CN 0%-100%), 10-35 min (CH_3CN 100%-50%). The product was obtained as a yellow solid (238 mg, 0.41 mmol, 3.5%). %). ^{1}H NMR (400 MHz, $CDCl_3$) δ 8.25 (m, 4H), 8.19 (s, 1H), 7.74 (m, 2H), 3.59 (m, 16H), 3.49 (m, 2H), 2.91 (t, *J* = 5.2, 2H), 2.75 (t, *J* = 5.2, 2H), 2.60 (m, 2H), 2.48 (q, *J* = 6.0, 4H), 1.83 (quintet, *J* = 5.6, 2H), 1.03 (t, *J* = 6.0, 6H); ^{13}C NMR (400 MHz, $CDCl_3$) δ182.2, 181.3, 171.4, 144.9, 135.0, 134.5, 133.3, 128.7, 128.5, 127.4, 124.9, 116.7, 72.8, 72.5, 71.6, 66.7, 52.1, 51.6, 50.4, 45.1, 35.6, 29.8, 12.3; (^{1}H NMR & ^{13}C NMR spectra are in list of figures).

3.2.5 *Isothermal Titration Calorimetry (ITC).*

ITC experiments were carried out at 25 ^{o}C using a VP-ITC microtitration calorimeter (Microcal, Inc., Northhampton, MA). The experiments were conducted by injecting 3 μL of a 0.5 mM anthraquinone solution in MES10 buffer every 300 s for a total of 98 injections into a 0.01 mM AT-rich DNA hairpin (5'-biotin-GCATATATATCCCCATATATATGC) solution in the same buffer. Integration of the area under each peak of the titration plot as a function of time gave the heat produced for each injection. Control experiments to determine the heats of dilution for the DNA into buffer were carried out by injecting MES buffer solution into DNA or ligand into buffer alone. The dilution heat for the DNA was negligible and constant and was therefore subtracted from the interaction heats of ligand into DNA titration. The corrected binding isotherm for ligand binding to DNA was fitted to a "one set of sites" binding model with Origin 7.0

to determine the binding parameter, equilibrium binding constant, $K_{observed}$, number of ligands binding to DNA, n, and the binding enthalpy, $\Delta H_{observed}$. The measured heat of dissociation for similar anthraquinone dimers was ~ 1.0 ± 0.1 kcal/mol, (see discussion in Chapter 2). This value was used in each case to correct the observed enthalpy of interaction of AQ ligands with DNA:

$$\Delta H_{observed} = \Delta H_{dissociation} + \Delta H_{binding}$$

The determined $\Delta H_{dissociation}$ value was subtracted from the $\Delta H_{observed}$ value to give a corrected value for the binding-induced enthalpy change, $\Delta H_{binding}$. The change in entropy, ΔS, was calculated from $\Delta G = \Delta H_{binding} - T\Delta S$.

3.3 Results and Discussion

The dicationic anthraquinone amides, **AQD I-IV**, were designed for further elucidation of the effect of side chain length on DNA binding affinity, as well as enthalpic and entropic changes as a function of changes in the ligand's side chain. The ITC data for **AQD I-IV** binding to the AT-rich DNA was fitted to a "one set of sites" equilibrium binding model to obtain their binding affinities, K, binding enthalpies, ΔH and entropies, ΔS, and the number of ligands bound per hairpin, n. The equilibrium binding constants were of the order of magnitude of 5.3×10^4 – 9.1×10^4 M^{-1} (Table 1), in no particular order as a function of chain length. The equilibrium binding constants were similar to their mono-cationic counterparts, **AQ I-IV** (2.3×10^4 – 1.1×10^5 M^{-1}), as seen in Chapter 2. The n values obtained, that is the number of AQD ligand bound per hairpin, was ≥ 4 for all four compounds. For **AQD I**, ~7 ligands were bound to the hairpin, which is equivalent to a binding site-size of ~1. Based on the nearest neighbor-exclusion model for the binding of an intercalator to DNA[8], which states every second intercalation site along the DNA length remains unoccupied, a site size of ~1 is generally not expected. For **AQD I-III**, the DNA is about half neutralized. The AQD ligands must therefore bind non-specifically to DNA.

These non-standard complexes were not observed for their dicationic threading counterparts, **AQT I-IV**, which had n values of approximately two to three [9]. No further studies were conducted on these dicationic anthraquinone ligands.

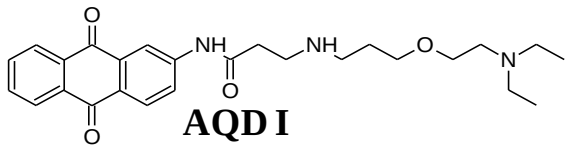

AQD I

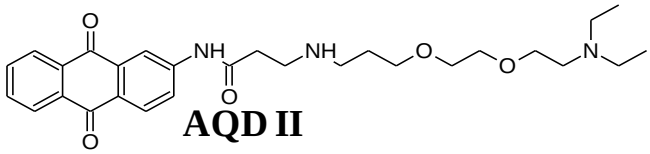

AQD II

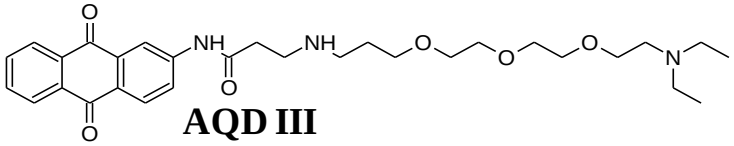

AQD III

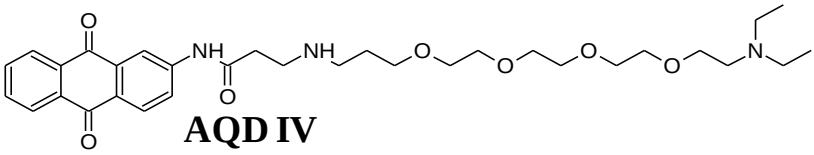

AQD IV

Figure 3.1: Anthraquinone intercalators, **AQD I-IV**, used in this study.

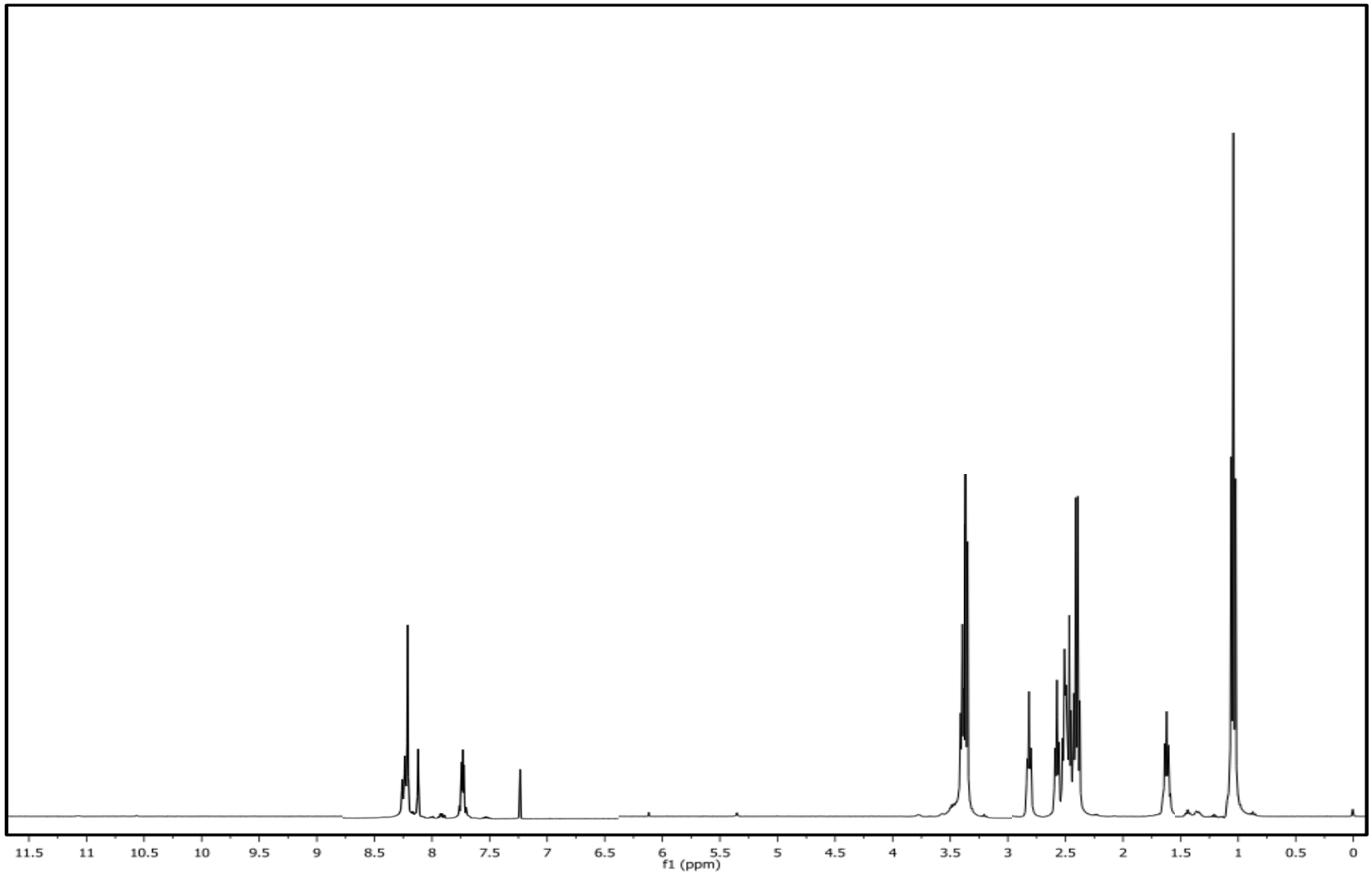

Figure 3.2: ^{1}H NMR spectrum of **AQD I** in chloroform

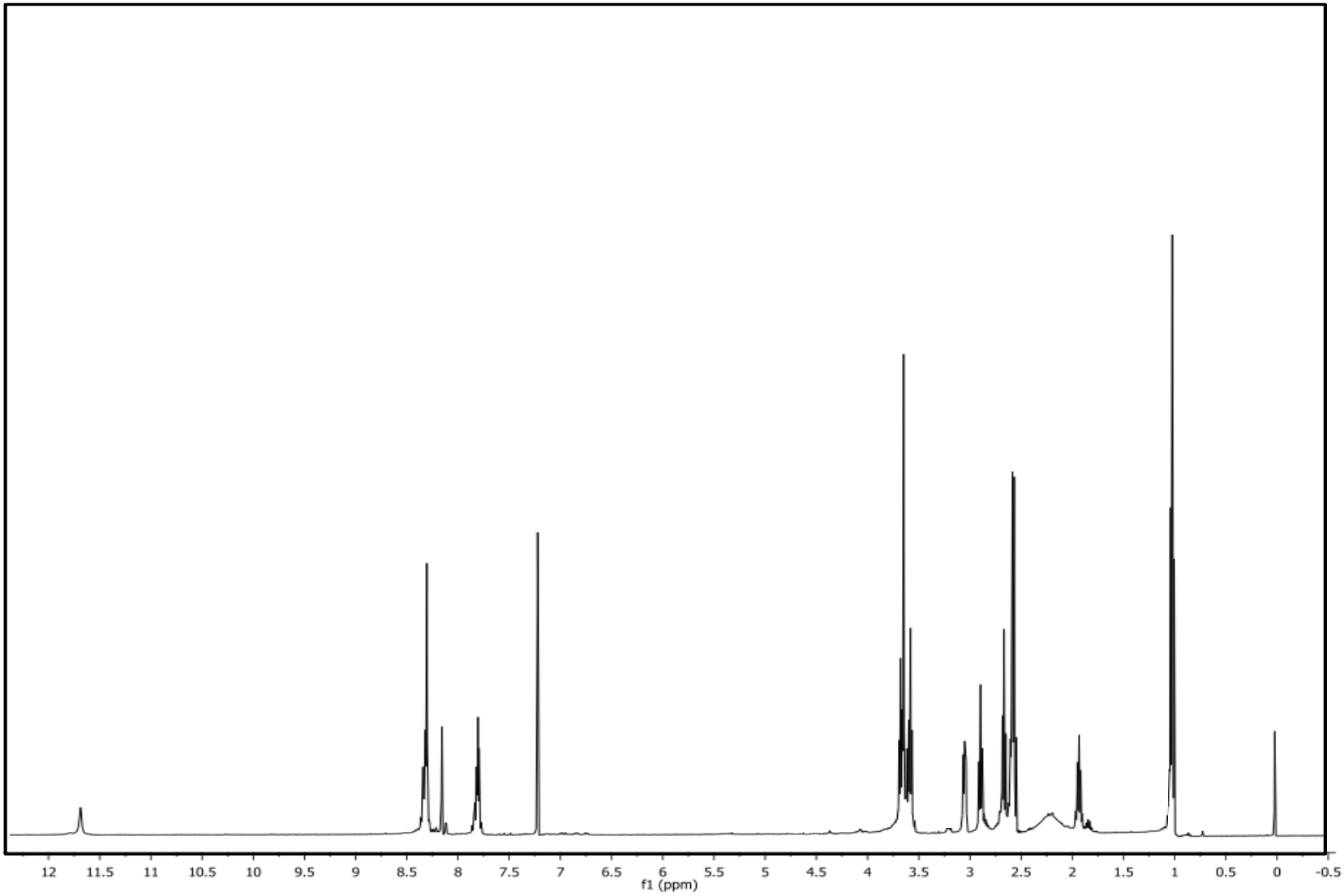

Figure 3.3: ^{1}H NMR spectrum of **AQD II** in chloroform

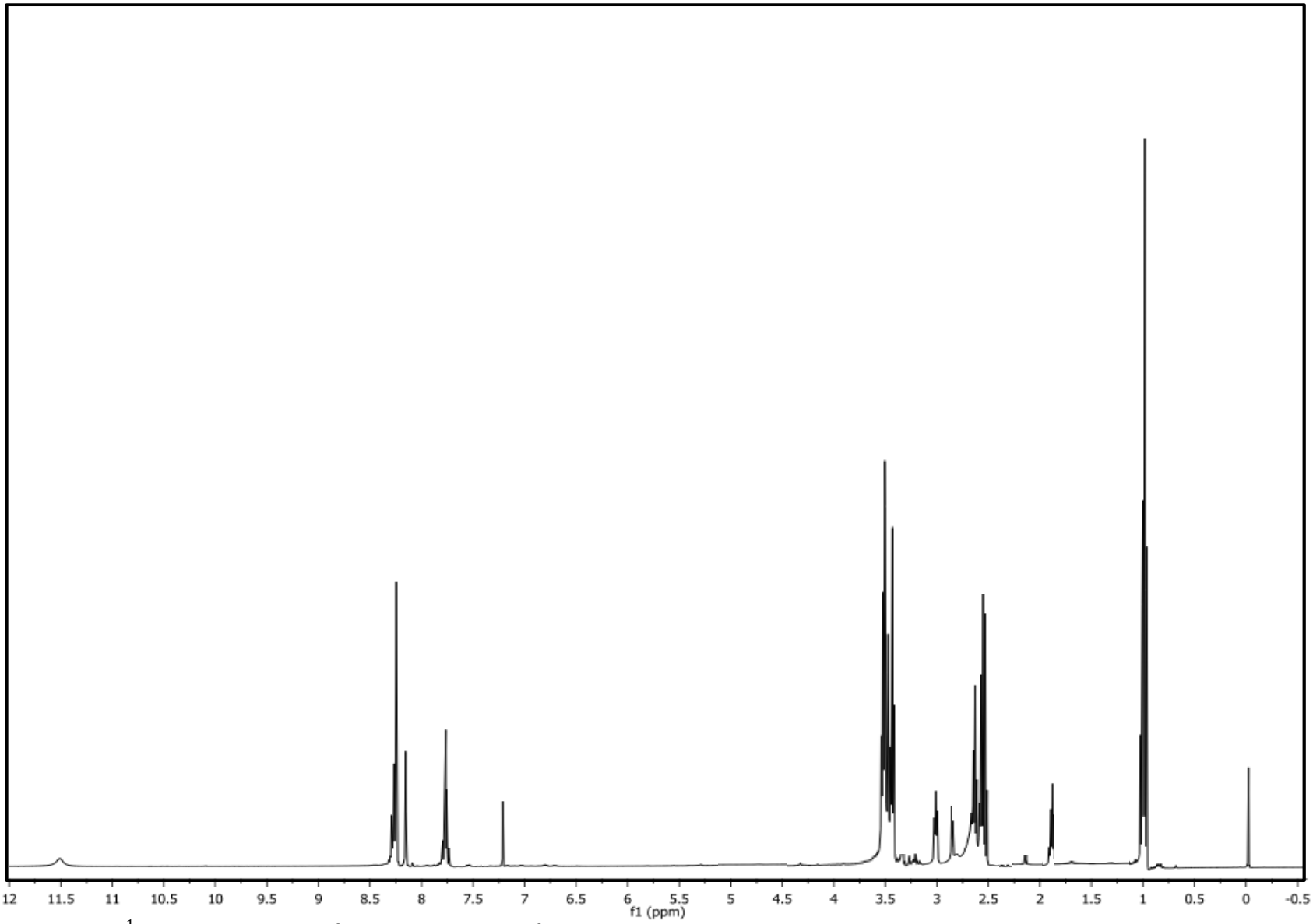

Figure 3.4: ^{1}H NMR spectrum of **AQD III** in chloroform

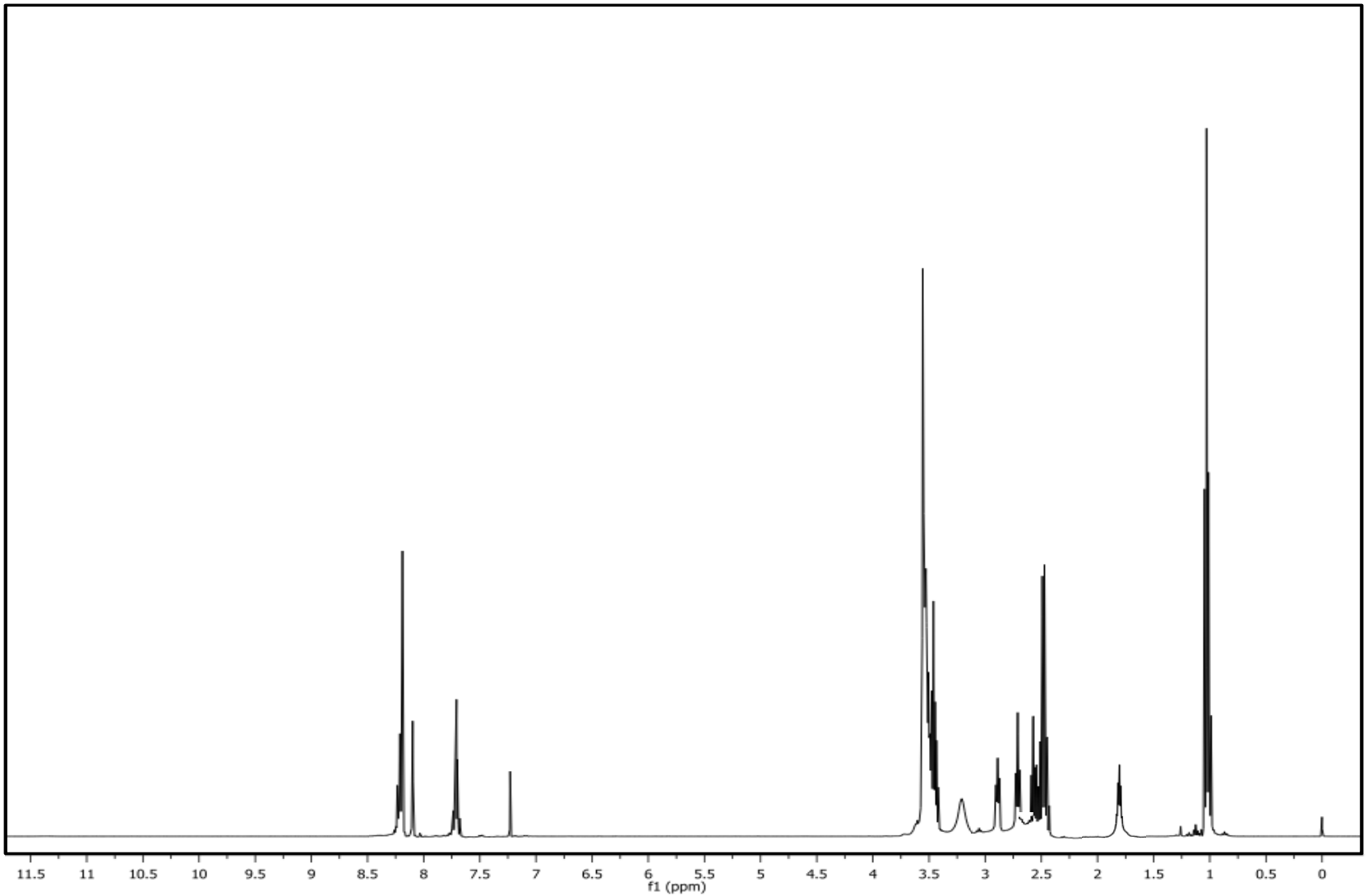

Figure 3.5: ^{1}H NMR spectrum of **AQD IV** in chloroform

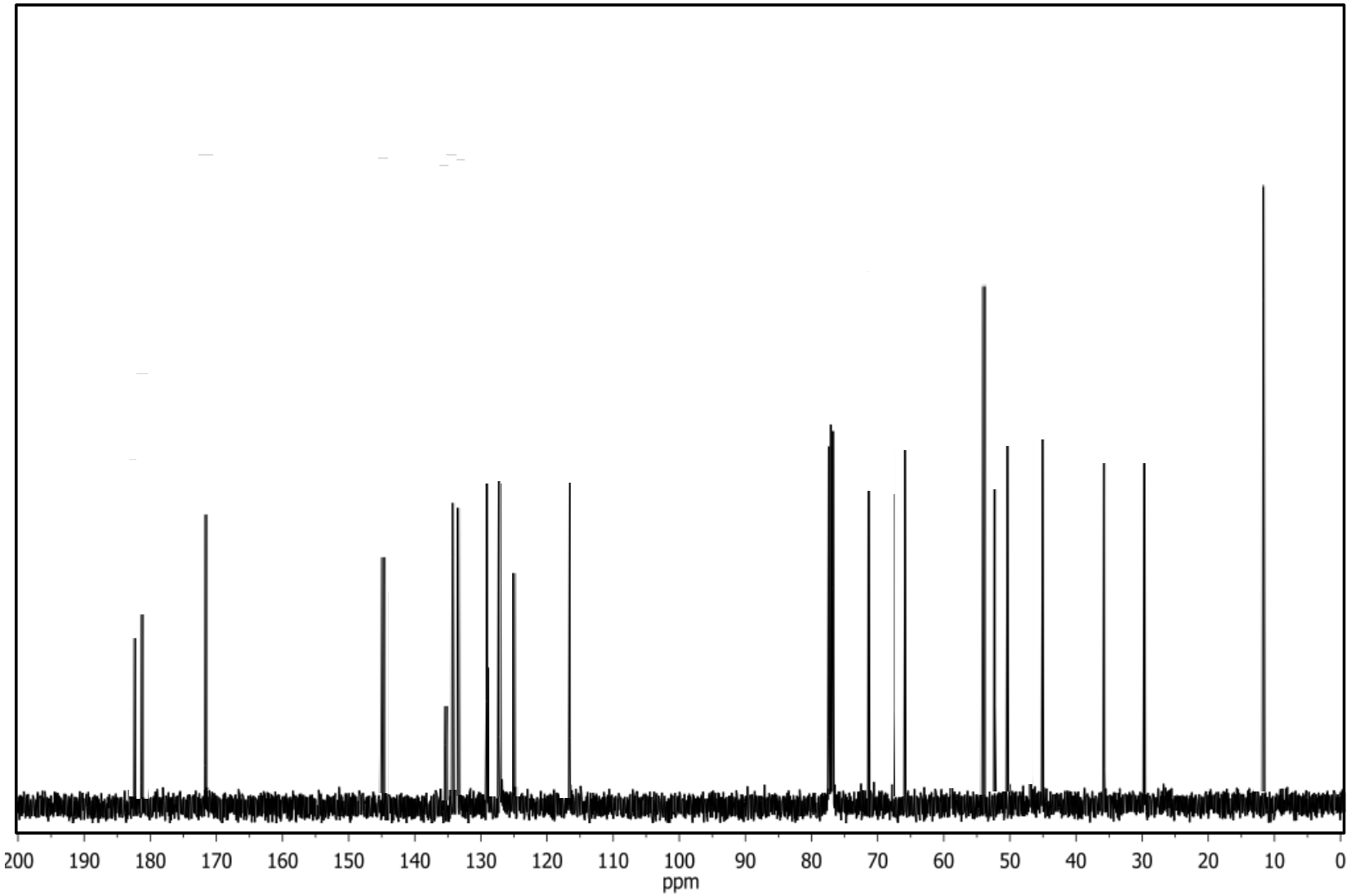

Figure 3.6: ^{13}C NMR spectrum of **AQD I** in chloroform

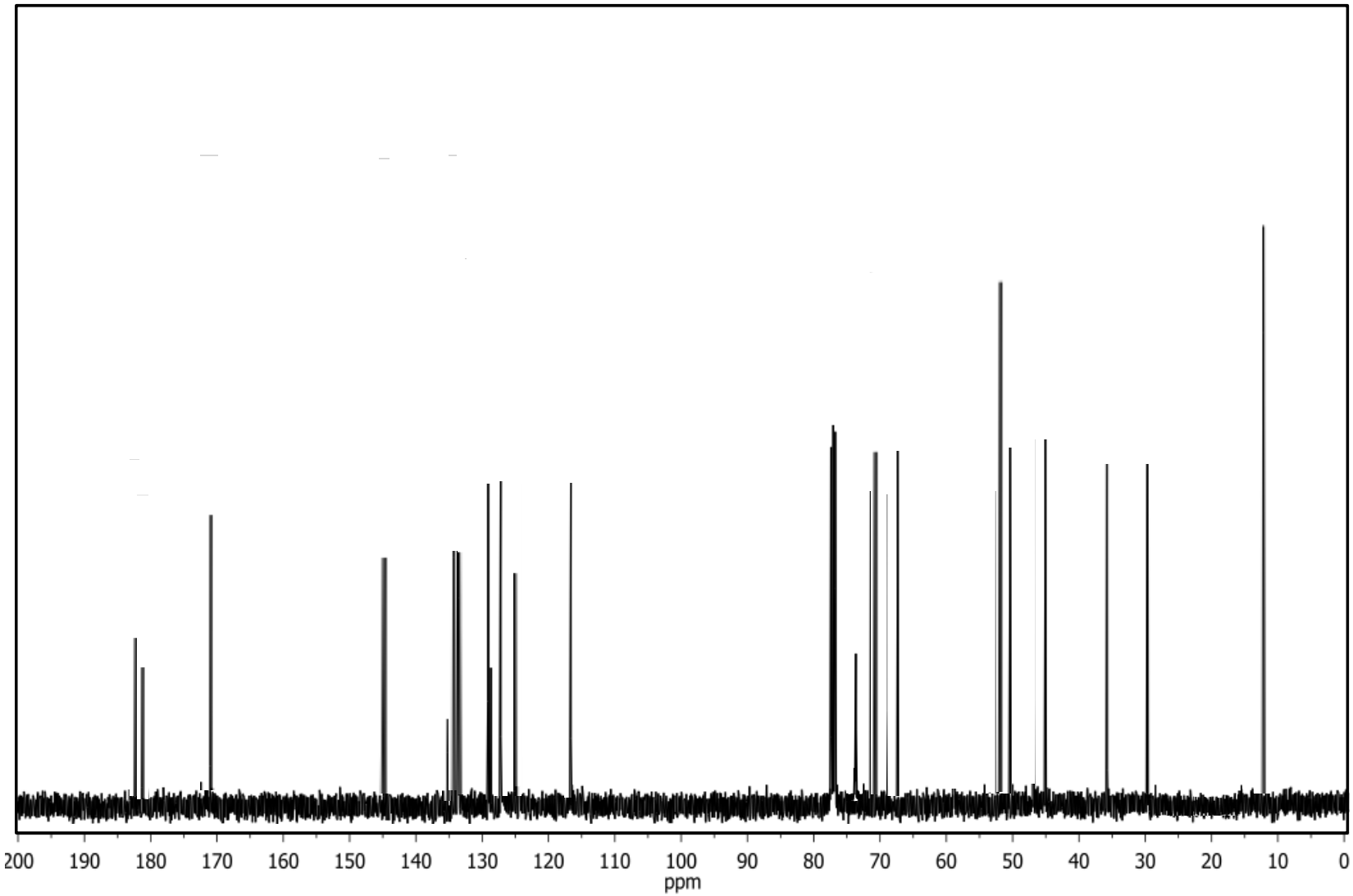

Figure 3.7: ^{13}C NMR spectrum of **AQD II** in chloroform

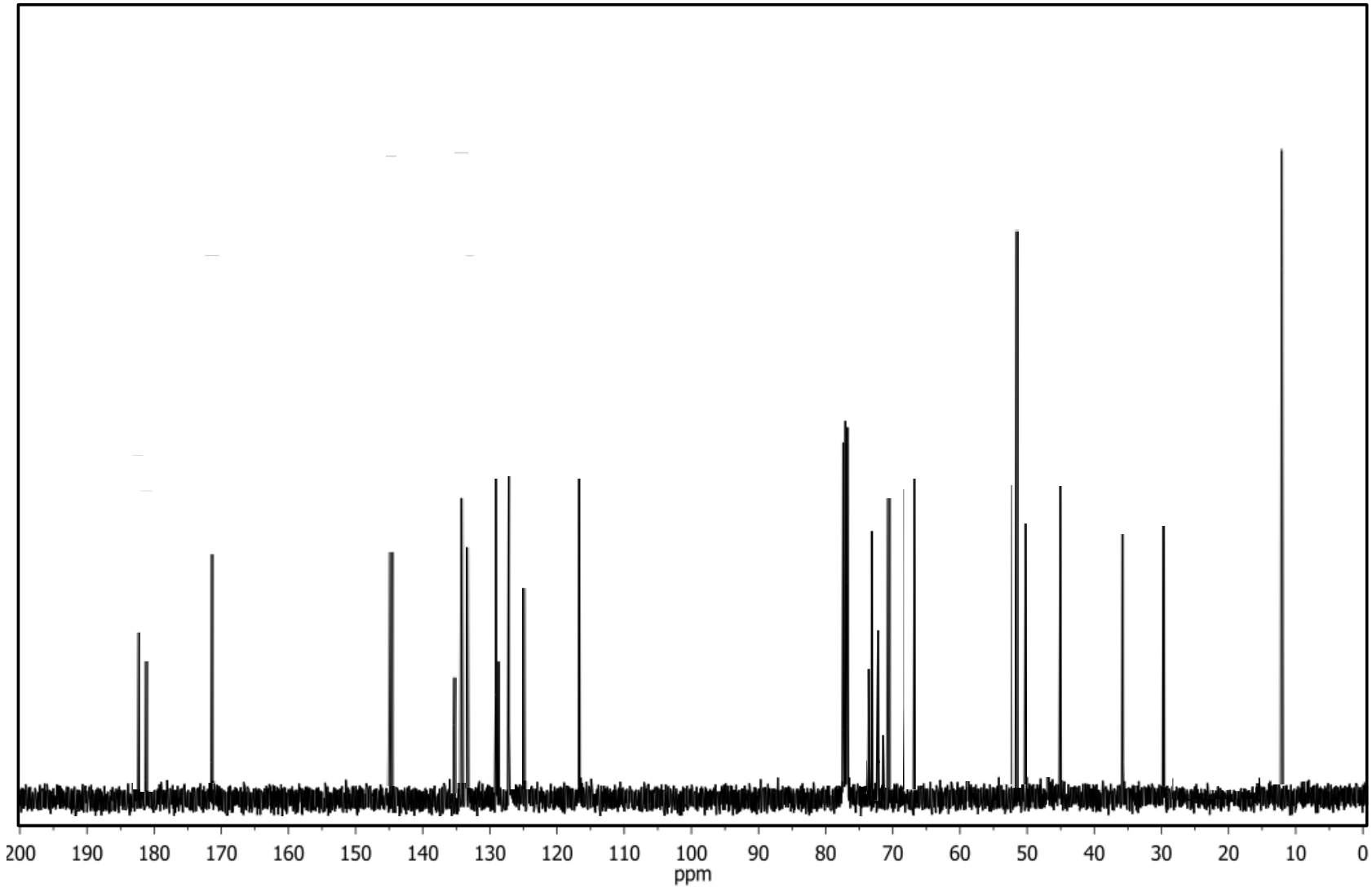

Figure 3.8: ^{13}C NMR spectrum of **AQD III** in chloroform

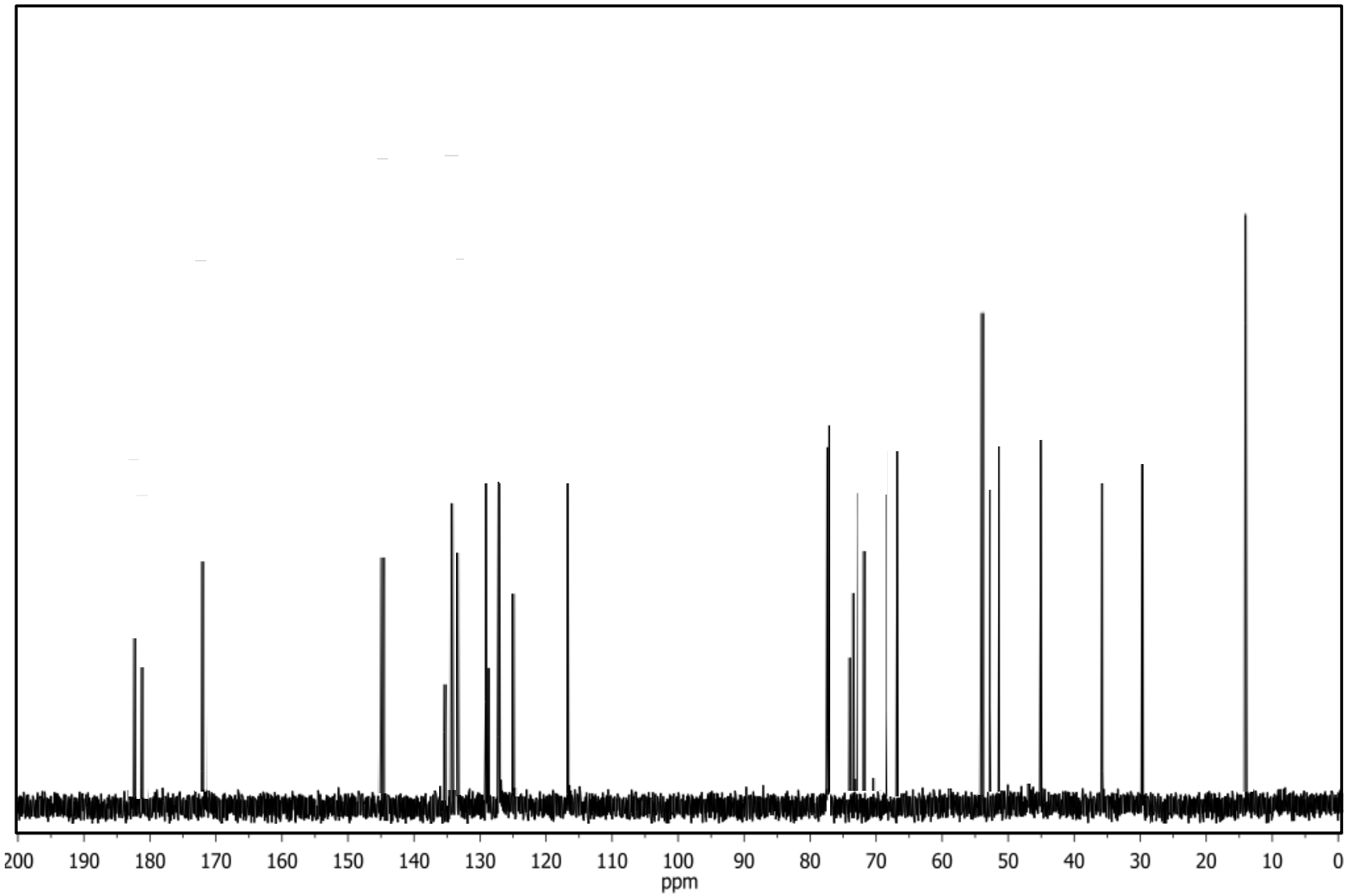

Figure 3.9: ^{13}C NMR spectrum of **AQD IV** in chloroform

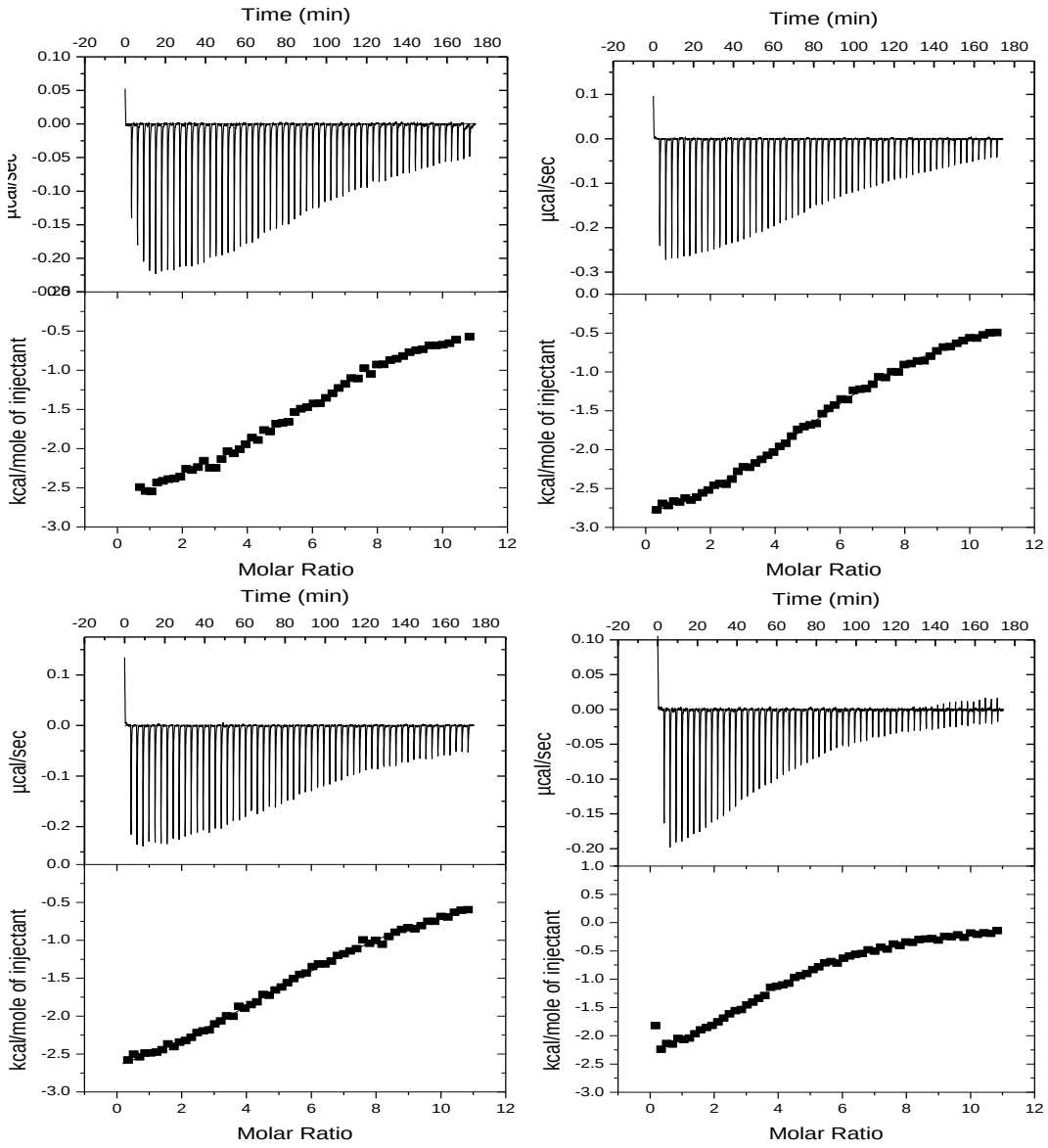

Figure 3.10: ITC heat of dissociation curves for a) **AQD I**, b) **AQD II**, c) **AQD III**, and d) **AQD IV**.
*Isothermal titrations consisted of ~95 injections (3 µL) of 500 µM **AQD I-IV** ligand into a calorimetric cell containing MES10 buffer. The data were fitted to a dimer dissociation model.*

Table 3.1: Binding parameters of **AQD I-IV** as determined by isothermal titration calorimetry.

Compound	K (10^4 M^{-1})	n	ΔH (kcal/mol)	TΔS (kcal/mol)	ΔG_{obs} (kcal/mol)
AQ I	7.70 ± 0.41	7.15 ± 0.05	-3.08 ± 0.04	-3.54	-6.62
AQ II	8.11 ± 0.27	6.55 ± 0.03	-3.35 ± 0.03	-3.30	-6.65
AQ III	5.32 ± 0.24	7.08 ± 0.05	-3.34 ± 0.05	-3.06	-6.40
AQ IV	9.13 ± 0.31	4.29 ± 0.04	-2.84 ± 0.03	-3.88	-6.72

3.4 References

1. Ruben, A. J., Kiso, Y., and Freire, E. (2006) Overcoming roadblocks in lead optimization: A thermodynamic perspective, *Chemical Biology & Drug Design 67*, 2-4.
2. Chaires, J. B. (2008) Calorimetry and thermodynamics in drug design, *Annual Review of Biophysics 37*, 135-151.
3. Weber, P. C., and Salemme, F. R. (2003) Applications of calorimetric methods to drug discovery and the study of protein interactions, *Curr. Opin. Struct. Biol. 13*, 115-121.
4. Hartman, W. W. (1943) Beta-diethylaminoethyl alcohol, *Org. Synth. 14*, 1.
5. Brustolin, F., Surin, M., Lemaur, V., Romanazzi, G., Sun, Q., Cornil, J., Lazzaroni, R., Sommerdijk, N., Leclere, P., and Meijer, E. W. (2007) The self-assembly of amphiphilic oligothiophenes: Hydrogen bonding and poly(glutamate) complexation, *Bull. Chem. Soc. Jpn. 80*, 1703-1715.
6. Utermohlen, W. P. (1945) Preparation of γ-alkoxy-n-propylamines, *J. Am. Chem. Soc. 67*, 1505-1506.
7. Bouzide, A., and Sauvé, G. (2002) Silver (I) oxide mediated highly selective monotosylation of symmetrical diols. Application to the synthesis of polysubstituted cyclic ethers, *Org. Lett. 4*, 2329-2332.
8. Crothers, D. M. (1968) Calculation of binding isotherms for heterogenous polymers, *Biopolymers 6*, 575-584.
9. McKnight, R. E., Zhang, J. G., and Dixon, D. W. (2004) Binding of a homologous series of anthraquinones to DNA, *Bioorg. Med. Chem. Lett. 14*, 401-404.

4 MOLECULAR DYNAMICS OF ANTHRAQUINONE DNA INTERCALATORS WITH POLYETHYLENE GLYCOL SIDE CHAINS

4.1 Direct Copy of Published Work

4.1.1 *Abstract*

The interactions of a homologous series of four anthraquinone (AQ) intercalators with increasing lengths of polyethylene glycol (PEG) side chains with DNA have been studied via molecular dynamics (MD) simulations. The geometry, conformation, interactions, and hydration of the complexes were examined. The geometries of the four ligands were similar with parallel stacking to the long axis of the adjacent DNA base pairs. Hydrogen bonding between the AQ amide and DNA led to a preference for the *trans-syn* conformer. As the side chain lengthened, binding to DNA reduced the conformational space, resulting in an increase in unfavorable entropy. Increased localization of the PEG side chain in the DNA groove, indicating some interaction of the side chain with DNA, also contributed unfavorably to the entropy. The changes in free energy of binding due to entropic considerations (-3.9 to -6.3 kcal/mol) of **AQ I-IV** were significant. The hydration of the PEG side chain decreased upon binding to DNA. Understanding of side chain conformations, interactions, and hydration changes that accompany the formation of a ligand-DNA complex may be important in the development of new applications of pegylated small molecules that target biological macromolecules.

4.1.2 *Introduction*

The design of genome-directed small molecules that target specific DNA sequences and structures has been a recurring theme in anticancer drug development [1-5]. Study of the interac-

tions of these small molecules with DNA is especially important in elucidating the specificity of DNA-ligand interactions and developing new and more effective drugs. Previous studies have shown that interactions formed between the drug and DNA fall into two main categories: intercalation and groove binding [6-12]. Most DNA-interacting molecules possess flexible degrees of freedom, which give rise to a complex potential energy surface with several conformational minima. Quite frequently, even though many conformational possibilities exist in the free form, these molecules adopt only one or perhaps a few preferred conformations when bound to DNA. For a small rigid molecule, it may be reasonable to ignore the conformational change on binding, but not for more flexible ligands or those bearing long side chains. Understanding the favorable and unfavorable contributions to the binding free energy of a ligand binding to DNA is important for the design process of drug molecules.

Anthraquinones are an important class of molecules for cancer chemotherapy; several derivatives have been successfully administered in the clinic, including daunomycin and adriamycin [13-18]. In this context, researchers have explored the possibility of modifying the structure of anthraquinones to improve the overall effectiveness and decrease the toxicity of this drug class. The introduction of an amide substituent into the anthraquinone (AQ) ring system allows elaboration of the system through the attachment of side chains. Studies of anthraquinone amides with the nitrogen bound in the 2-position have included interaction with DNA structures including duplexes [19-22], triplexes [21, 23-24], and quadruplexes [25-29], as well as cleavage of the DNA in the minor groove [30], at abasic sites [31], and under irradiation [32]. Members of this class of molecules continue to be studied as anticancer agents [33-38].

We chose to synthesize the AQ intercalators, **AQ I-IV**, bearing a homologous series of polyethylene glycol (PEG) side chains (Figure 1A) connected through an amide linkage to probe

the effect of the side chain length on DNA binding [39]. The PEG structure was chosen because the addition of each subunit is expected to have only a very small effect on the hydrophobicity of the molecule [40-41]. In addition, PEG of various lengths are widely used as osmolytes in studies of DNA due to their minimal interaction with DNA, water solubility, lack of toxicity, stability, commercial availability, and varying molecular weights [42-49].

The observed free energy of binding for an intercalator, ΔG_{obs}, has been parsed into five components [50]:

$$\Delta G_{obs} = \Delta G_{conf} + \Delta G_{hyd} + \Delta G_{t+r} + \Delta G_{pe} + \Delta G_{mol} \qquad [1]$$

ΔG_{hyd} is the free energy of hydrophobic transfer of the molecule from solution to the DNA binding site. ΔG_{t+r} is the free energy cost resulting from losses in translational and rotational degrees of freedom upon complex formation. ΔG_{pe} has to do with polyelectrolyte contributions resulting from the release of condensed counter ions from the DNA upon binding. ΔG_{mol} is the free energy from noncovalent molecular interactions between the molecule and DNA including hydrogen bonds, and van der Waals, electrostatic, and dipole-dipole interactions. ΔG_{conf} is the free energy contribution from conformational changes in the DNA and ligand upon binding. The interpretation of experimental binding studies usually assumes that conformational changes arising in the ligand upon binding to DNA are negligible compared to that of the DNA itself, and hence do not contribute significantly to the binding free energies. Although it may be reasonable to ignore the conformational changes in a small rigid molecule upon binding to DNA, changes in conformation should be considered for more flexible ligands or those bearing long side chains. In this work, **AQ I-IV** have PEG-based side chains of increasing length. Because PEG is not expected to interact with the DNA, this is an ideal homologous series to investigate the effect of side chain conformational flexibility on DNA binding.

Molecular dynamics (MD) simulations provide an important complement to experimental data. These simulations are well suited to provide insights into the conformational properties of a ligand, DNA or their complex. Simulation on a sufficiently long timescale will allow for characterization of the structure at the molecular level. In this paper, we report the MD simulation of the AQ series when free in solution and when bound to DNA.

There are a number of MD simulation studies that have probed the interaction, geometry, conformational changes, mechanism of binding, and free energies of AQ intercalators with DNA duplexes [10, 51-66]. The AQ intercalators studied include mitoxantrone, doxorubicin, daunomycin, and nogalamycin. Our work extends these studies by evaluating how side chains with multiple degrees of freedom interact with the DNA grooves. We compare the conformations available to the molecules both free in solution and when bound to a DNA hairpin.

4.1.3 ***Materials and Methods***

4.1.3.1 NMR and IR of Anthraquinones, AQ I-IV

NMR samples of **AQ I** [39] were prepared in $CDCl_3$. Two dimensional ROESY (Rotating-frame Overhauser Enhancement SpectroscopY) NMR spectra were recorded on a 400 MHz Bruker spectrometer with mixing time of 350 ms. The ROESY data were measured with a total of 512 t_1 increments, and 2048 data points in t_2. Spectral widths of 5600 Hz were used in both dimensions. Data processing was carried out with the MestReNova 5.0.3 software [67].

IR spectra were taken on a Perkin-Elmer 257 spectrophotometer. The spectra of neat AQ ligands were obtained by co-addition of 5 scans at a resolution of 1 cm^{-1}.

4.1.3.2 Computational Methods

MD simulations (50 ns) were performed for the four anthraquinone ligands both free in solution and when bound to DNA. Starting from a model-built B-DNA hairpin (GCGCGCGCTTTTGCGCGCGC), the anthraquinone-DNA complexes were generated employing the AQ-DNA orientation and spacing of the anthraquinone respinomycin bound to DNA [1N37 in the Protein Data Bank (PDB)] [68]. The system was then subjected to energy minimization on a Sybyl 8.0 (Tripos, Inc., St. Louis, MO) program by using MMFF94s force field by including the MMFF94 partial atomic charges [69].

The atomic charges of the ligand were derived by means of the RESP technique [70] based on the electrostatic potential calculated at the HF/6-31G* level using the Gaussian 03 package [71]. The MD simulations were carried out using the *sander* module [72] in the Amber 9.0 suite of programs with the modified version (ff99SB) of the parm99 all-atom force field [73]. The starting structures and input files were generated using the *xleap* program [73]. Both the free ligand and the ligand-DNA complexes were solvated in cubic periodic boxes with the TIP3P (transferable intermolecular potential 3P) water model [74-75], up to 10 Å away from the ligand or complex. For the free ligands and bound complex, each periodic box was filled with approximately 2700 and 4900 water molecules, respectively.

The starting structures were equilibrated to a pressure of 1 bar (100 kPa) and a temperature of 300 K using the ff99SB force field [73] implemented in the *sander* module with the particle mesh Ewald (PME) method [76]. Equilibration was conducted according to the following three steps: a minimization of 10000 steps with the first 2000 being steepest descent (to remove unfavorable contacts) and the remainder being conjugate gradient. The solvent and ions were minimized while the DNA and the ligand were restrained by a 100 kcal mol^{-1} $Å^{-2}$. A short MD run of

50 ps in which the solute molecules were restrained and the water molecules allowed to relax was performed. During the MD, the system was gradually heated from 0 to 300 K. The restraints on the solvent and ions were applied at 50 kcal mol^{-1} $Å^{-2}$. For the final step of equilibration, a 100 ps MD run in which both the solute and the water molecules were allowed to relax was done. The final density of the system was ~ 0.989 g/mL.

The production simulations (50 ns) were carried out with a fixed volume in which the temperature was maintained at 300 K. The electrostatic interactions were treated by using the smooth particle mesh Ewald method [76] with grid spacing of 0.5 Å. The cutoff distance for the non-bonded interactions was 9 Å. The SHAKE algorithm [77] was used to restrain all bonds involving a hydrogen atom. Snapshots were saved every 500 steps for further analyses. To create all the overlaid snapshots, frames from the simulation were chosen randomly. The DNA shown in the overlaid snapshots is representative of the average DNA structure.

4.1.3.3 Entropy Calculations

The starting point of our analyses, chosen to be 10 ns, allowed the system to equilibrate further. The ptraj module of the Amber 9 suite was used for analysis of the molecular trajectories and VMD for visualization. The entropic contributions of the free AQ side chains and penalties resulting from the restriction of the side chain upon binding to the hairpin duplex were derived. Ptraj calculations of configurational entropy follows the formulation by Schlitter [78] which employs a quantum mechanical harmonic oscillator ([2]). The entropy takes into account both the configurational and vibrational entropy contributions arising from conformational changes in the ligand and addition of new modes upon binding to DNA. The translational and rotational motions were eliminated by spatially superimposing the structures in the trajectory to a common reference structure. This ensures eliminating the possibility of convergence problems. The defi-

nition for the entropy based on covariance matrix of atomic positional fluctuations of the Cartesian coordinates of the particles in the system is given as:

$$S = \tfrac{1}{2} k_B \ln \det [1 + k_B T e^2/\hbar^2 M\sigma] \qquad [2]$$

where k_B is the Boltzmann constant, T is the temperature, e is the Euler value, $\hbar = h/2p$; h is Planck's constant, and M is the mass diagonal matrix. The σ value is the covariance matrix of the atomic positional fluctuations with elements ([3]):

$$\sigma_{ij} = \langle (x_i - \langle x_i \rangle)(x_j - \langle x_j \rangle) \rangle \qquad [3]$$

Schlitter's formula is convenient when the entropy of only subgroups of atoms is of interest, in our case, the side chain atoms. The application of the covariance matrix calculation was performed only on the side chain heavy atoms (C, N and O) as a reduced representation of the system, avoiding an estimate of the entropy from fluctuations of other atoms within the ligand.

4.1.3.4 Water Occupancy

Water distribution around the DNA was calculated using ptraj grid of the AMBER 9.0 suite of programs. The water distribution was calculated by binning atom positions from RMS coordinate fit frames over all the DNA-complex atoms at 1 ps intervals into 0.5 $Å^3$ grids. The value of each grid element represents the number of times the coordinates of the water oxygen were within the 0.5 $Å^3$ represented by that particular grid element. These grids were then contoured using VMD [79]. Contouring of waters was performed at two or more times the expected bulk water density.

VMD was used for analysis of the bridging water molecules. The bridging water molecules in the simulations are characterized by Tcl scripts. To capture the residence time of the water molecule bridging the DNA and AQ ligands or within the AQ ligand itself, the dwell time

distribution of waters within 3.5 Å of selected atoms was counted as described previously [80]. The time distribution was then fit to an exponential to get the residence time.

4.1.4 *Results and Discussion*

Herein, we describe a systematic study of the DNA binding interactions of four AQ ligands bearing increasing side chain lengths of PEG. We first determined the conformation of the AQ amide in solution. Results from IR and NMR indicated that the NH-CO (ω) bond was found in the *trans* conformation (Figure 1B). MD simulations were used to assess the torsional behavior of the NH-CO (ω) and AQ-NHCO (Φ) linkages, interactions between the AQ-ligand and DNA, and the conformations of the side chain. We also evaluated the binding geometry and stacking interactions of the four ligands upon binding to DNA, which were similar for all the ligands. In contrast, the side chain conformations of **AQ I - IV** were different, as discussed below.

4.1.4.1 Conformational Assignment of the Free AQ-amide in Solution

The amide link in our AQ intercalators can adopt four conformations (Figure 1B): *trans-syn*, *trans-anti*, *cis-anti*, and *cis-syn*. A clear view of the conformations adopted by this linker, and the relation of these conformations to the structure of the side chain, can be important in understanding the binding of AQ to DNA.

This conformation was first assessed by IR spectroscopy. The IR of **AQ I** showed a single N-H stretching band at 3338 cm^{-1} (Figure 4.2). Previous studies have indicated that the N-H stretching band is sensitive to the conformation and that the *cis*- and *trans*-conformers usually appear approximately 20 - 40 cm^{-1} apart [81]. It can be assumed that the single sharp band for **AQ I** indicates the presence of only one amide isomer. This is presumably the *trans*-conformer, because studies of other *N*-phenylamides have found that the *trans*-conformer is approximately 2.5 kcal mol^{-1} energetically more favorable than the *cis*-conformer [82-84].

A single peak in the N-H region was seen in the ^{1}H NMR 1D spectrum of **AQ I** (Figure 4.3). Shin et al. have seen completely separated signals (by approximately 0.5 ppm) of the N-H protons of the *cis* and *trans* amide isomers [85]. Evans and Miller also observed the separation of proton signals between the *cis* and *trans* isomers, in their examples of up to 3 ppm [86]. In our study, the observation of a single N-H peak in the NMR spectrum established the presence of only a single isomer. In a ROESY spectrum, only two cross-peaks for the amide proton at 11.6 ppm were seen, those for the H1 and H3 protons (the two protons *ortho* to the side chain at position 2, Figure 4.4). The lack of cross peaks between the H1/H3 protons and the methylene groups in the side chain indicated that only the *trans* isomer was present.

4.1.4.2 Conformational Assignment of the Free AQ-amide in Solution

Using the *trans-anti* isomers as the starting structures, rotations about the NH-CO ω-amide bond and the AQ-NHCO Φ-bond for the free **AQ I-IV** amide were assessed. Throughout the 50 ns simulations, there were no observations of *cis-trans* isomerization of the ω-bond, as measured by the torsional angle between the NH and CO groups (Figure 4.5); the *trans* isomer was the only species seen. *Cis/trans* isomerization is an extremely slow process due to the existence of a large rotational barrier of the ω-bond, in the range of 15 - 20 kcal mol^{-1} [81, 84]. The absence of rotation about the ω-bond in our study was therefore not surprising.

The MD simulations showed free rotation about the AQ-NHCO Φ-bond. The distribution of dihedral angles about the Φ-bond for **AQ I-IV** showed ensembles of amide conformations centered at ±45^{o} (designated *trans-syn*) and ±135^{o} (designated *trans-anti*) (Figure 4.6, top). We note that a modeling study on an amido-anthraquinone with a different side chain found a preferred amide conformation of 0^{o} [29]. In our work, the free energy profile of the dihedral angles [87] for the Φ-bond showed that the *trans-syn* and *trans-anti* isomers were similar in energy (Figure

4.6, bottom). The lack of substituents at the H1 and H3 positions on the AQ ring resulted in similar probabilities of sampling both conformers.

To assess the binding characteristics of the **AQ** ligands to DNA, the *trans-anti* conformer of each was docked between the second and third base pairs of the DNA hairpin. The AQ-ligands were oriented so that the side chain was in the minor groove, as observed with other anthracene molecules binding to DNA [66, 88-94]. The starting point of our analyses, chosen to be 10 ns, allowed the system to equilibrate further.

Figure 4.7 shows the stacking interactions of the AQ I-DNA complex, where only the four surrounding base pairs (C1:G16, G2:C15, C3:G14, and G4:C13) in close contact with the ligand are drawn for clarity. The initial starting structure for the simulation had the AQ perpendicular to the base pairs, based on other examples such as nogalamycin [66], daunomycin [88], and idarubicin [89]. During the simulation, AQ I reoriented to a position in which it was stacked almost parallel to the DNA base pair axis. This geometry resulted in extensive chromophore-base overlaps, with the side chain components coming close to the sugar-phosphate groups in the minor grooves. The geometry was presumably influenced by favorable DNA interactions with the quinone oxygens of the AQ, as well as the amido and amino groups of the side chain. In the binding of other AQ-ligands to DNA, Williams and Searle have suggested that nogalamycin binding to DNA is driven by favorable interactions of the side chains, especially between the 2"-OH on the bicycloaminoglucose sugar and N7 of the nearby guanine [66]. Tanious *et al.* have proposed that the substituent position on AQ ligands dictates the intercalative DNA binding geometry [20].

The MD simulations showed restricted rotation about the AQ-NHCO Φ-bond when **AQ I** was bound to DNA (Figure 4.8A). The *trans-syn* conformation was favored (-45^{o}, carbonyl

pointed towards the terminus of the hairpin), but both *trans-syn* and *trans-anti* conformations were observed. Visual inspection of the simulation showed that the N<u>H</u> of the AQ amide was closest to <u>O</u>4' of the C3 sugar. About 70% of the structures had the N<u>H</u> and <u>O</u>4' atoms situated within H-bonding distance of one another (< 3 Å, Figure 4.8B). This set of structures generally had the amide in the *trans-syn* conformation. The remaining structures (30% of the simulation) did not have a hydrogen bond to the amide. In these structures, the amide was generally in the *trans-anti* conformation and positioned such that it could not hydrogen bond with the O4' group (or other nearby hydrogen bond acceptors).

Binding of **AQ II-IV** were similar to that of **AQ I**. The AQ ring systems stacked almost parallel to the G2:C15 and C3:G14 base pair axis, similar to the geometry observed for **AQ I**. The side chain NH-amides sampled both the *trans-anti* and *trans-syn* conformations (Figure 4.8). The *trans-syn* conformer accounted for the majority of conformations. However, in comparison to **AQ I**, as the side chain increased in length, a wider range of *trans-syn* conformers appeared (-60^{o} to 15^{o} for **AQ II** and -60^{o} to 30^{o} for **AQ III** and **AQ IV**), some of which were not stabilized by a hydrogen bond between the NH-amide and O4' of the C3 sugar. Overall, in comparison to **AQ I**, there was a decrease in correlation between the *trans-syn* conformer and the hydrogen bond between the NH-amide and C3 O4' groups.

4.1.4.3 Electrostatic Interactions between the Ligand and DNA.

For the **AQ I**-DNA complex, about half of the structures had an apparent electrostatic interaction between the ammonium group in the side chain and the nearest phosphate group, C3 ($R_2\underline{N}H_2^+$ - $\underline{P}O_4^-$ distances of ~ 3 to 4 Å, Figure 4.8C). This interaction is presumably involved in helping to anchor the ligand into the DNA binding site. The other half of the structures had

$R_2\underline{N}H_2^+$ - $\underline{P}O_4^-$ distances of > 4 Å. There was moderate correlation between the shorter $R_2\underline{N}H_2^+$ - $\underline{P}O_4^-$ distances and hydrogen bonding of the amide NH to O4' of the C3 sugar.

The **AQ II-IV** derivatives maintained distances of ~ 3 to 4 Å between the $R_2\underline{N}H_2^+$ group and $\underline{P}O_4^-$ of C3 for about 40 - 50% of the simulation (Figure 4.8C). This interaction, like that for **AQ I**, is presumably involved in helping to anchor the ligand into the DNA binding site. A decrease in the correlation between the *trans-syn* conformer and hydrogen bond between the NH-amide and C3 O4' groups as well as some decrease in the percentage of apparent electrostatic contacts between the $R_2\underline{N}H_2^+$ and C3 $\underline{P}O_4^-$ groups may be attributed to other structures favored by the side chain in **AQ II-IV**.

4.1.4.4 Conformational Analysis of the Side Chains in AQ I-IV.

Visual analyses of the dynamic trajectories of both the free and bound **AQ** ligands in solution showed that the side chains were very flexible (snapshots of **AQ I** and **AQ IV** are shown in Figure 4.9). We noted that the free ligands exhibited a wider range of motion, sampling more conformers compared to the bound ligands.

Using the distance between the ammonium group and terminal methyl in the side chain ($R_2\underline{N}H_2^+$ - $\underline{C}H_3$ distances) as a metric, we observed that the side chain had a shorter average distance in the free AQ as compared to the DNA-bound AQ in each case (Figure 4.10). The effect is fairly small for **AQ I**, with the bound AQ having only a slightly greater average distance than the free AQ. The difference became greater as the side chain lengthened. Free **AQ IV** had a fairly equal distribution of conformers with distances of 5 - 13 Å whereas bound **AQ IV** had an ensemble of favored conformers at a significantly greater distance: 10 - 14 Å. The difference in the free and bound forms was in part due to the presence of DNA restricting the conformational

space of the side chain. For all the bound AQ ligands, the side chain spent more time sampling conformations away from the DNA groove.

In addition, we noted an increased localization of the PEG side chain in the DNA groove as the chain length increased (Figure 4.11). The distances between the second oxygen of the side chain and DG5:O2 of the DNA were used as a metric for groove localization. Structures having distances of less than 5 Å between the side chain and DNA were considered localized in the DNA groove; these accounted for about 25% of the simulation for **AQ IV**. Snapshots of **AQ IV** with the side chain in the groove are shown in Figure 4.12. The significant number of PEG structures in the DNA groove was an indication of interactions between the PEG side chain and the DNA. These interactions further restrict motions of the side chain and thereby contribute unfavorably to the entropy. PEG is not generally considered to interact with DNA; however, the forced high local concentration of the PEG side chain in the DNA groove could favor these interactions.

We quantitated the entropies of the side chains using Schlitter's equation, [2] [78]. For the free **AQ I-IV** ligands, the configurational entropies increased from ~47 to 71 kcal/mol as the side chain length increased (Table 4.1). The increased entropy along the series **AQ I-IV** was attributed primarily to the increase in the number of rotatable bonds in the side chain. The calculated entropies of the side chain for the bound **AQ I-IV** ligands ($T\Delta S_{bound}$) ranged from ~43 to 65 cal/mol. Using the equation $T\Delta S_{conf} = T\Delta S_{bound} - T\Delta S_{free}$, changes in entropy of -3.9 to -6.3 kcal/mol were obtained for **AQ I-IV** binding to DNA. This indicated a decrease in entropy upon binding to DNA, becoming more unfavorable along the series **AQ I** to **AQ IV**. This $T\Delta S_{conf}$ term can be compared to the loss in translational and rotational degrees of freedom upon ligand-host complex formation, the $T\Delta S_{t+r}$ term in ΔG_{t+r} ([2]). The $T\Delta S_{t+r}$ term is estimated as 14.4 ± 3

kcal/mol [95]. The $T\Delta S_{conf}$ contributions of **AQ I-IV** are therefore significant when compared to $T\Delta S_{t+r}$. The free energy of conformational change for intercalators bearing a long or flexible side chains can contribute significantly to the overall free energy of binding of a ligand to DNA.

4.1.4.5 Side Chain Conformation and Water Bridges.

The difference in the side chain conformations between the bound and unbound AQ can also be viewed from the standpoint of water interactions. We analyzed the data set in terms of the internal water bridges within the side chain. Two types of internal water bridges were observed throughout the simulation, 1:2 bridges (bridging adjacent ether oxygen atoms) and 1:3 bridges (bridging every other ether oxygen). These bridges are commonly seen in simulations of PEG in water; leading references are found in Wahab *et al.* [96] and Juneja *et al.* [97].

Looking first at **AQ IV** free in solution, water bridges were maintained for > 85% of the simulation. The majority (~ 75%) of the structures had at least two water bridges (Table 4.2). The situation changed when **AQ IV** was bound to DNA. Considering first the structures in which the side chain was localized in the DNA groove (distances of less than 5 Å between second oxygen of the side chain and DG5:O2 of the DNA), we saw that only approximately 25% of the structures had two or more water bridges, the other structures had either one or no water bridge. The set of structures with the side chain not localized in the groove had approximately half of its structures with two or more water bridges. Overall, binding to DNA appeared to decrease the number of internal water bridges in the AQ side chain.

Fewer ether oxygens in the side chain resulted in fewer water bridges, as expected. For the bound **AQ IV** side chain, 1:2 and 1:3 water bridges were maintained for > 65% and 20% of the simulation, respectively. The bound **AQ III** ligand maintained 1:2 and 1:3 water bridges for approximately 40% and 7% of the simulation, respectively. The 1:2 water bridges in **AQ II** were

maintained for only 25% of the simulation; **AQ I** cannot form bridges. Overall, comparing the free and bound AQ ligands, the free ligands showed 10 - 25% more 1:2 water associations than the bound, but the 1:3 water bridges were about the same in both forms. Water occupancy of the free side chain ether oxygens, counting both bridged and nonbridged waters, ranged from a low of about 50% in **AQ I** to a high of greater than 80% for each of the ether oxygens in **AQ IV**.

4.1.4.6 Bridged Waters between the Ligand and DNA.

To probe the possible mediating role of water molecules, we identified water molecules that were involved in H-bonds between the ligand and DNA (distances ≤ 3.5 Å). For all of the series, both carbonyl oxygen atoms on the AQ chromophore were significantly hydrated throughout the simulation. The oxygen pointing in the minor groove (bridged to G14 and C15) was hydrated for greater than 90% of the simulation while that in the major groove (bridged to G2) was hydrated for over 80% of the simulation. The ammonium hydrogens also participated in water-mediated H-bonds with the C3 phosphate; however, this was seen for less than 10% of the simulation. The amide carbonyl oxygen had bound water occupancy greater than 90%, but these bound waters were not seen to mediate interactions with the DNA. The role of DNA hydration in structure stabilization and mediating drug-DNA interactions in DNA-ligand complexes have been discussed [98-99]. In general, bridging waters can play an important role in the structure of AQ-DNA complexes.

4.1.4.7 Hydration of the AQ-DNA Complexes.

To assess structural water, the simulations were analyzed for site occupancy, taken as two or more times bulk water density. As an example, Figure 4.13 shows high occupancy water solvation sites for **AQ I** and **AQ IV**. The most obvious structural waters were along the spine of hydration in the minor groove. The positioning of the waters in the DNA minor groove for **AQ I**

and **AQ IV** were somewhat different. Higher density water regions appeared to decrease as the side chain increased in length. The interaction of the PEG side chain in **AQ IV** with the DNA groove seemed to influence the binding of water to the DNA groove. Ligands that bind to the minor groove of DNA have been shown to affect the hydration of the groove, e.g., Hoechst 33258 [100], DAPI [101], the benzimidazole derivatives DB183 and DB185 [102], and netropsin [103].

It has previously been noted that small changes in the side chains of an intercalator can make significant changes in the water associated with the DNA-intercalator complex. For example, the adriamycin-DNA complex binds 18 more water molecules than does the daunomycin complex, although these anthraquinone derivatives differ only by a single hydroxyl group in the side chain [104]. Propidium binds DNA with six more water molecules in the complex than does ethidium [105].

4.1.5 ***Conclusions.***

We have used MD simulations to assess the DNA binding characteristics of four homologous AQ intercalators bearing increasing lengths of PEG side chain. In all four AQ-ligands, the amide was found mainly in the *trans-syn* conformation, generally stabilized by hydrogen bonding interactions between the DNA and amide. An apparent electrostatic interaction between the side chain ammonium group and the close-by C3 phosphate was seen in all four AQ-DNA complexes; however, the length of time it was maintained decreased as the side chain increased in length. This is presumably due to an increasing number of other favorable conformers as the side chain becomes longer.

Our MD simulations indicated increasingly unfavorable entropic contributions to the free energy of binding as the side chain became longer. This seemed to be due in part to restricted conformational space and perhaps in part due to increasing localization of longer chains in the

DNA groove. The magnitude of these entropic contributions can be significant, especially for long and flexible side chains.

DNA binding of this AQ series resulted in a forced high local concentration of PEG in the DNA groove. PEG is widely used as an osmolyte in DNA studies and generally viewed as having minimal interaction with the DNA. We found that **AQ IV** had a significant percentage of structures localized in the DNA groove. This may be an indication of PEG interacting with the DNA groove. There was a high correlation between conformations with the side chains localized in the DNA groove and a decrease in the number of internal water bridges. The decrease in the number of internal water bridges observed between the free and bound ligands was presumably due to the formation of favorable structures with the DNA.

Overall, the AQ and PEG side chains bring together multiple conformational preferences to define ligand binding to DNA. Comparison of free and bound **AQ IV** indicated that interactions with the DNA have a significant effect on the conformations of the side chain. The effects of intramolecular cross-linking via water bridges may important when designing nucleic acids conjugated to PEG groups. These studies on DNA-intercalator binding can aid in the development of new DNA binding agents.

4.2 Unpublished Data.

Figure 4.15 gives a summary of the hydrated oxygens in **AQ IV**; Table 4.3 gives a summary of the percent time each oxygen is hydrated in **AQ I-IV**, both free and bound.

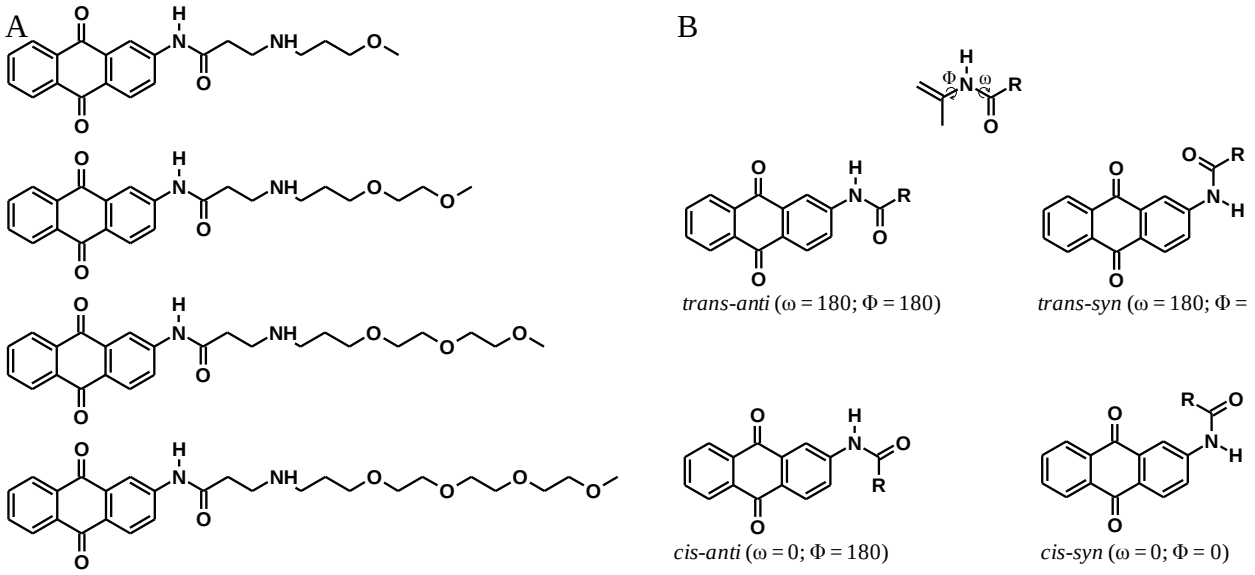

Figure 4.1: (A) Chemical structures of anthraquinone amides, **AQ I – IV**. (B) Representation of the amide bond conformers, drawn as planar structures.

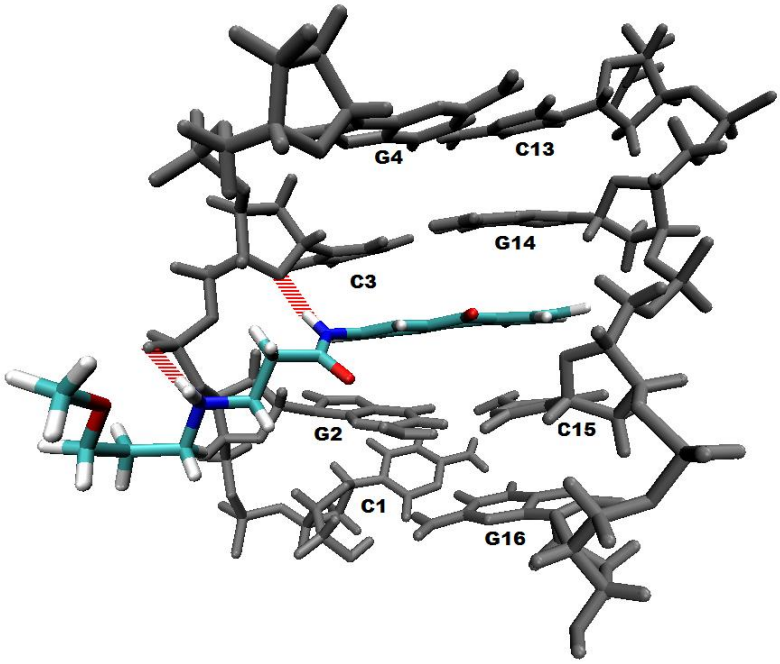

Figure 4.2: Representative snapshot of the interaction of **AQ I** with the DNA hairpin.
The $R_2\underline{N}H_2^+$ - PO_4^- and NH-O4' interactions are shown. The amide is in the trans-syn conformation.

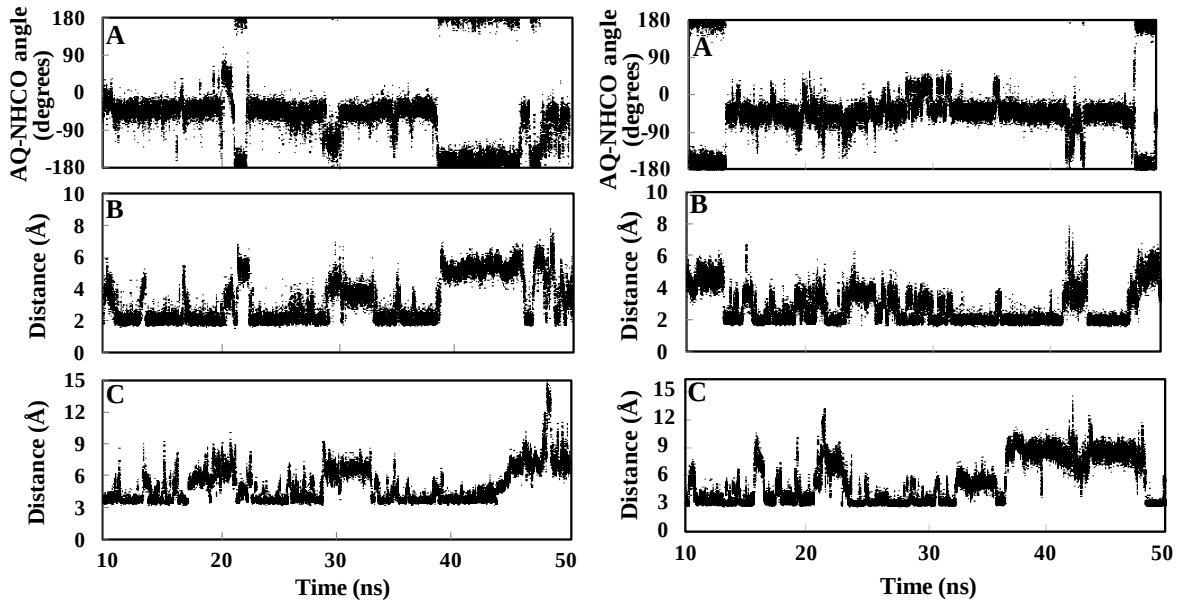

Figure 4.3: Analysis of the binding of **AQ I** (left) and **AQ IV** (right) to DNA; data are presented as a function of time.
(A) Rotation about the AQ-NHCO Φ-bond. (B) Distance between N<u>H</u>-amide and O4' of the C3 sugar of DNA. (C) Distance between the side chain ammonium group ($R_2\underline{N}H_2^+$) and $\underline{P}O_4^-$ of C3.

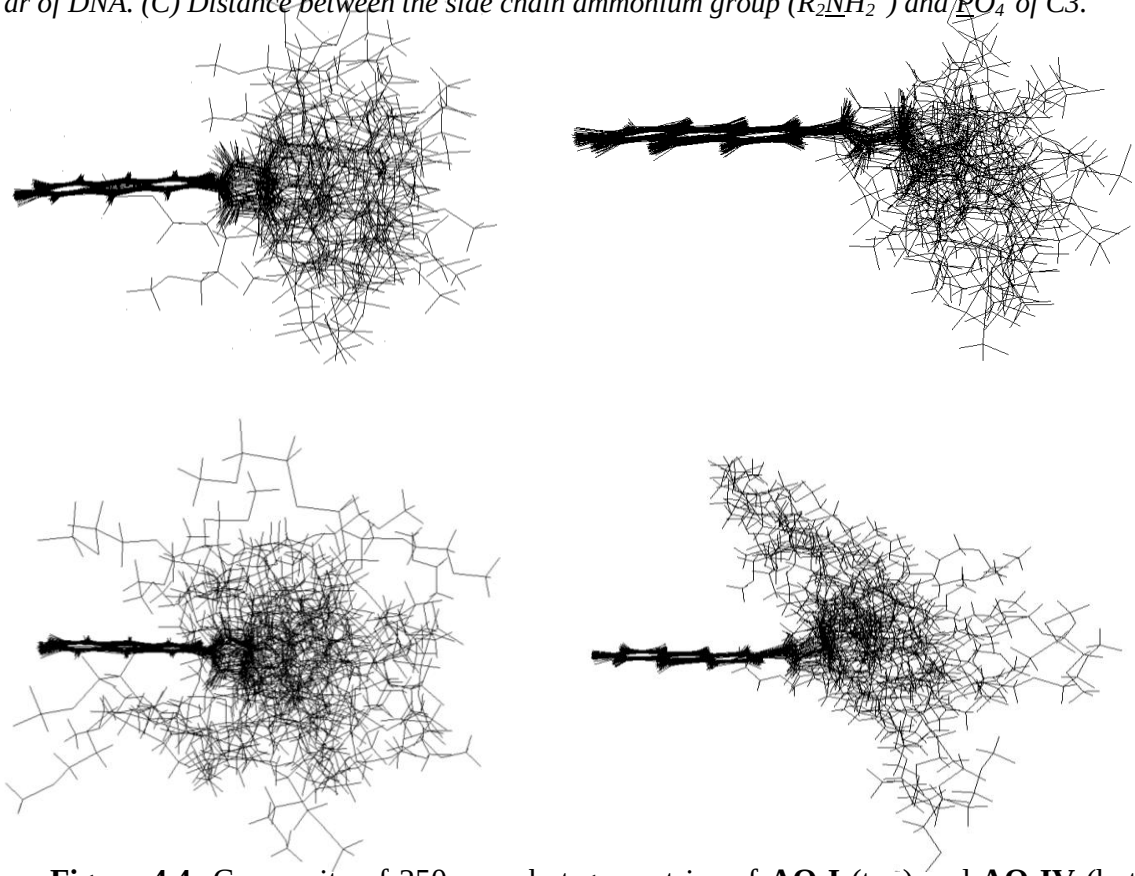

Figure 4.4: Composite of 250 snapshot geometries of **AQ I** (top) and **AQ IV** (bottom) between 10 to 50 ns for the free (left) and bound (right) ligands.

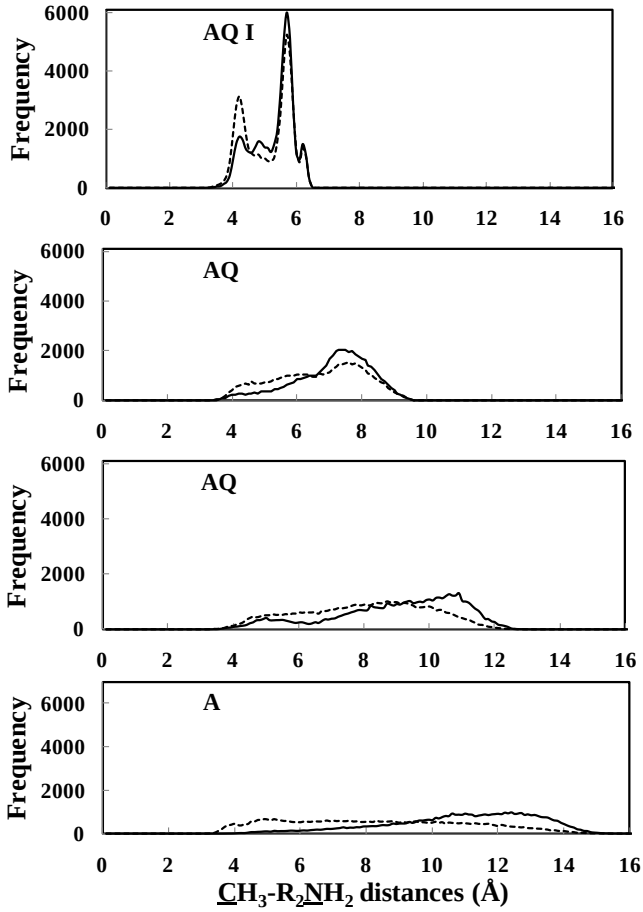

Figure 4.6: Analysis of the side chain conformation of **AQ I-IV**; data are presented as a function of distances between the $R_2\underline{N}H_2^+$ group and terminal methyl of the side chain.
The dashed lines are the free AQ ligand and the solid lines are the bound AQ ligand.

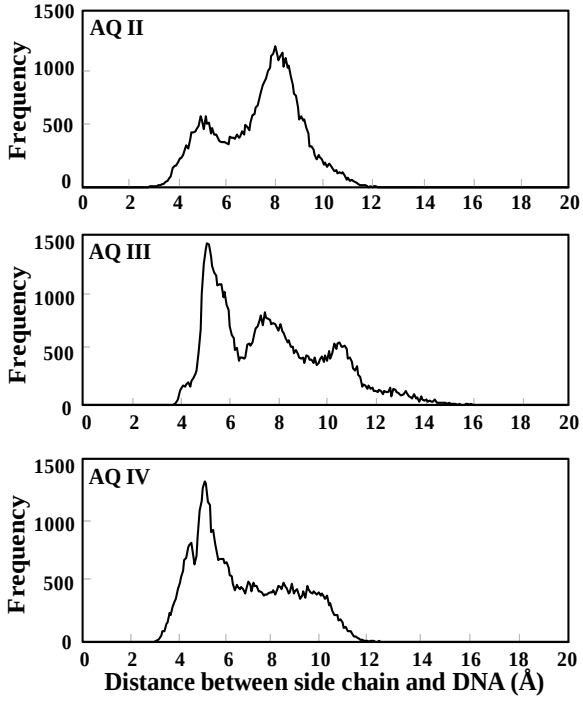

Figure 4.5: Analysis of localization of **AQ II-IV** side chain in the DNA minor groove; data are presented as a function of the distance between the second oxygen of the side chain and DG5:O2 of the DNA.

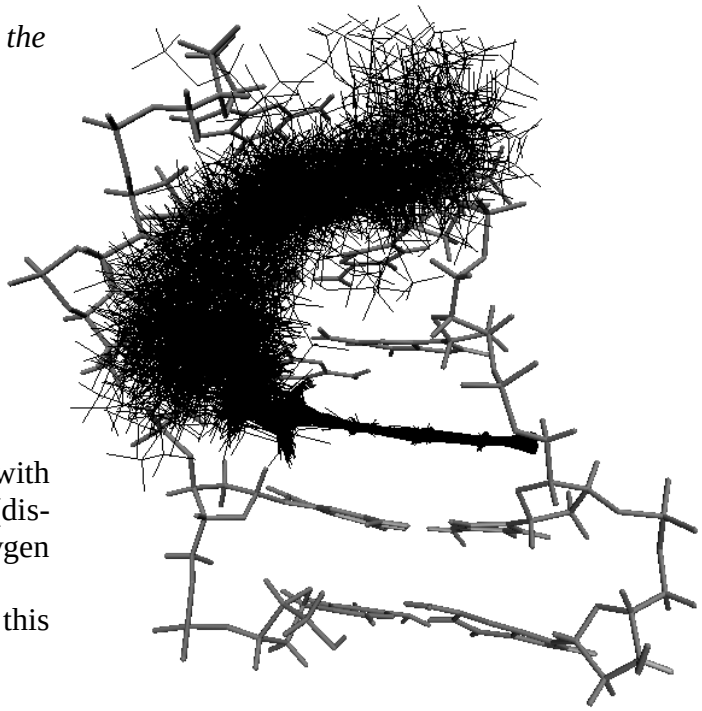

Figure 4.7: Subset of **AQ IV** structures with the side chain localized in the DNA groove (distances of less than 5 Å between second oxygen of the side chain and DG5:O2 of the DNA).
Shown are 250 shots taken randomly from this subset collected between 10 and 50 ns.

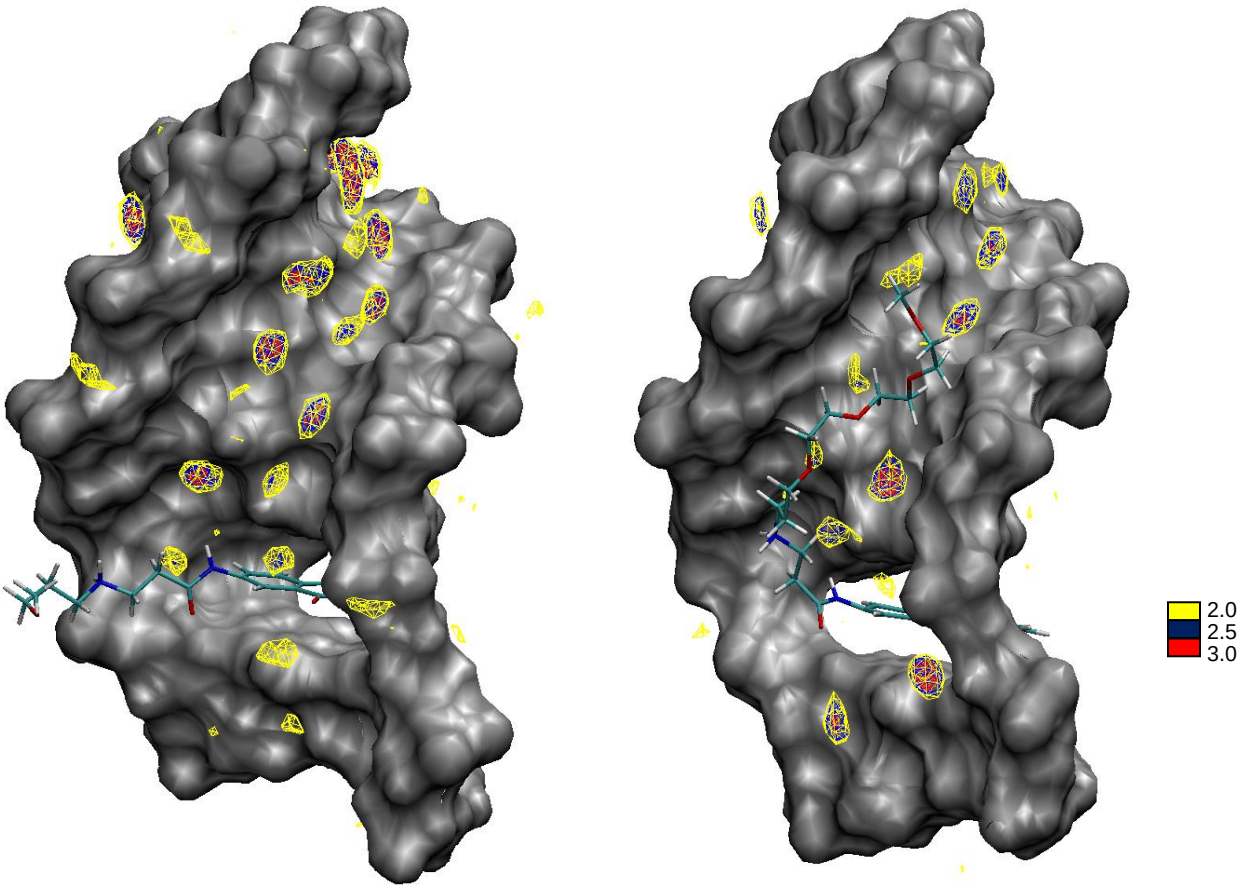

Figure 4.8: Minor groove view of the hydration of the **AQ I**-DNA complex (left) and **AQ IV**-DNA complex (right).
*The contour thresholds correspond to 2.0 or more times the average bulk water density (shown in key) during the simulation. The DNA and AQ ligand for both **AQ I** and **AQ IV** are single snap-shots representing the average structure of these complexes.*

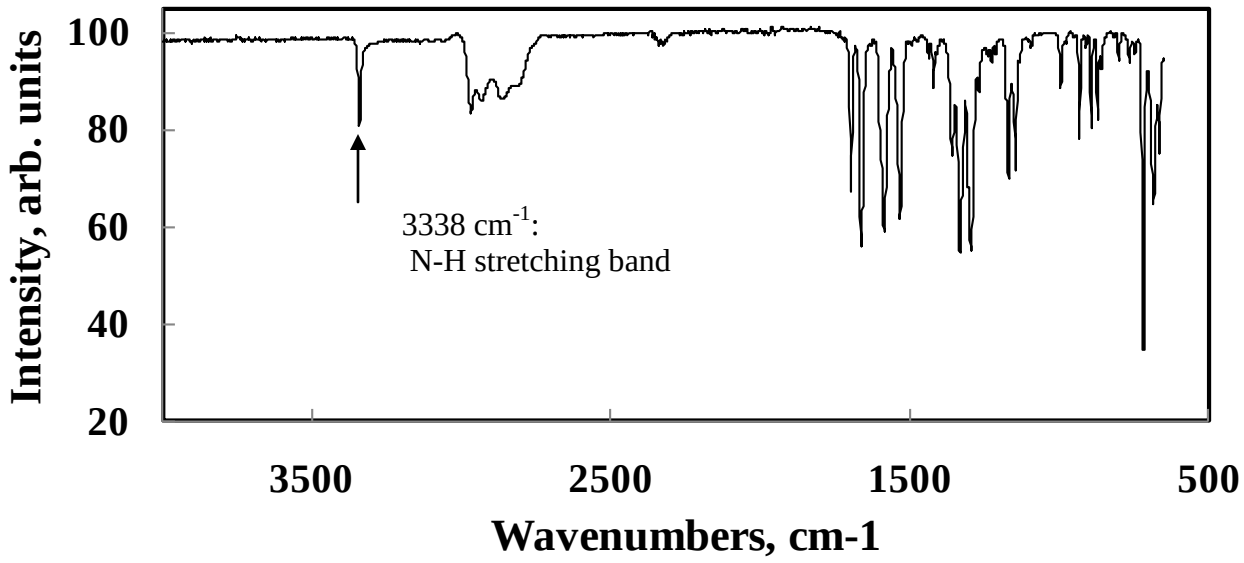

Figure 4.9 (S1): Infrared spectrum of neat **AQ I**.

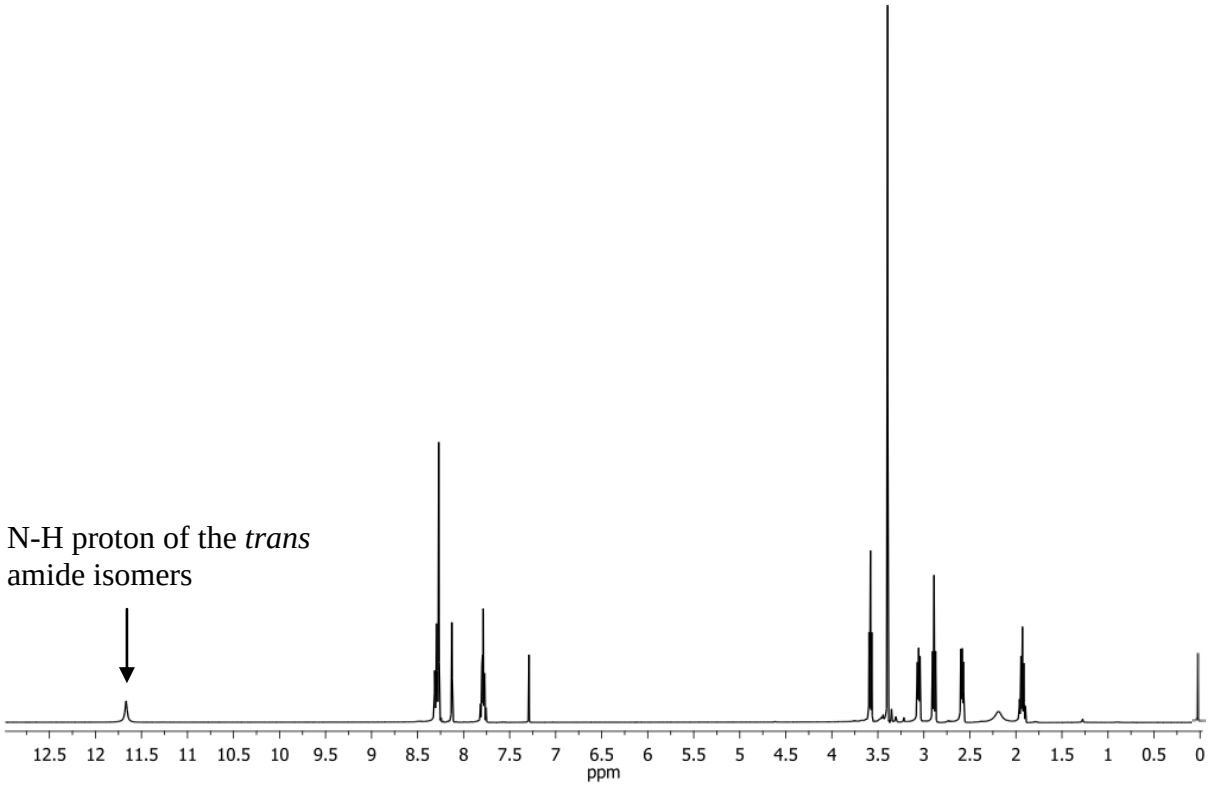

Figure 4.10 (S2): ^{1}H NMR spectrum of **AQ I** in $CDCl_3$**.**

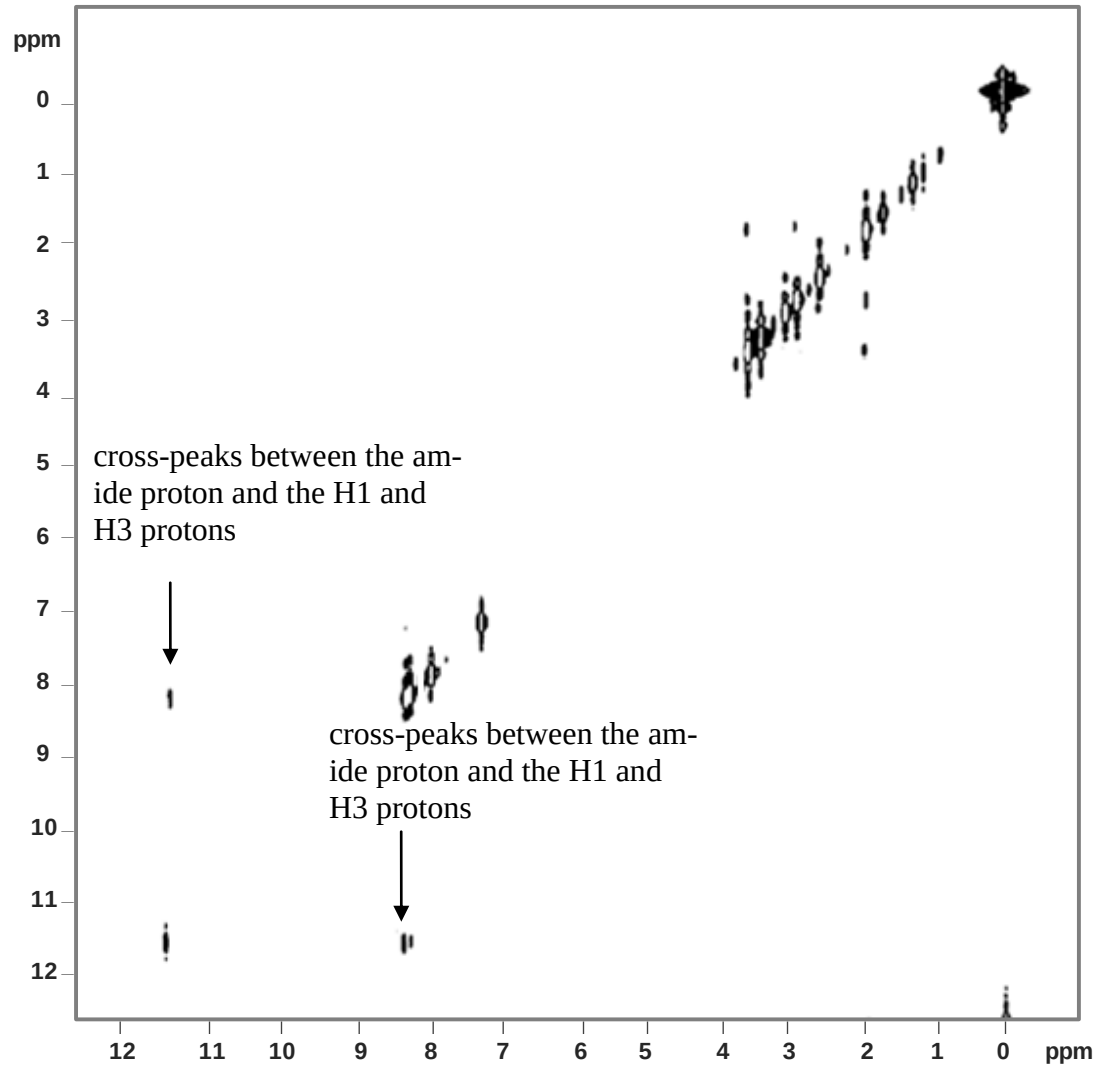

Figure 4.11 (S3): 2D ROESY NMR spectrum of **AQ I.**

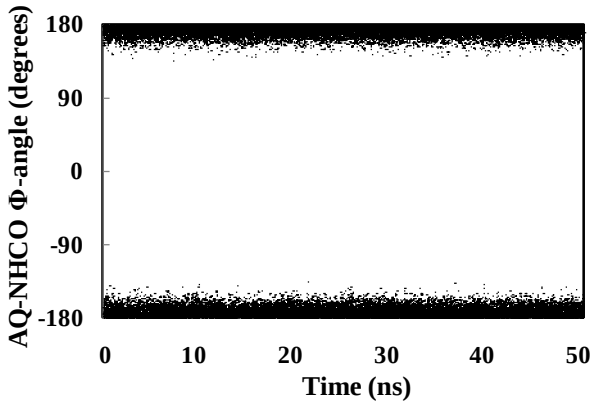

Figure 4.12 (S4): The NH-CO ω-dihedral angle as a function of time for the **AQ I** free ligand.

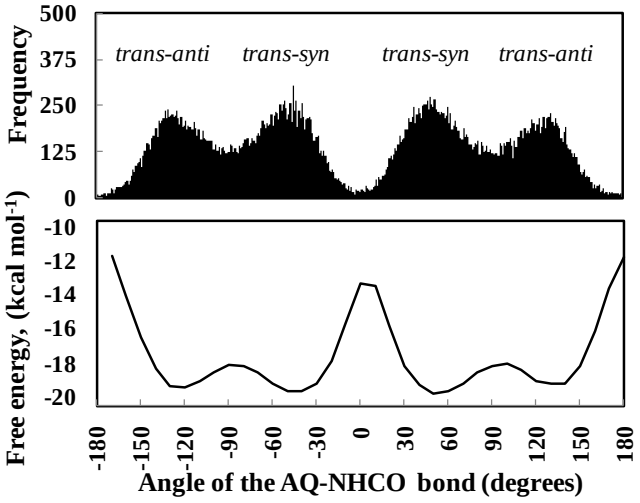

Figure 4.13 (S5): Probability plot of the AQ-NHCO Φ-dihedral angle for the free **AQ I** ligand (top). Conversion of the probability plot to its corresponding free energy profile (bottom).

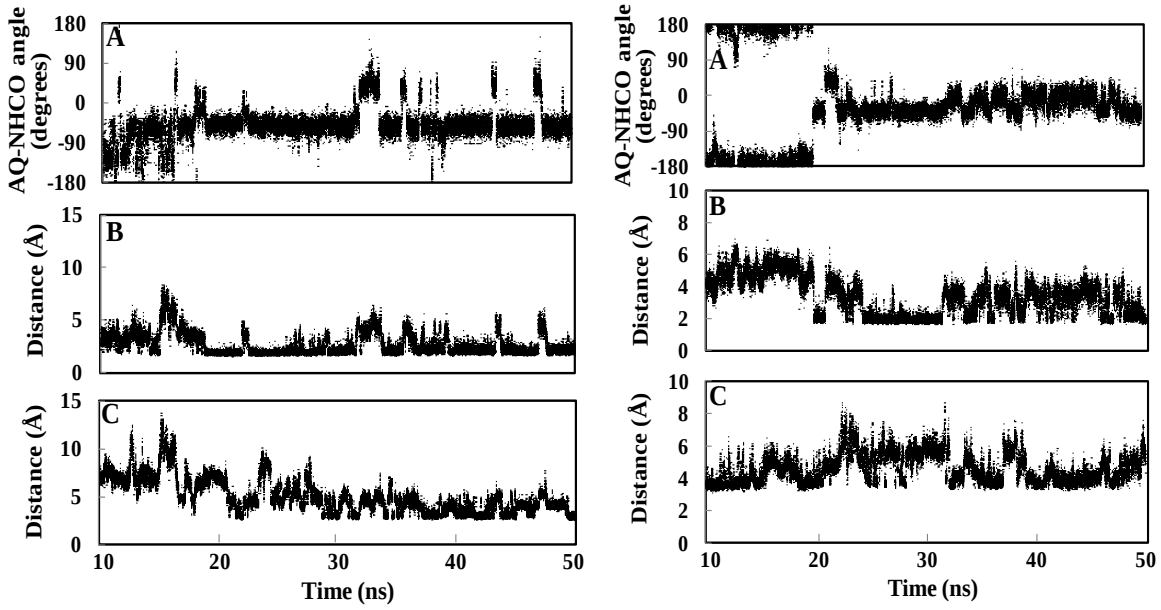

Figure 4.14 (S6): Analysis of the binding of **AQ II** (left) and **AQ III** (right) to DNA; data are presented as a function of time.
(A) Rotation about the AQ-NHCO Φ-bond. (B) Distance between NH-amide and O4' of the C3 sugar of DNA. (C) Distance between the side chain ammonium group ($R_2\underline{N}H_2^+$) and $\underline{P}O_4^-$ of C3.

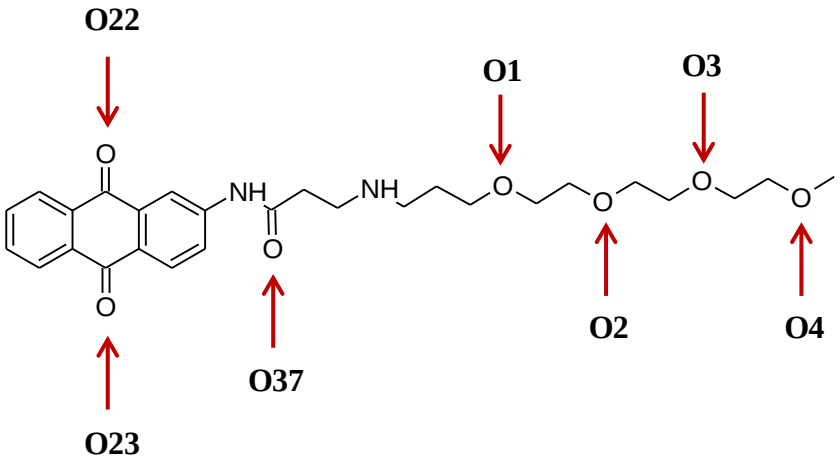

Figure 4.15: Hydration of AQ-ligand.

Table 4.1: Entropy change of the **AQ I-IV** side chain when free in solution and bound to DNA.

Ligand	$T\Delta S_{free}$ (kcal/mol)	$T\Delta S_{bound}$ (kcal/mol)	$T\Delta S_{conf}$ (kcal/mol)
AQ I	46.5	42.6	-3.9
AQ II	52.3	47.8	-4.5
AQ III	60.2	55.7	-4.5
AQ IV	71.1	64.8	-6.3

Table 4.2: Hydration of the **AQ IV** side chain when free in solution and bound to DNA.

Side chain conformation	Zero water bridge (%)	One water bridge (%)	Two water bridges (%)	Three water bridges (%)	Four water bridges (%)
Bound **AQ IV** localized in the DNA groove*	28	44	20	6	1
Bound **AQ IV** not localized in the DNA groove†	16	34	32	14	3
Free **AQ IV**	14	12	45	25	4

* Localization was defined by using distances of < 5 Å between the second oxygen of the side chain and DG5:O2 of the DNA .

† Defined by using distances of ≥ 5 Å between the second oxygen of the side chain and DG5:O2 of the DNA.

Table 4.3: Hydration of the oxygens in **AQ I-IV** when free in solution and bound to DNA.

	AQ I	**AQ I**	**AQ II**	**AQ II**	**AQ III**	**AQ III**	**AQ IV**	**AQ IV**
	Free	Bound	Free	Bound	Free	Bound	Free	Bound
O22	99	95	97	96	98	93	96	91
O37	89	92	93	90	94	92	92	90
O23	88	86	85	87	83	81	84	81
O4							94	72
O3					88	67	92	64
O2			68	53	82	63	86	56
O1	53	49	65	52	71	50	86	67
Internal Bridges								
O1-O2			37	25	33	26	57	40
O2-O3					47	35	24	18
O3-O4							62	39
O1-O3					11	7	17	16
O2-O4							21	17

4.3 References

1. Wemmer, D. E. (2000) Designed sequence-specific minor groove ligands, *Annu. Rev. Biophys. Biomol. Struct. 29*, 439-461.
2. Wilson, W. D., and Li, K. (2000) Targeting RNA with small molecules, *Curr. Med. Chem. 7*, 73-98.
3. Ebbinghaus, S. W. (2003) Site-selective DNA binding drugs, *Chem. Biol. 10*, 895-897.
4. Tse, W. C., and Boger, D. L. (2004) Sequence-selective DNA recognition: Natural products and nature's lessons, *Chem. Biol. 11*, 1607-1617.
5. Wang, B. C., Tan, J., and Zhu, L. C. (2010) Selective binding of small molecules to DNA: Application and perspectives, *Colloids Surf., B 79*, 1-4.
6. Kakkar, R., Suruchi, and Grover, R. (2005) Theoretical study of molecular recognition by Hoechst 33258 derivatives, *J. Biomol. Struct. Dyn. 23*, 37-47.
7. Kanakis, C. D., Tarantilis, P. A., Polissiou, M. G., Diamantoglou, S., and Tajmir-Riahi, H. A. (2005) DNA interaction with naturally occurring antioxidant flavonoids quercetin, kaempferol, and delphinidin, *J. Biomol. Struct. Dyn. 22*, 719-724.
8. Vardevanyan, P. O., Antonyan, A. P., Parsadanyan, M. A., Davtyan, H. G., Boyajyan, Z. R., and Karapetian, A. T. (2005) Complex-formation of ethidium bromide with poly d(A-T)·poly d(A-T), *J. Biomol. Struct. Dyn. 22*, 465-470.
9. Ovchinnikov, A. V., Baranovsky, S. F., Rozvadovska, A. O., Rogova, O. V., Veselkov, K. A., Ermolaev, A. V., ParkeS, H., Davies, D. B., and Evstigneev, M. P. (2007) Structural basis for the binding affinity of a homologous series of synthetic phenoxazone drugs with DNA: NMR and molecular mechanics analysis, *J. Biomol. Struct. Dyn. 24*, 443-453.
10. Barone, G., Guerra, C. F., Gambino, N., Silvestri, A., Lauria, A., Almerico, A. M., and Bickelhaupt, F. M. (2008) Intercalation of daunomycin into stacked DNA base pairs. DFT study of an anticancer drug, *J. Biomol. Struct. Dyn. 26*, 115-129.
11. Bazhulina, N. P., Nikitin, A. M., Rodin, S. A., Surovaya, A. N., Kravatsky, Y. V., Pismensky, V. F., Archipova, V. S., Martin, R., and Gursky, G. V. (2009) Binding of Hoechst 33258 and its Derivatives to DNA, *J. Biomol. Struct. Dyn. 26*, 701-718.
12. Saha, B., Mukherjee, A., Santra, C. R., Chattopadhyay, A., Ghosh, A. N., Choudhuri, U., and Karmakar, P. (2009) Alprazolam Intercalates into DNA, *J. Biomol. Struct. Dyn. 26*, 421-429.
13. Lown, J. W. (1993) Anthracycline and anthraquinone anticancer agents: Current status and recent developments, *Pharmacol. Ther. 60*, 185-214.
14. Arcamone, F., Animati, F., Capranico, G., Lombardi, P., Pratesi, G., Manzini, S., Supino, R., and Zunino, F. (1997) New developments in antitumor anthracyclines, *Pharmacol. Ther. 76*, 117-124.
15. Monneret, C. (2001) Recent developments in the field of antitumour anthracyclines, *Eur. J. Med. Chem. 36*, 483-493.
16. Minotti, G., Menna, P., Salvatorelli, E., Cairo, G., and Gianni, L. (2004) Anthracyclines: Molecular advances and pharmacologic developments in antitumor activity and cardiotoxicity, *Pharmacol. Rev. 56*, 185-229.
17. Asche, C. (2005) Antitumour quinones, *Mini-Rev. Med. Chem. 5*, 449-467.
18. Kratz, F., Warnecke, A., Schmid, B., Chung, D. E., and Gitzel, M. (2006) Prodrugs of anthracyclines in cancer chemotherapy, *Curr. Med. Chem. 13*, 477-523.

19. Agbandje, M., Jenkins, T. C., McKenna, R., Reszka, A. P., and Neidle, S. (1992) Anthracene-9,10-diones as potential anticancer agents. Synthesis, DNA-binding, and biological studies on a series of 2,6-disubstituted derivatives, *J. Med. Chem. 35*, 1418-1429.
20. Tanious, F. A., Jenkins, T. C., Neidle, S., and Wilson, W. D. (1992) Substituent position dictates the intercalative DNA-binding mode for anthracene-9,10-dione antitumor drugs, *Biochemistry 31*, 11632-11640.
21. Haq, I., Ladbury, J. E., Chowdhry, B. Z., and Jenkins, T. C. (1996) Molecular anchoring of duplex and triplex DNA by disubstituted anthracene-9,10-diones: Calorimetric, UV melting, and competition dialysis studies, *J. Am. Chem. Soc. 118*, 10693-10701.
22. McKnight, R. E., Zhang, J. G., and Dixon, D. W. (2004) Binding of a homologous series of anthraquinones to DNA, *Bioorg. Med. Chem. Lett. 14*, 401-404.
23. Fox, K. R., Polucci, P., Jenkins, T. C., and Neidle, S. (1995) A molecular anchor for stabilizing triple-helical DNA, *Proc. Natl. Acad. Sci. U. S. A. 92*, 7887-7891.
24. Keppler, M. D., Read, M. A., Perry, P. J., Trent, J. O., Jenkins, T. C., Reszka, A. P., Neidle, S., and Fox, K. R. (1999) Stabilization of DNA triple helices by a series of mono- and disubstituted amidoanthraquinones, *Eur. J. Biochem. 263*, 817-825.
25. Sun, D. Y., Thompson, B., Cathers, B. E., Salazar, M., Kerwin, S. M., Trent, J. O., Jenkins, T. C., Neidle, S., and Hurley, L. H. (1997) Inhibition of human telomerase by a G-quadruplex-interactive compound, *J. Med. Chem. 40*, 2113-2116.
26. Han, H. Y., and Hurley, L. H. (2000) G-quadruplex DNA: A potential target for anti-cancer drug design, *Trends Pharmacol. Sci. 21*, 136-142.
27. Harrington, D. J., Cemeli, E., Carder, J., Fearnley, J., Estdale, S., Perry, P. J., Jenkins, T. C., and Anderson, D. (2003) Genotoxicity studies on DNA-interactive telomerase inhibitors with application as anti-cancer agents, *Teratog. Carcinog. Mutagen. 23*, 31-41.
28. Zagotto, G., Sissi, C., Lucatello, L., Pivetta, C., Cadamuro, S. A., Fox, K. R., Neidle, S., and Palumbo, M. (2008) Aminoacyl-anthraquinone conjugates as telomerase inhibitors: Synthesis, biophysical and biological evaluation, *J. Med. Chem. 51*, 5566-5574.
29. Zagotto, G., Sissi, C., Moro, S., Dal Ben, D., Parkinson, G. N., Fox, K. R., Neidle, S., and Palumbo, M. (2008) Amide bond direction modulates G-quadruplex recognition and telomerase inhibition by 2,6- and 2,7-bis-substituted anthracenedione derivatives, *Bioorg. Med. Chem. 16*, 354-361.
30. Helissey, P., Bailly, C., Vishwakarma, J. N., Auclair, C., Waring, M. J., and Giorgi-Renault, S. (1996) DNA minor groove cleaving agents: Synthesis, binding and strand cleaving properties of anthraquinone-oligopyrrolecarboxamide hybrids, *Anticancer. Drug Des. 11*, 527-551.
31. Steullet, V., Edwards-Bennett, S., and Dixon, D. W. (1999) Cleavage of abasic sites in DNA by intercalator-amines, *Bioorg. Med. Chem. 7*, 2531-2540.
32. Breslin, D. T., and Schuster, G. B. (1996) Anthraquinone photonucleases: Mechanisms for GG-selective and nonselective cleavage of double-stranded DNA, *J. Am. Chem. Soc. 118*, 2311-2319.
33. Shammas, M. A., Koley, H., Beer, D. G., Li, C., Goyal, R. K., and Munshi, N. C. (2004) Growth arrest, apoptosis, and telomere shortening of Barrett's-associated adenocarcinoma cells by a telomerase inhibitor, *Gastroenterology 126*, 1337-1346.
34. Huang, H. S., Huang, K. F., Li, C. L., Huang, Y. Y., Chiang, Y. H., Huang, F. C., and Lin, J. J. (2008) Synthesis, human telomerase inhibition and anti-proliferative studies of a

series of 2,7-bis-substituted amido-anthraquinone derivatives, *Bioorg. Med. Chem. 16*, 6976-6986.
35. Huang, H.-S., Chen, T.-C., Chen, R.-H., Huang, K.-F., Huang, F.-C., Jhan, J.-R., Chen, C.-L., Lee, C.-C., Lo, Y., and Lin, J.-J. (2009) Synthesis, cytotoxicity and human telomerase inhibition activities of a series of 1,2-heteroannelated anthraquinones and anthra[1,2-d]imidazole-6,11-dione homologues, *Bioorg. Med. Chem. 17*, 7418-7428.
36. Shangguan, G. Q., Huang, L. L., and Qu, X. G. (2007) The synthesis and cytotoxic activity of novel organogermanium sesquioxides with anthraquinone or naphthalene moiety, *Chin. Chem. Lett. 18*, 1347-1350.
37. Shchekotikhin, A. E., Glazunova, V. A., Luzikov, Y. N., Buyanov, V. N., Susova, O. Y., Shtil, A. A., and Preobrazhenskaya, M. N. (2006) Synthesis and structure-activity relationship studies of 4,11-diaminonaphtho[2,3-f]indole-5,10-diones, *Bioorg. Med. Chem. 14*, 5241-5251.
38. Perry, P. J., Gowan, S. M., Reszka, A. P., Polucci, P., Jenkins, T. C., Kelland, L. R., and Neidle, S. (1998) 1,4- and 2,6-Disubstituted amidoanthracene-9,10-dione derivatives as inhibitors of human telomerase, *J. Med. Chem. 41*, 3253-3260.
39. Jackson Beckford, S., and Dixon, D. W. (2012) Molecular dynamics of anthraquinone DNA intercalators with polyethylene glycol side chains, *J. Biomol. Struct. Dyn. 29*, 1065-1080.
40. Jain, N., and Yalkowsky, S. H. (2001) Estimation of the aqueous solubility I: Application to organic nonelectrolytes, *J. Pharm. Sci. 90*, 234-252.
41. Mills, N. (2006) ChemDraw ultra 10.0, *J. Am. Chem. Soc. 128*, 13649-13650.
42. Lavery, P. E., and Kowalczykowski, S. C. (1992) Enhancement of recA protein-promoted DNA strand exchange activity by volume-occupying agents, *J. Biol. Chem. 267*, 9307-9314.
43. Ellis, R. J. (2001) Macromolecular crowding: Obvious but underappreciated, *Trends Biochem. Sci. 26*, 597-604.
44. Goobes, R., Kahana, N., Cohen, O., and Minsky, A. (2003) Metabolic buffering exerted by macromolecular crowding on DNA-DNA interactions: Origin and physiological significance, *Biochemistry 42*, 2431-2440.
45. Miyoshi, D., and Sugimoto, N. (2008) Molecular crowding effects on structure and stability of DNA, *Biochimie 90*, 1040-1051.
46. Muhuri, S., Mimura, K., Miyoshi, D., and Sugimoto, N. (2009) Stabilization of three-way junctions of DNA under molecular crowding conditions, *J. Am. Chem. Soc. 131*, 9268-9280.
47. Zheng, K., Chen, Z., Hao, Y., and Tan, Z. (2010) Molecular crowding creates an essential environment for the formation of stable G-quadruplexes in long double-stranded DNA, *Nucl. Acids Res. 38*, 327-338.
48. Kilburn, D., Roh, J. H., Guo, L., Briber, R. M., and Woodson, S. A. (2010) Molecular crowding stabilizes folded RNA structure by the excluded volume effect, *J. Am. Chem. Soc. 132*, 8690-8696.
49. Rajendran, A., Nakano, S., and Sugimoto, N. (2010) Molecular crowding of the cosolutes induces an intramolecular i-motif structure of triplet repeat DNA oligomers at neutral pH, *Chem. Commun. 46*, 1299-1301.

50. Chaires, J. B., Satyanarayana, S., Suh, D., Fokt, I., Przewloka, T., and Priebe, W. (1996) Parsing the free energy of anthracycline antibiotic binding to DNA, *Biochemistry 35*, 2047-2053.
51. Zhu, S. H., Yan, L. M., Ji, X. B., and Lu, W. C. (2010) Conformational diversity of anthracycline anticancer antibiotics: A density functional theory calculation, *THEOCHEM 951*, 60-68.
52. Kostjukov, V. V., Khomytova, N. M., Davies, D. B., and Evstigneev, M. P. (2008) Electrostatic contribution to the energy of binding of aromatic ligands with DNA, *Biopolymers 89*, 680-690.
53. Kostjukov, V. V., Khomytova, N. M., and Evstigneev, M. P. (2009) Partition of thermodynamic energies of drug-DNA complexation, *Biopolymers 91*, 773-790.
54. Mukherjee, A., Lavery, R., Bagchi, B., and Hynes, J. T. (2008) On the molecular mechanism of drug intercalation into DNA: A simulation study of the intercalation pathway, free energy, and DNA structural changes, *J. Am. Chem. Soc. 130*, 9747-9755.
55. Sarma, R. L., Kalita, R., Karim, M., Bezbaruah, B., and Medhi, C. (2008) Ab initio molecular orbital and force field calculations on the interaction of daunomycin with GC base-pair and intercalation within DNA, *Indian J. Chem., Sect B 47*, 1605-1610.
56. Kostjukov, V. V., Lantushenko, A. O., Davies, D. B., and Evstigneev, M. P. (2007) On the origin of the decrease in stability of the DNA hairpin d(GCGAAGC) on complexation with aromatic drugs, *Biophys. Chem. 129*, 56-59.
57. Jain, M., Barthwal, S. K., Barthwal, R., and Govil, G. (2005) Restrained molecular dynamics studies on complex of adriamycin with DNA hexamer sequence d-CGATCG, *Arch. Biochem. Biophys. 439*, 12-24.
58. Cashman, D. J., and Kellogg, G. E. (2004) A computational model for anthracycline binding to DNA: Tuning groove-binding intercalators for specific sequences, *J. Med. Chem. 47*, 1360-1374.
59. Trieb, M., Rauch, C., Wibowo, F. R., Wellenzohn, B., and Liedl, K. R. (2004) Cooperative effects on the formation of intercalation sites, *Nucl. Acids Res. 32*, 4696-4703.
60. Trieb, M., Rauch, C., Wellenzohn, B., Wibowo, F., Loerting, T., Mayer, E., and Liedl, K. R. (2004) Daunomycin intercalation stabilizes distinct backbone conformations of DNA, *J. Biomol. Struct. Dyn. 21*, 713-724.
61. Shi, Y. Y., Zhao, H. M., and Wang, C. X. (1993) Relative binding free-energy calculations of DNAto daunomycin and its 13-dihydro analog, *Int. J. Biol. Macromol. 15*, 247-251.
62. Song, M. Y., and Jhon, M. S. (1992) Molecular dynamics study of the effect of ion concentration on the B-DNA, Z-DNA and DNA-daunomycin complex, *THEOCHEM 89*, 33-47.
63. Islam, S. A., Neidle, S., Gandecha, B. M., and Brown, J. R. (1983) Experimental and computer graphics simulation analyses of the DNA interaction of 1,8-bis-(2-diethylaminoethylamino)-anthracene-9, 10-dione, a compound modelled on doxorubicin, *Biochem. Pharmacol. 32*, 2801-2808.
64. van Houte, L. P. A., van Garderen, C. J., and Patel, D. J. (1993) The antitumor drug nogalamycin forms 2 different intercalation complexes with d(GCGT)•d(ACGC), *Biochemistry 32*, 1667-1674.

65. Mazerski, J., Martelli, S., and Borowski, E. (1998) The geometry of intercalation complex of antitumor mitoxantrone and ametantrone with DNA: Molecular dynamics simulations, *Acta Biochim. Pol. 45*, 1-11.
66. Williams, H. E. L., and Searle, M. S. (1999) Structure, dynamics and hydration of the nogalamycin-d(ATGCAT)$_2$ complex determined by NMR and molecular dynamics simulations in solution, *J. Mol. Biol. 290*, 699-716.
67. Willcott, M. R. (2009) MestRe Nova, *J. Am. Chem. Soc. 131*, 13180-13180.
68. Searle, M. S., Maynard, A. J., and Williams, H. E. L. (2003) DNA recognition by the anthracycline antibiotic respinomycin D: NMR structure of the intercalation complex with d(AGACGTCT)(2), *Org. Biomol. Chem. 1*, 60-66.
69. Halgren, T. A. (1999) MMFF VII. Characterization of MMFF94, MMFF94s, and other widely available force fields for conformational energies and for intermolecular-interaction energies and geometries, *J. Comput. Chem. 20*, 730-748.
70. Dupradeau, F. Y., Pigache, A., Zaffran, T., Savineau, C., Lelong, R., Grivel, N., Lelong, D., Rosanski, W., and Cieplak, P. (2010) The R.ED. tools: advances in RESP and ESP charge derivation and force field library building, *Phys. Chem. Chem. Phys. 12*, 7821-7839.
71. Frisch, M. J., Trucks, G. W., Schlegel, H. B., Scuseria, G. E., Robb, M. A., Cheeseman, J. R., Montgomery, J. A., Vreven, T., Kudin, K. N., Burant, J. C., Millam, J. M., Iyengar, S. S., Tomasi, J., Barone, V., Mennucci, B., Cossi, M., Scalmani, G., Rega, N., Petersson, G. A., Nakatsuji, H., Hada, M., Ehara, M., Toyota, K., Fukuda, R., Hasegawa, J., Ishida, M., Nakajima, T., Honda, Y., Kitao, O., Nakai, H., Klene, M., Li, X., Knox, J. E., Hratchian, H. P., Cross, J. B., Bakken, V., Adamo, C., Jaramillo, J., Gomperts, R., Stratmann, R. E., Yazyev, O., Austin, A. J., Cammi, R., Pomelli, C., Ochterski, J. W., Ayala, P. Y., Morokuma, K., Voth, G. A., Salvador, P., Dannenberg, J. J., Zakrzewski, V. G., Dapprich, S., Daniels, A. D., Strain, M. C., Farkas, O., Malick, D. K., Rabuck, A. D., Raghavachari, K., Foresman, J. B., Ortiz, J. V., Cui, Q., Baboul, A. G., Clifford, S., Cioslowski, J., Stefanov, B. B., Liu, G., Liashenko, A., Piskorz, P., Komaromi, I., Martin, R. L., Fox, D. J., Keith, T., Laham, A., Peng, C. Y., Nanayakkara, A., Challacombe, M., Gill, P. M. W., Johnson, B., Chen, W., Wong, M. W., Gonzalez, C., and Pople, J. A. (2003) *Gaussian 03, Revision C.02*, Gaussian, Inc., Wallingford, CT.
72. Walker, R. C., Crowley, M. F., and Case, D. A. (2008) The implementation of a fast and accurate QM/MM potential method in Amber, *J. Comput. Chem. 29*, 1019-1031.
73. Case, D. A., Cheatham, T. E., Darden, T., Gohlke, H., Luo, R., Merz, K. M., Onufriev, A., Simmerling, C., Wang, B., and Woods, R. J. (2005) The Amber biomolecular simulation programs, *J. Comput. Chem. 26*, 1668-1688.
74. Jorgensen, W., Chandrasekhar, J., Madura, J., Impey, R., and Klein, M. (1983) Comparison of simple potential functions for simulating liquid water, *J. Chem. Phys. 79*, 926-935.
75. Mahoney, M. W., and Jorgensen, W. L. (2000) A five-site model for liquid water and the reproduction of the density anomaly by rigid, nonpolarizable potential functions, *J. Chem. Phys. 112*, 8910-8922.
76. Darden, T., York, D., and Pedersen, L. (1993) Particle mesh Ewald - an N.LOG(N) method for Ewald sums in large systems, *J. Chem. Phys. 98*, 10089-10092.

77. Ryckaert, J.-P., Ciccotti, G., and Berendsen, H. J. C. (1977) Numerical integration of the cartesian equations of motion of a system with constraints: Molecular dynamics of *n*-alkanes, *J. Comput. Phys. 23*, 327-341.
78. Schlitter, J. (1993) Estimation of absolute and relative entropies of macromolecules using the covariance matrix, *Chem. Phys. Lett. 215*, 617-621.
79. Humphrey, W., Dalke, A., and Schulten, K. (1996) VMD: Visual molecular dynamics, *J. Mol. Graph. 14*, 33-38.
80. Hamelberg, D., Shen, T., and McCammon, J. A. (2005) Relating kinetic rates and local energetic roughness by accelerated molecular-dynamics simulations, *J. Chem. Phys. 122*, 241103.
81. Stewart, W. E., and Siddall, T. H. (1970) Nuclear magnetic resonance studies of amides, *Chem. Rev. 70*, 517-551.
82. Pedersen, B. F., and Pedersen, B. (1965) The stable conformation of *N*-methylacetanilide, *Tetrahedron Lett. 6*, 2995-3001.
83. Bourn, A. J. R., Gillies, D. G., and Randall, E. W. (1966) *Cis-trans* isomerism in *N*-methyl and *N*-ethylformanilide, *Tetrahedron 22*, 1825-1829.
84. Manea, V. P., Wilson, K. J., and Cable, J. R. (1997) Conformations and relative stabilities of the *cis* and *trans* isomers in a series of isolated *N*-phenylamides, *J. Am. Chem. Soc. 119*, 2033-2039.
85. Shin, S., Kurawaki, A., Hamada, Y., Shinya, K., Ohno, K., Tohara, A., and Sato, M. (2006) Conformational behavior of *N*-methylformamide in the gas, matrix, and solution states as revealed by IR and NMR spectroscopic measurements and by theoretical calculations, *J. Mol. Struct. 791*, 30-40.
86. Evans, F. E., and Miller, D. W. (1983) Conformation and dynamics of carcinogenic *N*-substituted 2-aminofluorene compounds studied by NMR, *J. Am. Chem. Soc. 105*, 4863-4868.
87. Shell, M., Panagiotopoulos, A., and Pohorille, A. (2007) Methods Based on Probability Distributions and Histograms, In *Free Energy Calculations* (Chipot, C., and Pohorille, A., Eds.), pp 77-118, Springer Berlin Heidelberg.
88. Wang, A. H., Ughetto, G., Quigley, G. J., and Rich, A. (1987) Interactions between an anthracycline antibiotic and DNA: Molecular structure of daunomycin complexed to d(CpGpTpApCpG) at 1.2 Å resolution, *Biochemistry 26*, 1152-1163.
89. Gao, Y. G., and Wang, A. H. (1991) Influence of aglycone modifications on the binding of anthracycline drugs to DNA: The molecular structure of idarubicin and 4-*O*-demethyl-11-deoxydoxorubicin complexed to d(CGATCG), *Anticancer. Drug Des. 6*, 137-149.
90. Leonard, G. A., Brown, T., and Hunter, W. N. (1992) Anthracycline binding to DNA - high resolution structure of d(TGTACA) complexed with 4'-epiadriamycin, *Eur. J. Biochem. 204*, 69-74.
91. Dautant, A., d'Estaintot, B. L., Gallois, B., Brown, T., and Hunter, W. N. (1995) A trigonal form of the idarubicin d(CGATCG) complex - crystal and molecular structure at 2.0 Å resolution, *Nuc. Acids Res. 23*, 1710-1716.
92. Temperini, C., Cirilli, M., Aschi, M., and Ughetto, G. (2005) Role of the amino sugar in the DNA binding of disaccharide anthracyclines: crystal structure of the complex MAR70/d(CGATCG), *Bioorg. Med. Chem. 13*, 1673-1679.

93. Duff, M. R., Tan, W. B., Bhambhani, A., Perrin, B. S., Thota, J., Rodger, A., and Kumar, C. V. (2006) Contributions of hydroxyethyl groups to the DNA binding affinities of anthracene probes, *J. Phys. Chem. B 110*, 20693-20701.
94. Adnan, N., Buck, D. P., Evison, B. J., Cutts, S. M., Phillips, D. R., and Collins, J. G. (2010) DNA binding by pixantrone, *Org. Biomol. Chem. 8*, 5359-5366.
95. Spolar, R., and Record, M. (1994) Coupling of local folding to site-specific binding of proteins to DNA, *Science 263*, 777-784.
96. Wahab, S. A., Harada, T., Matsubara, T., and Aida, M. (2006) Quantum chemical study of the interaction of the short-chain poly(oxyethylene)s $CH_3(OCH_2CH_2)_mOCH_3$ ($C_1E_mC_1$; m = 1 and 2) with a water molecule in the gas phase and in solutions, *J. Phys. Chem. A 110*, 1052-1059.
97. Juneja, A., Numata, J., Nilsson, L., and Knapp, E. W. (2010) Merging implicit with explicit solvent simulations: Polyethylene glycol, *J. Chem. Theory Comput. 6*, 1871-1883.
98. Pal, S. K., and Zewail, A. H. (2004) Dynamics of water in biological recognition, *Chem. Rev. 104*, 2099-2123.
99. Li, Z., and Lazaridis, T. (2007) Water at biomolecular binding interfaces, *Phys. Chem. Chem. Phys. 9*, 573-581.
100. Kiser, J. R., Monk, R. W., Smalls, R. L., and Petty, J. T. (2005) Hydration changes in the association of Hoechst 33258 with DNA, *Biochemistry 44*, 16988-16997.
101. Vlieghe, D., Sponer, J., and Meervelt, L. V. (1999) Crystal structure of d(GGCCAATTGG) complexed with DAPI reveals novel binding mode, *Biochemistry 38*, 16443-16451.
102. Tanious, F. A., Hamelberg, D., Bailly, C., Czarny, A., Boykin, D. W., and Wilson, W. D. (2004) DNA sequence dependent monomer-dimer binding modulation of asymmetric benzimidazole derivatives, *J. Am. Chem. Soc. 126*, 143-153.
103. Van Hecke, K., Nam, P. C., Nguyen, M. T., and Van Meervelt, L. (2005) Netropsin interactions in the minor groove of d(GGCCAATTGG) studied by a combination of resolution enhancement and *ab initio* calculations, *FEBS J. 272*, 3531-3541.
104. Yu, H. J., Ren, J. S., Chaires, J. B., and Qu, X. G. (2008) Hydration of drug-DNA complexes: Greater water uptake for adriamycin compared to daunomycin, *J. Med. Chem. 51*, 5909-5911.
105. Qu, X., and Chaires, J. B. (2001) Hydration changes for DNA intercalation reactions, *J. Am. Chem. Soc. 123*, 1-7.

5 INVESTIGATION OF THE KINETICS OF A SERIES OF THREADING ANTHRAQUINONE INTERCALATORS

5.1 Introduction

Threading intercalators represent a class of high affinity DNA binding agents that interact by inserting the chromophore between the DNA bases and locating one substituent into each groove [1-7]. For association as well as dissociation to occur, one of the bulky and/or charged side chains must pass through the DNA bases; this requires significant conformational changes in the DNA structure and, in some cases, opening of at least one base pair [5, 8]. These structural constraints generally lead to slow association and dissociation rates compared to classical intercalators [2-3, 5, 7, 9-12]. The major classes of threading intercalators include naphthalene diimides [13-28], anthraquinones [1, 29-34], acridines [35-43], and binuclear ruthenium complexes [10, 12, 44-47]. The kinetics of threading intercalators have been postulated to be a feature in their cytotoxic properties for some members of this class [38, 40, 42-43, 48-51].

The naphthalene diimide (NDI) derivatives have become significant players in the field of threading intercalators, due to synthetically easy derivatization of the parent naphthalene diimide structure [13-28]. Early kinetic studies showed an apparent association rate constant of k_a ~1.4 x 10^5 M^{-1} sec^{-1}, and dissociation rate constant of k_d ~ 0.20 sec^{-1} (dependent on the salt concentration) for small members of this class with symmetrical side chains [15]. Iverson's group has more recently developed a new class of poly-threading intercalators by connecting several NDI units via flexible linkers [9, 28]. Their efforts involved developing longer poly-intercalators as well as investigating linkers of various compositions in an attempt to improve the intercalator's specificity. The dissociation half-life of a threading tetra-intercalator was ~16 days [9]. Dissociation

rates correlated with relative affinities for some members of this class [28]. The group also showed that altering the symmetry, direction, and charge in the linker allowed discrimination of up to 14 bp DNA binding sites that differed by 1 or 2 base pairs linkers by as much as 30-fold [28].

A series of binuclear ruthenium complexes with different auxiliary and bridging ligands have recently been investigated for their threading intercalating properties. Members of this class with very slow intercalation kinetics have been used to study the effect of the ligand's nature on their threading efficiency. In this context, several groups have investigated the effect of the ligand's chirality on the threading mechanism and rates [12, 52-54]. Onfelt et al. have studied the interactions of two bis-threading ruthenium enantiomers with ct-DNA [54]. The two enantiomers had similar thermodynamic affinities, but varied considerably in their binding kinetics. Dissociation from ct-DNA was markedly faster and also more dependent on the ionic strength for one of the enantiomers, possibly due to differences in the conformational changes of the DNA (which was thought to define the rate-limiting step). Andersson et al. have also shown differences in the rates due to the chirality of the ligand [12]. They postulated that for shorter bridging ligands, the interactions between the non-intercalating side chain and DNA became increasingly important and dominated the enantio-selectivity. In contrast, for longer bridging ligands, the chirality around the intercalating part seemed more important. Additional work in the area of the kinetics of metal-polypyridine complexes with DNA has been reviewed by Biver et al. [55] and by Wilhelmsson et al. [56]

There have also been several studies on the effect of structural changes in large ruthenium complexes on the DNA binding mechanism. Nordell et al. have investigated the mechanism of threading ruthenium complexes, one bearing two ruthenium phenanthroline side chains and the other, two bipyridine groups [57-58]. The mechanism of the bipyridine system was proposed to

be an initial formation of a semi-intercalated species which slowly converted to the final threaded complex. In contrast, binding of the phenanthroline analogue fit a mechanism of two parallel paths. One pathway passed through a semi-intercalated complex before the final threaded state, and the other through a groove-aligned complex before the fully intercalated state. The steric hindrance of the larger phenanthroline ligand presumably disfavored the semi-intercalated pathway. Li et al. have studied four ruthenium threading derivatives with different bulky quaternary ammonium substituents to find relationships between molecular structure and intercalation kinetics [59]. The intercalation kinetics were found to be dependent on both the charge and the distance between the bulky substituent and the ruthenium center. They proposed that the kinetic properties of the threaders were important for consideration as a chemotherapeutic agent.

Intercalators with large and rigid side chains have been used to probe the relationship between DNA dynamics and the threading process. For example, dissociation from a long stretch of alternating A–T can be more than three orders of magnitude greater than that from a mixed sequence, due to the increased structural flexibility of the AT base pairs [57, 60]. Studies of binuclear ruthenium complexes with AT-rich hairpins revealed a significant increase in the threading association rate for sequences with AT base pairs for more than one helix turn of the B-DNA [61]. The dissociation rate constants did not show a pattern in this regard and the mechanism did not depend on an open end of the hairpin. The threading process was also enhanced by loops or mismatches in the sequence. Recently, Kogan et al. have shown that a binuclear ruthenium complex can thread efficiently into reannealed polymorphic DNA in comparison to native DNA, leading to the conclusion that the threader is binding to local areas of the DNA that do not have duplex structure [62]. A dimeric ruthenium complex has been found to thread into negatively supercoiled plasmid DNA two orders of magnitude more quickly than into the cleaved linear

form of the DNA, indicating that torsional strain can have a significant controlling effect on the kinetics of intercalation [45]. In other work, threading intercalation into lambda DNA stretched with optical tweezers was interpreted in terms of binding to one or more melted base pairs [46]. The association mechanism may involve slow relaxations in the conformations of the initially bound species [47].

The final DNA structure in these DNA-intercalator complex need not be a duplex. For example, Choudhury et al. have found that a platinum-acridine bisintercalator can stabilize either the classical B-form or a non-B-form of the DNA depending on the stereochemistry around the metal center and the nature of the acridine's side chain [42]. In one instance, a structure with base pairing of a Hoogsteen nature was observed. Other work has shown that some systems have complicated mechanistic patterns. For example, an acridine with an appended polyamine center shows two binding processes depending on the DNA/intercalator ratio, with the binding mode at low ratios interpreted largely in terms of external binding and that at higher ratios in terms of intercalation of the aromatic moiety [63].

The majority of the studies to date involve changes in the three dimensional structure of the side chain, often with rigid groups that lie in the DNA grooves in the final structures. In these cases, the mechanism of the intercalation is intrinsically tied with the geometry of the final structure. In our study, we are interested in widening our understanding of the threading process by studying a series of complexes in which the final structures of the intercalated complexes, with respect to placement of the intercalating moiety itself in the DNA and their side chains, are very similar. This is a series for which the threading process is essentially uncoupled from the final structures of the intercalated species. To achieve this, we have studied a series of four ho-

mologous threading intercalators, which differ only in the lengths of the appended polyethylene-based side chains.

5.2 Work to be published

Investigation into the Kinetics of a Homologous Series of Threading Intercalators Binding to DNA

5.2.1 *Abstract*

The association rate constants of a homologous series of anthraquinone intercalators with calf thymus DNA have been studied using stopped-flow spectrophotometry. The threading mechanisms of the anthraquinones' binding to DNA showed sensitivity to the side chain length of the molecule. The curves for the three longer side chains were bi-exponential. We propose a three step mechanism which involves formation of an external bound anthraquinone-DNA complex followed by intercalation of the anthraquinone, and isomerization to another complex with similar thermodynamic stability. The kinetic curve for the shortest side chain was mono-exponential, probably corresponding to the first two steps of the three step mechanism. Our work indicates the apparent mechanistic consequences of even small changes in a flexible side chain of a DNA intercalator.

5.2.2 *Introduction*

The intercalation of molecules into DNA continues to be of interest in terms of the design of pharmaceutical agents, toxicity, and the fundamental biophysical processes that are involved in the intercalation event [2-3, 6-7, 64-68]. Threading intercalators are a subset of intercalators that bind with side chains in both the major and minor groove [1-6]. For association as well as dissociation to occur, one of the bulky and/or charged side chains must pass through the DNA bases,

which requires significant conformational changes in the DNA structure and may give complex mechanistic pictures. One of the earliest kinetic studies was on nogalamycin, an anthracycline antibiotic with appended sugars [5, 30, 69]. The association kinetics are complex and require not less than three exponentials to fit its profile with ct-DNA [69]. Other studies have also been conducted with a cis-platinum threading derivative of proflavine [70-71]. The kinetic process for this derivative was discussed in terms of a three step mechanism in which an initial external complex is formed followed by partial and then full intercalation. Much of the recent work in the area, however, has focused on large intercalators consisting of aromatic units surrounding a central metal atom [5]. Some of these structures have very slow on ($t_{1/2}$ = 132 min into AT-rich DNA) and off ($t_{1/2}$ = 17 min) rates [60]. It has been shown that the changes to the intercalator's structure can result in changes of the binding mechanism [12, 57, 59-60]. It is clear that even complex structures can eventually adopt a fully intercalated geometry, as shown by a study of a threading tetra-bisintercalator [9].

For the design of new pharmaceutical compounds, it is of interest to understand how small molecules with flexible side chains intercalate into DNA. Presumably both the ligand and DNA are required to change their conformation upon binding. In this work, we have focused on 2,6-substituted anthraquinones, which adopt a threading geometry [29, 72]. Early work on anthraquinones with small flexible side chains showed association rates that were $\leq 2 \times 10^5$ $M^{-1}s^{-1}$ [29]. The dissociation rates were $\leq$ 5-6 s^{-1}. The anthraquinones required two exponentials to fit their binding kinetics, with differences between the two rate constants of <4 fold for both association and dissociation kinetics.

In the current study, we were interested in probing the effect of larger flexible side chains. This can allow evaluation of more complex mechanisms of intercalation where the main

differences are in the threading processes *per se;* that is, a situation in which the threading process is essentially uncoupled from the final structures of the intercalated species. To achieve this, we have studied a series of four homologous threading intercalators, which differ only in the lengths of the appended polyethylene-based side chains. The final structures are expected to be very similar with respect to placement of the intercalating moiety itself in the DNA.

5.2.3 ***Results and Discussion***

The compounds used in our study, **AQT I – AQT IV** (Fig. 1), were synthesized according to the procedure reported by McKnight et al. [72] We have used a combination of fluorescence spectroscopy [73] and stopped-flow kinetics [74] to assess the equilibrium binding parameters and the association and dissociation rate constants for the binding of the four anthraquinone ligands to ct-DNA.

Figure 2 shows the equilibrium titration of **AQT IV** in the presence of ct-DNA; the anthraquinone fluorescence signal became less emissive upon binding to DNA. The equilibrium constant (4.0×10^4 M^{-1}) and the number of bases per binding site (~4) were obtained by fitting the titration data to Supplementary Equation 2. The binding constant of **AQT IV** to AT- and GC-rich DNA hairpins was previously determined to be 19×10^4 M^{-1} (n = ~3) and 9.0×10^4 M^{-1} (n = ~4), respectively, using surface plasmon resonance [72]. The small differences presumably reflect the different DNA and techniques used. Equilibrium fluorescence titrations of **AQT I**, **AQT II**, and **AQT III** gave binding constants of 3.3×10^5 M^{-1} (n = ~3), 1.6×10^5 M^{-1} (n = ~3), and 0.93×10^5 M^{-1} (n = ~3), respectively (Supplementary Figures 1-3).

The binding process for **AQT IV** to DNA showed distinct fast and slow kinetic phases. For both phases, the derived rate constants showed a hyperbolic dependence on the concentration of DNA (Figure 3). This type of dependence indicates a rapid equilibrium followed by a kinet-

ically measureable step. The simplest model consistent with the data is given in equation 1; equations appropriate for non-linear least squares fitting are in the Supplementary Data. It should be noted that all fitting takes into account the site size of the DNA-threader complex, based on the McGhee-von Hippel formalism [75] as developed by Jovin and Striker [76].

$$AQ + DNA \underset{}{\overset{K_1}{\rightleftharpoons}} AQ\text{-}DNA_1 \underset{k_{-2}}{\overset{k_2}{\rightleftharpoons}} AQ\text{-}DNA_2 \underset{k_{-3}}{\overset{k_3}{\rightleftharpoons}} AQ\text{-}DNA_3 \qquad \text{eq 1}$$

For **AQT IV**, about 60% of the fast phase was completed at the highest concentration of DNA (130 μM) within the instrument's dead time. Fitting the observed data with a site size of 4 gave an equilibrium binding constant, K_1 of 5.9 x 10^4 M^{-1}, an association rate constant, k_2 of 340 s^{-1}, and dissociation rate constant, k_{-2} of 71 s^{-1}. A site size of 3 did not give a good hyperbolic fit; a site size of 5 gave values of K_1 = 4.5 x 10^4 M^{-1}, k_2 = 290 s^{-1}, and k_{-2} = 115 s^{-1}. These data indicate the sensitivity of the calculated values to the site size assumed for the complex.

Fitting of the slow phase gave an equilibrium constant for the first two steps of 4.1 x 10^4 M^{-1}, a k_3 of 21 s^{-1} and a k_{-3} of 19 s^{-1}. The slow phase, while not as sensitive to site size as the fast phase, also displayed differences in the fitted kinetic parameters. The overall calculated equilibrium binding constant $K_{123} = K_1 [1+K_2(1 + K_3)]$ [77] was ~4.3 x 10^5 M^{-1}. This was within a factor of approximately 10 of the equilibrium constant determined by direct titration. The differences in the calculated equilibrium constant and that measured from static fluorescence titration are presumably due to partial completion of the reaction within the instrument's dead time, to the sensitivity of the calculated parameters to the DNA binding site size, and to the mathematical approach, which collapses binding at many similar, but not equivalent, sites to a simple four-component model.

The intercalation kinetics for both **AQT II** and **AQT III** showed a fast phase followed by a slow phase, similar to **AQT IV**. In these cases, however, the first phase was significantly faster than for **AQT IV**, with extents of completion that precluded good fitting of this phase (Supplementary Figures S4 and S5). The second phase of **AQT II** and **AQT III** binding to DNA was slower. Fitting to equation 7 (Supplementary Data) showed similar association and dissociation rate constants for these two homologs (Table 1). These compounds fit the intercalation model for **AQT IV**.

The intercalation model we propose for the three longer homologs involves initial formation of a weak electrostatic complex (AQ-DNA_1). Conformational changes in the DNA open an intercalation site allowing the anthraquinone to thread through the opening to give AQ-DNA_2. This slowly isomerizes to form AQ-DNA_3. The second step in equation 1 (formation of the AQ-DNA_2 complex) was visualized only for **AQT IV.** This is presumably simply a function of the longer side chain in this system, which slows its binding rate to DNA. We have previously shown that the long polyethylene glycol side chain of **AQT IV** adopts a helical conformation, and it is possible that this propensity may also affect the kinetics in this system [78].

A slow phase, with forward and reverse rate constants of about 20 s^{-1} and a K_3 equilibrium constant of about 1, was observed for all three of **AQT II**, **AQT III**, and **AQT IV**. Similar K_3 equilibrium constants have been observed for the anthraquinone based intercalator daunomycin [77] as well as proflavines [70, 79]. The most likely explanations are a conformational rearrangement of the DNA or redistribution of the ligand to other sites on the DNA. In the former instance, an AQ-DNA complex would be formed in which the ligand is only partially intercalated. This would be in equilibrium with an AQ-DNA complex that is fully intercalated and the ligand is now enveloped by the DNA bases. A second explanation is that the intercalator ini-

tially finds a kinetically favorable site, and gradually rearranges to a suite of complexes in which the intercalator is bound to other sites that are of similar thermodynamic stability. It has been shown that intercalation into AT-rich sites is generally more kinetically favorable than into GC-rich sites [60-61, 80-82]. Previous work on rigid threading intercalators has also found a significant kinetic preference for AT-rich DNA sequences. However, in that we have previously shown that these anthraquinone threaders preferentially bind to AT-sites rather than GC-sites in a thermodynamic sense [72], redistribution to a GC-site is presumably not thermodynamically favorable in this instance. It may be, however, that the initial kinetic complex is the result of binding to a stretch of AT-rich sequence, while the final complex is redistribution of the bound ligand more evenly along the DNA (perhaps still with preference for AT sites).

In contrast to **AQT II-IV** which fitted to a double exponential equation, the association kinetics of **AQT I** to ct-DNA only required a single exponential to fit the reaction trace. The apparent association rate was linearly dependent on the DNA concentration (Figure 4). The reaction was fast enough that about 60% of the process (at the highest concentration of DNA, 130 μM) occurred during the dead time of the instrument. Fitting the observed trace gave an association rate constant, k_1, of 5.2 x 10^5 $M^{-1}s^{-1}$ and a dissociation rate constant, k_{-1}, of 58 s^{-1} (n = 3, and similar for n = 4 and 5). The simple kinetic data obtained correspond to an apparent one-step mechanism for **AQT I** binding to DNA.

One possibility for the observation of the simple linear dependence kinetics is that we are observing only the first two steps of equation 1 with a small value for K_1. Indeed, the data would have a linear dependence on the concentration of DNA if the first equilibrium binding constant, K_1, were $\leq 10^3$ M^{-1}, and association rate constant for intercalation, k_2, had a value >300. A K_1 value of ~10^2 - 10^3 M^{-1} has been previously estimated for formation of an electrostatic complex

between ligands and DNA [83] and this value for k_2 is in line with that observed for the other homologs in the series. The apparent simplicity of the kinetics for **AQT I** is presumably because the side chains of this threader can easily move through local openings in the DNA that are smaller, and formed more frequently, than those required by the larger homologs in the series.

5.2.4 *Conclusion*

In conclusion, our study of the binding mechanism of anthraquinone threading intercalators to DNA has shown a high sensitivity of rates on the ligand's side chain length. The three derivatives bearing longer side chains bound via a three step mechanism. For all of them, the last step was a slow process, independent of the concentration of DNA, which had forward and reverse rate constants of about 20 s^{-1}. Although the shortest side chain ligand, **AQT I**, appeared to bind via a simple one step mechanism, it is likely that this process is the first two steps of the three step mechanism (with the last, slow, step, not observed for this ligand). Threading intercalation of ligands into DNA is influenced by two main factors: the DNA dynamics and the nature of the ligand. Smaller side chains are able to thread through small local openings in the DNA bases created by thermal fluctuations. This results in faster association rates, and an apparently simpler binding mechanism. Longer side chains are not able to thread through the local openings in the DNA, and therefore must either find locally melted regions or bind to the DNA and facilitate conformational changes in its structure. After initial threading of the ligand, the complex isomerizes to another complex with very similar energy, most seemingly via redistribution of the ligand more evenly along the DNA. However, this step may be the ligand becoming fully intercalated into the DNA. Such schemes have been observed before, but generally in complexes with rigid side chains designed to slow the threading intercalation process. Our work

shows that even small changes in a flexible intercalator side chain can lead to significant changes in the apparent intercalation process.

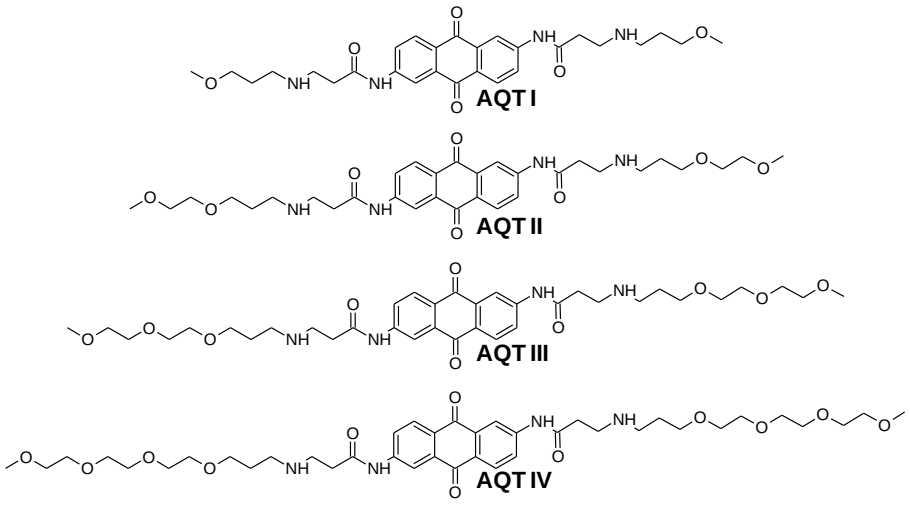

Figure 5.1 Threading anthraquinone intercalators, **AQT I - AQT IV** used in this study.

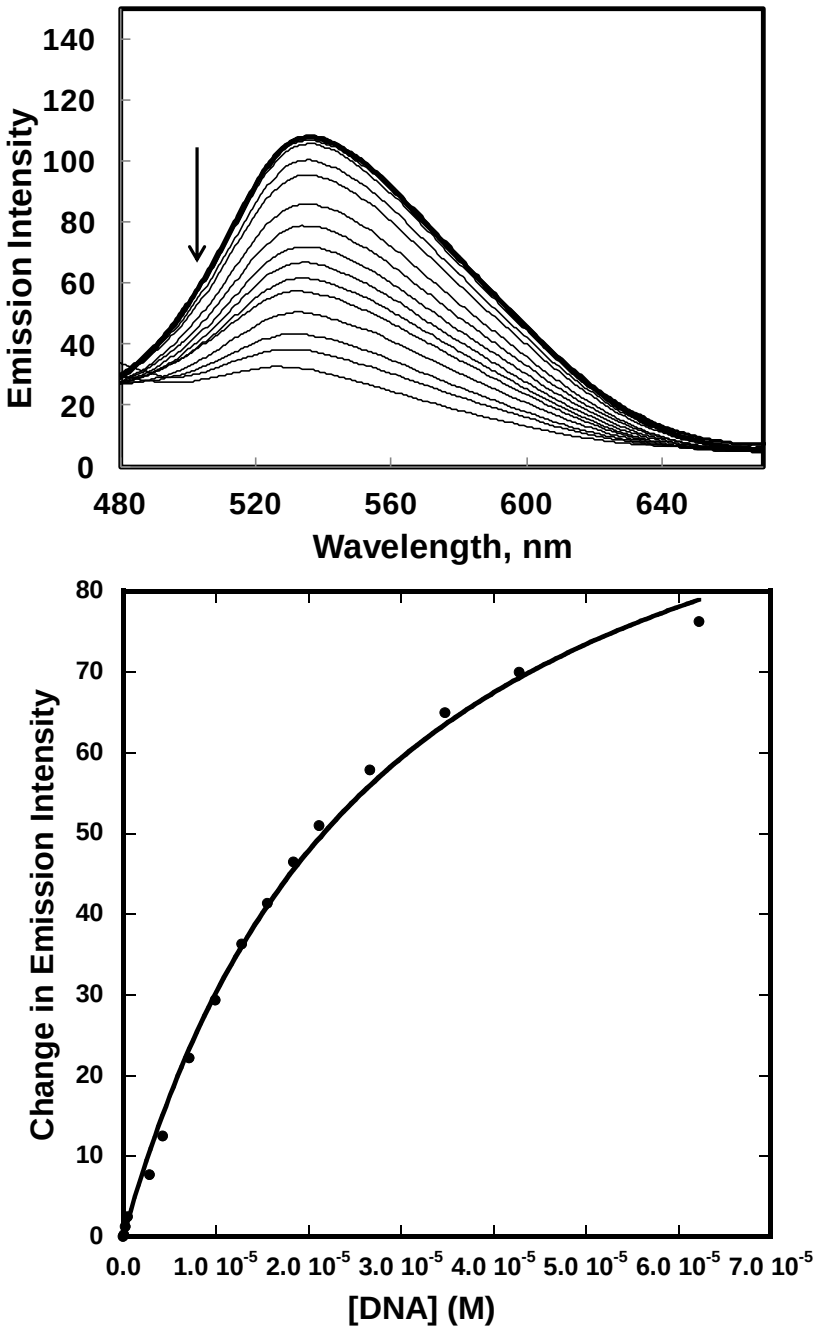

Figure 5.2: Fluorescence spectral titration of ct-DNA with 3.3 μM **AQT IV** in MES10 buffer, 0.15 M NaCl, pH 6.24 and 25 ^{o}C (λ_{ex}:354 nm; λ_{em}:536 nm).
*Top: Fluorescence spectra of **AQT IV** with ct-DNA at various DNA:**AQT IV** ratios (r_i = 0 to 60; concentration of DNA given in base pairs). Bottom: The observed change in emission intensity at 536 nm as a function of the concentration of ct-DNA were fitted with a multiple-site binding model to obtain an equilibrium binding constant and the binding site size.*

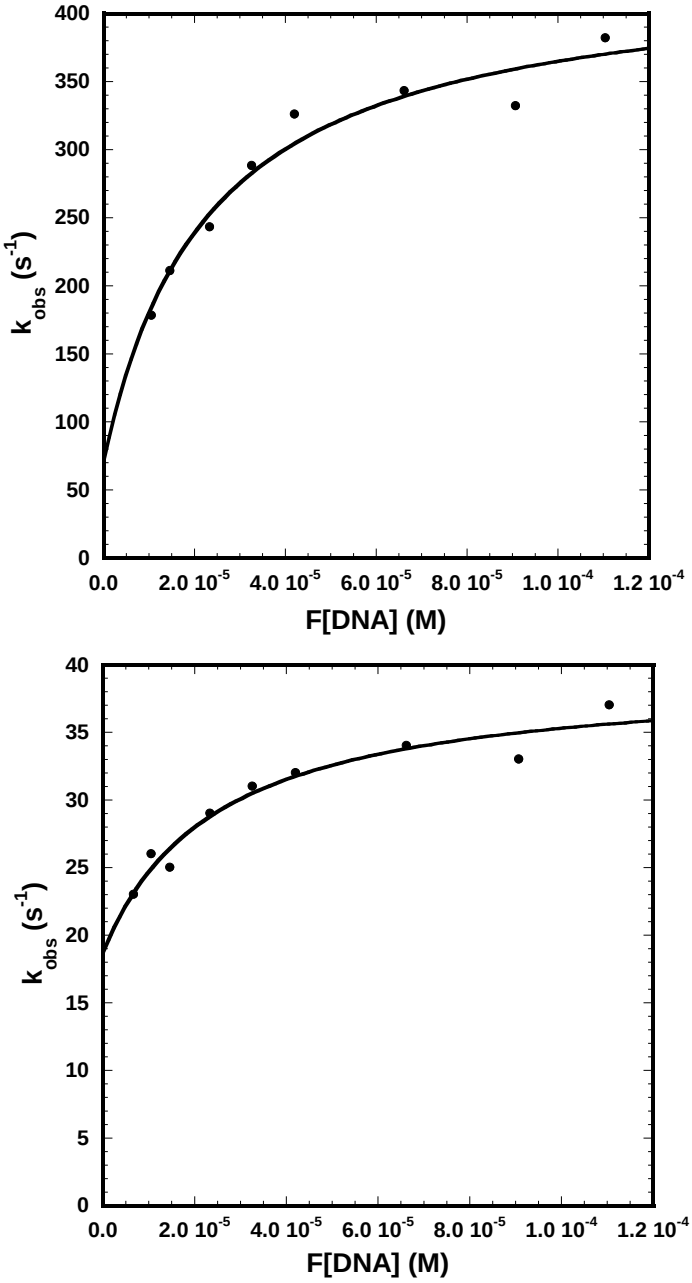

Figure 5.3: Dependence of the observed rates of the **AQT IV**/ct-DNA system on the concentration of DNA in MES10 buffer, pH 6.4, 0.15 M NaCl at 25 ^{o}C.
(A) Fast process; (B) slow process. The fitting assumed a site size of 4.

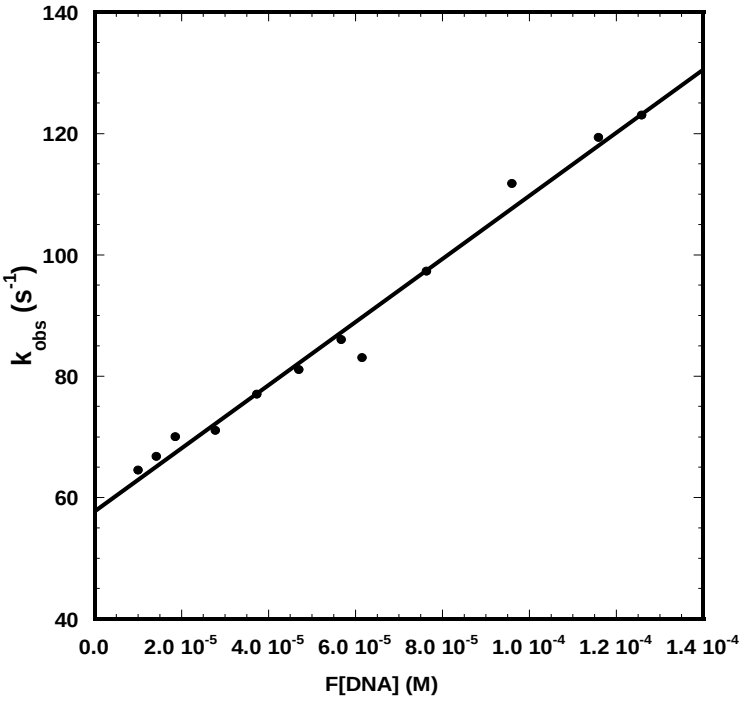

Figure 5.4: Dependence of the observed rates of the **AQT I**/ct-DNA system on the concentration of DNA in MES10 buffer, pH 6.4, 0.15 M NaCl at 25 ^{o}C.
The fitting assumed a site size of 3.

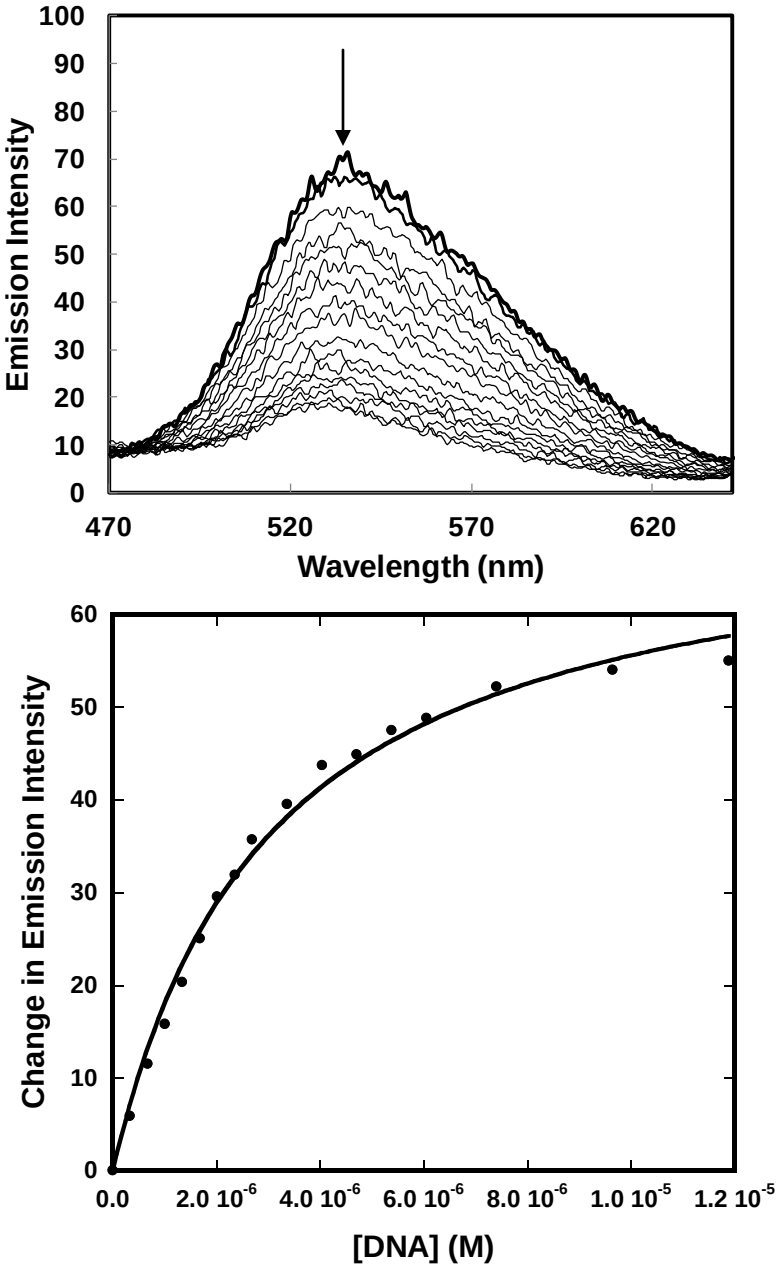

Figure 5.5 (S1): Fluorescence spectral titration of ct-DNA with 3.3 µM **AQT I** in MES10 buffer, 0.15 M NaCl, pH 6.24 and 25 ^{o}C (λ_{ex}: 354 nm; λ_{em}:536 nm).
*Top: Fluorescence spectra of **AQT I** with ct-DNA at various DNA:**AQT I** ratios (r_i = 0 to 12). Bottom: The observed change in emission intensity at 536 nm as a function of the concentration of ct-DNA were fitted with equation 2 to obtain an equilibrium binding constant and the binding site size.*

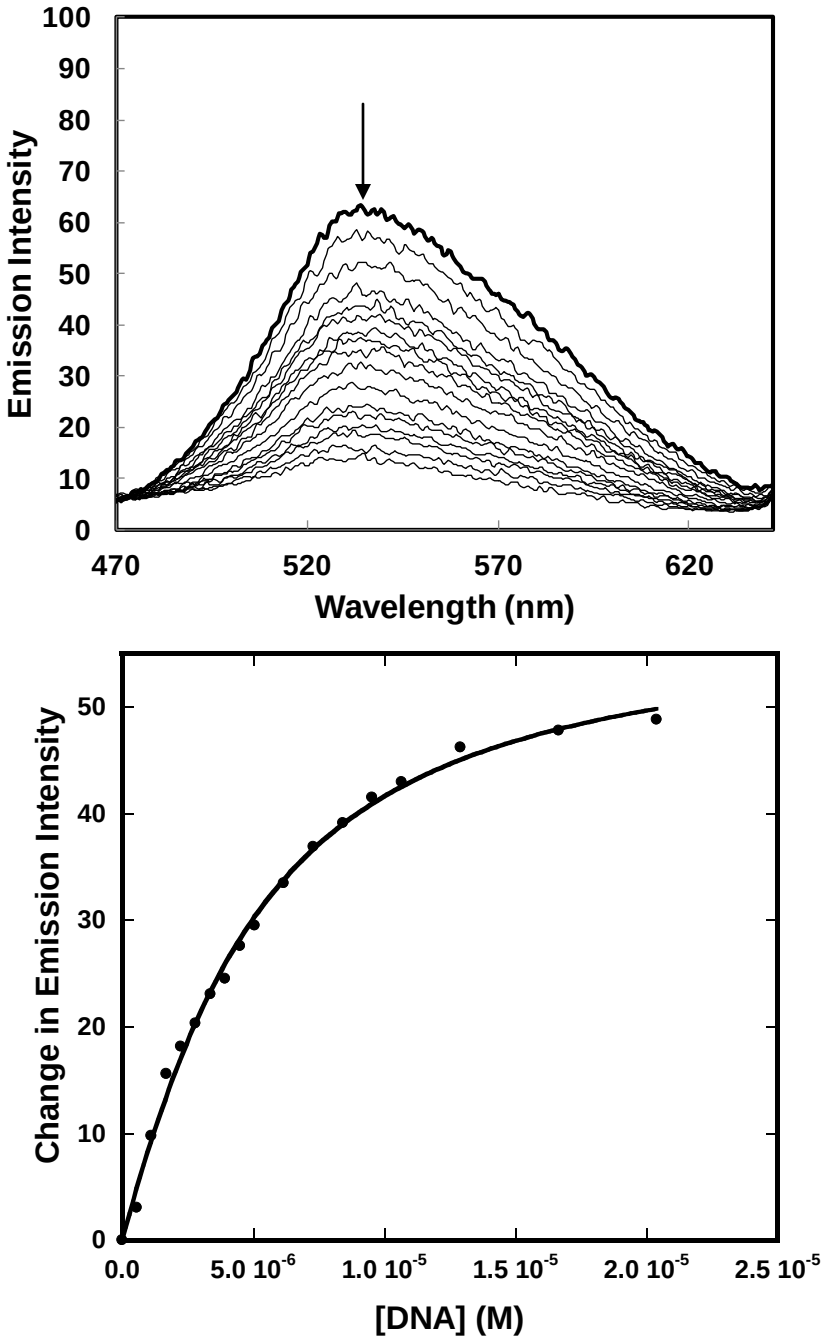

Figure 5.6 (S2): Fluorescence spectral titration of ct-DNA with 3.3 μM **AQT III** in MES10 buffer, 0.15 M NaCl, pH 6.24 and 25 ^{o}C (λ_{ex}: 354 nm; λ_{em}:536 nm).
*Top: Fluorescence spectra of **AQT III** with ct-DNA at various DNA:**AQT III** ratios (r_i = 0 to 25). Bottom: The observed change in emission intensity at 536 nm as a function of the concentration of ct-DNA were fitted with equation 2 to obtain an equilibrium binding constant and the binding site size.*

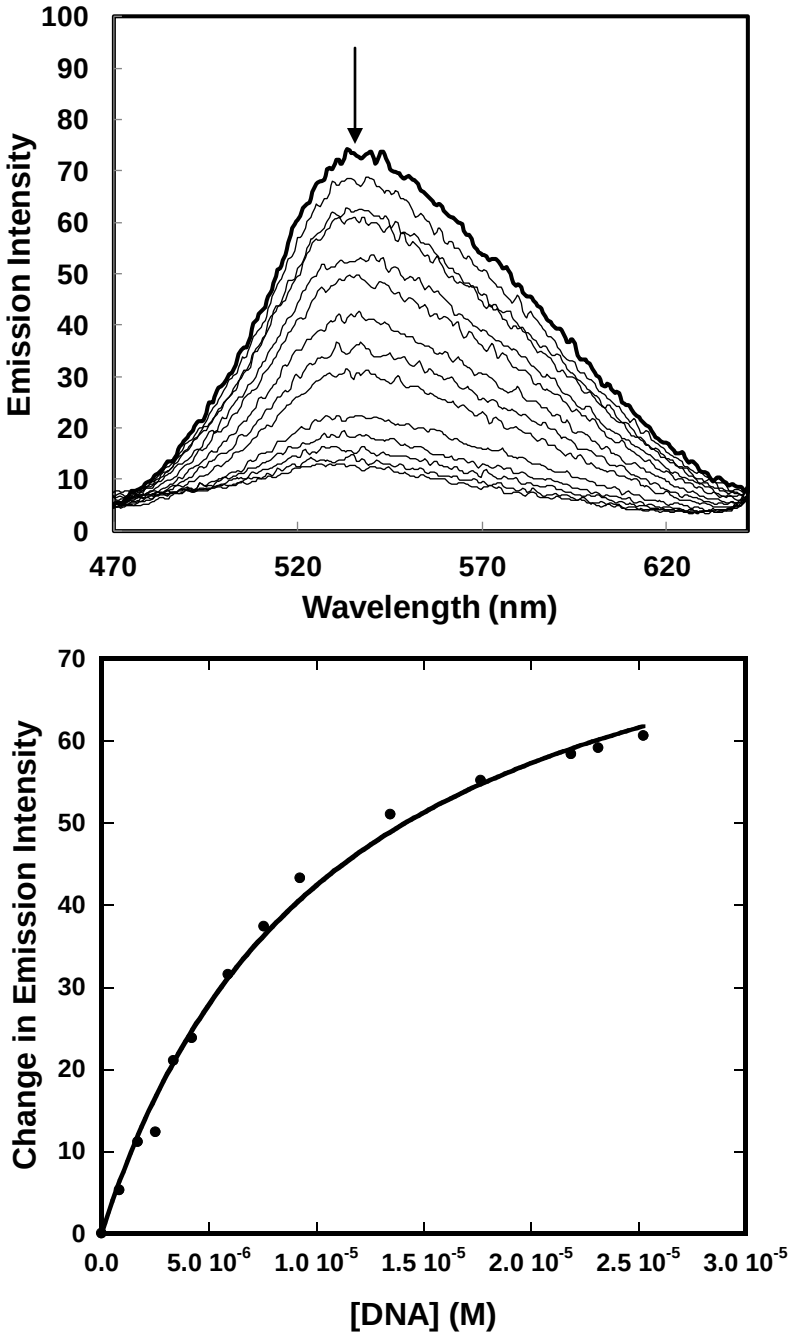

Figure 5.7 (S3): Fluorescence spectral titration of ct-DNA with 3.3 μM **AQT III** in MES10 buffer, 0.15 M NaCl, pH 6.24 and 25 ^{o}C (λ_{ex}: 354 nm; λ_{em}:536 nm).
*Top: Fluorescence spectra of **AQT III** with ct-DNA at various DNA:**AQT III** ratios (r_i = 0 to 25). Bottom: The observed change in emission intensity at 536 nm as a function of the concentration of ct-DNA were fitted with equation 2 to obtain an equilibrium binding constant and the binding site size.*

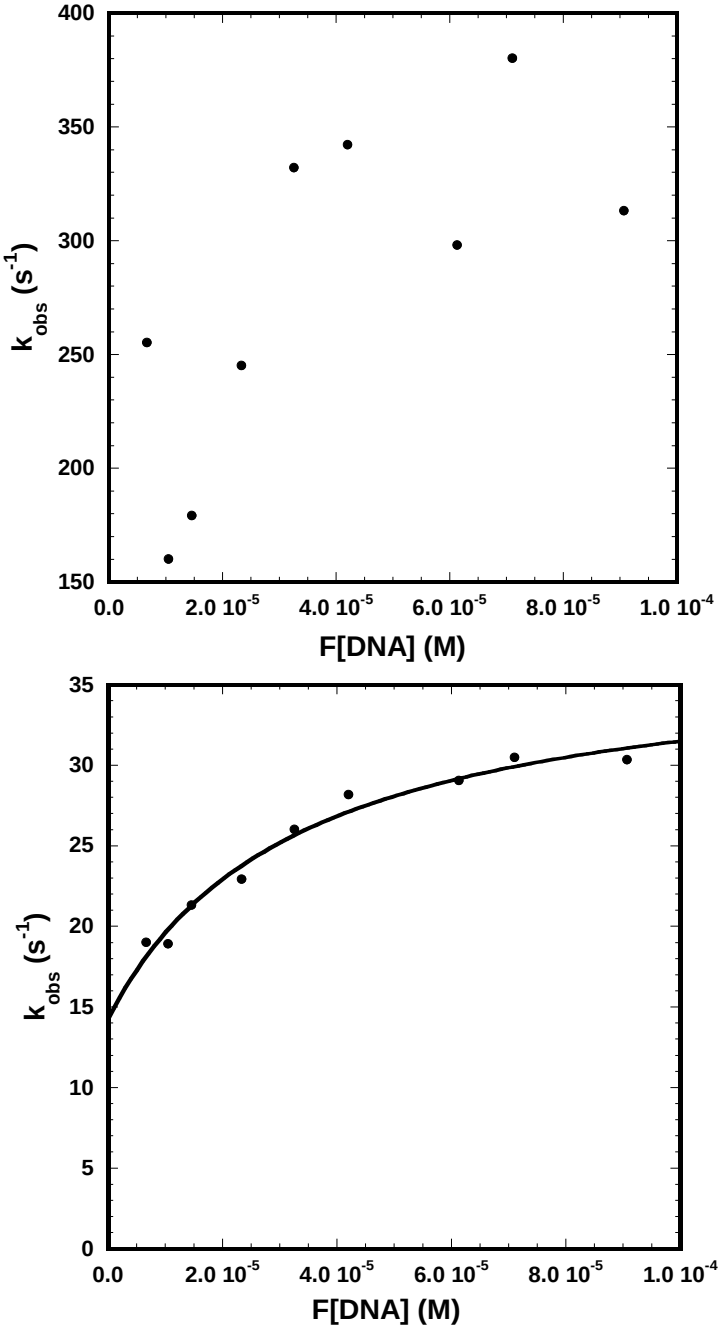

Figure 5.8 (S4): Dependence of the observed rates of the **AQT II**/ct-DNA system on the concentration of DNA in MES10 buffer, pH 6.4, 0.15 M NaCl at 25 ^{o}C.
(A) Fast process; (B) slow process. The fitting assumed a site size of 3. The faster process was not fitted because it was almost completed at the highest concentration of DNA and the signal to noise ratio was high.

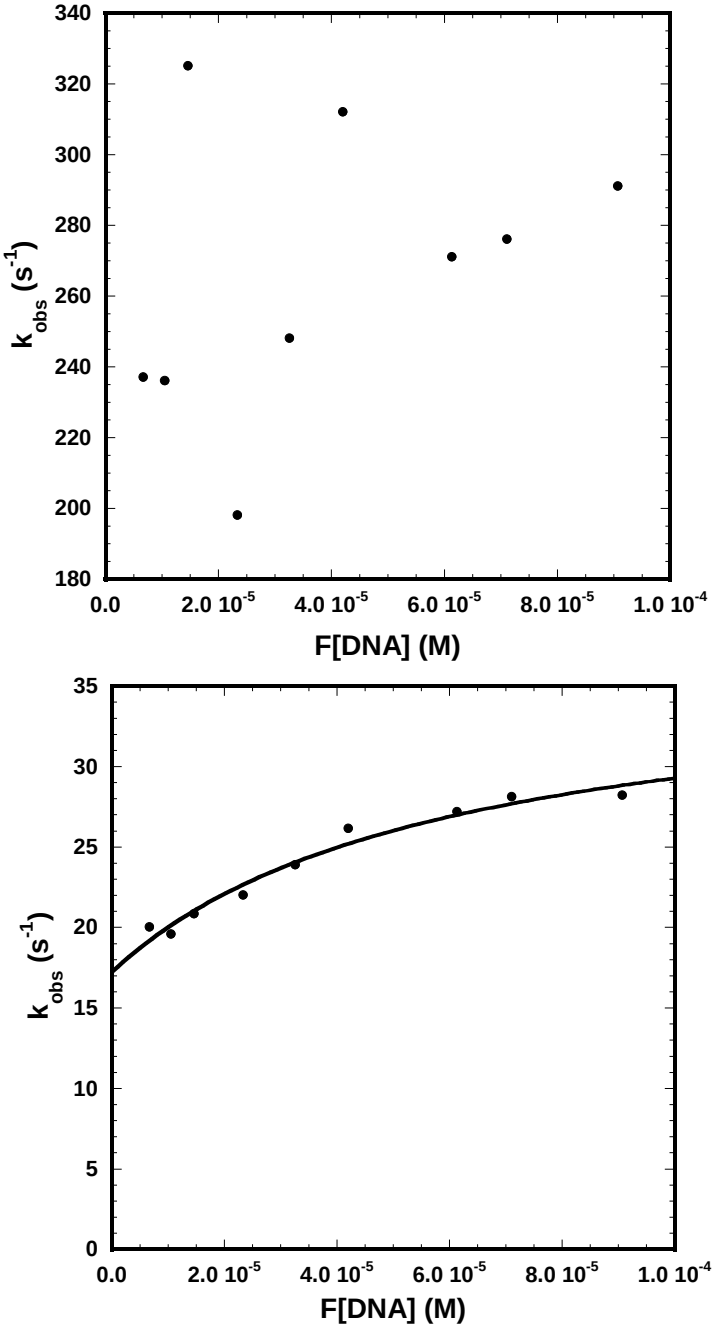

Figure 5.9 (S5): Dependence of the observed rates of the **AQT III**/ct-DNA system on the concentration of DNA in MES10 buffer, pH 6.4, 0.15 M NaCl at 25 ^{o}C. *(A) Fast process; (B) slow process. The fitting assumed a site size of 3. The faster process was not fitted because it was almost completed at the highest concentration of DNA and the signal to noise ratio was high.*

Table 5.1: Kinetic constants for the anthraquinone-DNA interaction

Ligand	K_1 (M^{-1}) 10^4	k_2 (s^{-1})	k_{-2} (s^{-1})	k_3 (s^{-1})	k_{-3} (s^{-1})	K_3	K* (M^{-1}) 10^4
AQT II	-	≥630	-	23 ± 1.7	14 ± 1.9	2.6	16 ± 1.2
AQT III	-	≥470	-	19 ± 3.3	17 ± 1.1	2.1	9.3 ± 0.5
AQT IV	5.9 ± 0.20	340 ± 16	71 ± 13	21 ± 2.2	19 ± 3.2	2.1	4.0 ± 0.6

K is the overall equilibrium binding constant obtained from plotting the change in emission as a function of the DNA concentration.*

5.2.5 *Supplementary Information*

Fluorescence Spectroscopy: Data manipulation and plotting was done using the program Kaleidagraph version 4.0. To obtain the binding constant of anthraquinone to DNA, the data was fitted to a non-competitive interaction model for nonlinear least-squares optimization of the binding parameters [84]:

$$y = 0.5R\ \{A + B + x - (\sqrt{((A + B + x)^2 - 4Bx)})\} \qquad eq\ 2$$

where $R = R_b/n$, (R_b is the instrument response sensitivity and is given by the fluorescence of the ligand when it is fully bound divided by the total concentration of the ligand; n is the site size); $A = n/K$, (K is the equilibrium binding constant); and $B = nL_t$, (L_t is the total concentration of ligand). The equilibrium binding constant and site size are calculated as $K = B/(A*L_t)$ and $n = B/L_t$.

Kinetics Experiments

Analysis of AQT I binding to ct-DNA. The dependence of the observed rate constant, k_{obs}, on the free DNA site concentration is given by the equation below:

$$k_{obs} = k_1 * F([DNA]) + k_{-1} \qquad eq\ 3$$

where k_1 is the association rate constant, k_{-1} is the dissociation rate constant, and F([DNA]) the concentration of potential binding sites calculated as outlined by Macgregor et al. [85] The calculation was developed by Jovin and Striker [76], based on the McGhee-von Hippel formalism [75]. The concentration of potential binding sites, F[DNA], depends upon the fraction of sites already occupied such that

$$F[DNA] = [DNA]_o\ f(r) \qquad eq\ 4$$

where $[DNA]_o$ is the total concentration of potential binding sites in the unoccupied DNA. Base on the McGhee and von Hippel model, $f(r)$ is the exclusion of potential binding sites arising from the distribution of the ligands on the DNA and is given by

$$f(r) = (1-nr)^n[1-(n-1)r]^{1-n} \qquad eq\ 5$$

where the number of intercalation sites occupied or perturbed (and as such, cannot participate in further binding) by a ligand is equal to 2n-1. At saturating ligand concentrations, the fractional DNA occupancy reaches the limit of 1/n.

Analysis of AQT IV binding to ct-DNA. The kinetic data for the binding of **AQT IV** to ct-DNA was analyzed by plotting the observed rate constants, k_{obs}(fast) and k_{obs}(slow), as a function of the DNA concentration and fitted to equations 6 and 7 as described below:

$$k_{obs}(\text{fast}) = K_1k_2 * F([DNA]) / (1 + K_1 * F([DNA])) + k_{-2} \qquad \textit{eq 6}$$

and

$$k_{obs}(\text{slow}) = K_{12}k_3 * F([DNA]) / (1 + K_{12} * F([DNA])) + k_{-3} \qquad \textit{eq 7}$$

where $K_{12} = K_1(1 + K_2)$. The overall equilibrium binding constant can be calculated using the equation $K^*(1+ K_2(1 + K_3)$.

5.3 References

1. Takenaka, S., and Takagi, M. (1999) Threading intercalators as a new DNA structural probe, *Bull. Chem. Soc. Jpn. 72*, 327-337.
2. Braña, M. F., Cacho, M., Gradillas, A., de Pascual-Teresa, B., and Ramos, A. (2001) Intercalators as anticancer drugs, *Curr. Pharm. Des. 7*, 1745-1780.
3. Wilson, W. D. (1999) DNA Intercalators, In *DNA and Aspects of Molecular Biology* (Kool, E. T., Ed.), pp 427-476, Pergamon, New York.
4. Guelev, V. M., Cubberley, M. S., Murr, M. M., Lokey, R. S., and Iverson, B. L. (2001) Design, synthesis, and characterization of polyintercalating ligands, In *Methods Enzymol.* (Chaires, J. B., and Waring, M. J., Eds.), pp 556-570, Academic Press, New York.
5. Wilhelmsson, L. M., Lincoln, P., and Nordell, P. (2006) Slow DNA Binding, In *Sequence-Specific DNA Binding Agents* (Waring, M., Ed.), pp 69-95, The Royal Society of Chemistry, Cambridge, UK.
6. Wheate, N. J., Brodie, C. R., Collins, J. G., Kemp, S., and Aldrich-Wright, J. R. (2007) DNA intercalators in cancer therapy: Organic and inorganic drugs and their spectroscopic tools of analysis, *Mini Rev. Med. Chem. 7*, 627-648.
7. Strekowski, L., and Wilson, B. (2007) Noncovalent interactions with DNA: An overview, *Mutat. Res. Fund. Mol. Mech. Mut. 623*, 3-13.
8. Fox, K. R., Brassett, C., and Waring, M. J. (1985) Kinetics of dissociation of nogalamycin from DNA: Comparison with other anthracycline antibiotics, *Biochim Biophys Acta. 830*, 383-392.
9. Holman, G. G., Zewail-Foote, M., Smith, A. R., Johnson, K. A., and Iverson, B. L. (2011) A sequence-specific threading tetra-intercalator with an extremely slow dissociation rate constant, *Nat. Chem. 3*, 875-881.
10. Li, M., Lincoln, P., and Andersson, J. (2011) Slow threading intercalation of monomeric Ru(II) complexes with 10,13-diarylsubstituted dppz ligands, *J. Phys. Chem. B 115*, 7923-7931.
11. Westerlund, F., Nordell, P., Nordén, B., and Lincoln, P. (2007) Kinetic characterization of an extremely slow DNA binding equilibrium, *J. Phys. Chem. B 111*, 9132-9137.
12. Andersson, J., and Lincoln, P. (2011) Stereoselectivity for DNA threading intercalation of short binuclear ruthenium complexes, *J. Phys. Chem. B 115*, 14768-14775.
13. Ohtsuka, K., Komizo, K., and Takenaka, S. (2010) Synthesis and DNA binding behavior of a naphthalene diimide derivative carrying two dicobalt hexacarbonyl complexes as an infrared DNA probe, *J. Organomet. Chem. 695*, 1281-1286.
14. Sato, S., Nojima, T., Waki, M., and Takenaka, S. (2005) Supramolecular complex formation by beta-cyclodextrin and ferrocenylnaphthalene diimide-intercalated double stranded DNA and improved electrochemical gene detection, *Molecules 10*, 693-707.
15. Tanious, F. A., Yen, S. F., and Wilson, W. D. (1991) Kinetic and equilibrium analysis of a threading intercalation mode: DNA sequence and ion effects, *Biochemistry 30*, 1813-1819.
16. Yen, S. F., Gabbay, E. J., and Wilson, W. D. (1982) Interaction of aromatic imides with DNA spectrophotometric and viscometric studies, *Biochemistry 21*, 2070-2076.
17. Liu, Z. R., Hecker, K. H., and Rill, R. L. (1996) Selective DNA binding of (*N*-alkylamine)-substituted naphthalene imides and diimides to G+C-rich DNA, *J. Biomol. Struct. Dyn. 14*, 331-339.

18. Lokey, R. S., Kwok, Y., Guelev, V., Pursell, C. J., Hurley, L. H., and Iverson, B. L. (1997) A new class of polyintercalating molecules, *J. Am. Chem. Soc. 119*, 7202-7210.
19. Guelev, V., Sorey, S., Hoffman, D. W., and Iverson, B. L. (2002) Changing DNA grooves - A 1,4,5,8-naphthalene tetracarboxylic diimide bis-intercalator with the linker (beta-ala)(3)-lys in the minor groove, *J. Am. Chem. Soc. 124*, 2864-2865.
20. Sato, S., Nojima, T., Takagi, M., Kondo, H., and Takenaka, S. (2002) Synthesis of adamantyl naphthalene diimide and its interaction with double stranded DNA, *Nucleic Acids Res Suppl*, 213-214.
21. Lee, J., Guelev, V., Sorey, S., Hoffman, D. W., and Iverson, B. L. (2004) NMR structural analysis of a modular threading tetraintercalator bound to DNA, *J. Am. Chem. Soc. 126*, 14036-14042.
22. Sato, S., Hokazono, K., Irie, T., Ueki, T., Waki, M., Nojima, T., Kondo, H., and Takenaka, S. (2006) Ferrocenylnaphthalene diimide-based electrochemical detection of methylated gene, *Anal. Chim. Acta 578*, 82-87.
23. Chu, Y., Sorey, S., Hoffman, D. W., and Iverson, B. L. (2007) Structural characterization of a rigidified threading bisintercalator, *J. Am. Chem. Soc. 129*, 1304-1311.
24. Sato, S., and Takenaka, S. (2008) Linker effect of ferrocenylnaphthalene diimide ligands in the interaction with double stranded DNA, *J. Organomet. Chem. 693*, 1177-1185.
25. Sato, S., Hirano, A., and Takenaka, S. (2010) Selective immobilization of double stranded DNA on a gold surface through threading intercalation of a naphthalene diimide having dithiolane moieties, *Anal. Chim. Acta 665*, 91-97.
26. Watanabe, S., Ohtsuka, K., Sato, S., and Takenaka, S. (2011) Discrimination of phosphorylated double stranded DNA by naphthalene diimide having zinc(II) dipicolylamine complexes, *Bioorg. Med. Chem. 19*, 1361-1365.
27. McKnight, R. E., Reisenauer, E., Pintado, M. V., Polasani, S. R., and Dixon, D. W. (2011) Substituent effect on the preferred DNA binding mode and affinity of a homologous series of naphthalene diimides, *Bioorg. Med. Chem. Lett. 21*, 4288-4291.
28. Smith, A. R., Ikkanda, B. A., Holman, G. G., and Iverson, B. L. (2012) Subtle recognition of 14-base pair DNA sequences via threading polyintercalation, *Biochemistry 51*, 4445-4452.
29. Tanious, F. A., Jenkins, T. C., Neidle, S., and Wilson, W. D. (1992) Substituent position dictates the intercalative DNA-binding mode for anthracene-9,10-dione antitumor drugs, *Biochemistry 31*, 11632-11640.
30. Fox, K. R., Brassett, C., and Waring, M. J. (1985) Kinetics of dissociation of nogalamycin from DNA comparison with other anthracycline antibiotics, *Biochim. Biophys. Acta 840*, 383-392.
31. McKnight, R. E., Zhang, J., and Dixon, D. W. (2004) Binding of a homologous series of anthraquinones to DNA, *Bioorg. Med. Chem. Lett. 14*, 401-404.
32. Gatto, B., Zagotto, G., Sissi, C., and Palumbo, M. (1997) Preferred interaction of D-peptidyl-anthraquinones with double-stranded B-DNA, *Int. J. Biol. Macromol. 21*, 319-326.
33. Searle, M. S., Maynard, A. J., and Williams, H. E. L. (2003) DNA recognition by the anthracycline antibiotic respinomycin D: NMR structure of the intercalation complex with d(AGACGTCT)(2), *Org. Biomol. Chem. 1*, 60-66.

34. Williams, L. D., Egli, M., Gao, Q., Bash, P., Van Der Marel, G. A., Van Boom, J. H., Rich, A., and Frederick, C. A. (1990) Structure of nogalamycin bound to DNA hexamer, *Proc. Natl. Acad. Sci. U. S. A. 87*, 2225-2229.
35. Jourdan, M., Garcia, J., Lhomme, J., Teulade-Fichou, M. P., Vigneron, J. P., and Lehn, J. M. (1999) Threading bis-intercalation of a macrocyclic bisacridine at abasic sites in DNA: Nuclear magnetic resonance and molecular modeling study, *Biochemistry 38*, 14205-14213.
36. Bourdouxhe-Housiaux, C., Colson, P., Houssier, C., Waring, M. J., and Bailly, C. (1996) Interaction of a DNA-threading netropsin-amsacrine combilexin with DNA and chromatin, *Biochemistry 35*, 4251-4264.
37. Martelli, A., Jourdan, M., Constant, J. F., Demeunynck, M., and Dumy, P. (2006) Photoreactive threading agent that specifically binds to abasic sites in DNA, *Bioorg. Med. Chem. Lett. 16*, 154-157.
38. Searcey, M., Martin, P. N., Howarth, N. M., Madden, B., and Wakelin, L. P. G. (1996) DNA threading agents: Effect of sidechain bulk on DNA binding and cytotoxicity of 9-anilinoacridine-4-carboxamides, *Bioorg. Med. Chem. Lett. 6*, 1831-1836.
39. Carlson, C. B., and Beal, P. A. (2000) Solid-phase synthesis of acridine-based threading intercalator peptides, *Bioorg. Med. Chem. Lett. 10*, 1979-1982.
40. Wakelin, L. P. G., Bu, X., Eleftheriou, A., Parmar, A., Hayek, C., and Stewart, B. W. (2003) Bisintercalating threading diacridines: relationships between DNA binding, cytotoxicity, and cell cycle arrest, *J. Med. Chem. 46*, 5790-5802.
41. Badr, S., El-Kerdawy, M. M., Tanious, F. A., Wilson, W. D., and Boykin, D. W. (2008) Synthesis of acridine based threading intercalators, *Heterocyc. Comm. 14*, 15-20.
42. Choudhury, J. R., Guddneppanavar, R., Saluta, G., Kucera, G. L., and Bierbach, U. (2008) Tuning the DNA conformational perturbations induced by cytotoxic platinum-acridine bisintercalators: Effect of metal *cis/trans* isomerism and DNA threading groups, *J. Med. Chem. 51*, 3069-3072.
43. He, Z., Bu, X., Eleftheriou, A., Zihlif, M., Qing, Z., Stewart, B. W., and Wakelin, L. P. G. (2008) DNA threading bis(9-aminoacridine-4-carboxamides): Effects of piperidine sidechains on DNA binding, cytotoxicity and cell cycle arrest, *Bioorg. Med. Chem. 16*, 4390-4400.
44. Bazzicalupi, C., Biagini, S., Bianchi, A., Biver, T., Boggioni, A., Giorgi, C., Gratteri, P., Malavolti, M., Secco, F., Valtancoli, B., and Venturini, M. (2010) DNA interaction with Ru(II) and Ru(II)/Cu(II) complexes containing azamacrocycle and dppz residues. A thermodynamic, kinetic and theoretical study, *Dalton Trans. 39*, 9838-9850.
45. Nordell, P., Jansson, E. T., and Lincoln, P. (2009) Supercoil-accelerated DNA threading intercalation, *Biochemistry 48*, 1442-1444.
46. Paramanathan, T., Westerlund, F., McCauley Micah, J., Rouzina, I., Lincoln, P., and Williams Mark, C. (2008) Mechanically manipulating the DNA threading intercalation rate, *J. Am. Chem. Soc. 130*, 3752-3753.
47. Westerlund, F., Nordell, P., Blechinger, J., Santos, T. M., Nordén, B., and Lincoln, P. (2008) Complex DNA binding kinetics resolved-by combined circular dichroism and luminescence analysis, *J. Phys. Chem. B 112*, 6688-6694.
48. Muller, W., and Crothers, D. M. (1968) Studies of the binding of actinomycin and related compounds to DNA, *J. Mol. Biol. 35*, 251-290.

49. Janovec, L., Kozurkova, M., Sabolova, D., Ungvarsky, J., Paulikova, H., Plsikova, J., Vantova, Z., and Imrich, J. (2011) Cytotoxic 3,6-bis((imidazolidinone)imino)acridines: Synthesis, DNA binding and molecular modeling, *Bioorg. Med. Chem. 19*, 1790-1801.
50. Denny, W. A. (2004) Acridine-4-carboxamides and the concept of minimal DNA intercalators, In *Small Molecule DNA and RNA Binders* (Demeunynck, M., Bailly, C., and Wilson, W. D., Eds.), pp 482-502, Wiley-VCH Verlag GmbH & Co. KGaA, Weinheim.
51. Denny, W. A. (2002) Acridine derivatives as chemotherapeutic agents, *Curr. Med. Chem. 9*, 1655-1665.
52. Westerlund, F., Pierard, F., Eng, M. P., Nordén, B., and Lincoln, P. (2005) Enantioselective luminescence quenching of DNA light-switch Ru(phen)(2)dppz (2+) by electron transfer to structural homologue Ru(phendione)(2)dppz (2+), *J. Phys. Chem. B 109*, 17327-17332.
53. Wilhelmsson, L. M., Esbjorner, E. K., Westerlund, F., Nordén, B., and Lincoln, P. (2003) *Meso* stereoisomer as a probe of enantioselective threading intercalation of semirigid ruthenium complex mu-(11,11'-bidppz)(phen)(4)Ru-2 (4+), *J. Phys. Chem. B 107*, 11784-11793.
54. Onfelt, B., Lincoln, P., and Nordén, B. (2001) Enantioselective DNA threading dynamics by phenazine-linked $[Ru(phen)_2dppz]^{2+}$ dimers, *J. Am. Chem. Soc. 123*, 3630-3637.
55. Biver, T., Secco, F., and Venturini, M. (2008) Mechanistic aspects of the interaction of intercalating metal complexes with nucleic acids, *Coord. Chem. Rev. 252*, 1163-1177.
56. Waring, M., and Editor (2006) *Sequence-specific DNA Binding Agents*.
57. Nordell, P., and Lincoln, P. (2005) Mechanism of DNA threading intercalation of binuclear Ru complexes: Uni or bimolecular pathways depending on ligand structure and binding density, *J. Am. Chem. Soc. 127*, 9670-9671.
58. Nordell, P., Westerlund, F., Wilhelmsson, M., Nordén, B., and Lincoln, P. (2005) DNA binding of bidppz Ru-complexes - Effect of ancillary ligands on intercalation kinetics, *Biophys. J. 88*, 410A-410A.
59. Li, M., and Lincoln, P. (2009) Synthesis and DNA threading properties of quaternary ammonium Ru(phen)(2)(dppz) (2+) derivatives, *J. Inorg. Biochem. 103*, 963-970.
60. Nordell, P., Westerlund, F., Wilhelmsson, L. M., Nordén, B., and Lincoln, P. (2007) Kinetic recognition of AT-rich DNA by ruthenium complexes, *Angew. Chem., Int. Ed. 46*, 2203-2206.
61. Nordell, P., Westerlund, F., Reymer, A., El-Sagheer, A. H., Brown, T., Nordén, B., and Lincoln, P. (2008) DNA polymorphism as an origin of adenine-thymine tract length-dependent threading intercalation rate, *J. Am. Chem. Soc. 130*, 14651-14658.
62. Kogan, M., Nordén, B., Lincoln, P., and Nordell, P. (2011) Transition state of rare event base pair opening probed by threading into looped DNA, *Chembiochem 12*, 2001-2006.
63. Bazzicalupi, C., Bencini, A., Bianchi, A., Biver, T., Boggioni, A., Bonacchi, S., Danesi, A., Giorgi, C., Gratteri, P., Ingrain, A. M., Secco, F., Sissi, C., Valtancoli, B., and Venturini, M. (2008) DNA binding by a new metallointercalator that contains a proflavine group bearing a hanging chelating unit, *Chem. Eur. J. 14*, 184-196.
64. Graves, D. E., and Velea, L. M. (2000) Intercalative binding of small molecules to nucleic acids, *Curr. Org. Chem. 4*, 915-929.
65. Haq, I. (2002) Thermodynamics of drug-DNA interactions, *Arch. Biochem. Biophys. 403*, 1-15.

66. Martínez, R., and Chacón-García, L. (2005) The search of DNA-intercalators as antitumoral drugs: What it worked and what did not work, *Curr. Med. Chem. 12*, 127-151.
67. Neto, B. A. D., and Lapis, A. A. M. (2009) Recent developments in the chemistry of deoxyribonucleic acid (DNA) intercalators: Principles, design, synthesis, applications and trends, *Molecules 14*, 1725-1746.
68. Biver, T. (2012) Use of UV-Vis Spectrometry to Gain Information on the Mode of Binding of Small Molecules to DNAs and RNAs, *Appl. Spectrosc. Rev. 47*, 272-325.
69. Fox, K. R., and Waring, M. J. (1984) Evidence of different binding sites for nogalamycin in DNA revealed by association kinetics, *Biochim. Biophys. Acta 802*, 162-168.
70. Biver, T., Secco, F., Tine, M. R., and Venturini, M. (2003) Equilibria and kinetics of the intercalation of Pt-proflavine and proflavine into calf thymus DNA, *Arch. Biochem. Biophys. 418*, 63-70.
71. Biagini, S., Bianchi, A., Biver, T., Boggioni, A., Nikolayenko, I. V., Secco, F., and Venturini, M. (2011) DNA binding of a proflavine derivative bearing a platinum hanging residue, *J. Inorg. Biochem. 105*, 558-562.
72. McKnight, R. E., Zhang, J. G., and Dixon, D. W. (2004) Binding of a homologous series of anthraquinones to DNA, *Bioorg. Med. Chem. Lett. 14*, 401-404.
73. Fluorescence titrations were performed on a Perkin Elmer Spectrofluorometer at λ_{exc} = 354 nm and λ_{em} = 536 nm. The titrations were carried out by adding increasing amounts of the DNA directly into the cell containing 3 µM anthraquinone ligand. The DNA concentration, given in base pair concentration, varied between 0.5 µM to 62 µM. Measurements were collected at 50 nm/min using a slit width of 5 mm. Data manipulation and plotting was done using the program Kaleidagraph (version 4.0). To obtain the binding constants of the anthraquinones binding to DNA, the data were fitted to the interaction model described in equation 2 (Supplementary Data).
74. The kinetic experiments were performed at 25 ^{o}C by using a Hi-Tech SF-61 stopped-flow spectrophotometer and monitoring the course of the reaction in the fluorescence detection mode. The acquired signal was recorded on a PC and then analyzed by suing the Hi-Kinetic Studio Software (Hi-Tech Scientific, Bradford on Avon, U.K.). The ligand concentration (AQ I-IV) were kept constant at 3 µM. Previous spectroscopic experiments and calculations revealed that anthraquinones are less than 1% self-aggregated, thus have minimum effect on the binding process. The ct-DNA concentration, in all cases refers to the basepair concentration. The DNA concentration varied within 15 µM and 150 µM. Each experiment was repeated at least seven times, and the kinetic traces were averaged in order to reduce the signal-to-noise ratio. Data manipulation and plotting was done using the program Kaleidagraph version 4.0.
75. McGhee, J. D., and von Hippel, P. H. (1974) Theoretical aspects of DNA-protein interactions: Co-operative and non-co-operative binding of large ligands to a one-dimensional homogeneous lattice, *J. Mol. Biol. 86*, 469-489.
76. Jovin, T. M., and Striker, G. (1977) Chemical relaxation kinetic studies of *E. coli* RNA polymerase binding to poly d(A--T) using ethidium bromide as a fluorescence probe, *Mol. Bio. Biochem. Biophys 24*, 245-281.
77. Chaires, J. B., Dattagupta, N., and Crothers, D. M. (1985) Kinetics of the daunomycin-DNA interaction, *Biochemistry 24*, 260-267.

78. Jackson Beckford, S., and Dixon, D. W. (2012) Molecular dynamics of anthraquinone DNA intercalators with polyethylene glycol side chains, *J. Biomol. Struct. Dyn. 29*, 1065-1080.
79. Biver, T., De Biasi, A., Secco, F., Venturini, M., and Yarmoluk, S. (2005) Cyanine dyes as intercalating agents: Kinetic and thermodynamic studies on the DNA/Cyan40 and DNA/CCyan2 systems, *Biophys. J. 89*, 374-383.
80. Nordell, P., Westerlund, F., Reymer, A., Nordén, B., and Lincoln, P. (2008) Finding AT-DNA - kinetic recognition of long adenine-thymine stretches by metal-ligand complexes, *Nucleic Acids Symp. Ser.*, 131-132.
81. Nordén, B., Lincoln, P., Nordell, P., Westerlund, F., and Wilhelmsson, M. (2007) DNA-threading intercalation rate studies: Dynamics is an efficient mechanism for biomolecular structure recognition, *J. Biomol. Struct. Dyn. 24*, 677-678.
82. Westerlund, F., and Lincoln, P. (2007) AT-dependent luminescence of DNA-threading ruthenium complexes, *Biophys. Chem. 129*, 11-17.
83. Meyer-Almes, F. J., and Porschke, D. (1993) Mechanism of intercalation into the DNA double helix by ethidium, *Biochemistry 32*, 4246-4253.
84. Stootman, F. H., Fisher, D. M., Rodger, A., and Aldrich-Wright, J. R. (2006) Improved curve fitting procedures to determine equilibrium binding constants, *Analyst 131*, 1145-1151.
85. Macgregor, R. B., Jr., Clegg, R. M., and Jovin, T. M. (1985) Pressure-jump study of the kinetics of ethidium bromide binding to DNA, *Biochemistry 24*, 5503-5510.